Estimating Fault Slip Rates over 10 to 10^6 yr timescales in
the Himalaya and Tibet

by

Richard Styron

B.S. Geology, 2005, University of Arkansas
M.S. Geology, 2008, University of Arkansas

Submitted to the graduate degree program in Geology
and the Graduate Faculty of the University of Kansas in partial fulfillment of
the requirements for the degree of Doctor of Philosophy

_____
Chairperson Michael H. Taylor

_____
J. Douglas Walker

_____
Andreas Moller

_____
Daniel F Stockli

_____
Ross Black

_____
Xingong Li

Date Defended: 12 October 2012

The Dissertation Committee for Richard Styron
certifies that this is the approved version of the following dissertation:

Estimating Fault Slip Rates over 10 to 10^6 yr timescales in
the Himalaya and Tibet

_____

Chairperson Michael H. Taylor

Date Approved:

1 November 2012

ii

ABSTRACT

The Himalayan-Tibetan orogen is the highest on the modern Earth and an archetypal region for studying continental collisions. As such, its characteristics have been the basis for many different models for orogenesis, in spite of a lack of data on deformation styles and rates in many parts of the orogen. More data on deformation rates and histories are needed to create, modify or reject hypotheses seeking to explain aspects of this orogeny. This work comprises four studies of deformation over vastly different temporal scales, with a spatial emphasis on the western Himalaya and Tibet. The first study combines global positioning system (GPS) geodesy and structural field observations to study arc-parallel extension and translation of the Himalaya. Arc-parallel extension is estimated at ~3 cm yr^{-1} over the length of the Himalaya, with the highest rates in eastern Nepal. Arc-parallel translation is expressed as slip on the Karakoram fault and decreases in rate and magnitude from northwest to southeast. Results from this study indicate that a model of variably-oblique convergence between the Indian plate and the Himalaya is likely responsible for the observed deformation, while other models considered fail to match observations. The second study combines field mapping, zircon (U-Th)/He thermochronology, zircon U-Pb geochronology and thermokinematic modeling to determine the deformation history of the previously unstudied South Lunggar Rift in southwestern Tibet. Results indicate that extension started in the middle Miocene and accelerated in the late Miocene to modern horizontal extension rates of 1-3 mm yr^{-1}. Cumulative extension in the rift varies from 3 to 21 km along strike. The third study extends the thermokinematic modeling performed in the South Lunggar Rift to the North Lunggar Rift; key results include a northward propagation in rapid extension that may result from the underthrusting of the Indian plate beneath Tibet. The fourth study is a neotectonic slip rate study on the southeastern Karakoram fault. Mapping results suggest that late Quaternary offsets of geomorphic features may be considerably lower than previously estimated. Slip rate estimates await laboratory results but are likely much lower than earlier estimates, consisitent with the oblique convergence hypothesis for Himalayan deformation. These combined results provide much-needed data on deformation rate and style in the orogen and highlight the role of the Indian plate in driving orogenesis.

Acknowledgements

First and foremost, none of the work contained here could have been done without the constant support of my advisor, Mike Taylor. In addition to providing financial and logistical support for the expensive and logistically challenging research here, Mike thoroughly and consistently reviewed my work in an extremely timely fashion, pushed me farther in methods, interpretation and efficiency, and introduced me into the larger research community. Over the past four years, the dynamics of our relationship have evolved as well, reflecting both my growth as a scientist and his as an advisor; this dynamic has made it much easier to get things done with a minimum of fuss or restraint. I look forward to a continued relationship with him as a collaborator.

Secondly, the other members of my committee have all contributed to my development and the progress of my dissertation research as well as broader skill set. Danny Stockli and his lab group, too populous to list individually, provided excellent facilities, knowledge and expediency in (U-Th)/He thermochronomety, which is a vital organ in this body of work. An entire semester of one-on-one instruction in scientific computation from Ross Black also lead to the other methodological core of this work. Doug Walker proved more helpful than he may realize (or maybe not) in forcing me to be more rigorous in my interpretations, though we will see if I have gone far enough at my defense. Andreas Moller was helpful not only in acquiring valuable data, but in quickly and fulsomely responding to inquiry over matters geochronological and otherwise, and providing advice and interpretation from the valuable perspective of someone not entrenched in the ubiquitously biased world of Tibetan geology. Xingong Li taught me much about GIS analysis, which has been extremely useful not only in this research but in my teaching and in ongoing projects.

My classmates while at KU have also been indispensable. Kurt Sundell and Andrew McCallister worked hard to make the fieldwork successful, provided necessary training in the helium lab, and sharpened my thoughts on Tibet through hours and hours of discussion. Other members of our research group, A.J Herrs, Gabriel Veloza and Maureen Logan, gave great feedback to

1

presentations and helped in many ways. Willy Rittase and Beate Mocek helped me tremendously through training me in the cosmogenics lab. The IGL group is a wonderful research group to be a part of; learning the thermo- and geochronology ropes could not have been easier or more fun. Great discussions on tectonics and related processes from the group members, especially Tandis Bidgoli and Jeff Oalmann, were crucial in developing my understanding of these processes. And of course the fun only increased when we left the lab. Many students in other disciplines helped me with various things as well, be it computer coding or understanding complicated physical and chemical phenomena: Kwan Yee Cheng, Ben Rickards and Ian Bowen were particularly helpful.

Individuals outside of KU were also critical. Nothing here could have been done without my coauthors, both those named above and Mike Murphy, Deliang Liu, Ding Lin, Guang Yang and John Gosse--each faultlessly contributing to our work. Paul Kapp provided considerable advice as well; Will Woodruff and Brian Horton were both open with their work and fun in the field. Speaking of the field, this reasearch would be pitiful without our dear Tibetan collaborators: Jhoma Tsering, Tentzen, Dawa, Deng Ju, Uncle and Kadup were dependably excellent, and exceeded both expectations and typical behavioral standards in making this happen.

There are many more who made these years memorable. Love from the incredible Lydia Staisch, my amazing parents and my brothers also exceeded high expectations. And then there are those whom I won't incriminate by naming here, whose friendship through good times and bad, full beverages and empty, will stay friends for a lifetime.

Table of Contents

Table of Contents, con't.

Table of Contents, con't.

Chapter 1

Introduction

This dissertation comprises several studies that all involve studying tectonic deformation of Tibet and the Himalaya, with special emphasis on southwestern Tibet and the central-western Himalaya. Though the locations studied, the methods employed and timescales of consideration vary significantly from project to project, the tectonics of southern Tibet and the Himalaya over the time and space studied remain consistent enough that a coherent picture of regional deformation emerges. In particular, the role of the Indian plate as a major cause of extensional deformation within the Himalayan-Tibetan orogen becomes more clear, though this is often neglected in the literature. Additionally, this research reveals much about the variability through time of regional deformation, providing new and important information on the evolution of orogeny.

Four different studies are included in this dissertation. Chapter 2 is not a study per se, but introduces a fault database used throughout the rest of the dissertation. The first study (Chapter 3), published in *Geosphere* in April 2011, is titled 'Oblique convergence, arc parallel extension, and the role of strike-slip faulting in the high Himalaya'. This study combines published Global Positioning System (GPS) geodetic data from throughout northern India, the Himalaya and southern Tibet, as well as geologic data indicating the geometry, timing and magnitude of fault deformation throughout the Himalaya, to test four prominent models of Himalayan and south Tibetan crustal extension. The results of the analysis show that arc-parallel extension of the Himalaya occurs at ~3 cm yr^{-1}, and the only model whose predictions are consistent with all observations is the 'oblique convergence' model, where systematic variation in the angle of convergence between India and Tibet causes arc-parallel extension of the Himalaya. This model also predicts that horizontal displacements and rates on the Karakoram fault will decrease to the southeast. This prediction forms the hypothesis to be tested in Chapter 6.

The second study (Chapter 4), entitled, 'Miocene initiation and acceleration of extension

in the South Lunggar rift, western Tibet: evolution of an active detachment system from structural mapping and (U-Th)/He thermochronology' was submitted to Tectonics in August 2012. This work is the seminal study on the South Lunggar Rift in southwest Tibet. The study uses structural and neotectonic mapping, zircon (U-Th)/He thermochronology, zircon U-Pb LA-ICP-MS geochronology, and thermokinematic modeling with the Pecube code to decipher the tectonic history of the rift. Our mapping results show that the South Lunggar Rift is made up of a central horst block (forming the Surla Range) bound on the west by the South Lunggar detachment, a west-dipping low-angle normal fault, and on the east by the east-dipping Palung Co normal fault. Zircon (U-Th)/He analytical results and thermokinematic modeling indicate that extension in the South Lunggar Rift began in the middle Miocene (18-10 Ma) and accelerated at 8.5-8 Ma, as faulting on the South Lunggar Detachment commenced.

The third study (Chapter 5), entitled 'Northward propagation of rapid east-directed extension in the Lunggar Rift, western Lhasa Terrane, Tibet: a consequence of Indian underthrusting?' is prepared for submission to a short-format, high-readership journal such as *Geology*, following submission of (U-Th)/He data from the North Lunggar Rift to a peer-reviewed journal. In this study, six apatite and zircon (U-Th)/He bedrock transects from the Lunggar Rift (two from the South Lunggar Rift, included in Chapter 4, and four from the North Lunggar Rift) are modeled using methods developed in Chapter 4. The results from this work show that though extension in the Lunggar Rift began in the middle Miocene (similar to elsewhere in Tibet and the Himalaya), initial extension rates were low and a wave of rapid extension has been propagating north through the rift, with a location and rate similar to the tip of Indian plate, which is underthrusting the Tibetan crust. We then develop a conceptual model tying the two observations together, where the Tibetan middle to lower crust flows to the east, locally thinning the crust to counteract deeper crustal thickening due to Indian underthrusting.

The fourth study (Chapter 6) is a summary of work to date on a late Quaternary slip rate project on the southeastern Karakoram Fault. This project consists of mapping geomorphic

features (alluvial fans and fluvial terraces) offset by the Karakoram Fault, and dating them through *in situ* terrestrial cosmogenic nuclide (TCN) dating techniques. Mapping and sampling were performed in September 2010. TCN sample preparation was done in July and August 2012, but isotopic measurements have not been completed. As part of the project, Python computer code was developed to construct slip and slip rate histories for faults using Monte Carlo simulations and capable of incorporating arbitrary probabilty density functions for the age and offset determinations. This code, which is fully functional, brings new rigor in uncertainty propagation to slip rate determinations. It is presented and described in this chapter.

A summary of the work presented here, and a discussion of how it fits together and its implications, is presented in the Conclusions (Chapter 7).

Fault scarps in Quaternary sedimnents in the North Lunggar Rift

Chapter 2:

HimaTibetMap-1.0: New 'Web-2.0' Database of Active Structures from the Indo-Asian Collision

Published in *Eos*, May 2010

Richard Styron, Mike Taylor, Kelechi Okoronkwo

The ongoing collision of India and Asia has produced a vast system of folds and faults, many of which are active today, as evidenced by recent devastating earthquakes, such as the 2005 Kashmir event [Pathier, et al., 2006] and the 2008 Wenchuan event [Parsons, et al., 2008], which caused considerable loss of life. These events underscore the need for a public, comprehensive database of active structures. Taylor and Yin (2009) assembled such a database, HimaTibetMap-1.0, now publicly available through the University of Kansas's (KU) Hawk Drive, a 'Web-2.0'-style system that allows for the addition of user-generated content and comments. HimaTibetMap-1.0 is intended to be a resource for geoscientists interested in the region, a framework on which other field geologists may contribute their work to the community, a forum for informal discussions about Indo-Asian neotectonics. The database is found at https://documents.ku.edu:443/collaboration/Geologic Data in Tibet.

HimaTibetMap-1.0

HimaTibetMap-1.0 contains >900 active structures in central Asia. Information on most structures was taken from the literature and compiled using ESRI's ArcMap. Structures in poorly-documented regions were inferred from remote sensing imagery and elevation data. The geometry and kinematics of inferred structures are based on geomorphic criteria (e.g., triangular facets) and circumstantial evidence (e.g., earthquake focal mechanisms) (Taylor and Yin, 2009).

Additionally, the database includes the main suture zones in the Himalayan-Tibetan Orogen and the distribution of Tibetan Cenozoic volcanism.

HimaTibetMap-1.0 is available in several formats. The ESRI Shapefile version contains the structures, with kinematics for each structure included as attributes and as a code for use with a 'styles' file to display symbology. The styles file, developed by Eric Cowgill at UC Davis, may be found and implemented following directions beginning in Section 2 of this manual: http:// keckcaves.geology.ucdavis.edu/software/RIMSG3/MANUALS/RIMS_Manual_v1b.pdf. HimaTibetMap-1.0 is also available in ASCII format for use with the open-source software Generic Mapping Tools (GMT, Wessel and Smith, 1995) and as Google Earth-compatible KML files.

Hawk Drive

HimaTibetMap-1.0 is intended to be a starting point for a collaborative compilation of Indo-Asian neotectonic data. KU's Hawk Drive is an installment of the popular Xythos Internet-based collaboration software. The 'Geologic Data in Tibet' web page, within Hawk Drive, is a wiki containing public-access content (e.g., HimaTibetMap-1.0) but also has more functionality for registered users, who may upload data or modifications of extant data and comment on message boards about the data or Indo-Asian tectonics. Although contributors must be added manually, permission will be granted on request. Those with Xythos accounts at other institutions may access Geologic Data in Tibet from their system, while users without are granted access through hyperlink-based 'tickets'. Users who upload materials will retain full rights to those materials, and may control access. We highly encourage contribution, and hope that these new technologies spark collaboration that will further our understanding of this fascinating region. For registration or more information, contact Richard Styron.

References

Parsons, T., C. Ji, and E. Kirby (2008), Stress changes from the 2008 Wenchuan earthquake and increased hazard in the Sichuan basin, Nature, 454, 509-510.

Pathier, E., et al. (2006), Displacement field and slip distribution of the 2005 Kashmir earthquake from SAR imagery, Geophys. Res. Lett., 33, L20310.

Taylor, M., and A. Yin (2009), Active structures on the Tibetan plateau and surrounding re-gions, Geosphere, in press.

Wessel, P. and W. H. F. Smith (1998), New, improved version of the Generic Mapping Tools released, EOS Trans. AGU, 79, p. 579
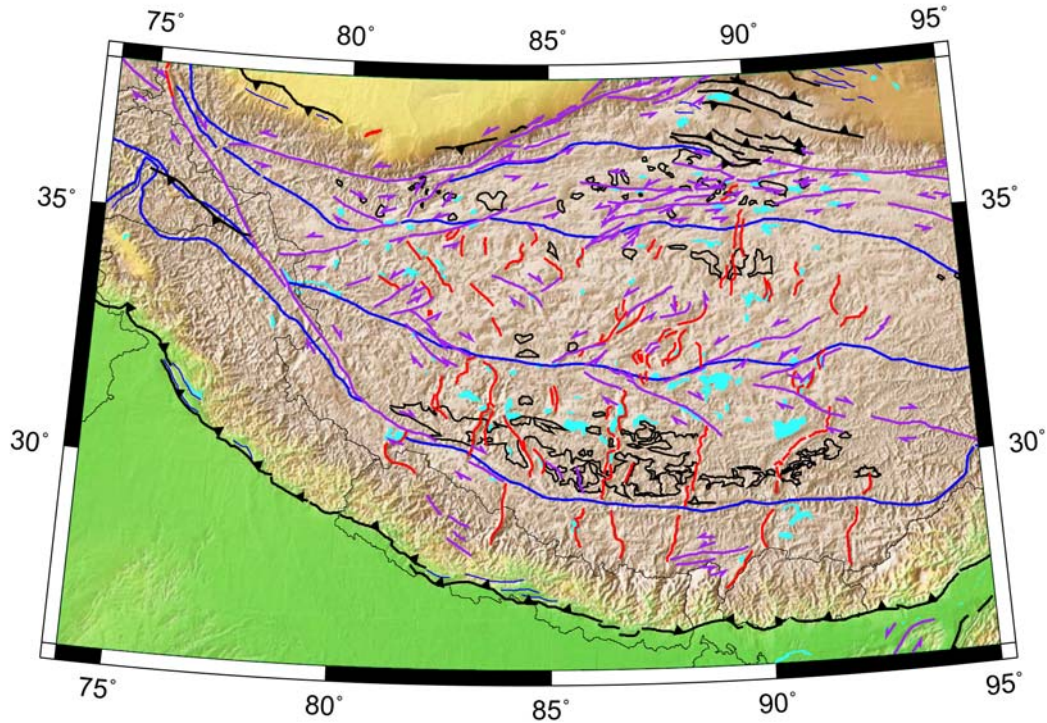
Figure 1: GMT map of Tibet incorporating HimaTibetMap-1.0 data. Purple lines indicate strike-slip faults. Red lines indicate normal faults. Thick black lines indicate thrust faults. Thinner black lines indicate distribution of Tibetan Cenozoic volcanism. Thick blue lines indicate sutures. Thin blue lines indicate folds.
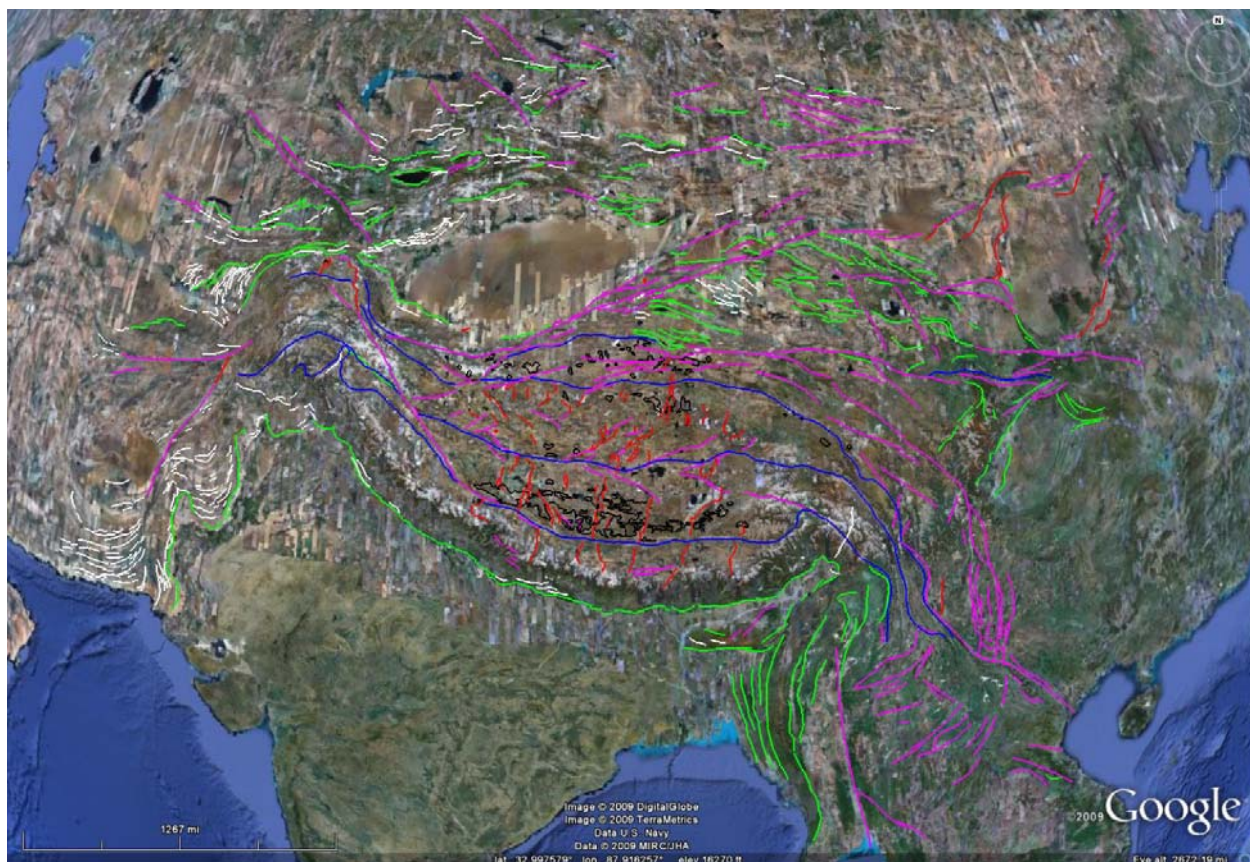
Figure 2: HimaTibetMap-1.0 data in Google Earth. Color scheme is the same as Figure 1 except green lines indicate folds and white lines indicate thrusts.

Gurla Mandhata from the northern Pulan Basin, which together compose a major Himalayan arc-parallel extensional structure.

Chapter 3

Oblique convergence, arc-parallel extension, and the role of strike-slip faulting in the High Himalaya

Richard H. Styron [1*]

Michael H. Taylor [1]

Michael A. Murphy [2]

Abstract

Arc-parallel extension is an important component of the active deformation of the Himalaya. This extension is accommodated via arc-perpendicular normal faults linked to arc-parallel strike-slip faults. Analysis of ~130 global positioning system geodetic velocities indicates >3 cm yr^{-1} of arc-parallel extension of the Himalaya. Several models have sought to explain Himalayan arc-parallel extension and strike-slip faulting, including lateral extrusion of Tibet, oroclinal bending of the Himalaya, radial spreading of Tibet and the Himalaya, and variably-oblique convergence between India and the Himalaya. Predictions of each model are tested against structural and geodetic observations. These tests indicate that the oblique convergence model best describes Himalayan extensional and strike-slip deformation.

Introduction

Throughout much of the Phanerozoic, the southern margin of Eurasia has been tectonically active; the collision and subsequent accretion of continental lithospheric fragments against Eurasia since the middle Paleozoic have produced the highly deformed crust that now makes up the orogens of central Asia (Yin and Harrison, 2000). This process is ongoing; India's Late Cretaceous-early Paleogene collision and continued convergence with Eurasia have produced an active deformation zone extending for >2000 km (Taylor and Yin, 2009). This deformation has uplifted the Himalaya range and portions of the Tibetan Plateau, producing the highest topography on Earth, where most of the Indo-Eurasian relative motion is accommodated (Gan, et al., 2007). This convergence is the primary cause for central Asian deformation, though many models have been proposed to explain the observations of the geometry and active tectonics of the Indo-Asian collision zone or subsets of it, especially in Tibet and the Himalaya. These include, but are not limited to, models of rapid uplift of the Tibetan Plateau due to detachment and sinking of the lithospheric mantle (e.g., Molnar, et al., 1993); northeast stepwise uplift of Tibet (Tapponnier, et al., 2001); gravitationally-driven collapse of the plateau (e.g. Dewey, 1988; Jade, et al., 2004), possibly accommodated by lower crustal flow from under the plateau to the east (e.g. Royden, et al., 1997); viscous (continuous) deformation of Tibetan lithosphere (e.g. England and Houseman, 1988); and deformation of Tibet and the Himalaya via motion of a number of relatively small internally-rigid blocks (e.g. Chen, et al., 2004a; Meade, 2007; Thatcher, 2007).

Though the Himalayan-Tibetan orogen is often considered the type model of a continental collisional orogen, active shortening structures are limited to the margins of the Tibetan Plateau, essentially the Himalayan front and where the plateau borders the Tarim, Qaidam and Sichuan Basins (Métivier et al., 1998; Taylor and Yin, 2009). Within Tibet, active deformation is widespread and consists of east-directed extension, accommodated by generally north-striking rifts and coeval north-south shortening via conjugate northeast- and northwest-striking strike-slip faults (Armijo, et al., 1986, 1989; Taylor, et al., 2003; Taylor and Yin, 2009) (Fig. 1). Active normal and strike-slip faulting is present within the Himalayan arc as well; these show slip directions to be generally

arc-parallel, resulting in both arc-parallel extension and translation (Nakata, 1989; Murphy, et al., 2002, 2009; Murphy and Copeland, 2005; Thiede, et al 2006; Jessup, et al., 2008; Li and Yin, 2008). Various mechanisms have been proposed to explain deformation in the Himalaya and south Tibet, including lateral extrusion of a rigid Tibet along the Karakoram fault (KF) and Indus-Yarlung suture zone (IYS) (Tapponnier, et al., 1982; Lacassin, et al., 2004); oroclinal bending (Li and Yin, 2008); outward, radial expansion of the Tibetan Plateau (Molnar and Lyon-Caen, 1989; Copley and McKenzie, 2007; Murphy et al., 2009); and variably-oblique Indo-Himalayan convergence (McCaffrey and Nábelek, 1998; Seeber and Pêcher, 1998). These models are described in more detail in the following, and specific, testable predictions of each are presented.

Here we combine and analyze several recently-published global positioning system (GPS) geodetic datasets in the Himalaya and immediate surroundings to evaluate the arc-parallel and arc-normal components of the velocity field in the Himalaya. We then use these results and structural observations from the geologic literature on the Himalaya and south Tibet to evaluate the more prominent models for modern Himalayan deformation.

Active structures of the Himalaya and south Tibet

Both the Himalaya and south Tibet show widespread active extensional and strike-slip faulting, though there are differences in deformational style. Active deformation in central Tibet consists of approximately east-west extension accommodated within the Lhasa and Qiangtang blocks via north-south-striking rifts (Armijo, et al., 1986, 1989; Yin et al., 1999a) (Figs. 1 and 2). Near the Bangong-Nujiang suture zone (BNS), the rifts link with conjugate northwest-striking dextral faults and northeast-striking sinistral faults the merge with the BNS (Armijo, et al., 1989) that accommodate N-S shortening and potentially more rapid E-W extension and eastward advection of central Tibetan lithosphere (Taylor, et al., 2003; Taylor and Peltzer, 2006). In the central Lhasa block, several of the major rifts cut southward through the IYS into the Himalayan arc (Yin, 2000). From east to west (Fig. 2), these include the Yadong-Gulu Rift (Cogan, et al.,

1998); the Pum Qu–Xainza Rift (Hager, et al., 2006), which may link to the south with the Nyönno Ri Detachment bounding the Ama Drime Massif (Jessup, et al., 2008; Kali, et al., 2010); the Tangra Yum Co–Tingri Rift (Dewane, et al., 2006; Taylor and Yin, 2009); the Kung Co Rift (Mahéo, et al., 2007; J. Lee, personal communication); and the Lopukangri Rift (Murphy, et al., 2010). Active rifting in the Lhasa block is not documented in western Tibet north of the Karakoram Fault, nor does this area display seismicity indicative of extension (Fig 1).

Active deformation in the Himalaya involves both extension and strike-slip faulting as well (Figs. 1, 2), though the orientation of the strain field is much more variable than in Tibet (Gan, et al., 2007). The dominant active structures within the Himalaya (north of the Main Frontal Thrust) are those accommodating arc-parallel extension (although studies have suggested recent activity of the Main Central Thrust (e.g., Hodges, et al., 2004)). Major active structures in the northwest Himalaya include the Leo Pargil core complex in northwest India, which is bound in the north by the KF and has accommodated some '10s of km' of extension (Thiede, et al., 2006), the Gurla Mandhata core complex, which has been interpreted to be a releasing bend in the right-lateral Karakoram-Humla fault system (Murphy and Copeland, 2005), and has accommodated 24-60 km extension, depending on the geometry of the core complex's major detachment at depth. The central Himalaya contains rifts cutting the range, such as the southern reaches of the south Tibetan rifts mentioned above, and the Thakkhola Graben (Hurtado, et al., 2001). With the exception of the Ama Drime Massif, (Jessup, et al., 2008) with a provisional extension estimate of 18-36 km on the western range-bounding Ama Drime Detachment and 15-30 km on the eastern Nyönno Ri Detachment, these rifts do not generally show the high magnitudes of extension as the western systems; estimates are often on the order of 10 km (Mahéo, et al., 2007, Wu et al., 1998).

Active strike-slip faulting has been described throughout much of the Himalaya. In northwestern India, NW-striking right-slip faults are associated with and often linked to east- and west- dipping normal faults (Steck, et al., 1998; Clark, 2005; Epard and Steck, 2008) including the Leo Pargil core complex (Thiede, et al., 2006) and arc-parallel dextral shear zones (Vannay and Steck, 1995; Epard and Steck, 2004). Farther to the southeast, dextral arc-parallel strike-slip

faulting has been observed in a zone from Gurla Mandhata SE into the Himalayan foothills in central Nepal. Murphy and Copeland (2005) mapped a right-slip fault, named the Humla Fault, extending east from the southern margin of Gurla Mandhata (Fig. 2). The Gurla Mandhata-Humla Fault system has been interpreted to transfer slip along the Karakoram Fault into the Himalaya (Murphy and Copeland, 2005; Murphy and Burgess, 2006). The Humla Fault may then feed slip into an en-echelon system of active dextral faults, including the Tibrikot, Dhaulagiri Southwest, and Bari Gad Faults (Nakata, 1989; Styron, et al., 2009; Murphy, et al., 2010).

The Karakoram Fault (KF) is the longest and most studied of the arc-parallel dextral faults in the western Himalaya region. The KF forms the boundary between the actively-extending northwest Himalaya and the relatively rigid southwest Tibet. Estimates of geologic offsets along the KF vary greatly. Initial estimates based on early mapping and tentative correlations of large-scale features such as batholiths (e.g. ~1000 km; Peltzer and Tapponnier (1988)) are significantly higher than more recent estimates, but even the recent estimates have significant variability. Although some of these are incompatible, as they are based on correlations of one offset feature on one side of the fault with different features on the opposite side of the fault (e.g. Lacassin, et al., 2004; cf. Searle, 1991), the lower set of slip estimates, which typically involve correlating narrower and more unique offset features (e.g. Murphy, et al., 2000; Robinson, 2009) may be reconciled by the recognition that slip may not be consistent along strike due to internal deformation of the crust to either side of the fault. Robinson (2009) compiled estimates of geologic offsets from locations distributed along much of the KF. These offsets are based on separation of a variety of features, including sedimentary and igneous rock bodies, fault and suture zones, and the course of the Indus River (Murphy and Copeland, 2005; Murphy, et al., 2002; Murphy, et al., 2000; Searle, 1996; Searle, et al., 1998; Phillips, et al., 2004; Robinson, 2009). These offsets are plotted with respect to distance along strike of the arc in Fig. 3. If these offset estimates are accurate, the Himalaya has had to have undergone significant (>100 km) extension where bounded by the KF. Although it has often been suggested that slip along the KF feeds into the IYS, Murphy, et al. (2010) found that the northern margin of the IYS is cut and offset 15 kilometers by the Lopukangri rift system. This

westernmost disruption of the IYS by north-trending rifts, in addition to the central Himalayan examples of rifting of the IYS cited above, strongly suggests that the IYS has hosted no significant strike-slip motion since the mid-Miocene, and that KF slip is transferred to the south into the Himalaya along the Gurla Mandhata-Humla fault system.

Significant right-lateral arc-parallel strike-slip faulting in the Himalaya has not been described east of the Bari Gad fault (Fig. 2). Instead, strike-slip faulting becomes left-lateral east of central Nepal. Strike-slip motion is taken up both by discrete arc-parallel sinistral structures (Li and Yin, 1998) and transtensional faults such as segments of the Yadong-Gulu rift (Armijo, et al., 1986; Kapp and Guynn, 2004) (Fig. 1, 2). Focal mechanisms suggest steeply-dipping, arc-parallel left-lateral faulting in Bhutan (Drukpa, et al., 2006). These sinistral faults are somewhat less organized than the dextral faults of the western Himalaya and probably have accommodated significantly smaller amounts of translation (Li and Yin, 2008).

Timing of initiation of extension

Figure 2 shows published age estimates that bracket the time initiation of syncollisional extension and strike-slip faulting. Studies of the Ama Drime Massif utilizing ^{40}Ar/^{39}Ar dating of micas and (U-Th)/He dating of apatite suggest the inception of arc-parallel extension at 13-12 Ma, immediately following the local cessation of activity on the Main Central Thrust and South Tibetan Detachment (Jessup, et al., 2008; Kali, et al., 2010). Thermochronologic analysis of the Kung Co granite in the footwall of the Kung Co Fault by J. Lee (personal communication) led to an interpretation involving initiation of normal faulting at 13-12 Ma and acceleration of fault-assisted exhumation at 10 Ma. The Thakkhola Graben is the most physiographically prominent graben in the Himalaya. Geologic mapping since the 1970s by Bordet (1971) and Colchen et al. (1986) have shown that it is bounded on the west by a major east-dipping normal fault referred to as the Dangardzang fault (DF). Little is known about the thermal history of its footwall, but investigations of its basin fill (Tetang and overlying Thakkhola Formations) preserved in its hanging wall show that it is syndeformational. The older Tetang Formation is between 11 and 9.6 Ma (Garzione et

al., 2003) implying slip along the Dangardzang Fault was active at this time, and that it initiated sometime before 11 Ma. At its southern end, the Dangardzang Fault cuts the Dhaulagiri-Annapurna Detachments (the local segments of the South Tibetan Detachment (STD)). In the Annapurna and Dhaulagiri ranges, structural, metamorphic, and intrusive histories of rocks exposed on either side of the STD indicate that it was moving between 22-16 Ma (Hodges et al., 1996; Godin et al., 2001; Searle and Godin, 2003; Searle, 2010), thereby placing an upper age constraint on the timing of extension within the Thakkhola Graben.

West of Thakkhola, the two most prominent, large-scale active extensional fault systems, the Gurla Mandhata-Humla fault system (GMH) and the Leo Parghil shear zone, have have received geochronological and thermochronological investigations. Th-Pb monazite dating of mylonitic leucogranite dikes within the GMH bracket the timing of ductile extension between 15-7 Ma (Murphy and Copeland, 2005). ^{40}Ar/^{39}Ar analyses of white mica and biotite from rocks in the footwall of the Leo Pargil shear zone are interpreted to reflect the onset of fault-facilitated exhumation ca. 15 Ma (Theide et al., 2006). The Karakoram Fault borders both of these extensional systems to the north and is kinematically linked, at least in the case of the GMH (Murphy et al., 2002). Near Banggong Co, U-Pb zircon dating of syndeformational granite bodies brackets the time of initiation between 15.68 ± 0.52 and 13.73 ± 0.28 Ma (Phillips et al., 2004). Lacassin et al. (2004) and Valli et al. (2007) estimate much older ages for the timing of initiation along the Karakoram fault (23 to 34 Ma). Zhang et al. (2010) showed through geologic mapping that rocks and structures (Great Counter Thrust) they associate with the Karakoram Fault are part of an older structural system referred to as the Ayi Shan Detachment.

These data together indicate a common mid-Miocene initiation of arc-parallel extension and translation throughout the central and northwestern Himalaya.

Tibrikot Fault

Nakata (1989) recognized the presence of active right-lateral strike-slip faulting in the western Nepalese Himalaya. He documented the Tibrikot, Dhaulagiri Southwest, and Bari Gad Faults through remote sensing and field observations (Fig. 2). Preliminary field observations of the

arc-parallel Tibrikot Fault (Styron, et al., 2009) indicate late Quaternary dextral slip on a steeply-dipping arc-parallel fault near the base of the MCT zone. Both bedrock and fluvial geomorphic features are clearly offset in a right-lateral sense, as shown in CORONA imagery (Fig. 4). The fault zone is narrow, and shows brittle deformation, in contrast to the ductilely-deformed rocks it cuts. Though net slip on the Tibrikot is unknown, the fault's short length suggests displacement is lower than on other arc-parallel strike-slip faults in the Himalaya, such as the KF, and likely younger.

The Tibrikot Fault's geometry, kinematics and location in a zone of right-lateral shear strongly suggest that the fault represents the propagation of KF slip from the IYS region through the High Himalaya via the GMH and into the frontal Himalaya. Though displacement is likely relatively small, the Tibrikot appears to be a significant structure as it and adjacent dextral faults appear to represent the propagation of KF slip through the Himalaya instead of along the IYS, which has implications for the validity of models of Himalayan and south Tibetan deformation outlined below.

Models for Himalayan and south Tibetan active deformation

The recent decades of research in the Indo-Asian collision zone have produced several models to explain the multifaceted deformation in the region. Several of the most common models are briefly discussed here, along with specific predictions that may be tested with the observations and analysis presented in this work. It is important to note that these predictions may or may not have been explicitly discussed by any of the researchers who published the models; however, we feel that these predictions come directly out of the models.

Lateral Extrusion

The lateral extrusion model of Indo-Asian tectonics was one of the first models put forth to explain the first-order structural features of the Tibetan Plateau and its surrounding areas visible in early satellite images (e.g. Tapponnier, et al., 1982). Essentially, this model describes Tibet as

23

undergoing tectonic escape and translating eastward relative to stable Eurasia and India as India indents into Asia. The lateral extrusion of Tibet is accommodated along the left-lateral Altyn Tagh and Kunlun faults in the north (Fig. 1) and the right-lateral KF and right-slip along the IYS in the south (Tapponnier, et al., 1982; Lacassin, et al., 2004; Schill, et al., 2004; Valli, et al., 2007, 2008). While this model was not initially proposed to explicitly explain deformation in the Himalaya, it implies high magnitudes of slip and slip rate along the KF continue as dextral shear into the IYS (Fig. 5a).

Oroclinal Bending

The oroclinal bending model describing the curvature of the Himalayan arc involves rotational bending of an initially linear belt. The primary lines of evidence for this process are clockwise paleomagnetic rotations in the NW Himalaya (e.g. Klootwijk, et al., 1985; Schill, et al., 2001, 2002) and right-lateral arc-parallel faulting in the western Himalaya and adjacent Tibet mirrored by left-lateral faulting in the eastern Himalaya and southern Tibet (e.g. Ratschbacher, et al., 1994; Li and Yin, 2008). The predictions for this model vary based on the locations of the 'hinge-lines' around which the range rotates, and the mechanism by which this folding occurs: neutral surface folding or flexural slip. Flexural flow may be a viable mechanism for oroclinal bending at depth but the upper crust is not expected to shear ductilely; therefore the brittle upper crust would deform by faulting localizing the distributed shear below, replicating the effects of flexural slip. More recent models (Schill, et al., 2001, 2002; Li and Yin, 2008), have the Himalayan arc bending around its central part such that the Himalayan syntaxes approach each other and the arc becoming more folded in map view. The kinematic predictions that arise for neutral surface folding are (1) there will be E-W contraction across southern Tibet, and potentially (2) arc-parallel extension in the outer (India-facing) Himalaya decreasing to a region of no extension or contraction along the center of the orocline (analogous to extension in the outer part of a fold's hinge and contraction in the inner part). For flexural slip, the prediction is (3) arc-parallel strike-slip faulting along preexisting structural discontinuities such as the Indus-Yarlung Suture Zone or the faults in the Himalaya itself

24

such as those in the MCT or STD zones, analogous to flexural slip in folded sedimentary layers. Given the geometry of the orogen, the arc-parallel strike-slip faults west of the central Himalaya would be sinistral and the faults east of the hinge zone would be dextral (Fig. 5b).

Radial Spreading

The Tibetan Plateau's extremely hot, thick crust may be capable of lateral flow at geodetically-observable velocities (Bird, 1991; Beaumont, et al., 2004). Consequently, Tibet has been proposed to be flowing towards its margins to reduce the gravitational potential energy excess caused by the ~5 km elevation difference between the plateau and its surroundings (e.g. England and Houseman, 1988; Copley and McKenzie, 2007; Copley, 2008; Cook and Royden, 2008). In the radial spreading model of Himalayan deformation, this applies to the Himalayan margin as well as the eastern margin of the plateau. As Tibet spreads out southward over India, it causes radial as well as circumferential expansion (Jade, et al., 2004; Murphy and Copeland, 2005; Copley and McKenzie, 2007; Copley, 2008). The following predictions may be made from this model: (1) as Tibet expands towards India, the circumference of the Himalayan arc will expand, causing arc-parallel extension. (2) south-directed radial spreading of the Tibetan Plateau will result in ~N-S extension, so the Himalaya will move south with respect to both stable Eurasia and to the central Tibetan Plateau. Some researchers have modified this model to allow for a presumably more viscous NW Himalaya to act as a gate or barrier, allowing the less viscous interior of Tibet to pour out past the Himalaya along the KF, so that (3) right-lateral, arc-parallel strike-slip faulting between the NW Himalaya and Tibet occurs (Murphy, et al., 2002, 2009; Murphy and Copeland, 2005), though this prediction is not necessarily a part of the radial spreading model, especially as envisaged with a rheologically homogeneous Tibet and Himalaya (e.g., Copley and McKenzie, 2007) (Fig. 5c)

Oblique Convergence

The model for Himalayan deformation caused by the variation in convergence obliquity is based on two observations: (1) there is a smooth variation in the strike of the Himalayan arc from the eastern to the western syntaxes, between which the arc may be approximated by a small circle, as judged by several criteria (Bendick and Bilham, 2001); and (2) India-Asia convergence vectors (relative to Asia) are generally parallel, and are normal to the strike of the Himalaya only in the Everest region of Nepal. Therefore, there is an increasing arc-parallel component to the convergence vectors away from the central Himalaya, which causes arc-parallel extension. Arc-parallel extension is most rapid where the along-strike *rate of change* of the arc-parallel velocities is highest. In the northwestern (and potentially eastern) regions of the Himalaya, the arc is translating along the Himalaya-Tibet boundary, approximated by the Karakoram Fault zone (McCaffrey and Nábelek, 1998; Seeber and Pêcher, 1998). This requires the net slip and slip rate along the KF to increase to the northwest, analogous to a translating and extending forearc sliver such as that observed in Sumatra (McCaffrey, 1992). This model is very commonly applied at subduction zones worldwide (e.g. McCaffrey, 1992; Avé Lallemant and Oldow, 2000), which are almost always convex towards the underthrusting plate, as observed in the Himalaya. It is critical to note that Seeber and Pêcher (1998) refer to the pattern of earthquake slip vectors along the Himalaya to reflect 'radial thrusting.' Despite the similarity of the terminalogy, this is distinct from the radial spreading model, discussed above; 'radial thrusting' simply refers to the radial orientation of thrust slip vectors, which are normal to the strike of the arc. It does not imply that the radius of the arc grows during thrusting, only that the divergence in slip vectors causes circumferential or arc-parallel extension along the range. This is complimented by contraction at the syntaxes, and accommodated by right-lateral slip along the KF which strikes roughly normal to the thrust events along the northwestern range front, consistent with slip partitioning. Unlike the oroclinal bending and radial spreading models, the oblique convergence model does not propose to explain the curvature of the Himalayan arc; this model only shows the consequences of the regular variation of Indo-Himalayan convergence obliquity along the arc. The oblique convergence model makes the following testable predictions (1) the gradient observed in arc-parallel geodetic velocities away

from the region of pure normal Indo-Himalayan convergence in eastern Nepal is correlated with the degree of convergence obliquity; (2) there is significant arc-parallel extension in the Himalaya; and (3) arc-parallel extension in the northwest Himalaya is accommodated by arc-parallel strike-slip faults and arc-perpendicular normal faults (Fig. 5d).

Geodetic analysis

The most spatially and temporally comprehensive geodetic dataset for the Himalayan-Tibetan system yet published is that of Gan, et al. (2007), a compilation of the datasets of Zhang, et al. (2004), Paul, et al. (2001), Wang, et al. (2001) and Banerjee and Bürgmann (2002). This set of ~1300 GPS vectors in and around China is given in both a Eurasia-fixed reference frame in the International Terrestrial Reference Frame 2000 (ITRF2000), and a Tibet-fixed reference frame. GPS vectors from the Eurasia-fixed dataset in and around the Himalaya were selected. Several other datasets were compiled to increase data coverage and density. Jade, et al. (2004) presented a network of GPS vectors in Ladakh and far western Xizang, relative to ITRF97. These data were transformed into ITRF2000 using the National Geodetic Survey's Horizontal Time Dependent Positioning tool (http://www.ngs.noaa.gov/TOOLS/Htdp/Htdp.shtml). Additional GPS data from Bettinelli, et al. (2006), and Banerjee, et al., (2008) were also included. These three datasets were then transformed into a Eurasia-fixed reference frame by using the ITRF2000-Eurasia Euler pole at 57.965 ± 1.211°N, -99.374 ± 2.71°E of Altamimi (2002).

Convergence between India and Eurasia has been described by Jade, et al. (2007) by a rotation of 0.341 ± 0.005° Ma^{-1} around a pole at 26.5 ± 3.4° N, 13.9 ± 7.8° E. These rotation parameters were used to generate convergence vectors between India and Eurasia in a Eurasia-fixed reference frame at every GPS site; these are referred to as the 'plate motion vectors'. The observed geodetic and predicted plate motion vectors are shown in Fig. 6. A comparison of the geodetic and plate motion vectors illustrates the degree and spatial extent to which the overriding plate is moving with underthrusting India. Along the Himalayan front, the vectors are very similar. Farther inboard of the thrust front, the velocity of the geodetic vectors lessens as strain is

27

accumulated across the arc, though the vectors generally remain parallel to each other and to the Indo-Asian plate motion vectors. Previous studies can well explain the observed velocities with elastic strain accumulation along the MHT with a locking depth of about 20 km (e.g. Jouanne, et al., 1999; Larson, et al., 1999; Lavé and Avouac, 2000; Chen, et al., 2004a, b). It is also clear that the geodetic vectors are oriented purely normal to the Himalayan arc only in eastern Nepal; convergence is progressively more oblique along strike in either direction. The largest divergence between the geodetic and plate motion vectors is near the eastern Himalayan syntaxis, where there appears to be significant clockwise vertical-axis rotation, also consistent with previous studies (Shen, et al., 2005; Allmendinger, et al., 2007). Some of this divergence may also be explained by the absorption of a fraction of the total Indo-Asian convergence within the Shillong Plateau (e.g. Bannerjee, et al., 2008; Clark and Bilham, 2008; cf. Jade, et al., 2007).

The consequence of the observed variation in convergence obliquity is that the arc-normal and arc-parallel components to Indo-Himalayan relative motion vary systematically along the arc. Though the amount of Indo-Himalayan convergence obliquity varies significantly along strike, the seismic events along the Himalayan front have slip vectors dominantly oriented perpendicular to the strike of the arc (Seeber and Pêcher, 1998; Bendick, et al., 2007; Fig. 1), not oblique and in the direction of plate convergence and elastic strain accumulation. The few focal mechanisms along the Karakoram Fault or the arc-parallel strike-slip faults in Nepal are also strike-slip, not oblique-slip. From a geologic perspective, the presence of a large thrust or system of thrust faults (the MFT and MBT) in the frontal Himalaya and arc-parallel strike-slip faults (the KF, Humla, Tibrikot, and Bari Gad Faults) farther inboard, as well as normal faults striking perpendicular to the arc, all suggest that strain in the Himalayan arc is well-partitioned into fairly pure arc-normal shortening and arc-parallel extension and translation along discrete fault systems. Therefore, in a region where convergence between the Indian plate and the Himalaya is oblique, a thrust event along the MFT will only relieve the arc-normal component of the elastic strain field; the arc-parallel component will only be relieved by an event on a strike-slip fault such as the Karakoram Fault.

In order to assess this quantitatively, each geodetic vector is decomposed into its arc-

parallel and arc-normal components, using the definition of the arc as a small circle with a pole at 91.6° E, 42.4° N of Bendick and Bilham (2001) for the western and central segments of the arc, a pole at 89.5° E, 37° N for sites between 88° E to 91.5° E, and a pole at 90.7° E, 35° N for sites west of 91.5° E. The latter two poles are necessary because the radius of curvature for the Himalayan arc decreases east of Sikkim and a small circle about the first pole does not fit the observed arc geometry, and were fit visually. The arc-normal vector is the component of the geodetic velocity in the direction of the pole, and the arc-parallel vector is the velocity component tangential to the small circle at that point. The arc-parallel vectors are shown in Fig. 7a. Fig. 7b shows the arc-parallel velocities within the Himalayan arc (between the KF/IYS and the MFT) plotted with respect to their distance along strike (where the position of each is projected onto a small circle approximating the Himalayan arc of radius 1696 km around the pole of Bendick and Bilham (2001). Although the full 2 dimensional velocity error ellipses are shown in the maps, the 1 dimensional error bars shown in the plots are calculated as the diameters of the 1-σ error ellipses in the direction of the velocity vectors.

The arc-parallel velocities suggest that the Himalayan arc is stretching at ~3 cm/yr between the India-Pakistan border and the western border of Bhutan. This is about 1500 km along strike, leading to an extension rate of 20 nstrain yr^{-1}. The extension rate is not completely uniform along strike; the sites in the northwestern-most 400 kilometers of the arc have similar arc-parallel velocities, ~ 20 mm yr^{-1}. However, from near ~78 E to ~89 E (400 km to 1400 km along-strike distance from GPS site STAKSHA), the velocity gradient is fairly uniform, representing about 35 nstrain yr^{-1} of extension (Fig. 7b). The ~10 mm yr^{-1} extension rates from the Humla Fault region northwest through the end of the study area broadly agree with >100 km arc-parallel extension of this region (based on the KF displacement gradient) given a mid-Miocene age for the onset of extension.

It is also of interest to study how these velocities change across the arc rather than along it. Therefore the arc is divided into seven regions along strike (Fig. 7a), and the arc-normal and arc-parallel components of the GPS site velocities in each region are binned and plotted with

respect to their distance from the pole of Bendick and Bilham (2001) (Fig. 8). For each region, the mean arc-parallel and arc-normal velocities for several sites in the Himalayan foreland are subtracted from the mean velocities of several sites in the interior of Tibet. This gives estimates of the amount of shear strain (positive values are right-lateral) and convergence across the arc, and highlights potential along strike-velocity gradients. These results are presented in Table 1. In general, the estimates of shear strain accumulation across the arc decrease from the northwestern Himalaya towards the center of the range, and appear to increase again in the east. The estimates of arc-normal convergence are remarkably consistent across the northwestern and central portions of the arc, though again there is an increase in these rates in the eastern Himalaya. However, this area seems to be undergoing clockwise vertical-axis rotation about the eastern syntaxis with little internal strain (Allmendinger, et al., 2007); therefore, the rates calculated for the eastern two regions may simply reflect the effects of vector projections of this rotational velocity field, and not reflect shear strain or shortening across the range; for this reason, the results from these regions are not taken into account when evaluating deformational models, though they are given for completeness.

The transects across the arc (Fig. 8, Table 1) show that arc-parallel shear is dextral throughout the arc and statistically different than zero at the 68% confidence level only in the northwestern Himalaya. The rates of shear strain accumulation, $\sim 6.5 \pm 4.5$ mm yr^{-1} (1-σ) for the Ladakh and Himachal regions, are similar to the rates of longer term Quaternary slip along the Karakoram Fault from offset Quaternary glacial moraines and debris flows (Brown, et al., 2002; Chevalier, et al., 2005). However, it is interesting to note that this shear strain accumulation does not appear to be localized on the Karakoram Fault (Jade, et al., 2004). The Gurla Mandhata and Everest regions show about half the arc-parallel shear strain accumulation in comparison to the northwest regions, albeit with significantly larger errors. The Thakkhola region has the highest rate of shear strain accumulation, though that rate is still less than the 1-σ uncertainty; this error is primarily due to the large uncertainty in the velocities at remote sites in the interior of Tibet.

Though the extant geodetic sites are not positioned so that a good estimate of slip rate along

the Tibrikot fault can be made (Fig. 9), the site DLP0 is located ~2 km south of the fault (in between the Tibrikot and Dhaulagiri Southwest faults) and has an arc-parallel velocity of 5.71 ± 2.25 mm yr^{-1}, and the site JML0 is located ~10 km south of the Humla fault (the along-strike continuation of the Tibrikot fault) about 70 km west, and has an arc-parallel velocity of 10.50 ± 2.05 mm yr^{-1}. The next site to the south-southwest (directly towards the foreland), of DLP0 is MUL0, some 90 km away, with an arc-parallel velocity of 11.99 ± 2.05 mm yr^{-1}. While this data is certainly not sufficient to effectively bracket slip rates on the Tibrikot fault, if this velocity gradient represents half of the strain accumulation across the fault (e.g. Savage and Burford, 1973) it does suggest that the Humla-Tibrikot system accumulates shear strain at several mm yr^{-1}, similar to rates on the Karakoram Fault. The across-arc arc-parallel velocity profiles in Fig. 8 also suggest that all of the arc-parallel shear strain in that sector of the Himalaya is accumulating on the Humla, Tibrikot, Dhalagiri Southwest and Bari Gad faults. This is a good indication that KF slip is transferred into the Himalaya instead of continuing along the IYS.

The arc-normal velocities vary along the Himalayan arc from ~10 to ~35 mm yr^{-1} (Figs. 8, 10). The highest velocities are where convergence between India and the Himalaya is arc-normal. However, despite the threefold variation in the velocities, the rates of convergence between geodetic sites in the Himalayan foreland and south Tibet remain remarkably consistent at near 12 mm yr^{-1} in the northwestern and central Himalaya (Fig. 8). This estimate is lower than many estimates from geology (e.g. Lavé and Avouac, 2000) and early geodesy (e.g. Larson, et al., 1999) but similar to some more recent geodetic studies (e.g. Chen, et al., 2004b; c.f. Bettinelli, et al., 2006). The along-strike consistency of the arc-normal convergence rate may indicate a dynamic equilibrium between shortening and crustal thickening in the Himalaya and extension and translation within the Tibetan Plateau.

Discussion

Evaluation of deformational models

We use our geodetic results and geologic observations from the literature to evaluate models of Himalayan and south Tibetan deformation by addressing the specific predictions for each model mentioned above.

The lateral extrusion model as applied to Tibet predicts that there will be high rates and magnitudes of slip along the Karakoram Fault, which continues along the Indus-Yarlung Suture Zone accommodating the eastward escape of Tibet. Previous geologic observations (Searle, 1991; Searle, et al., 1998; Murphy, et al., 2000; Phillips, et al., 2004; Robinson, 2009a) show a decrease in displacement magnitude along the KF to the southeast. Furthermore, Murphy and Copeland (2005), Murphy, et al. (2010) and this study suggest that the majority of slip along the KF is transferred south into the Himalaya via the Gurla Mandhata-Humla fault system and continues southeast along the Tibrikot Fault. Exactly how slip is transferred to the southeast from the TF is unknown. One possibility is that the Tibrikot Fault links up with either the faults bounding the Thakkhola Graben or the Dhaulagiri Southwest and Bari Gad Faults. Our geodetic analysis shows that slip rates along the Karakoram Fault are much less than early estimates of several cm yr^{-1}, and are not statistically different from zero along the IYS, though the errors in the dextral shear accumulation rates across the central Himalaya are large enough to allow for low (less than 1 cm yr^{-1}) slip along the IYS. However, the lack of seismicity indicative of right-slip faulting on the IYS and the uninterrupted rifting across the IYS into the central Himalaya (Murphy, et al., 2010) strongly suggest that the IYS is not currently an active right-slip shear zone, and has not been at least since the inception of rifting in the region. The observations of an eastward increase in clockwise rotation observed in paleomagnetic data of Schill, et al. (2004) in the hanging wall of the STD in the north central Himalaya may be related to faulting on of the STD, as the timing constraints on those data are insufficient to bracket them as post-STD fautling. Furthermore, the eastward increase of clockwise rotation suggested by these data is inconsistent with through-going dextral shear on the IYS, which would produce a consistent amount of rotation along the structure. Therefore, the compiled observations do not favor it as a major active structure in

regional kinematics.

The oroclinal bending model predicts that rotation of the Himalayan orocline will result in (1) E-W contraction in Tibet, (2) outer arc-parallel extension (i.e., in the frontal Himalaya) which decreases to zero along the midline of the orocline, and contraction in the interior, and possibly (3) sinistral arc-parallel strike-slip faulting in the western orogen and dextral arc-parallel strike-slip faulting in the eastern orogen. Prediction (1) is not supported by either geodetic or geologic observations, which clearly show active and well-developed E-W rifting in the Lhasa block, which in the central part of the range propagates into the Himalayan arc. Prediction (2) is partially met, as there is ample evidence for arc-parallel extension in the range; however, a switch to a contractional regime in the inner arc similar to that observed in the hinge zone of folds is not observed. Prediction (3) is also not supported by geologic or geodetic evidence, which indicate arc-parallel strike-slip faulting with opposite slip sense of that predicted. Therefore the oroclinal bending model is not supported by this study. The clockwise paleomagnetic rotations in the northwestern Indian Himalaya must be explained through other models.

The radial spreading model as applied to the Himalaya predicts that (1) the Himalayan arc will undergo arc-parallel extension, (2) the arc will move south with respect to stable Eurasia and the interior of Tibet, and (3) that arc-parallel strike-slip faulting is possible. We see that prediction (1) is confirmed by both geologic and geodetic observations. Prediction (2), however, is not supported by either geologic or geodetic observations; in fact, the opposite is observed: the Himalayan arc is moving north with respect to both Eurasia and the interior of Tibet. This is not immediately apparent in the geodetic studies that utilized an India-fixed reference frame, because they either do not extend far enough north so that the N-S contraction across Tibet is observable (Jade, et al., 2007; Banerjee, et al., 2008), or the data are too sparse for this to be apparent (Jade, et al., 2004). However, the northward velocities observed near the Bangong-Nujiang Suture Zone (Fig. 6) are too far north of the MHT to be significantly influenced by elastic effects due to locking on the MHT (Bettinelli, et al., 2006; cf. Feldl and Bilham, 2006). Furthermore, shortening in the direction of Indo-Eurasian relative motion continues throughout the entirety of the plateau, between

the Himalaya and the rigid basins to the north, at significant (>10 mm yr^{-1}) rates (Zhang, et al., 2004). This cannot be coeval with the radial, southwest- to southeast-directed extension required by the radial spreading model (Copley and McKenzie, 2007). The only geologic observations that could support (2) are those describing the South Tibetan Detachment System, an early Miocene structure whose recent activity has been suggested (e.g. Hurtado, et al., 2001), but active slip on this system would be inconsistent with the geodetic strain field. Prediction (3), which is not a firm requirement of the model but a modification made to incorporate geologic observations, is not inconsistent with this analysis. The geologic evidence supporting radial spreading is primarily arc-parallel extension and strike-slip faulting within the Himalaya (Murphy, et al., 2002, 2009). Therefore, this study does not support radial spreading as a viable mechanism for modern Himalayan deformation.

The variably oblique convergence model for Himalayan deformation predicts (1) an increasing arc-parallel velocity gradient away from the region of purely normal Indo-Himalayan convergence in eastern Nepal, (2) arc-parallel extension of the Himalaya; and (3) increasing rates and magnitudes of Himalayan arc-parallel translation away from the central range along arc-parallel strike-slip faults. This study confirms prediction (1); arc-parallel velocities are near zero near Everest, and velocities increase towards the syntaxes. To the west, this velocity gradient is geologically expressed as extension of the Himalayan arc from the Thakkhola Graben region to the northwest that is bounded to the north by the Karakoram Fault - net slip estimates across the Karakoram (Robinson, 2009), Humla (Murphy and Copeland, 2005), and likely the Tibrikot faults increases to the northwest. This results in the observation of prediction (2), arc-parallel extension distributed throughout the Himalaya. Prediction (3) is also confirmed by this study and many others: Rates of dextral shear accumulation across the arc increase to the northwest as well, though the uncertainties are large enough that all values may be equal at the 68% confidence level. Therefore, the results of this study support the oblique convergence model for Himalayan deformation over the other models considered. These results only apply for the present deformational phase (to which all of the data discussed here applies), characterized by arc-parallel extension and translation of the Himalayan arc, which seems to have begun in in the middle Miocene, as discussed above.

In the next section we discuss the implications of variably oblique convergence as applied to the Himalaya.

Oblique convergence and Himalayan deformation

As the Indian plate underthrusts Tibet, it exerts a shear stress on the base of the Himalayan orogenic wedge. The orientation of this shear stress with respect to the strike of the wedge changes along strike, so that there is an increasing component of traction parallel to the wedge away from the region of normal convergence in eastern Nepal. This causes extension of the Himalayan arc. Where this convergence is oblique to the strike of the arc, the arc-parallel component induces translation of the Himalaya relative to south Tibet. In the northwest Himalaya, the extending Himalayan arc translates differentially along the Karakoram Fault against a relatively unextended western Lhasa block, so that the slip rates and magnitudes along the KF increase to the northwest. Slip on the Karakoram Fault steps to the south at Gurla Mandhata, which is interpreted to be a releasing bend having undergone several tens of kilometers of extension (Murphy, et al., 2002), and continues as dextral slip along a series of en-echelon faults (including the Humla, Tibrikot and Bari Gad Faults) cutting across the Nepalese Himalaya. Net slip on the Humla is estimated at 25-30 km (Murphy and Copeland, 2005). The faults to the southeast likely have less displacement (Murphy, et al., 2010). The initiation of strike-slip faulting seems to be diachronous; Phillips, et al. (2004) describe the central Karakoram Fault as being active at 15 Ma, while to the southeast, the KF cannot have began cutting the South Kailas thrust until thrusting ceased after 13 Ma (Yin, et al., 1999b; Murphy, et al., 2000). The Humla fault, which cuts the South Tibetan Detachment system, also must have initiated after the latter's cessation (Murphy and Copeland, 2005). The Tibrikot Fault must have begun cutting the MCT zone rocks after thrusting ceased, as late as 4 Ma (Harrison, et al., 1997). This southeastward propagation of dextral faulting may be related to a shear stress gradient along this zone (highest in the NW), as well as the successive southward propagation of the Himalayan active thrust front as material is accreted to the front and base of the Himalayan wedge. In the central Himalaya, both the range and the Tibetan Plateau are

extending in the same general direction, and many of the rifts that accommodate this extension are common to both domains and are apparently continuous across the IYS. The rates of extension are similar to the north and to the south of the IYS zone, thus a transfer zone along the IYS is not necessary. Farther east, arc parallel and sub-parallel sinistral faulting occurs, but this faulting is not as developed as in the west (Li and Yin, 2008). This transitions into clockwise rotation around the eastern Himalayan syntaxis (Allmendinger, et al., 2007; Shen, et al., 2005) as the MHT meets the dextral, N-striking Sagaing fault, which is the boundary between the Indian and Sunda plates (Liu and Bird, 2007).

Though the Himalaya and Tibet are both actively extending, the differences in the orientation and location of the extension direction suggests that the style of extension throughout the orogen arises from two different mechanisms—variably-oblique convergence causing Himalayan arc-parallel extension, while extension in the Tibetan Plateau likely results from a combination of excess of gravitational potential energy in Tibet (e.g. England and Houseman, 1988; Copley, 2008), compression applied to the southern Eurasia plate by the Indian plate (e.g. Vergnolle, et al., 2007), and possibly by widespread basal tractions (Taylor and Yin, 2009).

Conclusions

Analysis of GPS velocities in the Himalaya and southern Tibet shows that the central and northwestern Himalaya is undergoing arc-parallel extension. This extension is bound by dextral shear in the northwest, which may be accommodated on the Karakoram Fault. Shortening across the central and northwestern Himalaya is very consistent at ~12 mm yr^{-1}. The northward movement of the Himalaya with respect to central Tibet and stable Eurasia, the arc-parallel extension of the Himalaya, and the lack of significant dextral slip along the IYS all suggest that arc-parallel extension and translation in the Himalaya are the result of variably-oblique convergence between India and the Himalaya.

Acknowledgements

References

Allmendinger, R.W., Reilinger, R., and Loveless, J., 2007, Strain and rotation rate from GPS in Tibet, Anatolia, and the Altiplano: Tectonics, v. 26, TC3013, doi:10.1029/2006TC002030.

Altamimi, Z., Sillard, P., and Boucher, C., 2002, ITRF2000: A new release of the International Terrestrial Reference Frame for earth science applications: Journal of Geophysical Research-Solid Earth, v. 107, p. 2214.

Armijo, R., Tapponnier, P., Mercier, J., and Tong-Lin, H., 1986, Quaternary extension in southern Tibet: Field observations and tectonic implications: Journal of Geophysical Research, v. 91, p. 13803-13872.

Armijo, R., Tapponnier, P., and Han, T., 1989, Late Cenozoic right-lateral strike-slip faulting in southern Tibet: Journal of Geophysical Research, v. 94, p. 2787–2838.

Avé Lallemant, H.G., and Oldow, J.S., 2000, Active displacement partitioning and arc-parallel extension of the Aleutian volcanic arc based on Global Positioning System geodesy and kinematic analysis: Geology, v. 28, p. 739-742.

Baltz, T., and Murphy, M.A., Structural evolution of the Thakkhola graben and implications on the architecture of the central Himalaya: Eos Transactions American Geophysical Union, v. 90, no. 58, Fall Meeting Supplement, Abstract T43C-2110.

Banerjee, P., and Bürgmann, R., 2002, Convergence across the northwest Himalaya from GPS measurements: Geophysical Research Letters, v. 29, doi: 10.1029/2002GL015184.

Banerjee, P., Bürgmann, R., Nagarajan, B., and Apel, E., 2008, Intraplate deformation of the Indian subcontinent: Geophysical Research Letters, v. 35, L18301, doi:10.1029/2008GL035468.

Beaumont, C., Jamieson, R.A., Nguyen, M.H., and Medvedev, S., 2004, Crustal channel flows: 1. Numerical models with applications to the tectonics of the Himalayan-Tibetan orogen: Journal of Geophysical Research, v. 109, B06406, doi:10.1029/2003JB002809

Bendick, R., and Bilham, R., 2001, How perfect is the Himalayan arc?: Geology, v. 29, p. 791-794.

Bendick, R., Bilham, R., Khan, M.A., and Khan, S.F., 2007, Slip on an active wedge thrust from geodetic observations of the 8 October 2005 Kashmir earthquake: Geology, v. 35, p. 267-270.

Bettinelli, P., Avouac, J.-P., Flouzat, M., Jouanne, F., Bollinger, L., Willis, P., and Chitrakar, G., 2006, Plate Motion of India and Interseismic Strain in the Nepal Himalaya from GPS and DORIS Measurements: Journal of Geodesy, v. 80, p. 567-589.

Bilham, R., and England, P., 2001, Plateau 'pop-up' in the great 1897 Assam earthquake: Nature, v. 410, p. 806-809.

Bird, P., 1991, Lateral extrusion of lower crust from under high topography, in the isostatic limit: Journal of Geophysical Research, v. 96, p. 10275-10286.

Bordet, P., Colchen, M., Krummenacher, D., Le Fort, P., Mouterde, R., and Remy, M., 1971, Recherches géologiques dans l'Himalaya du Népal, région de laThakkhola: Paris, Centre National de la RechercheScientifique, 279 p.

Brown, E.T., Bendick, R., Bourlès, D.L., Gaur, V., Molnar, P., Raisbeck, G.M., and Yiou, F., 2002, Slip rates of the Karakorum fault, Ladakh, India, determined using cosmic ray exposure dating of debris flows and moraines: Journal of Geophysical Research, v. 107, no. B9, doi:10.1029/2000JB000100

Calais, E., Vergnolle, M., San'kov, V., Lukhnev, A., Miroshnitchenko, A., Amarjargal, S., and Déverchère, J., 2003, GPS measurements of crustal deformation in the Baikal-Mongolia area (1994–2002): Implications for current kinematics of Asia: Journal of Geophysical Research, v. 108, no. B10, doi:10.1029/2002JB002373.

Chen, Q.Z., Freymueller, J.T., Wang, Q., Yang, Z.Q., Xu, C.J., and Liu, J.N., 2004a, A deforming

block model for the present-day tectonics of Tibet: Journal of Geophysical Research, v. 109, B09401, doi:10.1029/2002JB002350.

Chen, Q.Z., Freymueller, J.T., Yang, Z.Q., Xu, C.J., Jiang, W.P., Wang, Q., and Liu, J.N., 2004b, Spatially variable extension in southern Tibet based on GPS measurements: Journal of Geophysical Research, v. 109, B01403, doi:10.1029/2002JB002151.

Chevalier, M.-L., Ryerson, F.J., Tapponnier, P., Finkel, R.C., Van Der Woerd, J., Haibing, L., and Qing, L., 2005, Slip-Rate Measurements on the Karakorum Fault May Imply Secular Variations in Fault Motion: Science, v. 307, p. 411-414.

Clark, M.K., Bilham., R., 2008, Miocene rise of the Shillong Plateau and the beginning of the end for the eastern Himalaya: Earth and Planetary Science Letters, v. 269, p. 337–350, doi: 10.1016/j.epsl.2008.01.045.

Clark, R.J., 2005, Structural constraints on the exhumation of the Tso Morari Dome, NW Himalaya: MS Thesis, Massachusetts Institute of Technology, 52 p.

Cogan, M.J., Nelson, K.D., Kidd, W.S.F., Wu, C., and Project, I.T., 1998, Shallow structure of the Yadong-Gulu rift, southern Tibet, from refraction analysis of Project INDEPTH common midpoint data: Tectonics, v. 17, p. 46-61.

Colchen, M., Le Fort, P., and Pêcher, A., 1986, Annapurna–Manaslu–Ganesh Himal: Paris, Centre National de laRecherche Scientifique, 136 p.

Cook, K.L., and Royden, L.H., 2008, The role of crustal strength variations in shaping orogenic plateaus, with application to Tibet: Journal of Geophysical Research, v. 113, B08407, doi:10.1029/2007JB005457.

Copley, A., 2008, Kinematics and dynamics of the southeastern margin of the Tibetan Plateau: Geophysical Journal International, v. 174, p. 1081-1100.

Copley, A., and McKenzie, D., 2007, Models of crustal flow in the India-Asia collision zone: Geophysical Journal International, v. 169, p. 683-698.

Dewane, T., Stockli, D., Hager, C., Taylor, M., Ding, L., Lee, J., and Wallis, S., 2006, Timing of Cenozoic EW Extension in the Tangra Yum Co-Kung Co Rift, south-central Tibet: EOS Transactions AGU, v. 87, no. 52, Fall Meeting Supplement, T34C-04.

Dewey, J.F., 1988, Extensional collapse of orogens: Tectonics, v. 7, no. 6, p. 1123-1139.

Drukpa, D., Velasco, A., and Doser, D., 2006, Seismicity in the Kingdom of Bhutan (1937–2003): Evidence for crustal transcurrent deformation: Journal of Geophysical Research, v. 111, B06301, doi:10.1029/2004JB003087.

England, P.C., and Houseman, G.A., 1988, The mechanics of the Tibetan Plateau: Philosophical Transactions, R., Soc., London, A., v. 326, p. 301-319.

Epard, J.-L., and Steck, A., 2004, The Eastern prolongation of the Zanskar Shear Zone (Western Himalaya): Eclogae Geologicae Helvetiae, v. 97, p. 193-212.

Epard, J.-L., and Steck, A., 2008, Structural development of the Tso Morari ultra-high pressure nappe of the Ladakh Himalaya: Tectonophysics, v. 451, p. 242-264.

Feldl, N., and Bilham, R., 2006, Great Himalayan earthquakes and the Tibetan plateau, Nature, v. 444, p. 165-170.

Gan, W., Zhang, P., Shen, Z., Niu, Z., Wang, M., Wan, Y., Zhou, D., and Cheng, J., 2007, Present-day crustal motion within the Tibetan Plateau inferred from GPS measurements: Journal of Geophysical Research, v. 112, B08416, doi:10.1029/2005JB004120.

Garzione, C.N., DeCelles, P.G., Hodkinson, D.G., Ojha ,T.P., and Upreti, B.N., 2003, East-west extension and Miocene environmental change in the southern Tibetan plateau: Thakkhola graben, central Nepal: Geological Society of America Bulletin, v. 115, p. 3–20.

Godin, L., Parrish, R.R., Brown, R.L., and Hodges, K.V., 2001, Crustal thickening leading to exhumation of the Himalayan metamorphic core of central Nepal: Insight from U-Pb geochronology and $^{40}Ar/^{39}Ar$ thermochronology: Tectonics, v. 20p. 729-747.

Hager, C., Stockli, D., Dewane, T., Ding, L., Taylor, M., and Lee, J., 2006, Episodic Mio-Pliocene rifting in south-central Tibet. Thermochronometric constraints from the Xainza rift: EOS Transactions AGU, v. 87, no. 52, Fall Meeting Supplement, T34C-02.

Harrison, T.M., Ryerson, F.J., LeFort, P., Yin, A., Lovera, O.M., and Catlos, E.J., 1997, A Late Miocene-Plicocen origin for the Central Himalayan inverted metamorphism: Earth and Planetary Science Letters, v. 146, p. E1-E7.

Hodges, K.V., Parrish, R.R., and Searle, M.P., 1996, Tectonic evolution of the central Annapurna Range, Nepalese Himalayas: Tectonics, v. 15, p. 1264–1291.

Hodges, K.V., Wobus, C., Ruhl, K., Schildgen, T., and Whipple, K., 2004, Quaternary deformation, river steepening, and heavy precipitation at the front of the Higher Himalayan ranges: Earth and Planetary Science Letters, v. 220, p. 379-389.

Hurtado, J., Hodges, K., and Whipple, K., 2001, Neotectonics of the Thakkhola graben and implications for recent activity on the South Tibetan fault system in the central Nepal Himalaya: Geological Society of America Bulletin, v. 113, p. 222.

Jade, S., Bhatt, B., Yang, Z., Bendick, R., Gaur, V., Molnar, P., Anand, M., and Kumar, D., 2004, GPS measurements from the Ladakh Himalaya, India: Preliminary tests of plate-like or continuous deformation in Tibet: Geological Society of America Bulletin, v. 116, p. 1385.

Jade, S., Mukul, M., Bhattacharyya, A., Vijayan, M., Jaganathan, S., Kumar, A., Tiwari, R., Kalita, S., and Sahu, S., 2007, Estimates of interseismic deformation in Northeast India from GPS measurements: Earth and Planetary Science Letters, v. 263, p. 221-234.

Jessup, M., Newell, D., Cottle, J., Berger, A., and Spotila, J., 2008, Orogen-parallel extension and

exhumation enhanced by denudation in the trans-Himalayan Arun River gorge, Ama Drime Massif, Tibet-Nepal: Geology, v. 36, p. 587.

Jouanne, F., Mugnier, J.L., Pandey, M.R., Gamond, J.F., Le Fort, P., Serrurier, L., Vigny, C., and Avouac, J.P., 1999, Oblique convergence in the Himalayas of western Nepal deduced from preliminary results of GPS measurements: Geophysical Research Letters, v. 26, no. 13, p. 1933-1936.

Kali, E., P. H. Leloup, N. Arnaud, G. Mahéo, D. Liu, E. Boutonnet, J. Van der Woerd, X. Liu, J. Liu-Zeng, and H. Li, 2010, Exhumation history of the deepest central Himalayan rocks, Ama Drime range: Key pressure-temperature-deformation-time constraints on orogenic models: Tectonics, v. 29, TC2014, doi:10.1029/2009TC002551.

Kapp, P., and Guynn, J.H., 2004, Indian punch rifts Tibet: Geology, v. 32, p. 993-996.

Klootwijk, C.T., Conaghan, P.J., and Powell, C.M., 1985, The Himalayan Arc - Large-Scale Continental Subduction, Oroclinal Bending and Back-Arc Spreading: Earth and Planetary Science Letters, v. 75, p. 167-183.

Lacassin, R., Valli, F., Arnaud, N., Leloup, P.H., Paquette, J.L., Haibing, L., Tapponnier, P., Chevalier, M.-L., Guillot, S., Mahéo, G., and Zhiqin, X., 2004, Large-scale geometry, offset and kinematic evolution of the Karakorum fault, Tibet: Earth and Planetary Science Letters, v. 219, p. 255-269.

Langille, J.M., Jessup, M.J., Cottle, J.M., Newell, D., and Seward, G., Kinematic evolution of the Ama Drime detachment: Insight into orogen-parallel extension and eshumation of the Ama Drime Massif, Tibet-Nepal: Journal of Structural Geology, vol. 32 no. 7, p. 900-919.

Larson, K.M., Bürgmann, R., Bilham, R., and Freymueller, J.T., 1999, Kinematics of the India-Eurasia collision zone from GPS measurements: Journal of Geophysical Research, v. 104, no. B1, p. 1077-1093.

Lavé, J., and Avouac, J.P., 2000, Active folding of fluvial terraces across the Siwaliks Hills, Himalayas of central Nepal: Journal of Geophysical Research, v. 105, no. B3, p. 5735-5770.

Li, D., and Yin, A., 2008, Orogen-parallel, active left-slip faults in the Eastern Himalaya: Implications for the growth mechanism of the Himalayan Arc: Earth and Planetary Science Letters, v. 274, p. 258-267.

Liu, Z., and Bird, P., 2007, Kinematic modelling of neotectonics in the Persia-Tibet-Burma orogen: Geophysical Journal International, v. 172, p. 779-797.

Mahéo, G., Leloup, P.H., Valli, F., Lacassin, R., Arnaud, N., Paquette, J.L., Fernandez, A., Haibing, L., Farley, K.A., and Tapponnier, P., 2007, Post 4 Ma initiation of normal faulting in southern Tibet. Constraints from the Kung Co half graben: Earth and Planetary Science Letters, v. 256, p. 233-243.

McCaffrey, R., 1992, Oblique Plate Convergence, Slip Vectors, and Forearc Deformation: Journal of Geophysical Research, v. 97, p. 8905-8915.

McCaffrey, R., and Nábelek, J., 1998, Role of oblique convergence in the active deformation of the Himalayas and southern Tibet plateau: Geology, v. 26, p. 691-694.

Meade, B., 2007, Present-day kinematics at the India-Asia collision zone: Geology, v. 35, p. 81–84, doi: 10.1130/G22924A.1.

Métivier, F., Gaudemer, Y., Tapponnier, P., and Meyer, B., 1998, Northeastward growth of the Tibet plateau deduced from balanced reconstruction of two depositional areas: The Qiadam and Hexi Corridor basins, China: Tectonics, v. 17, no. 6, p. 823-842.

Molnar, P., and Lyon-Caen, H., 1989, Fault plane solutions of earthquakes and active tectonics of the Tibetan Plateau and its margins: Geophysical Journal International, v. 99, p. 123–153.

Molnar, P., England, P., and Martinod, J., 1993, Mantle dynamics, uplift of the Tibetan Plateau, and the

Indian Monsoon: Reviews of Geophysics, v. 31, p. 357–396, doi: 10.1029/93RG02030.

Murphy, M.A., and Copeland, P., 2005, Transtensional deformation in the central Himalaya and its role in accommodating growth of the Himalayan orogen: Tectonics, v. 24, TC4012, doi:10.1029/2004TC001659.

Murphy, M. A., and Burgess, W. P., 2006, Geometry, kinematics, and landscape characteristics of an active transtension zone, Karakoram fault system, southwest Tibet: Journal of Structural Geology, v. 28, p. 268-283.

Murphy, M.A., Yin, A., Kapp, P., Harrison, T.M., Lin, D., and Guo, J.H., 2000, Southward propagation of the Karakoram fault system, southwest Tibet: Timing and magnitude of slip: Geology, v. 28, p. 451-454.

Murphy, M., Yin, A., Kapp, P., Harrison, T., Manning, C., Ryerson, F., Lin, D., and Jinghui, G., 2002, Structural evolution of the Gurla Mandhata detachment system, southwest Tibet: Implications for the eastward extent of the Karakoram fault system: Geological Society of America Bulletin, v. 114, p. 428.

Murphy, M.A., Saylor, J.E., Ling, D., 2009, Landscape evolution of southwest Tibet based on integrated paleoelevation reconstructions and structural history: Earth and Planetary Science Letters, v. 282, p. 1-9.

Murphy, M.A., Sanchez, V., and Taylor, M.H., 2010, Syncollisional extension along the India-Asia suture zone, south-central Tibet: Implications for crustal deformation of Tibet: Earth and Planetary Science Letters, doi:10.1016/j.epsl.2009.11.046

Nakata, T., 1989, Active faults of the Himalaya of India and Nepal: Tectonics of the western Himalayas: Geological Society of America Special Paper, v. 232, p. 243–264.

Paul, J., Bürgmann, R., Gaur, V.K., Bilham, R., Larson, K.M., Ananda, M.B., Jade, S., Mukal, M., Anupama, T.S., Satyal, G., and Kumar, D., 2001, The motion and ctive deformation of

India: Geophysical Research Letters, v. 28, p. 647–651, doi:10.1029/2000GL011832.

Peltzer, G., and Tapponnier, P., 1988, Formation and evolution of strike-slip faults, rifts, and basins during the India-Asia collision- An experimental approach: Journal of Geophysical Research, v. 93, p. 15085-15117.

Phillips, R.J., Parrish, R.R., and Searle, M.P., 2004, Age constraints on ductile deformation and long-term slip rates along the Karakoram fault zone, Ladakh: Earth and Planetary Science Letters, v. 226, p. 305-319.

Ratschbacher, L., Frisch, W., Liu, G., and Chen, C., 1994, Distributed deformation in southern and western Tibet during and after the India-Asia collision: Journal of Geophysical Research-Solid Earth, v. 99, no. B10, p.19,917-19,945.

Robinson, A.C., 2009, Geologic offsets across the northern Karakorum fault: Implications for its role and terrane correlations in the western Himalayan-Tibetan orogen: Earth and Planetary Science Letters, v. 279, p. 123-130.

Royden, L.H., Burchfi el, B.C., King, R.W., Wang, E., Chen, Z.L., Shen, F., and Liu, Y.P., 1997, Surface deformation and lower crustal fl ow in eastern Tibet: Science, v. 276, no. 5313, p. 788–790, doi: 10.1126/science.276.5313.788.

Savage, J., and Burford, R., 1973, Geodetic Determination of Relative Plate Motion in Central California: Journal of Geophysical Research, v. 78, p. 832-845.

Schill, E., Appel, E., Zeh, O., Singh, V., and Gautam, P., 2001, Coupling of late-orogenic tectonics and secondary pyrrhotite remanences: towards a separation of different rotation processes and quantification of rotational underthrusting in the western Himalaya (northern India): Tectonophysics, v. 337, p. 1-21.

Schill, E., Crouzet, C., Gautam, P., Singh, V.K., and Appel, E., 2002, Where did rotational shortening occur in the Himalayas? - Inferences from palaeomagnetic remagnetisations: Earth and

Planetary Science Letters, v. 203, p. 45-57.

Searle, M., 1991, Geology and tectonics of the Karakoram Mountains: John Wiley & Sons Inc, 358 p.

Searle, M.P., 1996, Geological evidence against large-scale pre-Holocene offsets along the Karakoram Fault: implications for the limited extrusion of the Tibetan Plateau: Tectonics v. 15, 171–186.

Searle, M., 2010, Low-angle normal faults in the compressional Himalayan orogen: Evidence from the Annapurna-Dhaulagiri Himalaya, Nepal: Geosphere, v. 6, no. 4, doi:10.1130/ GES00549.1

Searle, M.P., Weinberg, R.F., Dunlap, W.J., 1998, Transpressional tectonics along the Karakoram fault zone, northern Ladakh: constraints on Tibetan extrusion: In: Holdsworth, R.E., Strachan, R.A., Dewey, J.F. (Eds.), Continental Transpressional and Transtensional Tectonics. Geological Society of London Special Publication, vol. 135, p. 307–326.

Searle, M.P. and Godin, L., 2003. The South Tibetan Detachment and the Manaslu Leucogranite: A structural re-interpretation and restoration of the Annapurna-Manaslu Himalaya, Nepal: Journal of Geology, v. 111, p. 505-523.

Seeber, L., and Pêcher, A., 1998, Strain partitioning along the Himalayan arc and the Nanga Parbat antiform: Geology, v. 26, p. 791-794.

Shen, Z., Lu, J., Wang, M., and Bürgmann, R., 2005, Contemporary crustal deformation around the southeast borderland of the Tibetan plateau: Journal of Geophysical Research, v. 110, doi:10.1029/2004JB003421.

Steck, A., Epard, J.-L., Vannay, J.-C., Hunziker, J., Girard, M., Morard, A., and Robyr, M., 1998, Geological transect across the Tso Morari and Spiti areas: The nappe structures of the Tethys Himalaya: Eclogae Geologica Helvetica, v. 91, p. 103-121.

Styron, R., Taylor, M., Murphy, M., 2009, Himalayan Orogen-parallel Extension from GPS Geodesy and Structural Geology: The 5th International Symposium on Tibetan Plateau/ The 24th Himalaya–Karakorum–Tibet Workshop, Beijing, China. August 11–14.

Styron, R., Taylor, M., Okoronkwo, K., 2010, Database of Active Structures From the Indo-Asian Collision, Eos Transactions AGU, v. 91, no. 20, doi:10.1029/2010EO200001.

Tapponnier, P., Peltzer, G., Le Dain, A.Y., Armijo, R., and Cobbold, P., 1982, Propagating extrusion tectonics in Asia: New insights from simple experiments with plasticine: Geology, v. 10, p. 611-616.

Tapponnier, P., Xu, Z.Q., Roger, F., Meyer, B., Arnaud, N., Wittlinger, G., and Yang, J.S., 2001, Oblique stepwise rise and growth of the Tibet plateau: Science, v. 294, no. 5547, p. 1671–1677, doi: 10.1126/science.105978.

Taylor, M., and Peltzer, G., 2006, Current slip rates on conjugate strike slip faults in central Tibet using synthetic aperture radar interferometry: Journal of Geophysical Research, v. 111, B12402, doi: 10.1029/2005JB004014.

Taylor, M., and Yin, A., 2009, Active structures of the Himalayan-Tibetan orogen and their relationships to earthquake distribution, contemporary strain field, and Cenozoic volcanism: Geosphere, v. 5, p. 199-214.

Taylor, M., Yin, A., Ryerson, F., Kapp, P., and Ding, L., 2003, Conjugate strike-slip faulting along the Bangong-Nujiang suture zone accommodates coeval east-west extension and north-south shortening in the interior of the Tibetan Plateau: Tectonics, v. 22, no. 4, doi:10.1029/2002TC001361.

Thatcher, W., 2007, Micoplate model for the present-day deformation of Tibet: Journal of Geophysical Research, v. 112, B101401, doi: 10.1029/2005JB004244.

Thiede, R.C., Arrowsmith, J.R., Bookhagen, B., McWilliams, M., Sobel, E.R., and Strecker, M.R.,

2006, Dome formation and extension in the Tethyan Himalaya, Leo Pargil, northwest India: Geological Society of America Bulletin, v. 118, p. 635-650.

Upreti, B.N., 1999, An overview of the stratigraphy and tectonics of the Nepal Himalaya: Journal of Asian Earth Sciences, v. 17, p. 577-606.

Valli, F., Arnaud, N., Leloup, P.H., Sobel, E.R., Mahéo, G., Lacassin, R., Guillot, S., Li, H., Tapponnier, P., and Xu, Z., 2007, Twenty million years of continuous deformation along the Karakorum fault, western Tibet: A thermochronological analysis: Tectonics, v. 26, TC4004, doi:10.1029/2005TC001913

Valli, F., Leloup, P., Paquette, J., Arnaud, N., Li, H., Tapponnier, P., Lacassin, R., Guillot, S., Liu, D., and Deloule, E., 2008, New U-Th/Pb constraints on timing of shearing and long-term slip-rate on the Karakorum fault: Tectonics, v. 27, TC5007, doi:10.1029/2007TC002184.

Vannay, J., and Steck, A., 1995, Tectonic evolution of the High Himalaya in Upper Lahul (NW Himalaya, India): Tectonics, v. 14, no. 2, p.253-263.

Vergnolle, M., Calais, E., and Dong, L., 2007, Dynamics of continental deformation in Asia: Journal of Geophysical Research-Solid Earth, v. 112, B11403, doi:10.1029/2006JB004807.

Wang, Q., Zhang, P.Z., Niu, Z.J., Freymueller, J.T., Lai, X., Li, Y.X., Zhu, W.Y., Liu, J.N., Bilham, R., and Larson, K.M., 2001, Present-day crustal deformation in China constrained by global positioning system measurements: Science, v. 294, p. 574–577, doi: 10.1126/ science.1063647.

Wu, C., Nelson, K., Wortman, G., Samson, S., Yue, Y., Li, J., Kidd, W., and Edwards, M., 1998, Yadong cross structure and South Tibetan Detachment in the east central Himalaya (89 -90): Tectonics, v. 17, p. 28-45.

Yin, A., 2000, Mode of Cenozoic east-west extension in Tibet suggesting a common origin of rifts in Asia during the Indo-Asian collision: Journal of Geophysical Research, v. 105, B9,

doi:10.1029/2000JB900168.

Yin, A., and Harrison, T.M., 2000, Geologic evolution of the Himalayan-Tibetan orogen: Annual Review of Earth and Planetary Sciences, v. 28, p. 211–280, doi: 10.1146/annurev. earth.28.1.211

Yin, A., Kapp, P., Murphy, M., Manning, C. E., Harrison, T. M., Din, L., Xiguang, D.,Chunming, W., 1999a, Significant late Neogene east-west extension in north Tibet, Geology, v. 27, p.787-790.

Yin, A., Harrison, T.M., Murphy, M.A., Grove, M., Nie, S., Ryerson, F.J., Feng, W.X., and Le, C.Z., 1999b, Tertiary deformation history of southeastern and southwestern Tibet during the Indo-Asian collision: Geological Society of America Bulletin, v. 111, p. 1644-1664.

Zhang, P., Shen, Z., Wang, M., Gan, W., Bürgmann, R., Molnar, P., Wang, Q., Niu, Z., Sun, J., and Wu, J., 2004, Continuous deformation of the Tibetan Plateau from global positioning system data: Geology, v. 32, p. 809.

Zhang, R., Murphy, M.A., Lapen, T.J., Sanchez, V. and Heizler, M., 2010, Late Eocene crustal thickening followed by Early-Late Oligocene Extension along the India-Asia suture zone: Evidence for cyclicity in the Himalayan orogen, *in* Leech, M.L., and others, eds., Proceedings for the 25th Himalaya-Karakoram-Tibet Workshop: U.S. Geological Survey, Open-File Report 2010-1099, 2 p. [http://pubs.usgs.gov/of/2010/1099/zhangmurphy/].

Figures Tables with Captions

Region	Arc-parallel shear (mm yr⁻¹)	Error (1-σ, mm yr⁻¹)	Arc-normal shortening (mm yr⁻¹)	Error (1-σ, mm yr⁻¹)
Ladakh	6	4.4	13.7	5.6
Himachal	7	4.5	13.6	5.5
Gurla Mandhata	3.2	5.4	11.9	5.4
Thakkhola	8.1	8.9	11.7	8.0
Everest	3.1	7.5	12.5	6.9
Bhutan	7.9	7.2	16.1	6.1
Arunachal	6.8	5.4	24.1	4.1

Table 1: Arc-parallel shear and arc-normal shortening rates for the geodetic 'regions' along the Himalayan arc, calculated from the velocity profiles shown in Fig.6.
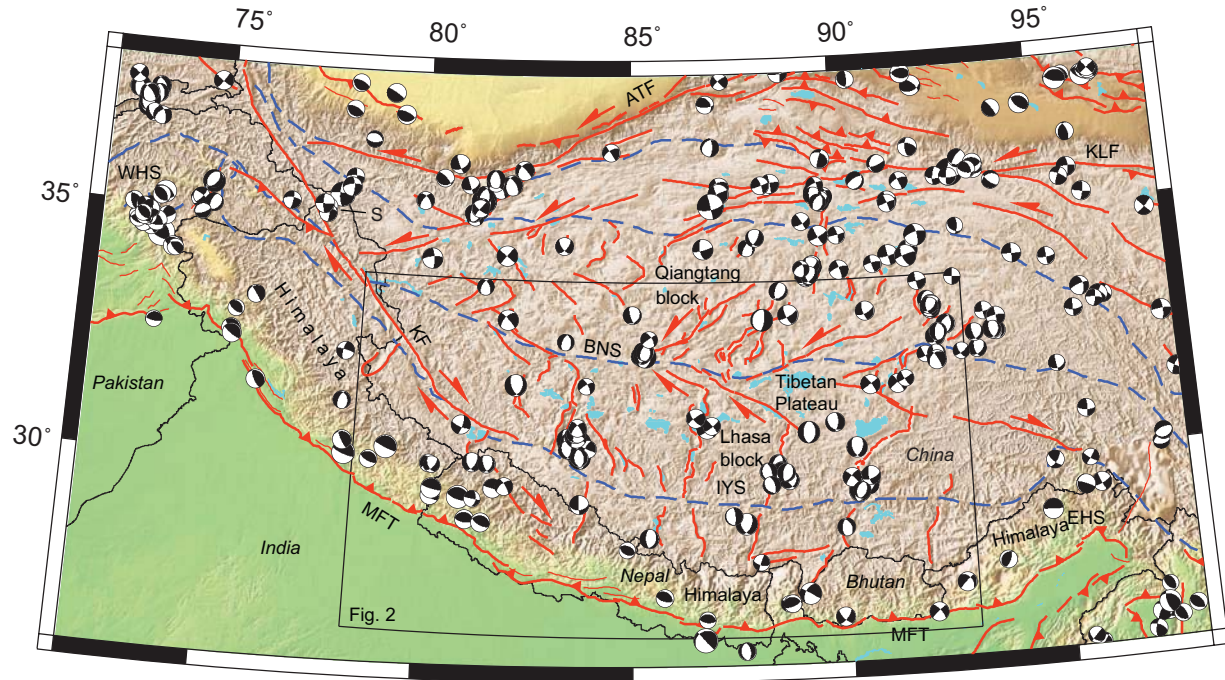
Figure 1: Active structures (orange lines) and suture zones (dashed blue lines) of the Himalayan-Tibetan orogen after Styron, et al. (2010). Focal mechanisms from the Global Centroid Moment Tensor catalog (www.globalcmt.org), 1976-2008. Topography is from the Shuttle Radar Topography Mission. MFT = Main Frontal Thrust. H = Himalaya range. WHS = western Himalayan syntaxis. EHS = eastern Himalayan syntaxis. IYS = Indus-Yarlung Suture. KF = Karakoram fault. BNS = Bangong-Nujiang Suture. LB = Lhasa block. QB = Qiangtang block. ATF = Altyn Tagh fault. S = GPS site STAKSHA.
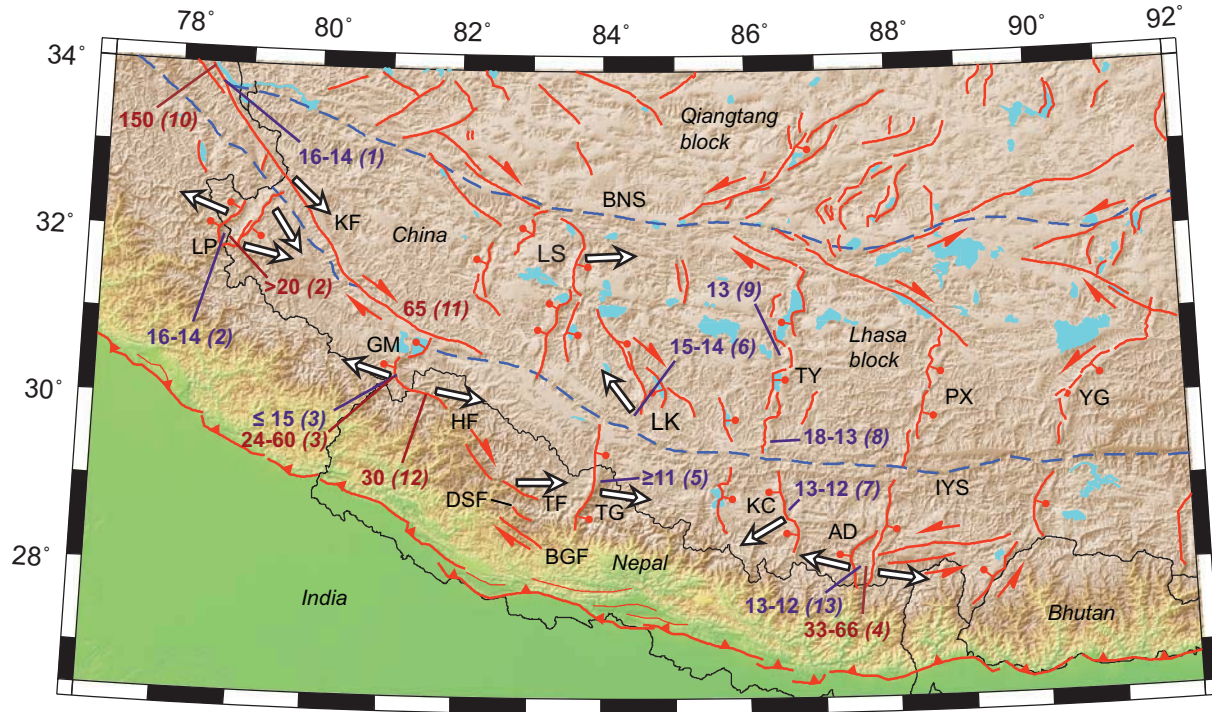
Figure 2: Active structures (orange lines) and sutures (dashed blue lines) after Styron, et al. (2010), Thiede, et al. (2006), and Jessup, et al., (2008). LP = Leo Parghil Dome. GM = Gurla Mandhata Dome. HF = Humla Fault. TF = Tribrikot Fault. TG = Thakkhola Graben. KC = Kung Co Rift. AD = Ama Drime Massif. IYS = Indus-Yarlung Suture. LK = Lopukangri Rift. LS = Lunggar Shan Rift. TY = Tangra-Yumco Rift. PX = Pum Qu-Xainza Rift. YG = Yadong-Gulu Rift. BNS = Bangong-Nujiang Suture. Numbers in purple indicate initiation ages (Ma). Numbers in reddish brown indicate fault heave (km). Sources are given in italics. 1 = Phillips, et al. (2004). 2 = Thiede, et al. (2006). 3 = Murpy, et al. (2002). 4 = Langille, et al. (2010). 5 = Garzione, et al. (2003). 6 = Murphy, et al. (2010). 7 = J. Lee, personal communication. 8 = Williams, et al. (2001). 9 = Dewane, et al. (2008). 10 = Searle (1996). 11 = Murphy, et al., 2000). 12 = Murphy and Copeland (2005). 13 = Kali, et al. (2010). Arrows indicate mean azimuth of fault heave, relative to the footwall in the case of nonvertical faults. Fault slip data sources: KF - Murphy, et al. (2009); LP - Thiede, et al. (2006); GM - Murphy, et al. (2002) LS - Sundell, et al. (2010); LK - Murphy, et al. (2010). TF - Styron, et al. (2009); TG - Baltz and Murphy (2009); KC – J. Lee, personal communication; AD - Jessup, et al. (2008), Kali, et al. (2010). Topography from Shuttle Radar Topography Mission (SRTM).
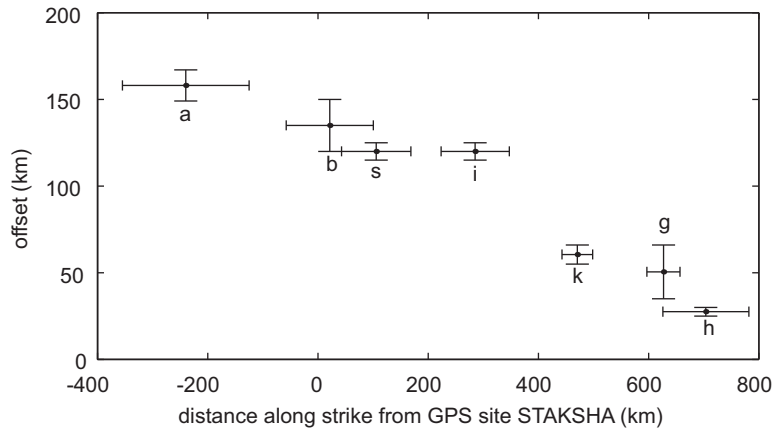
Figure 3: Offset estimates of geologic features along the Karakoram-Humla fault system plotted by their distance along strike of the Himalayan arc from GPS site STAKSHA (34.82 N, 77.52 E; Fig. 1), as compiled in Robinson (2009). Errors on the x-axis correspond to the along-strike distance spanned by the offset features. Errors on the y-axis indicate the error associated with the estimated offset. a = Aghil limestone. b = Baltoro granite. s = Shyok suture. i = Indus River. k = South Kailas thust. g = Gurla Mandhata detachment. h = Humla fault. See text for sources.
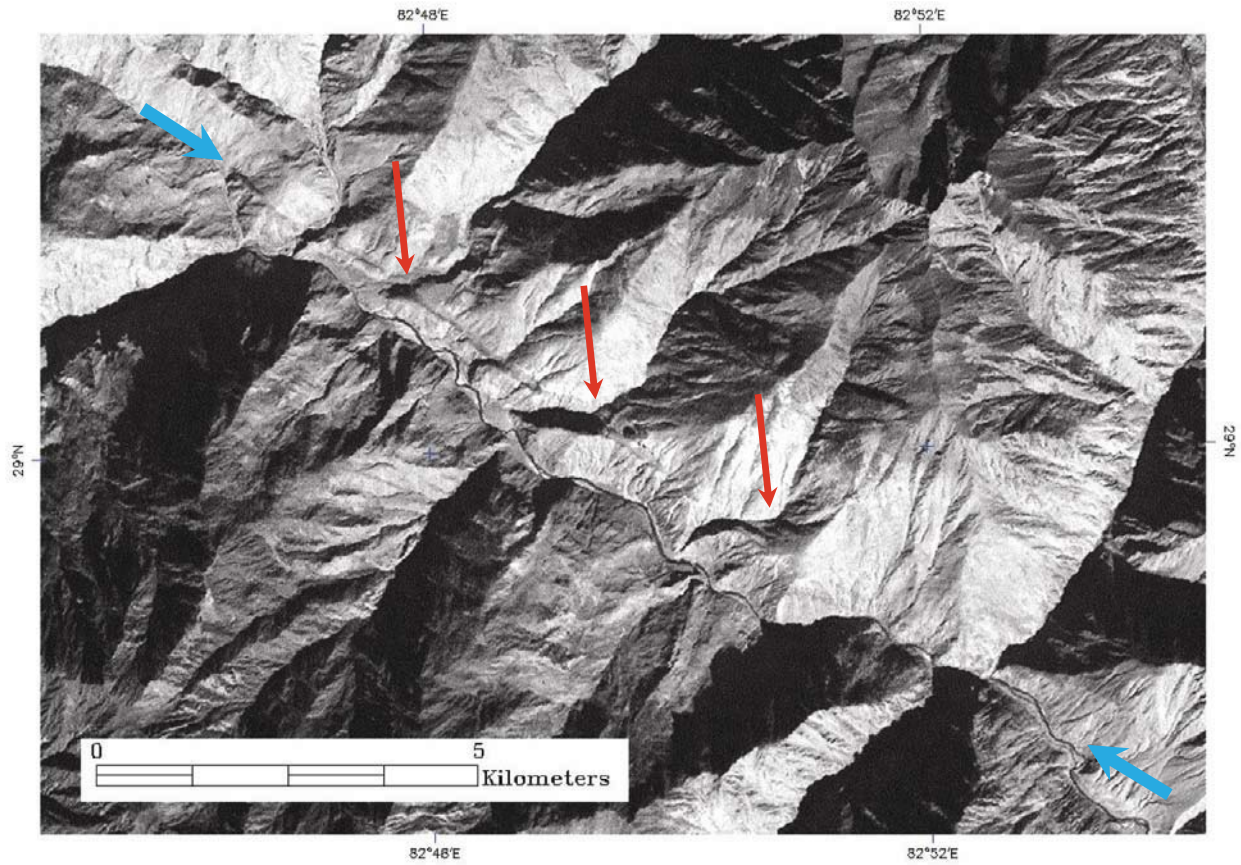
Figure 4: CORONA satellite imagery of the Tibrikot fault, Dolpo region, Nepal. Blue arrows indicate the trace of the fault. Red arrows indicate consistent right-lateral offsets of stream drainages crossing the fault. Note the sharpness of the fault trace, which suggests its recent activity.
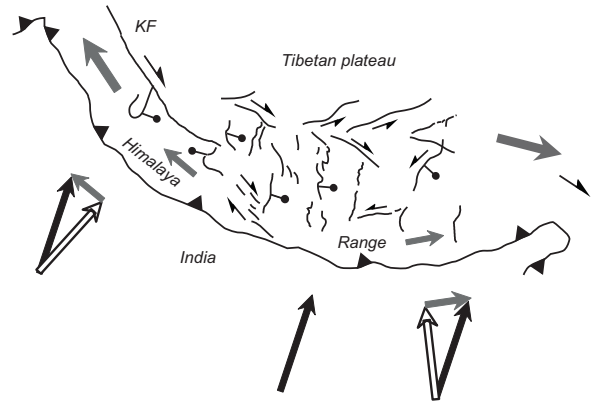
Figure 5: Models for Himalayan and south Tibetan deformation. A: Lateral extrusion model, where the Tibetan plateau translates to the east (grey arrows) along right-lateral structures along its southern margin and left-lateral structures along its northern margin. B: Oroclinal bending model, where the the Himalayan orogen bends such that the Eastern Himalayan syntaxis (EHS) and the Western Himalayan syntaxis (WHS) move towards each other, resulting in a decrease in the radius of curvature of the Himalayan arc. This causes extension of the outer (India-facing) Himalaya and contraction of the interior of the orogen (grey arrows), and strike-slip faulting analogous to flexural slip. C: Radial spreading model, where Tibet expands radially to the south (grey arrows) causing arc-parallel extension of the Himalaya. D: Oblique convergence model, where India's motion relative to Eurasia (black arrows) has an arc-normal (white arrows) and arc-parallel (grey arrows) component, causing arc-parallel extension and translation of the Himalaya (grey arrows). The dark grey arrow represents the eastward motion of central Tibetan lithosphere independent of oblique convergence.
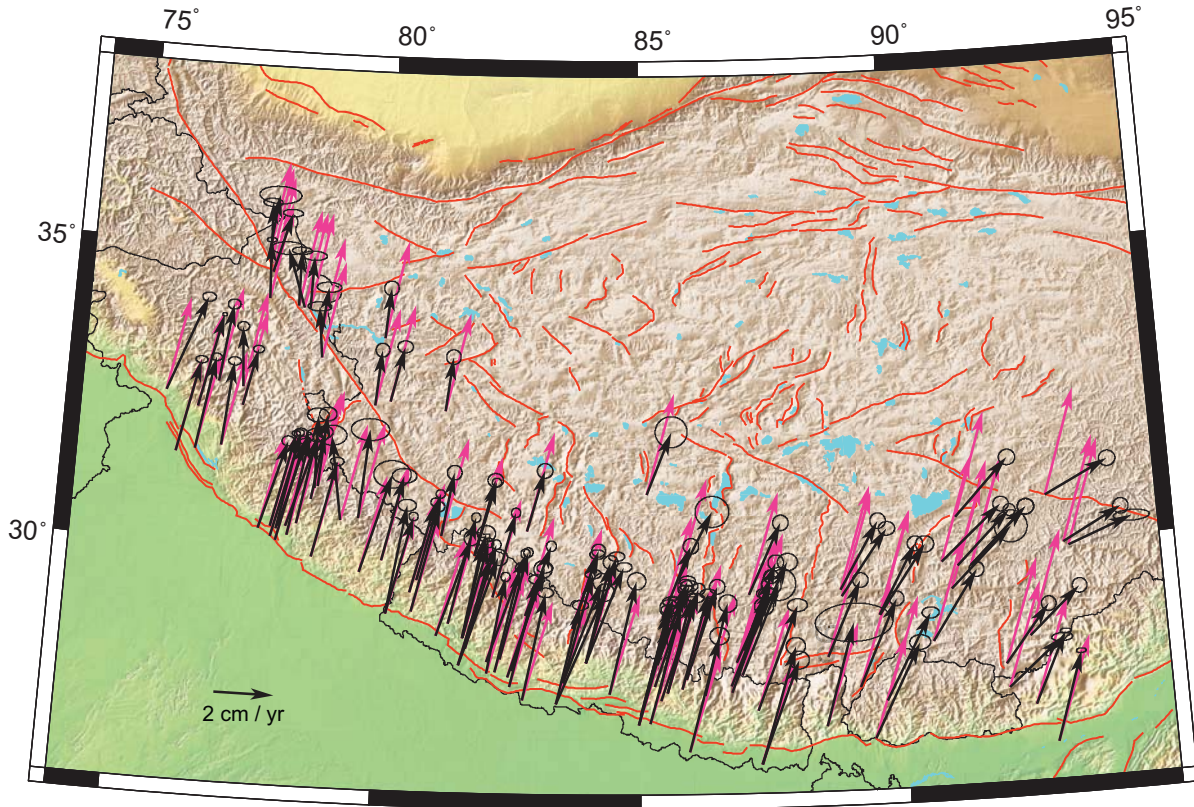
Figure 6: Observed GPS velocities (black) relative to stable Eurasia in the ITRF2000 reference frame and predicted India-Eurasia plate motion vectors (pink) relative to stable Eurasia in ITRF2000 at each GPS station using the India-Eurasia pole of of rotation from Jade, et al. (2007). All velocities are plotted using the same scale. Where the GPS and plate motion vectors are similar, the upper crust moves with the Indian plate (locked MHT). Where the GPS vectors are smaller (slower) than the plate motion vectors but still parallel (such as the interior of Tibet), strain accumulation of the upper plate between the MFT and the GPS site takes place at a rate equal to the difference of the vector magnitudes at that site. The significant divergence in the azimuths of the GPS and plate motion vectors in south Tibet indicates vertical-axis rotation around the EHS.
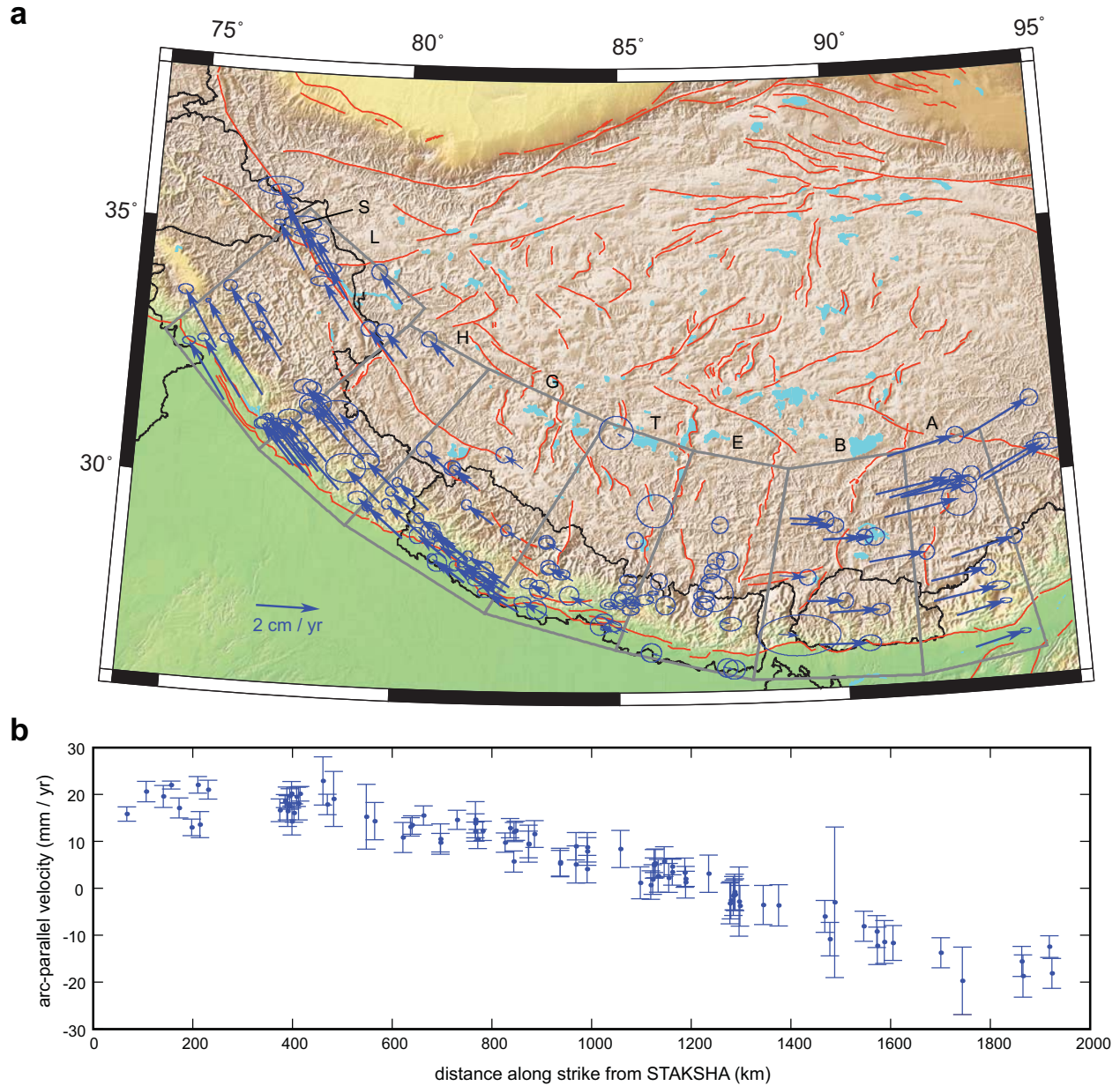
Figure 7a: Arc-parallel component of GPS velocities. Grey boxes outline 'regions' that define velocity bins. L = Ladakh region. H = Himachal region. G = Gurla Mandhata region. T = Thakkhola region. E = Everest region. B = Bhutan region. A = Arunachal region. S = GPS site STAKSHA.

Figure 7b: Arc-parallel component of GPS velocities from within the Himalayan arc (i.e. between the MFT and KF/IYS) plotted as a function of distance along strike from GPS site STAKSHA. Clockwise velocities are defined as positive. The uniform velocity gradient between 400 and 1400 km along strike indicates that arc-parallel extension is uniformly distributed throughout much of the Himalaya.
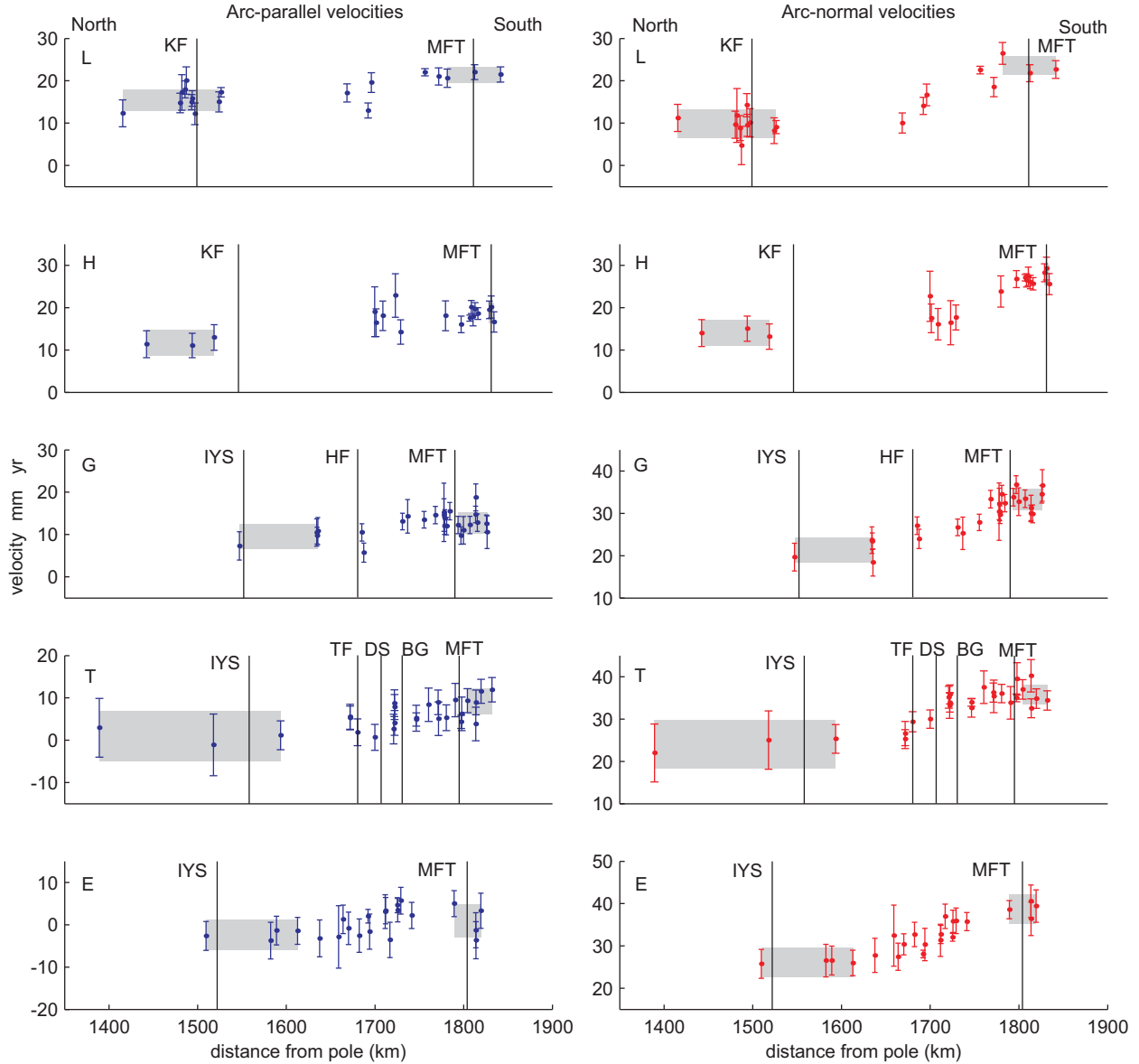
Figure 8: Arc-normal profiles of arc-parallel and arc-normal components of GPS velocities for the western and central Himalayan 'regions' shown in Figures 5 and 8. Velocities are plotted by the distance from the pole to the Himalayan arc of Bendick and Bilham (2001) at 41.4° N, 91.6° E. Positive arc-parallel velocities indicate clockwise (west- or northwest-directed) motion; increasing velocities with increasing radial distances indicate dextral shear across the arc. Positive arc-normal velocities indicate motion towards the pole; increasing velocities with increasing radial distances indicates shortening across the arc. Grey rectangles indicate the GPS sites used in the calculations of arc-normal convergence and arc-parallel shear discussed in the text. The height of the rectangles correspond to their associated error, with the mean value in the center of the rectangle. L = Lakakh region. H = Himachal region. G = Gurla Mandhata region. T = Thakkhola region. E = Everest region. KF = Karakoram Fault. IYS = Indus-Yarlung Suture Zone. MFT = Main Frontal Thrust. HF = Humla Fault. TF = Tibrikot fault. DS = Dhaulagiri Southwest fault. BG = Bari Gad fault.

59
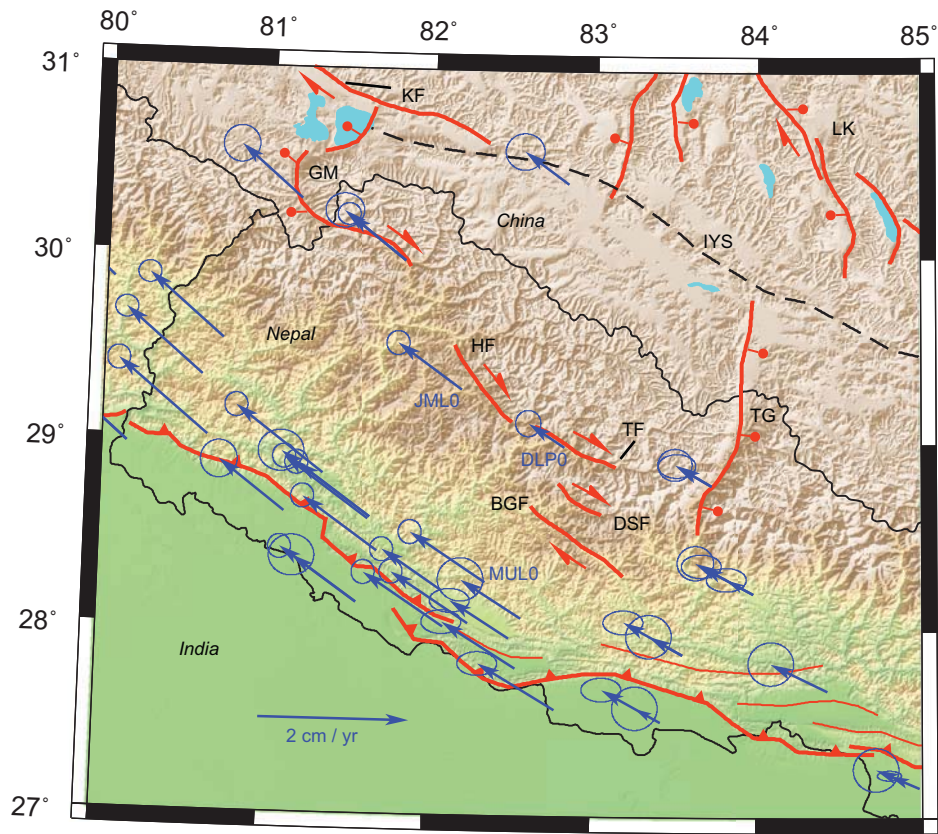
Figure 9: Active structures and arc-parallel GPS velocities in western Nepal and surrounding areas. JML0, DLP0, and MUL0 are GPS sites discussed in the text. BGF = Bari Gad fault. DSF = Dhaulagiri Southwest fault. TF = Tibrikot fault. HF = Humla fault. TG = Thakkhola graben. GM = Gurla Mandhata. IYS = Indus-Yarlung Suture. KF = Karakoram fault. LK = Lopukangri rift.
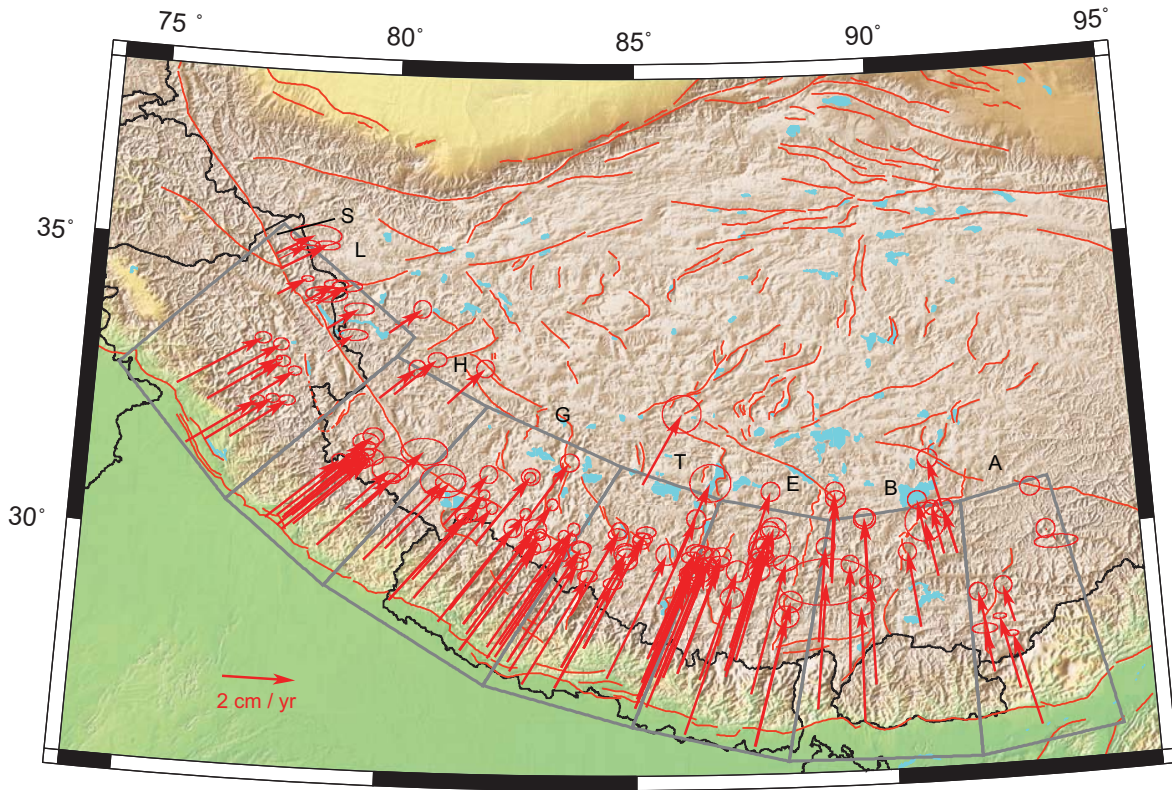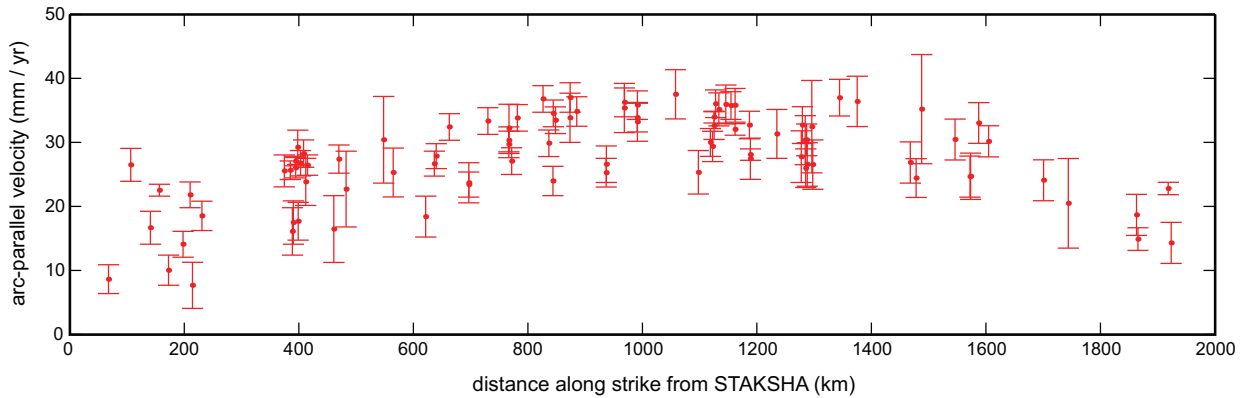
Figure 10a: Arc-normal component of GPS velocities. Grey boxes outline 'regions' that define velocity bins. L = Ladakh region. H = Himachal region. G = Gurla Mandhata region. T = Thakkhola region. E = Everest region. B = Bhutan region. A = Arunachal region. S = GPS site STAKSHA.

Figure 10b: Arc-normal component of GPS velocities from within the Himalayan arc (i.e. between the MFT and KF/IYS) plotted as a function of distance along strike from GPS site STAKSHA (34.82° N, 77.52° E). Velocities directed towards the pole of Bendick and Bilham (2001) are defined as positive.

Sta	Longitude	Latitude	Vn	Sn	Ve	Se	along_strike_length_(km)	distance_to_pole_(km)
J049	79.94	33.56	16.60	1.60	1.50	1.60	262.79	1415.41
JIPA	77.18	32.63	19.80	1.00	-1.30	1.30	172.54	1668.45
KOTH	77.19	32.32	18.70	0.80	4.10	1.20	197.84	1692.23
NADI	76.31	32.25	30.80	0.40	6.60	0.50	156.52	1756.28
REWL	76.82	31.63	27.90	0.90	2.60	1.40	230.61	1771.72
UDAI	76.69	32.70	25.50	1.10	3.30	1.40	140.81	1695.87
UNA0	76.31	31.54	30.60	0.80	5.00	1.20	210.02	1812.30
BOHA	75.94	31.48	30.60	0.80	6.30	1.30	195.33	1841.52
MANU	75.67	32.49	31.50	1.00	11.60	1.50	106.44	1781.48
STAKSH	77.52	34.82	20.77	1.90	2.21	4.60	0.00	1482.15
PNMK	77.57	34.73	19.99	0.90	-0.89	2.10	11.23	1485.67
LEH	77.60	34.13	19.50	0.50	-1.00	1.10	67.70	1526.34
TIRTH	77.62	34.57	20.01	0.80	5.10	2.20	28.63	1493.25
TNGS	78.18	34.03	18.45	0.80	-0.32	2.20	108.19	1493.85
MGLB	78.30	34.01	19.49	1.40	-6.72	3.80	117.07	1487.16
LKNG	78.41	34.00	17.62	1.00	0.18	2.70	124.68	1480.29
CHUS	78.66	33.58	15.78	1.10	1.46	2.70	177.33	1496.81
MUTH	78.70	33.19	16.99	1.00	-2.04	2.60	214.33	1524.05
JB56	79.80	32.43	18.40	1.50	1.70	1.50	352.40	1518.58
SHIQ	80.10	32.51	18.20	1.30	4.20	1.70	367.22	1493.81
QASI	77.63	30.28	29.30	1.10	8.40	1.40	374.57	1834.08
SABA	77.86	30.33	30.90	0.60	7.00	0.90	385.05	1815.93
SUKI	78.68	31.00	24.20	1.50	0.10	2.40	388.77	1708.78
HARS	78.75	31.04	23.90	1.50	2.20	1.90	390.39	1701.15
WIH2	78.01	30.33	31.10	0.30	8.60	0.50	394.29	1806.97
WILD	77.97	30.29	32.00	0.70	6.40	0.90	394.60	1812.84
MOND	77.87	30.15	34.50	1.20	8.40	1.50	398.12	1831.02
BHAT	78.62	30.81	22.40	1.30	3.70	1.70	398.79	1728.90
DHOU	78.16	30.34	29.80	0.90	9.20	1.10	402.94	1797.20
RAJA	77.98	30.10	33.40	0.90	7.90	1.30	408.34	1828.88
CHAM	78.37	30.40	29.40	1.50	5.50	2.40	412.02	1779.55
DOIW	78.19	30.19	32.70	0.70	6.00	0.90	415.25	1808.59
TUNG	79.21	30.49	27.90	2.20	-4.00	3.30	461.14	1723.00
J044	81.19	32.38	17.90	1.60	2.20	1.60	462.26	1442.36
LANS	78.68	29.85	31.90	0.90	7.20	1.50	470.00	1810.51
AULI	79.56	30.53	29.50	2.40	2.80	4.20	482.58	1699.66
KTML	79.62	29.64	32.60	3.00	9.70	4.10	548.09	1777.66
CHAU	80.04	29.84	28.30	1.60	6.60	2.70	564.91	1736.70
J045	81.18	30.29	21.00	1.60	3.80	1.60	621.62	1635.49
MAH0	80.15	28.96	32.37	0.95	8.24	1.01	629.60	1813.42
MAHE	80.15	28.96	36.00	1.30	6.00	2.00	629.94	1813.62
SHB0	80.72	29.53	28.83	0.95	7.23	1.01	636.73	1730.95
DAD2	80.60	29.33	29.99	0.95	7.63	1.01	640.01	1755.26
SHP0	80.64	29.01	34.90	1.05	8.54	1.01	662.91	1784.25
SMK0	81.83	29.97	24.42	0.95	6.82	1.01	696.79	1634.67
SIMI	81.83	29.97	25.10	1.50	6.40	1.70	696.88	1634.21
LMK1	81.12	28.61	32.73	1.65	11.05	1.61	724.01	1799.71
GUT0	81.35	28.82	35.39	1.05	8.45	1.01	730.14	1768.04
J046	82.83	30.39	20.20	1.60	5.70	1.70	756.96	1547.01
SKT0	81.64	28.59	31.67	1.05	7.95	1.01	766.83	1778.40
SKA0	81.63	28.58	32.17	1.05	6.15	1.01	766.92	1778.72
SURK	81.64	28.59	34.70	1.80	7.00	2.00	766.97	1777.77
JML0	82.19	29.28	28.12	1.05	7.23	1.01	771.72	1685.19
SPS2	81.69	28.41	34.68	1.05	9.56	1.01	781.62	1793.56
NEPA	81.57	28.13	36.00	1.80	12.40	2.00	787.61	1826.35
NPJ0	81.57	28.13	35.45	1.05	9.57	1.01	787.76	1825.73
BBP0	82.09	28.20	35.99	1.05	12.37	1.01	826.38	1796.88
KUS0	82.10	28.01	31.99	1.05	5.77	1.01	836.67	1815.42

DLP0	82.82	28.98	23.18	1.15	8.34	1.11	843.71	1687.34
MUL0	82.35	28.25	35.46	1.05	8.86	1.01	844.46	1780.75
AMP0	82.25	28.03	34.73	1.05	7.97	1.01	848.15	1806.98
RANJ	82.57	28.06	33.70	1.90	10.00	2.00	873.56	1790.53
CHP0	82.50	27.95	36.29	1.04	11.82	1.75	873.80	1804.25
BMT0	82.54	27.79	35.70	1.04	8.53	1.75	885.45	1819.50
KRN2	82.78	27.57	35.66	1.04	7.34	1.75	917.21	1831.85
JOM0	83.72	28.78	24.50	1.04	8.10	1.65	936.87	1671.83
JOMO	83.72	28.78	25.80	1.40	8.50	1.50	937.11	1671.82
TCOQ	85.14	31.02	20.60	3.40	8.30	3.50	951.02	1389.17
TANS	83.55	27.87	33.40	1.90	12.70	2.00	968.61	1771.66
TAN0	83.55	27.87	36.06	1.04	9.73	1.75	968.77	1771.13
BRW0	83.42	27.51	32.82	1.04	7.84	1.75	974.63	1813.92
BHAI	83.42	27.51	37.10	1.90	16.00	2.00	974.68	1813.56
PKR0	83.98	28.20	31.77	1.03	12.42	1.75	991.20	1722.10
POK0	83.98	28.20	35.27	1.03	10.02	1.75	991.20	1722.09
POKH	83.98	28.20	33.40	1.50	8.00	1.60	991.37	1721.90
BHAR	84.43	27.68	37.40	1.90	8.90	2.00	1057.93	1760.45
J040	85.44	28.96	23.50	1.70	9.50	1.70	1097.79	1593.50
SHOT	85.74	29.59	22.30	3.40	11.40	3.70	1099.02	1517.82
RAM0	85.22	28.02	27.69	1.03	11.54	1.75	1118.87	1699.91
SYA0	85.33	28.17	27.62	1.13	10.13	1.75	1122.67	1680.17
DAMA	85.11	27.61	33.06	0.43	9.15	1.05	1125.22	1746.44
DMN0	85.11	27.61	31.96	1.03	8.35	1.75	1125.22	1746.44
HET0	85.01	27.32	35.14	1.03	9.56	1.75	1127.89	1780.38
SIMR	84.98	27.16	38.70	1.90	10.00	2.00	1131.66	1797.73
SIMR	84.98	27.16	33.83	0.43	9.97	1.05	1131.89	1797.11
KKN0	85.28	27.80	33.31	1.23	11.54	1.95	1133.71	1720.91
AIRP	85.36	27.70	35.30	1.50	8.80	1.60	1145.83	1729.15
NIJ0	85.19	27.18	37.48	1.03	10.37	1.75	1150.18	1789.12
PKI0	85.40	27.57	33.84	1.03	11.75	1.75	1154.71	1741.33
NAGD	85.52	27.69	34.40	1.30	10.50	1.40	1161.94	1725.55
NAGA	85.52	27.69	31.37	0.43	7.95	1.35	1161.95	1725.23
BAL0	85.79	27.75	31.64	1.02	8.95	1.75	1186.96	1711.90
J041	85.97	28.15	26.00	1.60	8.90	1.70	1188.52	1663.88
GUMB	85.88	27.91	26.86	0.42	8.45	1.05	1188.77	1692.06
JIRI	86.23	27.64	30.50	1.90	7.80	2.00	1234.88	1711.56
JANK	85.92	26.71	38.20	1.90	10.30	2.10	1237.59	1819.39
J038	87.09	29.32	23.50	1.70	10.90	1.70	1263.54	1509.53
RONG	86.83	28.19	25.30	2.00	11.90	2.20	1277.40	1637.56
NAMC	86.72	27.80	30.20	1.40	12.80	2.10	1279.59	1682.25
LUKL	86.73	27.69	28.30	1.90	11.10	2.10	1284.44	1693.89
JB54	86.97	28.39	24.20	1.50	9.50	1.60	1285.34	1612.69
PHER	86.82	27.89	28.60	1.20	10.30	2.10	1286.95	1670.19
J030	87.06	28.59	24.80	1.70	9.60	1.70	1287.99	1588.99
SCOL	86.93	27.97	30.00	3.60	12.70	3.70	1295.83	1658.99
TING	87.16	28.63	24.10	1.90	11.70	2.20	1297.66	1582.38
KHAN	87.21	27.38	34.50	1.40	13.80	2.20	1344.40	1716.81
BIRA	87.26	26.48	34.16	1.95	13.09	2.22	1375.29	1813.73
BIRP	87.27	26.48	38.80	1.90	11.90	2.10	1376.28	1813.53
J021	91.11	30.48	18.60	1.70	18.10	1.80	1756.99	1326.16
BALA	90.80	29.74	18.00	1.60	20.50	1.70	1719.64	1409.54
DAGZ	91.36	29.66	18.10	1.70	19.10	1.80	1794.72	1416.79
LHAS	91.10	29.66	17.40	1.30	18.10	1.30	1760.14	1417.33
GGAR	90.96	29.28	19.50	3.50	20.70	3.60	1744.00	1460.00
J037	88.84	29.36	22.20	1.70	13.10	1.70	1472.92	1470.91
XIGA	88.86	29.25	21.70	1.50	15.60	1.80	1478.27	1482.70
JIAN	89.57	28.91	22.60	1.80	15.80	2.00	1573.35	1511.06
J039	89.56	28.91	23.00	1.60	12.80	1.70	1572.12	1511.17

J033	90.56	28.42	23.00	1.60	15.50	1.60	1700.73	1557.32
J029	88.56	28.24	25.00	1.60	11.50	1.70	1468.00	1598.19
J042	89.15	27.72	28.70	1.60	13.00	1.60	1546.20	1647.30
TIMP	89.64	27.47	28.38	1.21	15.52	1.88	1604.70	1669.42
RBIT	89.39	26.85	31.09	1.58	15.98	2.31	1587.46	1740.78
J028	92.87	30.75	10.40	1.70	21.30	1.80	2010.83	1300.33
J022	93.15	29.94	10.30	1.70	19.80	1.70	2036.57	1392.39
GONGB	93.24	29.88	8.05	1.18	21.64	3.96	2047.19	1399.71
J032	92.40	28.42	15.30	1.60	17.30	1.60	1923.62	1556.17
J034	91.91	27.97	19.00	1.60	15.20	1.60	1863.10	1604.79
TAWA	91.94	27.58	15.32	0.89	18.36	2.26	1865.57	1648.20
BOMD	92.42	27.27	23.44	0.48	11.19	1.16	1918.50	1684.02
TZPR	92.78	26.62	29.33	0.48	9.62	1.06	1953.26	1757.93

arc_normal_v	arc_normal_err	arc_normal_n	arc_normal_e	arc_parallel_v	arc_parallel_err	arc_parallel_n
11.22	3.20	6.78	8.94	12.32	3.20	9.82
10.03	2.36	5.63	8.30	17.12	2.14	14.17
14.08	2.02	8.07	11.54	12.97	1.77	10.63
22.53	0.92	12.46	18.77	22.01	0.85	18.34
18.53	2.29	10.91	14.98	21.02	2.02	16.99
16.67	2.57	9.09	13.97	19.58	2.34	16.41
21.80	2.01	12.62	17.77	22.05	1.77	17.98
22.67	2.10	12.97	18.60	21.50	1.79	17.63
26.49	2.58	13.99	22.49	20.62	2.18	17.51
11.79	6.36	5.59	10.38	17.25	4.21	15.19
8.81	2.95	4.22	7.73	17.96	2.00	15.76
9.06	1.56	4.61	7.80	17.30	1.12	14.90
14.23	2.75	6.96	12.42	14.96	1.80	13.05
9.49	2.61	5.02	8.06	15.83	1.84	13.43
4.71	4.53	2.51	3.99	20.07	3.22	16.97
9.62	3.22	5.17	8.11	14.76	2.31	12.45
10.09	3.35	5.69	8.34	12.21	2.57	10.09
8.21	3.03	4.77	6.68	15.02	2.37	12.22
13.17	3.00	8.50	10.06	12.96	3.00	9.90
15.05	2.98	9.81	11.41	11.06	2.87	8.39
25.55	2.49	16.74	19.30	16.63	2.41	12.56
25.65	1.45	16.93	19.27	18.59	1.38	13.97
16.09	3.70	10.64	12.06	18.08	3.50	13.56
17.48	3.38	11.58	13.09	16.45	3.28	12.32
27.08	0.75	17.98	20.25	17.54	0.71	13.12
26.04	1.59	17.29	19.47	19.67	1.54	14.71
29.24	2.68	19.46	21.82	20.15	2.62	15.04
17.68	2.96	11.78	13.19	14.24	2.88	10.62
26.75	1.99	17.87	19.91	16.04	1.95	11.93
28.25	2.13	18.93	20.96	19.49	2.06	14.47
23.83	3.68	16.01	17.65	18.08	3.52	13.39
26.45	1.58	17.81	19.56	20.14	1.55	14.89
16.45	5.22	11.40	11.86	22.89	5.14	16.50
14.00	3.20	9.71	10.09	11.37	3.20	8.19
27.39	2.20	19.09	19.65	17.87	2.17	12.81
22.70	5.92	15.94	16.17	19.04	5.87	13.56
30.41	6.78	22.17	20.81	15.24	6.91	10.43
25.29	3.82	18.61	17.13	14.31	3.97	9.69
18.40	3.20	13.95	12.00	10.82	3.20	7.05
29.99	1.95	22.82	19.45	14.73	1.97	9.55
31.29	2.99	23.82	20.29	18.78	3.19	12.18
26.68	1.95	20.38	17.22	13.08	1.97	8.45
27.86	1.95	21.32	17.94	13.48	1.97	8.68
32.41	2.07	25.08	20.54	15.51	2.05	9.82
23.41	1.95	18.41	14.47	9.73	1.98	6.01
23.69	3.14	18.62	14.64	10.48	3.23	6.48
32.74	3.28	26.06	19.82	11.01	3.25	6.67
33.34	2.08	26.61	20.08	14.58	2.05	8.78
19.67	3.27	15.89	11.60	7.31	3.33	4.31
30.34	2.08	24.60	17.75	12.08	2.05	7.07
29.69	2.08	24.08	17.37	13.83	2.05	8.09
32.24	3.72	26.15	18.86	14.62	3.85	8.55
27.07	2.08	22.00	15.77	10.50	2.05	6.12
33.83	2.08	27.61	19.55	12.24	2.05	7.08
36.58	3.72	29.93	21.04	10.56	3.85	6.07
34.51	2.08	28.23	19.84	12.56	2.05	7.22
36.79	2.08	30.57	20.46	9.74	2.05	5.42
29.87	2.08	24.93	16.46	12.81	2.05	7.06

23.97	2.28	20.05	13.13	5.71	2.25	3.13
34.53	2.08	28.90	18.90	11.99	2.05	6.56
33.46	2.08	28.04	18.25	12.26	2.05	6.69
33.85	3.85	28.64	18.04	9.50	3.94	5.06
37.01	2.31	31.32	19.71	9.33	2.84	4.97
34.83	2.30	29.60	18.35	11.56	2.85	6.09
34.40	2.28	29.57	17.58	11.91	2.88	6.09
25.27	2.25	21.87	12.66	5.26	2.80	2.64
26.59	2.85	23.01	13.32	5.56	2.95	2.79
22.01	6.85	19.14	10.87	2.95	6.95	1.46
35.37	3.84	30.94	17.14	5.08	3.95	2.46
36.26	2.25	31.72	17.57	8.96	2.92	4.34
32.54	2.25	28.52	15.67	8.93	2.93	4.30
40.22	3.84	35.25	19.37	3.84	3.95	1.85
33.87	2.24	29.84	16.02	4.08	2.94	1.93
35.82	2.24	31.56	16.94	7.85	2.94	3.71
33.21	3.04	29.27	15.70	8.74	3.15	4.13
37.52	3.84	33.73	16.43	8.38	3.96	3.67
25.32	3.40	23.02	10.55	1.16	3.40	0.48
25.02	6.89	22.75	10.41	-1.09	7.28	-0.45
29.99	2.17	27.42	12.16	0.68	3.05	0.27
29.36	2.37	26.87	11.84	1.87	3.16	0.75
33.95	0.92	31.09	13.65	4.91	1.56	1.97
32.62	2.17	29.87	13.11	5.20	3.06	2.09
36.03	2.17	33.01	14.43	5.31	3.06	2.13
39.48	3.83	36.21	15.73	6.25	3.97	2.49
35.00	0.92	32.11	13.94	4.33	1.57	1.73
35.15	2.58	32.26	13.97	2.64	3.50	1.05
35.93	3.03	33.08	14.04	5.69	3.17	2.22
38.57	2.16	35.54	14.98	5.00	3.08	1.94
35.75	2.16	32.98	13.80	2.21	3.09	0.85
35.80	2.63	33.09	13.68	3.44	2.77	1.31
32.03	0.91	29.60	12.23	4.63	1.77	1.77
32.71	2.15	30.41	12.05	3.33	3.12	1.23
27.45	3.22	25.53	10.09	1.28	3.37	0.47
28.09	0.90	26.12	10.32	2.01	1.61	0.74
31.33	3.82	29.44	10.71	3.10	3.97	1.06
39.42	3.84	37.07	13.42	3.32	4.15	1.13
25.77	3.40	24.36	8.40	-2.64	3.40	-0.86
27.77	4.04	26.33	8.84	-3.23	4.35	-1.03
32.70	2.88	31.01	10.37	-2.57	3.96	-0.81
30.35	3.83	28.82	9.54	-1.64	4.15	-0.52
25.96	3.02	24.65	8.15	-1.43	3.18	-0.45
30.39	2.48	28.86	9.51	-0.83	3.83	-0.26
26.56	3.40	25.23	8.29	-1.37	3.40	-0.43
32.45	7.22	30.88	9.99	-2.85	7.38	-0.88
26.53	3.85	25.25	8.14	-3.74	4.33	-1.15
36.99	2.87	35.50	10.38	-3.57	4.17	-1.00
36.40	3.94	35.12	9.57	-3.65	4.40	-0.96
40.56	3.82	39.14	10.65	-1.30	4.17	-0.34
13.72	3.41	13.32	-3.29	-22.03	3.59	5.28
14.10	3.21	13.88	-2.49	-23.35	3.39	4.12
12.85	3.41	12.46	-3.16	-22.96	3.59	5.64
13.15	2.60	12.84	-2.80	-21.39	2.60	4.56
15.31	7.01	15.05	-2.85	-23.96	7.19	4.45
23.25	3.40	23.16	2.00	-11.14	3.40	-0.96
22.91	3.00	22.83	1.89	-13.76	3.59	-1.13
22.46	3.60	22.46	-0.19	-15.99	4.00	0.14
22.90	3.20	22.90	-0.17	-12.97	3.40	0.10

20.93	3.20	20.77	-2.57	-18.20	3.20	2.23
26.08	3.20	25.94	2.78	-8.77	3.40	-0.94
29.17	3.20	29.15	1.10	-11.91	3.20	-0.45
28.16	2.42	28.15	-0.40	-15.92	3.77	0.23
31.26	3.16	31.25	0.33	-15.65	4.62	-0.17
-0.38	3.44	-0.34	0.17	-23.70	3.56	10.74
0.68	3.40	0.61	-0.29	-22.31	3.40	9.69
-2.36	2.60	-2.12	1.05	-22.97	4.56	10.17
10.52	3.20	10.18	-2.62	-20.56	3.20	5.12
16.17	3.20	15.94	-2.72	-18.18	3.20	3.06
12.11	1.79	11.95	-1.98	-20.62	4.21	3.37
20.47	0.99	19.99	-4.42	-15.99	2.09	3.45
26.17	0.99	25.41	-6.28	-16.37	1.91	3.93

arc_parallel_e	source	region
-7.44	Gan, et al., 2007	ladakh
-9.60	Gan, et al., 2007	ladakh
-7.44	Gan, et al., 2007	ladakh
-12.17	Gan, et al., 2007	ladakh
-12.38	Gan, et al., 2007	ladakh
-10.67	Gan, et al., 2007	ladakh
-12.77	Gan, et al., 2007	ladakh
-12.30	Gan, et al., 2007	ladakh
-10.89	Gan, et al., 2007	ladakh
-8.17	Jade, et al., 2004	ladakh
-8.62	Jade, et al., 2004	ladakh
-8.80	Jade, et al., 2004	ladakh
-7.31	Jade, et al., 2004	ladakh
-8.38	Jade, et al., 2004	ladakh
-10.71	Jade, et al., 2004	ladakh
-7.93	Jade, et al., 2004	ladakh
-6.88	Jade, et al., 2004	ladakh
-8.73	Jade, et al., 2004	ladakh
-8.36	Gan, et al., 2007	himachal
-7.21	Gan, et al., 2007	himachal
-10.90	Gan, et al., 2007	himachal
-12.27	Gan, et al., 2007	himachal
-11.96	Gan, et al., 2007	himachal
-10.89	Gan, et al., 2007	himachal
-11.65	Gan, et al., 2007	himachal
-13.07	Gan, et al., 2007	himachal
-13.42	Gan, et al., 2007	himachal
-9.49	Gan, et al., 2007	himachal
-10.71	Gan, et al., 2007	himachal
-13.06	Gan, et al., 2007	himachal
-12.15	Gan, et al., 2007	himachal
-13.56	Gan, et al., 2007	himachal
-15.86	Gan, et al., 2007	himachal
-7.89	Gan, et al., 2007	himachal
-12.45	Gan, et al., 2007	himachal
-13.37	Gan, et al., 2007	himachal
-11.11	Gan, et al., 2007	gurla mandhata
-10.53	Gan, et al., 2007	gurla mandhata
-8.20	Gan, et al., 2007	gurla mandhata
-11.21	Bettinelli, et al., 2006	gurla mandhata
-14.29	Gan, et al., 2007	gurla mandhata
-9.99	Bettinelli, et al., 2006	gurla mandhata
-10.31	Bettinelli, et al., 2006	gurla mandhata
-12.00	Bettinelli, et al., 2006	gurla mandhata
-7.65	Bettinelli, et al., 2006	gurla mandhata
-8.24	Gan, et al., 2007	gurla mandhata
-8.77	Bettinelli, et al., 2006	gurla mandhata
-11.64	Bettinelli, et al., 2006	gurla mandhata
-5.90	Gan, et al., 2007	gurla mandhata
-9.79	Bettinelli, et al., 2006	gurla mandhata
-11.21	Bettinelli, et al., 2006	gurla mandhata
-11.86	Gan, et al., 2007	gurla mandhata
-8.54	Bettinelli, et al., 2006	gurla mandhata
-9.99	Bettinelli, et al., 2006	gurla mandhata
-8.64	Gan, et al., 2007	gurla mandhata
-10.27	Bettinelli, et al., 2006	gurla mandhata
-8.09	Bettinelli, et al., 2006	gurla mandhata
-10.69	Bettinelli, et al., 2006	gurla mandhata

```
 -4.78  Bettinelli, et al., 2006  gurla mandhata
-10.03  Bettinelli, et al., 2006  gurla mandhata
-10.28  Bettinelli, et al., 2006  gurla mandhata
 -8.04  Gan, et al., 2007        thakkhola
 -7.89  Bettinelli, et al., 2006  thakkhola
 -9.83  Bettinelli, et al., 2006  thakkhola
-10.24  Bettinelli, et al., 2006  thakkhola
 -4.55  Bettinelli, et al., 2006  thakkhola
 -4.82  Gan, et al., 2007        thakkhola
 -2.57  Gan, et al., 2007        thakkhola
 -4.44  Gan, et al., 2007        thakkhola
 -7.84  Bettinelli, et al., 2006  thakkhola
 -7.83  Bettinelli, et al., 2006  thakkhola
 -3.37  Gan, et al., 2007        thakkhola
 -3.60  Bettinelli, et al., 2006  thakkhola
 -6.92  Bettinelli, et al., 2006  thakkhola
 -7.70  Gan, et al., 2007        thakkhola
 -7.53  Gan, et al., 2007        thakkhola
 -1.05  Gan, et al., 2007        thakkhola
  0.99  Gan, et al., 2007        thakkhola
 -0.62  Bettinelli, et al., 2006  thakkhola
 -1.71  Bettinelli, et al., 2006  thakkhola
 -4.50  Bettinelli, et al., 2006  thakkhola
 -4.76  Bettinelli, et al., 2006  thakkhola
 -4.87  Bettinelli, et al., 2006  thakkhola
 -5.73  Gan, et al., 2007        thakkhola
 -3.97  Bettinelli, et al., 2006  thakkhola
 -2.42  Bettinelli, et al., 2006  thakkhola
 -5.24  Gan, et al., 2007        everest
 -4.61  Bettinelli, et al., 2006  everest
 -2.04  Bettinelli, et al., 2006  everest
 -3.18  Gan, et al., 2007        everest
 -4.28  Bettinelli, et al., 2006  everest
 -3.10  Bettinelli, et al., 2006  everest
 -1.19  Gan, et al., 2007        everest
 -1.87  Bettinelli, et al., 2006  everest
 -2.91  Gan, et al., 2007        everest
 -3.12  Gan, et al., 2007        everest
  2.50  Gan, et al., 2007        everest
  3.06  Gan, et al., 2007        everest
  2.43  Gan, et al., 2007        everest
  1.56  Gan, et al., 2007        everest
  1.35  Gan, et al., 2007        everest
  0.79  Gan, et al., 2007        everest
  1.31  Gan, et al., 2007        everest
  2.71  Gan, et al., 2007        everest
  3.56  Gan, et al., 2007        everest
  3.42  Gan, et al., 2007        everest
  3.52  Bettinelli, et al., 2006  everest
  1.25  Gan, et al., 2007        everest
 21.39  Gan, et al., 2007        bhutan
 22.99  Gan, et al., 2007        bhutan
 22.26  Gan, et al., 2007        bhutan
 20.90  Gan, et al., 2007        bhutan
 23.55  Gan, et al., 2007        bhutan
 11.10  Gan, et al., 2007        bhutan
 13.71  Gan, et al., 2007        bhutan
 15.99  Gan, et al., 2007        bhutan
 12.97  Gan, et al., 2007        bhutan
```

18.07 Gan, et al., 2007   bhutan
 8.72 Gan, et al., 2007   bhutan
11.90 Gan, et al., 2007   bhutan
15.92 Jade, et al., 2007   bhutan
15.65 Jade, et al., 2007   bhutan
21.13 Gan, et al., 2007   arunachal
20.09 Gan, et al., 2007   arunachal
20.60 Gan, et al., 2007   arunachal
19.92 Gan, et al., 2007   arunachal
17.92 Gan, et al., 2007   arunachal
20.34 Gan, et al., 2007   arunachal
15.61 Jade, et al., 2007   arunachal
15.90 Jade, et al., 2007   arunachal

Our first look at the South Lunggar Rift.

Chapter 4:

Miocene initiation and acceleration of extension in the South Lunggar rift, western Tibet: evolution of an active detachment system from structural mapping and (U-Th)/He thermochronology

Authors

Richard H. Styron[1][*][†], Michael H. Taylor[1], Kurt E. Sundell[1], Daniel F. Stockli[1,2], Jeffrey A. G. Oalmann[1], Andreas Möller[1], Andrew T. McCallister[1], Deliang Liu[3], and Lin Ding[3]

Author Affiliations

1: Department of Geology, University of Kansas, Lawrence, Kansas, USA.

2: Department of Geology, Jackson School of Geosciences, University of Texas, Austin, Texas, USA.

3: Institute for Tibetan Plateau Research, Chinese Academy of Sciences, Beijing, China.

* Now at Department of Earth and Environmental Sciences, University of Michigan, Ann Arbor, MI, USA

[†] Corresponding author: richard.h.styron@gmail.com

Abstract

The modern extensional episode in Tibet may have begun in the middle to late Miocene, but there are few robust estimates of the rates, timing or magnitude of Neogene deformation within the Tibetan plateau. We present a comprehensive study of the seismically active, north-trending South Lunggar rift in the western Lhasa block of southern Tibet incorporating mapping, U-Pb geochronology and zircon (U-Th)/He thermochronology. The South Lunggar rift is the southern continuation of the North Lunggar Rift, and comprises a ~50 km N-S central horst bound by two major normal faults, the west-dipping South Lunggar detachment and the east-dipping Palung Co fault. The South Lunggar detachment has a dip at the rangefront of ~20° W, and brings up a well-developed mylonitic shear zone in its footwall displaying ductile and brittle kinematics indicative of normal-sense shear. The majority of the range is composed of felsic orthogneiss, mafic amphibolites, and pervasive leucogranite intrusions dated at ~16 and 63 Ma. Zircon (U-Th)/He cooling ages are Oligocene through late Pliocene, with the youngest ages observed in the footwall of the South Lunggar detachment. We tested ~25,000 unique thermokinematic forward models in Pecube against the structural and (U-Th)/He data to fully bracket the allowable ranges in fault initiations, accelerations and slip rates. We find that normal faulting in the South Lunggar rift began in the middle Miocene with horizontal extension rates of ~1 mm a^{-1}, and in the north accelerated at 8 Ma to 2.5-3.0 mm a^{-1} as faulting commenced on the South Lunggar detachment. Cumulative horizontal extension across the South Lunggar Rift ranges from <10 km in the south to 19-21 km in the north.

1 Introduction

Tibet is an archetypal example of an orogen undergoing syncontractional extension (Figure 1). Many models of Tibetan and Himalayan orogenesis have been proposed that explain or incorporate east-directed extension, such as convective removal of lithospheric mantle [e.g., *England*

and Houseman, 1988; *Molnar et al., 1993*], slab rollback in western Pacific subduction zones [*Yin, 2000*], orogenic collapse and radial spreading [e.g., *Dewey et al., 1988*; *Copley and McKenzie, 2007*], progressive underthrusting of Indian lithosphere [*DeCelles et al., 2002*; *Copley et al., 2011*], or other Himalaya-centric models [e.g., *Klootwijk et al., 1985*; *Styron et al., 2011a*]. Most of these models either make predictions or rely on estimates of the age of onset of Tibetan and Himalayan extension. Additionally, many of these and other models seek to characterize the nature of deformation in the orogen, such as the debate between a continuum-style [e.g., *England and Houseman, 1988*; *Bendick and Flesch, 2007*] vs. block-style deformation of the orogen [e.g., *Avouac and Tapponnier, 1993*; *Meade, 2007*; *Thatcher, 2007*], or the debate between deformation dominantly occurring along the orogen's boundaries [e.g., *Molnar and Tapponnier, 1975*; *Lacassin et al., 2004*] vs. internal deformation [e.g., *Taylor et al., 2003*; *Searle et al., 2011*]. These models are similarly reliant upon predictions or estimates of rates and magnitudes of deformation on faults in the orogen.

Despite the great interest in Tibetan rifting, only a small number of published studies document the onset of Cenozoic east-west extension within the plateau interior north of the Indus-Yarlung Suture Zone (Figures 1, 2), in contrast to the relatively well-studied Himalaya (see *Lee et al.* [*2011*] for a recent summary). In the eastern plateau, *Pan and Kidd* [*1992*] and *Harrison et al.* [*1995*] documented Pliocene cooling of the Nyainqentanglha detachment footwall (Figure 2). *Harrison et al.* [*1995*] modeled rifting beginning at 8 ± 1 Ma with a fault slip rate of 3 mm a^{-1}, a finding that was supported by *J. Kapp et al.* [*2005*]. A similar age was inferred by *Ratschbacher et al.,* [*2011*] to the northeast along the same fault system by ^{40}Ar/^{39}Ar dating of synkinematic micas from the mylonitic shear zone. *Blisniuk et al.* [*2001*] studied a fault zone in the Shuang Hu graben, a local releasing bend in the Muga Purou fault system in central Tibet [*Taylor et al., 2003*], and dated mineralized fault breccia at ~13.5 Ma through Rb-Sr and ^{40}Ar/^{39}Ar methods, which they interpreted as the minimum age of rift initiation on the plateau. At face value, these dates suggest that rift inception across the plateau was very diachronous, although the sample size is quite small. Furthermore, these studies do not robustly estimate slip rates on the faults by rigorously testing

many slip histories against the data in order to better constrain possible deformation histories.

In order to gain a more thorough understanding of the timing, rates and magnitude of Cenozoic exension in Tibet, as well as the potential spatial variations in extension, more data are needed, especially for western Tibet. This study presents structural and neotectonic mapping, zircon (U-Th)/He (zHe) thermochronology, and zircon U-Pb analysis of the little-known South Lunggar Rift (SLR) in the western Lhasa block of Tibet. We document a large (>50 km along strike) and active north-trending rift containing both high- and low-angle normal faulting. The footwall of the low-angle normal fault displays a well-developed mylonitic shear zone and is interpreted as a metamorphic core complex. Data collection was combined with extensive 3-D thermokinematic modeling (~25,000 forward models) to test possible deformation histories against the structural and thermochronometric observations. These results indicate up to 20 km E-W extension starting in the early to middle Miocene, at moderate rates (1-3 mm a^{-1}) following a late Miocene acceleration. Significant along-strike variability in fault geometry, slip rate and net displacement exist as well. In addition to providing new information on extension in SW Tibet, our results have implications for the thermal state of the Tibetan crust. Furthermore, the observations of low-angle normal 'detachment' faulting and large thermochronometric data collection allow for testing of various geometric models of detachment faulting.

1.1 Style and evolution of detachment faulting

Low-angle (<30° dip) normal 'detachment' faults, often exhibiting several to tens of kilometers of extension, have been mapped throughout the world over the past 30 years [e.g., *Wernicke, 1995*]. As these structures are not well understood due to the apparent conflict between their dip angle and standard Andersonian rock mechanical theory [e.g., *Anderson, 1951*] predicting normal fault dips of ~60° and fault locking at low angles, much effort has been put into resolving the contradiction of Andersonian fault theory with field [e.g., *Lee et al., 1987; Yin and Dunn, 1992*], geophysical [*Abers et al., 2002; Morley, 2009*] and geodetic [e.g., *Hreinsdottir and Bennett, 2009; Niemi et al., 2004*] observations. These studies often focus on the geometry of the detach-

ment at depth, and whether faulting initiated at low angle or was first high angle and later rotated to a low angle [e.g., *Spencer, 1984*; *Wernicke and Axen, 1988*]. Prominent models include planar, low-angle fault initiation [e.g., *Wernicke, 1981*]; the 'rolling hinge' model, where the very shallow and very deep parts of the detachment fault are low angle, but the majority of slip within the seismogenic crust occurs at a moderate to high angle [e.g., *Axen and Bartley, 1997*]; and antilistric models, where the detachment fault monotonically steepens with depth [e.g., *Buck, 1988*].

Many of the canonical field studies of detachment faults focused on the Cordillera of western North America (indeed, the typically sheared and metamorphosed antiformal footwalls of detachment faults were initially known as 'Cordilleran' metamorphic core complexes [*Crittenden et al., 1980*], now less parochially 'metamorphic core complexes' or more simply 'core complexes'), which were generally active in the late Cretaceous through Miocene [e.g., *Lister and Davis, 1989*]. Therefore, few studies [e.g., *Daczko et al., 2011*; *J. Kapp et al., 2005*; *Kapp et al., 2008*] have been done on active structures, where considerably more certainty exists on the geometric and geodynamic context, such as the thickness, strain rate and thermal state of the crust and upper mantle.

However, computational simulations of detachment faulting and core complex development are numerous. Though there has been significant variability in the modeling approach, the results typically show detachment faulting to form preferentially in areas of hot, thick crust capable of ductile flow at depth [e.g., *Buck, 1991; Rey et al., 2009*]. These studies also uniformly show the flexural or isostatic 'back' rotation of the footwall away from the detachment fault and hanging wall, leading to an up-dip shallowing of the fault dip, i.e. an 'antilistric' fault geometry [e.g., *Buck, 1988; Rey et al., 2009; Tirel et al., 2008; Wdowinski and Axen, 1992*]. In models that do not specify an initial detachment geometry, some material heterogeneity is often needed to initially localize deformation; this is typically a magmatic intrusion [e.g., *Brun et al., 1994; Tirel et al., 2008*], which is compelling because of the strong association of magmatism and core-complex formation [e.g., *Armstrong and Ward, 1991*].

Thermochronologic techniques have proven invaluable in understanding the rate and style of deformation in a variety of tectonic settings, especially in extensional regions, where progres-

sive down-dip exhumation of a normal fault footwall often leaves a clear thermal signature [e.g., *Stockli, 2005*]. Thermochronologic data in normal fault footwalls are typically interpreted in age vs. elevation or age vs. down-dip distance plots, often by the fitting of linear regression trend lines [e.g., *Fitzgerald et al., 2009*; *Maheo et al., 2007*]. However, this method makes questionable assumptions about the thermal state of the crust, particularly that the geothermal gradient is constant with depth and does not change during faulting, and radiogenic heating is not significant. These assumptions have been shown to be inaccurate enough to cause erroneous interpretations [*Ehlers et al., 2001; Ehlers, 2005*]. Additionally, structural complications such as progressive rotation of the footwall during extension may distort the geometrical relationship of the samples to horizontal geotherms; these complications have to be well-constrained [e.g., *Stockli et al., 2002*]; or ignored. Furthermore, simple regression lines are rarely weighted by age uncertainty, thereby failing to take this important age information into account.

Advances in 2-D and 3-D thermokinematic modeling [e.g., *Harrison et al., 1995; Ketcham, 1996; Braun, 2003; Ehlers et al., 2001*] have enabled the use of complicated fault geometries and dynamic, nonlinear geotherms incorporating radiogenic heating. Furthermore, iterative methods [e.g., *Campani et al., 2010; Ketcham et al., 2005*] allow for model fitting that incorporates formal uncertainties in thermochronometer data, producing much more robust interpretations than previously possible.

Many studies of Himalayan and Tibetan rifting have found evidence of active detachment faulting [e.g., *Burg et al., 1987; Harrison et al., 1995; Jessup et al., 2008; J. Kapp et al., 2005; Kapp et al., 2008; Murphy et al., 2002; Pan and Kidd, 1992; Robinson et al., 2004*], consistent with predictions of detachment fault formation in hot, thick crust [e.g., *Buck, 1991*]. Detachment faults have been mapped in both the North and South Lunggar rifts [*Kapp et al., 2008; Styron et al., 2011b*], and are interpreted to be active. The identification of rapidly-exhumed mid-crustal rocks in the detachment footwalls suggest that extension is locally very significant, and that faults are of significance to deformation of the Tibetan plateau. The structural and thermochronological work presented here on the South Lunggar rift give both an understanding of the rates and timing

of western Tibetan extension and a picture of core-complex activity in a hot and thick orogen.

1.2 Regional Geology

1.2.1 Pre-extensional geology

The southern margin of Eurasia has been tectonically active throughout the Phanerozoic. This activity mostly consists of the successive accretion of multiple terranes that now compose the Tibetan plateau. Accretion of these terranes is generally assumed to young southward, with docking of the Qilian and Kunlun terranes in the Paleozoic, the Qiangtang terrane in the early-mid-Mesozoic and the Lhasa terrane in the mid-late Mesozoic (forming the Bangong-Nujiang Suture Zone, Figure 1) [*Yin and Harrison, 2000*]. The late Cretaceous to early Eocene saw the beginning of India's ongoing collision with the Lhasa terrane along the Indus-Yarlung Suture Zone [*Ding et al., 2005*], creating much of the crustal shortening observed today.

Shortening in central Tibet began in the late Jurassic [*Murphy et al., 1997*] or early Cretaceous [*P. Kapp et al., 2005*] associated with the underthrusting of the Lhasa terrane beneath the Qiangtang terrane [e.g. *Yin and Harrison, 2000*; *Kapp et al., 2007*]. Shortening, accompanied by magmatism, continued throughout the Lhasa terrane until the Paleocene [*Murphy et al., 1997*; *P. Kapp et al., 2005*; *2007*]. Thin-skinned thrust sheets composed of Paleozoic strata were thrust over Mesozoic strata (and vice versa) in the south-central Lhasa terrane, and were sporadically intruded by granites throughout the Cretaceous [*Murphy, et al., 1997*]. During the mid to late Cretaceous, subduction of Neothethyan lithosphere underneath the southern Lhasa terrane produced the Gangdese magmatic arc [e.g., *Ding et al., 2003*].

Following the onset of India's collision, shortening generally ceased in the interior of the Lhasa terrane (inferred from the widespread and essentially flat-lying early Tertiary Linzizong volcanic rocks) [*Murphy et al., 1997*], but was still active until ~20 Ma on its northern and southern margins [*DeCelles et al., 2011*; *P. Kapp et al., 2005*; *2007*; *Yin et al., 1994*] as well as in northern Tibet [e.g., *Lease et al., 2011*]. Several hundred kilometers of shortening were accommodated in the Himalaya at this time, as well [*DeCelles et al., 2002*; *Robinson et al., 2006*; *Murphy, 2007*].

Synconvergent extension in the direction of plate convergence occurred episodically throughout the Oligocene and early Miocene, expressed as activity on the north-dipping South Tibetan Detachment system [*Burg et al., 1984*; *Burchfiel et al., 1992*] and the development of the South Kailas Basin between the Gangdese arc and the thrusts of the Indus-Yarlung Suture Zone [*DeCelles et al., 2011*; *Zhang et al., 2011*].

In the middle to late Miocene, a dramatic change in the style of deformation in the Himalaya and Tibet occurred. Activity on the Main Central Thrust and South Tibetan Detachment, the dominant early Miocene structures in the Himalaya, was significantly reduced if not halted altogether [e.g., *Murphy et al., 2002*] while the dominant zone of Himalayan shortening propagated south [*Meigs et a., 1995*; *DeCelles et al., 2001*]. At this time, the High Himalaya began arc-parallel extension along structures cutting the Main Central Thrust and South Tibetan Detachment [*Thiede et al., 2006*; *Murphy, et al., 2002*; *Styron et al., 2011a*; *Garzione et al., 2003*; *Lee et al., 2011*; *Jessup et al., 2008*]. Within the central and southern Tibetan plateau, shortening via folding and thrusting essentially ceased and an ongoing phase of east-west extension began [*Lee et al., 2011*; *Kapp et al., 2008*], with ongoing shortening, observed geodetically [e.g., *Zhang et al., 2004*] ostensibly accommodated on NE- and NW-striking V-shaped conjugate strike-slip faults in central Tibet [*Taylor et al., 2003; Yin and Taylor, 2011*].

1.2.2 Neogene rifts in Tibet

Neogene extension in Tibet is characterized by roughly north-trending graben in the central Lhasa and Qiangtang terranes [e.g. *Armijo et al., 1986*; *Blisniuk et al., 2001*] (Figures 1, 2). These graben are often linked to V-shaped conjugate strike-slip faults emanating from the Bangong-Nujiang Suture zone [e.g., *Taylor et al., 2003*], although in some cases, such as small graben in the Tanggula Shan and Gangdese Shan, extension may be isolated to areas of high topography (Figure 2). The southern Lhasa terrane contains five major rifts that essentially span the north-south length of the Lhasa terrane, and several subordinate rifts. From east to west, the major rifts are the Yadong-Gulu rift (this rift cuts from the Himalaya to the Bangong-Nujiang suture; the main segment

of the rift through the Lhasa block is called the Nyainqentanglha rift [*Pan and Kidd, 1992; J. Kapp et al., 2005*]), the Pumqu-Xainza rift [*Armijo et al., 1986; Hager et al., 2006*], the Tangra Yum Co rift [*Dewane et al., 2006*], and the Lunggar rift [*Kapp et al., 2008*, this study]. Subordinate rifts include an unnamed and unstudied (to our knowledge), but seismically active (Figure 2) rift to the west of the Lunggar Rift, the Lopukangri rift [*Murphy et al., 2010*] to the southeast of the Lunggar rift, the Xiagangjiang rift to the east of the North Lunggar rift [*Volkmer et al., 2007*], and numerous small graben throughout the western Gangdese range [e.g., Yin, 2000] (Figure 1, 2).

Some estimates have been made of net horizontal extension across the plateau. *Armijo et al.* [*1986*] estimated <3-4 km extension across the Yadong-Gulu and Pumqu-Xainza rifts, and extrapolate to suggest roughly 20 km extension across the plateau, assuming these rifts are representative of all major Tibetan rifts. More recently, *J. Kapp et al.* [*2005*], informed by modern ideas of detachment faulting and continental extension, studied the Nyainqentanglha segment of the Yadong-Gulu rift. They estimated a minimum of 8 km fault slip based on the down-dip length of the detachment fault's mylonitic shear zone, and combine structural and thermobarometric data to suggest 21-26 km of fault slip, assuming the detachment fault slipped at 35 degrees dip. Given this fault dip, their corresponding extension estimates would be 17-21 km based on all results with a minimum of 6.5 km. *Taylor et al.* [*2003*] suggest ~48 km of total right-lateral slip along the southern, right-slip faults in the conjugate fault zone along the Bangong-Nujiang suture that link into south Tibetan graben (i.e. west of the Jiali fault), based on mapping and remote sensing interpretation of the Lamu Co and Riganpei Co faults. Slip on these faults may be comparable to extension in the linked graben (Figure 1, 2). Preliminary mapping in the Tangra Yum Co [M. Taylor, unpublished mapping] and Pum Qu-Xainza rifts [C. Hager, personal electronic communication] suggest less than 10 km for each rift.

The Lopukangri rift to the southeast of the SLR (Figure 2) is a complex fault system interpreted either as part of the trailing end an extensional imbricate fan in a fault system extending from the Lamu Co fault through the Lunggar rift and southeastward into the Gangdese range, or as a more prominent member of a series of crustal tears with the same geographic extent [*Murphy*

et al., 2010; *Sanchez et al., in review, Journal of Asian Earth Sciences*]. Based on the work of Sanchez et al. [*in review*] and our preliminary field observations, the Lopukangri rift has a long northern segment, with a west-dipping, moderate-angle range-bounding normal fault. Although throw on this fault has not been enough to exhume basement in its footwall, the fault has extremely large normal fault scarps, offsetting Quaternary alluvium by up to 350 m vertically and locally display triangular facets several tens of meters high, suggesting that this segment of the rift is reasonably active. To the north of the rift proper is a rangefront fault striking NW that is interpreted as an oblique slip (dextral-normal) fault that terminates to the NW near the central Lunggar rift and may transfer slip from the North Lunggar rift to the Lopukangri rift. The southern segment of the Lopukangri rift cuts the southern slopes of the Gangdese range, offsetting contractional structures associated with the Indus-Yarlung Suture Zone by ~15 km [*Murphy et al., 2010; Sanchez et al., in review*]. ^{40}Ar/^{39}Ar dating of the footwall of the southern Lopukangri rift suggests rifting began at ~15 Ma [*Sanchez et al., in review*].

1.3 Lunggar Rift

The Lunggar Rift is a major north-trending rift in the western Lhasa terrane [*Armijo et al., 1986*; *Kapp et al., 2008*; *Elliott et al., 2010*] (Figure 2, 3). It is kinematically linked in the north to the Lamu Co right-lateral strike-slip fault, part of the V-shaped conjugate fault system running along the Bangong-Nujiang Suture Zone [*Taylor et al., 2003*] . The rift is over 150 km along strike, and made up of northern and southern segments separated by an accommodation zone (Figure 3). The northern segment, or the North Lunggar Rift (called the Lunggar Rift by *Kapp et al.* [*2008*] and *Woodruff et al., in review)*, consists of an east-dipping low-angle detachment fault separating a narrow (<10 km wide) supradetachment basin from an elevated footwall composed of variably-deformed granitoids, orthogneiss, and metamorphosed Paleozoic sedimentary rocks. The detachment is inactive at the rangefront, as indicated by unfaulted moraine and alluvial material overlying the fault trace. However, both east and west dipping normal faults offset Quaternary alluvium in the supradetachment basin and are parallel to the range-bounding detachment, suggesting they sole

into the detachment at depth [*Kapp et al., 2008*]. Relief in the North Lunggar Rift approaches 2 km, and maximum footwall elevations are ~6500 m. The accommodation zone between the North and South Lunggar rifts consists of a less-elevated (peak elevations generally <6000 m) footwall made up of the Cretaceous thin-skinned thrust belt that forms the pre-extensional surface in adjacent regions [*Murphy et al., 1997*].

The South Lunggar Rift (Figure 4) is made up of a central horst block, the Surla Range, which is bounded on both the east and west by normal faults. Well-developed basins are found on both sides of the Surla Range. Quaternary cumulative fault scarps on flanks of the Surla Range and active seismicity indicate that extension in the SLR is ongoing. The Swedish explorer Sven Hedin was likely the first Westerner to describe the geography and geology of the SLR during his passage through in June, 1908 [*Hedin, 1909*]. He noted the extensive glaciation and wide distribution of granite boulders in the western rift valley. He also described feeling moderate ground shaking due to an earthquake at approximately 9:30 PM (local time) on 28 June, 1908 while in Sailipu, a short distance to the west. To our knowledge, this is the first field geologic study of the SLR since Hedin's.

2 Bedrock and surficial geology of the South Lunggar Rift

2.1 Bedrock Units

The Surla Range in our map area is dominantly composed of amphibolite-grade metamorphic rocks (**ma**) and greenschist-facies volcanic rocks (**gv**) intruded by variably-deformed leucogranites (**g**, **myl**). Hanging wall rocks on both sides of the rift include unmetamorphosed volcanic rocks (**v**) and sedimentary rocks composing a Cretaceous thin-skinned thrust belt (**K**) (Figure 3, Figure 4). In general, ice and moraine cover and extensive talus development limited access to bedrock exposure, inhibiting more extensive sampling, measurement of structural data and contact identification, although high walls of glacial valleys and sporadic outcrop allowed for confident mapping of rock units.

The amphibolite-grade metamorphic unit (**ma**) is a composite unit of different rock types,

mapped as one unit. The unit is composed of coarse-grained biotite amphibolite, biotite granite orthogneiss, and biotite granodiorite orthogneiss. The orthogneiss is locally migmatitic. Contacts between the different subunits were not observed, and relationships are uncertain. Foliations in the orthogneiss are strongly developed with individual bands mm to 10s of meters in thickness. Amphibolites are unfoliated to moderately foliated at the hand sample to meter scale, and a well-developed foliation is visible in glacier-polished valley walls (Figure 5c). The foliation is generally north-dipping, though significant variability exists (Figure 4), and is therefore interpreted to be unrelated to the modern phase of extensional deformation. Leucogranite intrusion is widespread, and locally preferentially occurs along foliation planes (Figure 5c). Lower-grade (greenschist facies) felsic to intermediate fine-grained metavolcanic rocks (**mv**) are present in two major areas (Figure 4) and in small lenses (below map resolution) on the northern margin of the range. Biotite displays kink banding and alteration to chlorite, indicative of greenschist facies metamorphism. These rocks are observed to be intruded by granites, though the nature of contact between higher-grade metamorphic rocks was not observed. The unit may correlate to the Burial Hill volcanic rocks mapped by *Murphy et al.* [*1997*] along strike ~150 km to the east.

Biotite leucogranite intrusions (**g**) are widespread, from meter to up to 10s of km scales (Figure 4, 5c). These intrusions are observed in the metamorphic units (**ma**, **gv**). U-Pb ages (Section 4) indicate both Gangdese (~65 Ma) and early- to mid-Miocene (22-16 Ma) crystallization ages, although there are no significant petrologic differences between rocks of different ages. Therefore the large leucogranite bodies may be made up of smaller plutons that intruded episodically over 10s of m.y. In the northwestern Surla Range, structurally below the South Lunggar Detachment, the leucogranite is heavily sheared into a mylonitic zone (**myl**).

Hanging-wall rocks consist of a Cretaceous thrust belt of Paleozoic and Mesozoic supra-crustal rocks (**K**) [*Murphy et al., 1997*] and unmetamorphosed biotite-and hornblende-bearing felsic volcanic rocks (**v**). These volcanic rocks have a middle Miocene zHe cooling age (16.8 ± 0.8 Ma; Figure 4, Table 1), interpreted as an eruption age due to its vesicular texture suggesting little to no post-deposition burial and exhumation. The presence of hornblende, not found in the

leucogranites, suggests an eruptive source external to the Surla Range.

2.2 Quaternary units

Quaternary sedimentary units are dominantly the products of erosion of the Surla Range massif, and include two generations of Quaternary alluvium (**Qa** and **Qo**), Quaternary moraine and outwash (**Qm**) and Quaternary shorelines (**Qsh**). **Qo** is the older Quaternary unit, cut off from modern depositional systems by uplift or drainage reorganization. **Qa** is found in active to recently active depositional environments. The age of **Qm** is unknown, but it is reworked by the highest shorelines (**Qsh**), which are dated at the nearby Ngangla Ringco (Figure 3) at ~10.4 ka [A.M. Hudson, electronic personal communication, 2012].

3 Structural geology of the South Lunggar Rift

The Surla Range is uplifted on its eastern flank by a moderately east dipping normal fault, here named the Palung Co fault, and on its northwestern side by a low-angle west-dipping normal fault, here named the South Lunggar Detachment, which is linked with moderate to high angle west-dipping normal faults on the northwestern and southwestern margins of the Surla Range.

3.1 Palung Co Fault

The Palung Co Fault is a moderate-angle east-dipping normal fault striking 20˚ in the north and 350˚ in the south (Figure 3). The fault is ~80 km along strike, and cuts into the Gangdese (Transhimalaya) Range south of the Surla Range. Where it bounds the Surla Range, it forms 40˚ - 50˚ east-dipping triangular facets up to 1 km high. A lake, Palung Co, occupies much of the ~10 km wide rift basin east of the fault trace (Figure 4). The fault has uplifted leucogranites and amphibolites in the footwall 1.5 km above the sedimentary and volcanic rocks in the hanging wall, giving a minimum amount of throw of 1.5 km; however, the estimated sedimentary and volcanic cover thickness of ~8 km [*Murphy et al., 1997*; *2010*] and young zircon (U-Th)/He cooling ages (Section

5) suggests throw on the fault may be greater. Interpretation of rift morphology [e.g., *Friedmann and Burbank, 1995*] and thermochronology suggest that the area near Palung Co is the zone of maximum fault displacement. The Palung Co Fault is currently active, as indicated by small fault scarps in ground moraine visible in remote sensing imagery near the fault's northern tip (Figure 4). Additionally, in August 2008 a series of earthquakes occurred along the fault. The largest was a M_w 6.7 normal faulting event [*Elliott et al., 2010*; *Ryder et al., in press, Journal of Geophysical Research*]. Body-wave seismology and synthetic aperture radar interferometry (InSAR) indicate the rupture occurred on two fault planes, one projecting directly to the rangefront fault in the study area and the other several km to the south [*Elliott et al., 2010*]. Those authors estimated the northern rupture to be striking 20° and dipping 43 ± 2° E, in very close agreement with our field observations. Their modeling suggests that the top of the northern rupture patch was 2-5 km deep, and the bottom was 14-20 km deep. The shallow termination of seismic slip and InSAR phase continuity across the fault trace [*Elliott et al., 2010; Ryder et al., in press*] is consistent with our observations from mapping the area 12 months after the event indicating no obvious surface rupture. The southern rupture is roughly along strike of the northern rupture, but is south of a change in the mapped fault strike and cuts into the high topography in the Surla Range or Gangdese Range (the two ranges merge at this latitude), and has no clear geomorphic expression [*Elliot et al., 2010*]. This difference in strike between the rangefront and the rupture possibly represents the southward propagation of the northern Palung Co Fault and cessation of activity on the previous southern segment to the east, consistent with models of developing normal fault systems that hypothesize the simplification and organization of rift geometry into one relatively planar master fault through time [e.g., *Bosworth, 1985*].

3.2 South Lunggar Detachment

The northwestern portion of the Surla Range is uplifted along the South Lunggar Detachment (SLD). The SLD is a shallowly north- to west-dipping normal fault that is interpreted to link at depth with the steeper range-bounding normal faults to the north (Figure 3); however, thick

moraine cover obscures the fault linkage at the surface, though possible fault scarps in moraine suggest partitioning of normal and strike-slip motion into two main strands (Figure 4). To the south it is linked with a moderate-angle normal fault (Section 3.3), though we restrict the use of the name 'South Lunggar Detachment' to the northern fault. In its footwall, the SLD has exhumed leucogranite and amphibolite. In places on the western rangefront, triangular facets dipping ~20˚ W are preserved (Figure 7), though extensive glaciation has modified the rangefront elsewhere. Except in its southern extent, hanging wall rocks are not observed near the trace of the SLD due to thick moraine cover and the fault is not observed in bedrock.

Immediately below the detachment, footwall leucogranites display a mylonitic shear zone >100 m thick. Foliation planes in the mylonites strike parallel to the local trend of the rangefront, and where measured (at lower elevations) dip ~20˚, though the shear zone is observed to flatten out to <10˚ at the crest of the range (Figure 6c). Lineations, defined dominantly by ribbons of quartz, are consistently oriented WNW with much less variance than the strike of the foliations (Figure 4); slip on the northern part of the SLD is highly oblique (see kinematic data on Figure 4). Kinematic indicators such as S-C fabrics, sigma and delta clasts indicate a top down to the west, normal sense of shear (Figure 6a, b). Large feldspar crystals show brittle deformation instead of ductile deformation, indicating that mylonitization was not entirely in the ductile regime as might be expected if the shear zone formed during magma emplacement. The mylonitic shear zone is therefore interpreted to be the exhumed down-dip extension of SLD shear in the brittle-ductile transition zone. The orientation of foliations broadly defines an antiform that we suggest is a single corrugation of the detachment footwall, with the antiformal axis trending in the direction of extension (Figure 4). This configuration is similar to analogous structures well-defined in the Basin and Range extensional province of the western US [e.g., *Deubendorfer et al., 2010; John et al., 1987*], as well as in metamorphic core complexes world-wide [e.g., *Spencer, 2010*].

Brittle structures in the SLD footwall consist of chatter marks on the west- to north-dipping foliation planes, with steps consistent with top-W (normal sense) displacement. East-dipping low-angle normal faults with mm to cm scale offsets were also observed; these are interpreted to be

products of flexural rotation of the footwall through the upper (antilistric) part of a rolling hinge [e.g. *Buck, 1988*; *Axen and Bartley, 1997*]. This interpretation is supported by the observed shallowing of the mylonitic shear zone at the crest of the Surla Range, and by (U-Th)/He data and thermokinematic modeling (Section 5).

Though no seismic events on the SLD are represented in global catalogs, it is believed to have been recently active due to well-developed fault scarps along its trace (Figures 3, 6). The largest fault scarps associated with the SLD are 2 and 3 km basinward of the rangefront (Figure 4). These two west-dipping fault scarps cut a large lateral moraine extending into the basin and have a cumulative ~112 m of down-to-the-west throw, as determined by Jacob staff field measurements. These faults are considered to sole into the SLD at depth; observations of much smaller scarps at the SLD's trace at the rangefront immediately east implies that the SLD is active and uncut by the faults in its hanging wall. This arrangement of faults is similar to that observed in the North Lunggar Rift [*Kapp et al., 2008*], although in the North Lunggar Rift the detachment is inactive at the range front; the important point is that the dominant neotectonic expression of faulting has migrated away from the rangefront, but slip is interpreted to occur along the detachment at depth. The dissection of the detachment hanging wall by high-angle normal faults is a very common feature of low-angle normal fault systems in the Basin and Range and may be a consequence of isostatic uplift of the footwall following tectonic exhumation [*Kapp et al., 2008*], and possibly as part of an evolving rolling-hinge detachment system [e.g. *Axen and Bartley, 1997*].

The structure of the northern Surla Range, where bound by the SLD, is shown in a cross section across the range (Figure 8a). The observed gently antilistric geometry of the detachment fault and underlying shear zone are continued at depth. The maximum amount of possible extension in the South Lunggar Rift can be estimated by the horizontal distance between pre-extensional strata in the hanging walls. This distance is ~20 km at the latitude of the section, although it increases northward. This estimate is dependent on the depth of the flanking rift basins, which is unconstrained; the deeper the basins, the greater the distance between the pre-rift hanging wall strata. By limiting basin depth to less than 1 km, consistent with observations of other supradetachment

basins [*Cogan et al., 1998*; *Friedmann and Burbank, 1995*], we obtain a lower-bound estimate for maximum extension. ZHe ages young westward, suggesting that the SLD has accommodated significantly more exhumation (and therefore extension) than the Palung Co Fault at this latitude. This requires top-east horizontal-axis rotation of the Surla Range away from the detachment fault as has been suggested for detachment footwalls elsewhere in Tibet [e.g., *J. Kapp et al., 2005*; *Kapp et al., 2008*] and worldwide [e.g., *Buck, 1988*]. This is discussed in more detail in Section 5.

3.3 Moderate angle normal fault

To the south of the SLD, uplift of the Surla Range is accommodated by a moderate to high angle normal fault. The fault changes strike from NNE in the north, near the SLD, to E-W in the south as it wraps around west to bound the southern margin of the western South Lunggar rift basin (Figure 3). Though the fault is not exposed, subordinate high-angle (~55˚) west-dipping small-displacement faults in the footwall are likely parallel to the master fault. The rangefront of the Surla Range becomes significantly steeper south of the SLD as well. Quaternary fault scarps on the range-bounding fault were not definitively observed in the field. Cross-section B-B' (Figure 8b) characterizes the southern part of the Surla Range. Maximum extension across this section is ~16 km, with the same assumptions and caveats as the northern cross-section. As discussed in more detail in Sections 5 and 6, zHe data and thermokinematic modeling suggests that at this latitude, both the west-dipping and east-dipping (Palung Co Fault) structures have accommodated similar amounts of exhumation, and little to no horizontal-axis rotation of the Surla Range has occurred.

3.4 Footwall structures of the Surla Range

No major structures were mapped within the interior of the Surla Range; however, fault surfaces were found in almost every outcrop in the southern Surla Range, where older rocks were more exposed and accessible. These dominantly strike roughly E-W, although some high-angle N-striking fault surfaces were observed (Figure 4). No evidence was found for a shallowly west-dipping fabric that could have been reactivated during extension and influenced detachment fault

geometry..

A well-developed foliation, with planes meters to 10s of meters thick, dips northward moderately to gently (Figure 6); in places, it is unclear if this fabric is a true metamorphic foliation or if it is an intrusive complex, with younger leucosomes intruding older mafic and felsic rocks (possibly along a pre-existing fabric). In most locations, no foliation was observed in the mafic rocks (mostly amphibolites) at the outcrop scale, although they were generally more pervasively faulted. This may indicate that metamorphism occurred at relatively low temperatures, and the amphibolites deformed brittlely while the felsic orthogneisses deformed ductilely. Alternatively, this could indicate that the mafic rocks are younger than the foliation event; these may be basalt dikes that were subsequently metamorphosed to amphibolite facies under low differential stress.

3.5 Accommodation zone

The northern Surla Range decreases in elevation to the north, into the accommodation zone between the North and South Lunggar rifts. The Palung Co Fault and the North Lunggar Detachment tip out on the east side of the range here, and uplift is only accommodated on the western fault, which runs north from the SLD to the southern North Lunggar Shan. ZHe cooling ages are Oligocene for rocks in the footwall of this western fault, indicating limited exhumation (see Section 5). Steep topographic breaks and exhumation of granites and gneisses juxtaposed against lower grade rocks suggest that significant normal faulting exists within this zone in addition to the rangefront faults (Figure 3, Figure 4), although this area was not mapped in detail.

4 Zircon U-Pb geochronology

Zircons from a mylonite sample (SLW-NMT-02) from the SLD shear zone and a mildly deformed leucogranite sample (SLW-SFTR-02) were dated by the U-Pb method with laser ablation ICP-MS in order to bracket the timing of magmatism and place age constraints on other map units and geologic events through cross-cutting relationships. Two samples were selected because

they both display evidence of ductile deformation and have Pliocene zHe cooling ages, raising the possibility that ductile deformation was syn-kinematic, and that cooling ages may be young because of residual heat from magmatism. The first possibility is relevant because it may indicate that observed mylonitization may be a result of intrusive processes instead of detachment faulting [e.g., *Daoudene et al., 2012*], challenging our interpretation of the northern Surla Range as a metamorphic core complex. The second possibility is relevant because residual heat from magmatism would invalidate the assumption of cooling due to exhumation, rendering our thermochronologic interpretations inaccurate. Alternately, if these leucogranites are very old, the observed ductile deformation may be due to a previous deformational episode involving ~E-W extension, also challenging our core-complex interpretation.

4.1 Methods

U-Pb ages were determined by laser ablation inductively coupled plasma mass spectrometry (LA-ICP-MS) using a Thermo Scientific Element 2 ICP/MS at the University of Kansas. A Photon Machines 193nm ArF excimer laser was used to ablate 29 µm spots on whole zircon crystals placed on double sided-tape. The laser was set to 3.5 J cm^{-2} fluency at 10 Hz repetition rate, which produced ablation pits of ~20 µm depth, with the ablated material carried to the ICP/MS in He gas with a flow rate of 0.74 L min^{-1}, tied in with Ar gas at 1.0 L min^{-1} flow rate with a Y-connector 15 cm down flow from the ablation cell. Elemental fractionation, down-hole fractionation and calibration drift were corrected by bracketing measurements of unknowns with GJ1 zircon reference material [*Jackson et al., 2004*] and data reduction using the VisualAge data reduction scheme [*Petrus et al., 2011*] for the IOLITE software package [*Paton et al., 2011*]. Because the zircon crystals were not polished, multiple growth zones were ablated during some analyses. Ages were calculated only for the outermost growth zones (rims) in these cases. Within run reproducibility of the GJ1 reference material [*Jackson et al., 2008*] was better than 2% on the U-Pb age. Results were corrected for diffusive lead loss and common lead with the methods of *Andersen* [*2002*].

4.2 Results

Results are shown in Figure 9 and Data Table S1. Python code to calculate statistics is given in the auxiliary materials (calculate_weighted_means.py and geochron_stats.py). Sample SLW-SFTR-02 (Figure 9a) has a ^{238}U/^{206}U weighted mean age of 63.1 ± 0.78 Ma (95% confidence: $2\sigma/\sqrt{n}\sqrt{n}$, n=19, MSWD=0.51). This suggests it is related to Gangdese magmatism, as the sample is ~20 km from the northern margin of the Gangdese range. Zircons from sample SLW-NMT-02 (Figure 9b) display evidence of zoning (major, step-wise changes in isotopic ratios during laser ablation) and yield early Miocene rim ages, with a ^{238}U/^{206}U weighted mean age of 16.2 ± 0.77 Ma (n=15, MSWD=2.0). The sample also shows two populations of rim ages, a dominant group (n=11) with a ^{238}U/^{206}U weighted mean age of 15.9 ± 0.53 Ma (MSWD=2.2) and a lesser one (n=4) of 21.0 ± 0.84 (MSWD=0.29). These crystallization ages are ~58 and ~12-17 Ma older than the zHe ages for each sample (5.1 ± 0.5 Ma and 3.4 ± 0.2 Ma, respectively; Section 5, Table 1), confirming that Pliocene cooling age for sample SLW-SFTR-02 is not likely to be the result of residual magmatic heat. It is possible that some residual magmatic heat could influence the zHe age of sample SLW-NMT-02, although this effect is likely small, because the zHe age is only ~1.5 m.y. younger than the zHe age from the Paleocene granites to the south, and is from an area that appears to be exhumed more rapidly based on the much larger Quaternary fault scarps and localization of extension on the SLD at that latitude. Additionally, though SLW-NMT-02 displays evidence of zoning, U and Th concentrations are not systematically higher in the rims than in the cores of the zircons, indicating that the (U-Th)/He ages are not influenced by compositional zoning of parent isotopes.

Given that the fabrics in both the Paleocene and early Miocene leucogranites are indicative of ~E-W extension, which has not been documented in southern Tibet before the middle Miocene, these fabrics are likely the result of Neogene extensional processes and unrelated to magmatic processes. This is supported by the observation that feldspars within the mylonitic shear zone show only slight evidence for ductile deformation, and pervasive brittle deformation, suggesting that mylonitization took place at cooler temperatures than would be expected for syn-intrusive

deformation [see *Daoudenne et al., 2012* for the converse case].

5 Zircon (U-Th)/He thermochronology

In order to understand the history of deformation in the South Lunggar rift in a quantitative fashion, we used zircon (U-Th)/He, or zHe, thermochronology. This is a technique that utilizes the temperature-dependent diffusion of radiogenic ^{4}He out of a mineral grain to understand the cooling history of that grain. More specifically, it quantifies the time since a mineral grain cooled through a temperature range that is a function of the diffusion parameters for that type of mineral and the cooling rate, approximated by a 'closure temperature' [*Dodson, 1973*]. For rapidly-cooled zircons (e.g., cooling rates of 20-100 ˚C Ma^{-1}), this closure temperature is ~190-200 ˚C [*Reiners, 2005*]. The thermal sensitivity window (defined as a temperature range) yields a depth range termed the 'partial retention zone' via the geothermal gradient. Below the partial retention zone, radiogenic ^{4}He is diffused out of the grain as fast as it is produced, while above this zone, diffusion is extremely slow.

The temperature and depth sensitivity of zHe thermochronometry is ideal for studying rifts with significant amounts of exhumation, because the partial retention zone is deep enough to be less sensitive to surface processes such as erosion and hydrothermal circulation than for lower temperature thermochronometers such as apatite, while still being shallow enough to be responsive to tectonic exhumation [*Reiners, 2005*].

5.1 Zircon (U-Th)/He results

Zircons from 33 samples (2-6 single-grain aliquots per sample) were run for (U-Th)/He analysis at the University of Kansas Isotope Geochemistry Laboratory following procedures described by *Wolfe and Stockli* [*2010*]. Individual aliquot outliers were rejected according to Peirce's criterion [*Ross, 2003*] Mean sample results are shown in Table 1, and individual aliquot results are shown in Table DR2. The cooling ages of all samples in the Surla Range are late Miocene to Pliocene (Figure 4, Table 1), indicating that late Miocene to present exhumation for the entire range

has been greater than the depth of the pre-extensional zircon He partial retention zone, i.e. >5-10 km for mean geothermal gradients of 40–20 ˚C km^{-1}. In general, ages increase both with elevation and with distance from the SLD. For the northern sampling transect, corresponding to cross section A-A' (Figures 4, 8a), cooling ages decrease monotonically from 7.3 ± 0.6 (1σ) in the east to 3.4 ± 0.2 in the west, at the SLD trace (Figure 10b). This cooling pattern suggests that cooling has been accommodated by progressive exhumation and top-to-the-east rotation of the SLD footwall. For the southern sampling transect (Figures 4, 8b) cooling ages decrease from 7.3 ± 0.6 for the highest sample, in the center of the range, downhill and to the east and west (Figure 11). Age-elevation relationships are generally similar for both sides of the Surla Range, though there are more samples on the west side. This pattern suggests relatively vertical uplift of the Surla Range at this latitude, accommodated equally on both range-bounding faults. The eastern range-bounding fault, the PCF, has a stepover between two fault strands where this sampling transect crosses it. Samples from in between the two fault strands show 10-12 Ma cooling ages (Figure 4), suggesting that the tectonic sliver in between the fault strands was not exhumed as much or as rapidly as the main Surla Range.

Cooling ages older than late Miocene are found in two locations: an age of 16.8 ± 0.8 Ma for a tuff (unit **v**) in the western rift basin, which is interpreted to be the depositional age of the tuff, as its brittle, vesicular texture is not indicative of deep burial. A metavolcanic rock (**mv**) in the footwall of the accommodation zone between the North and South Lunggar Rifts and a leucogranite (**g**) that intrudes it yielded cooling ages of 32 ± 7 Ma, 26 ± 6 Ma, These samples are interpreted as being within in or above the mid-Miocene (pre-extensional) zircon He partial retention zone, which limits late Miocene to present exhumation of the accommodation zone to be less than ~5-10 km.

5.2 Thermal modeling with Pecube

Although the data provide a reasonable first-order picture of relative exhumation rates and some information on timing, they do not directly provide the fault slip rates or precisely estimate

93

the timing of rift initiation in the South Lunggar Rift. While some of this information can be obtained through analysis of (U-Th)/He age-elevation or age-fault distance relationships [e.g., *Stockli, 2005*], complications relating to the dynamic thermal (e.g. unknown or transient geothermal gradient, radiogenic heating) and structural (e.g., footwall rotation) state of the extending crust can introduce inaccuracies to such estimates [*Stockli, 2005*; *Robinson et al., 2010*; *Ehlers, 2003*]. We have therefore chosen to analyze our data with the thermochronological finite element modeling code Pecube [*Braun, 2003*]. Pecube iteratively solves the 3-D heat transport equation throughout an imposed tectonogeomorphic scenario, and is able to incorporate these aforementioned parameters that affect thermochronometric ages.

We modeled the data by constructing two 3-D thermokinematic models corresponding to each of our sampling transects. The geometry of each model is based on the cross-section for that transect, and is only wide enough (along strike) to incorporate the samples for that transect, as Pecube does not incorporate along-strike variation in slip rate or faults with varying strikes. The model incorporates modern topography and extends to 80 km depth, representing the modern thickness of the crust [*Nabelek et al., 2011*]. Model topography is steady-state. Sensitivity testing of thermal and fault parameters is given in Section 5.2.3.

Pecube is a forward modeling program that takes fault timing and slip rate parameters, and crustal thermal parameters (such as Moho temperature and radiogenic heat production) as inputs, and outputs thermochronometer ages as well as the model temperature and velocity field. As we seek to constrain the slip histories of all major faults in the study area, we chose to explore a broad range of fault parameters (given in Table 2) that is enough to fully encapsulate the realistic geological possibilities. We allow for a Pliocene change in slip rate (positive or negative), as an acceleration has been suggested for other Tibetan rifts [*Dewane et al., 2006*; *Hager et al., 2006*; *Lee et al., 2011; Sundell et al., 2011*]. Because the relationship between thermochronometer age and any single input parameter is highly nonlinear, it is necessary to iteratively model a large number of parameter combinations spanning the parameter space in order to rigorously estimate the probability distribution of the parameters. Our choice of fault parameters yields hundreds of

thousands of combinations (each combination represents a unique faulting history), not including any variation in thermal parameters. Though the Pecube code is capable of running in an iterative 'inversion' mode designed to seek the combination of parameters that best fits the observed (U-Th)/He cooling ages, our tests with it resulted in convergence towards combinations of parameters that were individually reasonable but yielded magnitudes of net extension that were unacceptably larger than our maximum estimates from geologic mapping. Furthermore, with iterative nonlinear inversion techniques and a large parameter space, it can be difficult to ascertain that the parameter space was fully explored.

Therefore, we chose to take all possible fault parameter combinations, calculate net extension for each combination, and only model those that yield magnitudes of extension consistent with our geologic cross-sections. This yielded 10,397 model runs for the north transect and 13,998 model runs for the south transect. This is a large number of possible fault parameter combinations, but is the minimum number necessary to rigorously characterize the history of normal faulting in the South Lunggar rift at a level of precision appropriate for the data. Fortunately, each model is independent of the others, so the problem lends itself well to running models in parallel on many processors; indeed, the number of independent computations qualifies this as an 'embarrassingly parallel' computational problem in computer science parlance.

In order to run the models in a time-efficient manner, we used PiCloud (www.picloud.com), a Python-based interface to Amazon's EC2 cloud servers. Identical Linux (Ubuntu 11.04) virtual environments were created on Amazon's servers, and Pecube v.3 was installed on each. A Python script was executed on a local machine that assembled and filtered the fault parameter combinations, ran Pecube in the cloud via PiCloud for each combination, and concatenated the results. Although official statistics weren't provided by PiCloud, the total run time versus individual run time suggests parallelization of 30-50x was achieved.

We chose to filter our model results by testing each run to see if all output zHe model ages at the sample locations matched the observed cooling ages at either 1 or 2 standard deviations. Because many ages have very low standard deviations (possibly a consequence of a low aliquot

95

sample size that does not represent the true uncertainty of the cooling age), we obtained no fits at 1σ or 2σ for either model. We re-filtered the data, using the larger of the observed 1σ value or an 8% uncertainty that represents the 2σ standard error for the analytical standard (Fish Canyon Tuff) as the sample error in the modeling. All Python code and binary (.npy) modeling results files are in the supplementary materials.

5.2.1 North Transect (A-A')

The northern transect generally corresponds to cross-section A-A' (Figure 8a; see Figure 16 for model location and Figure S1 for an image of the full FEM geometry). 58 model runs fit the data at 2σ, and none fit the data at 1σ. Initiation of faulting occurred on the PCF first in all model runs and is distributed fairly equally between 10 and 16 Ma, with a median at 12 Ma and a mode at 10 Ma (Figures 12 and 13b). Initiation of the SLD is younger, with the majority of runs (48 out of 58, or 82%) showing an initiation at 8 Ma, with the remainder at 9 Ma.

Initial extension rates (during initial PCF activity but before SLD initiation) were very low; all runs show the PCF slipping at 0.25 mm a^{-1}. Rapid extension began with the initiation of SLD slip, which has accommodated the large majority of extension across the SLR at this latitude. Results indicate initial slip on the SLD between 1.5 and 3 mm a^{-1}, with a median and strong mode at 2.5 mm a^{-1}. Because of the shallow dip of this fault and the small contribution of the PCF to the horizontal extension rate, this is essentially the extension rate across the rift at this latitude (Figure 13a). Results do not strongly suggest a change in slip rate in the Pliocene; median and modal values stay the same, although the runs with low initial rates increased to the modal values (Figure 13a).

Net extension is well constrained at 19-21 km, with only a few results between 19 and 20 km (Figure 13c). The median value is 20.62 km. Exhumation is also significantly greater in the west (due to the SLD) than in the east (due to the PCF). Exhumation of a sample currently at the SLD fault trace is ~10 km given our model geometry and 20 km of slip on the SLD (Figure 16.). However, exhumation along the PCF is less, between 2 and 4 km for 2σ fits. A vertical difference

of 8 km exhumation over the 20 km width of the range yields a differential tilt of ~21˚ to the east, indicating significant back rotation of the SLD footwall, consistent with many models of LANF and core complex evolution (e.g., *Buck, 1991*).

5.2.2 South Transect (B-B')

The south transect model corresponds to cross section B-B' (Figure 8b; see Figure 16 for model location and Figure S2 for an image of the full FEM geometry). The south transect had 786 model fits at 2σ and none at 1σ. Ages of fault initiation of both the PCF and the western fault are fairly similarly distributed between 10 and 18 Ma, with an increasing probability towards the younger ages (Figure 13e). Median initiations for both faults are 12 Ma. Modes for fault initiation are 11 Ma for the western fault and 10 Ma for the PCF (consistent with the northern model).

Extension rates across the SLR for this model are more poorly constrained, between 0.5 and 3 mm a^{-1}; however, there are significantly more fits between 1 and 1.5 mm a^{-1} (Figure 13d). Modal extension rates are 1.0 mm a^{-1} for both before and after a possible Pliocene change in fault slip rate, also giving little support to post-Miocene acceleration. However, the later distribution is more skewed to the high end, and the median values change from 1.0 to 1.3 mm yr^{-1}, owing to an increase in median slip rates (total slip, not simply horizontal extension) of 0.5 to 1 mm a^{-1} on the PCF; this acceleration has uniform distribution over the parameter space between 3 and 6 Ma. Median slip rates on the western fault are 1.0 mm a^{-1} before and after an acceleration. Therefore a subtle change in rate is not ruled out by the modeling, but is unlikely to be of significance.

Net extension across this part of the SLR ranges from 10 to 16 km, with a higher probability at the high end (Figure 13f). As the two faults show similar initiation ages and slip rates, footwall tilt is unlikely to be significant, but slight rotation toward the east is possible, as the PCF may have initiated slightly later and slipped slightly more slowly in its early history (Figure 16).

5.2.3 Sensitivity analysis of fixed model parameters

Though the possible fault slip rates and ages of fault initiation and acceleration were ro-

bustly tested in the previous section, the fault geometry and thermal parameters (radiogenic heat production and Moho temperature) where held fixed at values that produced good results in trials before the main testing phase. Here we analyze these parameters to see how their variations affect our results. For these analyses, we use the northern transect with a faulting history that corresponds to the best model fit from the previous testing, and individually vary one parameter at a time. The results (model ages) are compared to the best-fit model and to the observed zHe ages.

5.3.2.1 Variations in detachment geometry

Although the geometry of the mylonitic shear zone is constrained by field observations in the exhumed footwall of the model, the geometry of the detachment at depth is not. As discussed in Section 1.1, several models of detachment fault geometry exist. Here we run the prominent models (antilistic, planar and rolling-hinge) as well as a model where the northern Surla Range is bound on the west by a planar high-angle normal fault (instead of the low-angle SLD), essentially testing our interpretation of the northern Surla Range as a metamorphic core complex. As a point of clarification, references here to 'antilistic' geometry refer to the decrease in dip of the detachment fault above the exhumed footwall of the range (leading to folding and flattening of the footwall), as opposed to the fault's projection upward with the rangefront dip, which we call 'planar'. We run two 'antilistic' models: one with a low-angle geometry at depth ('low-angle antilistic') and one with a high-angle geometry at depth ('high-angle antilistic'); the fault geometry in the previous section has this same antilistic upper detachment and subsurface dip in between these ('moderate-angle antilistic'). Then, we test the 'rolling hinge' model, with a shallow antilistic geometry and a listric geometry at depth. We also test two 'planar' models, a 'low-angle planar' and a 'high-angle planar' model. Fault geometries are shown in Figure 14a.

The results are shown in Figure 14b. All the antilistic models, including the rolling hinge, produce similar age vs. longitude patterns, although only the moderate-angle antilistic model (used in the main model phase) fits all the data at 2σ. The low-angle antilistic model produces ages that are ~1m.y. older than the observed ages near the western rangefront, but good fits to the

east. The high-angle antilistric model produces ages that are ~1 m.y. too young in the west and good fits in the east. The rolling-hinge model, with a moderate-angle ramp, produces ages that are in between these two models, similar to the moderate-angle antilistric model. These models all incorporate the same antilistric geometry, which produces older cooling ages into the footwall, as is observed in the data. In contrast, the planar fault models produce ages that are slightly younger into the footwall. The low-angle planar model produces ages that are ~1 m.y. older than observations in the west (and identical to the low-angle antilistric model) but become 2-3 m.y. too young in the east. The high-angle model produces ages that are all younger than 2 Ma.

The increase in model ages into the footwall in all antilistric models and the decrease in ages into the footwall in all planar models is consistent with previous studies [e.g., *J. Kapp et al., 2005*; *Campani et al., 2010*; *Robinson et al., 2010*]. It is easily explained by the recognition that, in antilistric models, pre-extensional sample locations have significant vertical separation, and therefore pass through the PRZ at different times, and are rotated to roughly horizontal above the PRZ. In planar models, the footwall is not internally deformed, and the vertical separation of the samples remains constant; however, isotherms are convex upward in the footwall, as the footwall margins are cooled by the colder hanging wall. In all runs, steeper faults produce younger ages. We interpret this to indicate that a steeper fault exhumes deeper, and therefore hotter, rocks; in other words, a steeper fault advects heat upward more efficiently.

The results of this analysis show that the shallow geometry of the detachment fault has a great effect on the cooling ages, and that an antilistric geometry is necessary to reproduce the cooling patterns observed in the northern Surla Range; a planar geometry produces the opposite age-longitude trend. A similar cooling age pattern may be obtained by significant domino-style block rotation, as has been observed in Nevada [e.g. *Stockli et al., 2002*]; however, this is not a possibility in the Surla Range given the opposing dip directions of the range-bounding normal faults. The model results also indicate that the dip of an antilistric detachment at depth does not have a large control on the thermochronometer ages [e.g., *Ketcham, 1996*], and therefore precise determination of this dip would require other methods. Although only the moderate-angle antilistric model fits

the observations at 1σ, it is quite likely that slight variations in the slip rate and timing parameters with other antilistric models could yield similarly good fits.

5.2.3.2 Variations in thermal parameters

Our modeling has assumed a Moho temperature of 1200 ˚C and radiogenic heating of 20 ˚C Ma⁻¹. The Moho temperature is consistent with estimates of 1069-1248 ˚C from studies of middle Miocene xenoliths from the uppermost mantle (50-65 km depth, likely very close to the Moho before late Miocene crustal thickening) from the Sailipu area ~50 km west of the Lunggar Rift [*Liu et al., 2011*]. The heat production value converts to heat production of 2.39 μW m⁻³ for a granite with a density of 2700 kg m⁻³ and heat capacity of 224.607 J mol⁻¹ K⁻¹ (calculated at standard temperature and pressure using the equations of *Whittington et al.* [*2009*]). This heat production is low for granite [e.g., *Förster and Förster, 2000*], and lower than mean estimates for the Appalachian orogen of ~3 μW m⁻³ [*Jaupart et al., 2007*], which may be representative of Phanerozoic collisional orogens. Given the great thickness of the modeled crust, these thermal parameters result in very high temperatures in the middle crust.

Varying the heat production to half its value, 10 ˚C Ma⁻¹, caused a dramatic change in the modeled ages (Figure 14b). Given the colder resultant geotherm, faulting was insufficient to entirely exhume the footwall from below the pre-extensional zircon He partial retention zone. The samples near the trace of the SLD were exhumed from that depth, but are still several m.y. too old. Lowering the Moho temperature to 900 ˚C lead to ages several m.y. too old in the eastern part of the footwall, but samples near the SLD trace were of acceptable age.

The geothermal gradient in our preferred model is over 40˚ km⁻¹ in the upper several km of the crust before extension (Figure 15b). Within the footwall block near the detachment fault trace, rapid uplift and tectonic exhumation lead to vertical advection of heat and a compression of isotherms, giving a geothermal gradient of >70˚ km⁻¹ in the shallowest crust. Though these geothermal gradients decrease rapidly with depth, the geotherm for the crust remains elevated.

Because net extension in this preferred model is at the upper limit of what is acceptable

given the structural constraints, it is not possible to increase the slip rates on the faults in order to compensate for a colder upper crust. While Tibet is almost uniformly declared to have a hot crust [e.g., *Beaumont et al., 2001*; *Francheteau et al., 1984*; *Hu et al., 2000*; *J. Kapp et al., 2005*], the extremely high modeled temperatures in the lower crust are almost certainly too high. This may be the weakest result of our study. We suggest that radiogenic heat production in the crust is non-uniform, and is probably greatly concentrated in the upper 10-20 km of the crust, due to pervasive intrusions of leucogranites [e.g., *J. Kapp et al., 2005*; *Kapp et al., 2008*, this study] that are highly enriched in radioactive elements. However, it is not possible to implement depth-dependent radio-genic heating in the available version of Pecube.

6 Discussion

6.1 Evolution of the South Lunggar Rift

The geology, thermochronology and geochronology of the South Lunggar Rift indicate a rift characterized by a central horst block bounded by east- and west-dipping normal faults. In the northern SLR, extension and exhumation are dominantly accommodated on the west-dipping South Lunggar Detachment. Farther south, the east-dipping Palung Co fault becomes the dominant structure. Horizontal extension across the SLR ranges from 19-21 km at the latitude of the SLD to 10-16 km at the latitude of the southern transect. Extension decreases abruptly to the north and likely to the south as well, although perhaps more gradually. Extension rates also increase from south to north, from ~1 mm a^{-1} to ~2.5 mm a^{-1} at the latitude of the SLD. Fault initiation is broadly contemporaneous, though there is some probability of an earlier initiation in the south. The onset of more rapid extension in the north is much better constrained, and is most likely at ~8 Ma, with the initiation of the SLD (Figure 12). Extensional faulting appears to have initiated during or a few million years after episodic magmatism in the rift; it is possible that thermal weakening associated with magmatism allowed for the onset of extension.

6.2 Comparison with the nearby rifts

Observations and modeling results from the SLR are generally similar to the North Lunggar rift [*Kapp et al., 2008*; *Sundell et al., 2011*]. ZHe ages from the North Lunggar detachment footwall are the same age or up to 1-2 m.y. younger than samples from the same relative position in the SLD footwall, likely indicating more rapid extension, although the detachment could be steeper at depth in the north or the crust could be hotter. Furthermore, the structural and (U-Th)/He age distribution patterns in the North Lunggar rift are much more continuous along strike [*Sundell et al., 2011*].

The Lopukangri rift [*Sanchez et al., in review*] shows a similar age of fault initiation of ~15 Ma for the southernmost rift segment, which cuts the southern Gangdese range and structures of the Indus-Yarlung suture zone. The northern rift segment is undated, but the presence of supra-crustal rocks (dominantly volcanic rocks) in the footwall suggests that exhumation is less than in the SLR. However, Quaternary normal fault scarps up to 350 m high suggest that modern rifting is rapid.

6.3 Thermal state of the Tibetan crust

The distribution of late Miocene to Pliocene zHe ages and the upper bounds on net extension across the SLR indicate moderate exhumation rates of very hot upper crust. The inference of hot crust is supported by a variety of observations. Volcanism and magmatism are ubiquitous in southern Tibet, and appear to have continued at least until ~16 Ma in the SLR. Younger (~9 Ma) leucogranites have been dated in the footwall of the North Lunggar Rift [*Kapp et al., 2008*]. Leucogranites give evidence of magmatism derived from low degrees of partial melting, as might be expected of a high overall geotherm, and the ultrapotassic volcanic rocks containing very hot upper mantle xenoliths [*Liu et al., 2011*] indicate that the basal temperatures were high as well. Hot springs in the North Lunggar rift also provide independent evidence of elevated modern-day crustal heatflow, although these were not observed in the south. The 'Zhongba' 2008 earthquakes on the Palung Co fault may give some idea of the local geotherm, as well. InSAR and teleseismic body wave modeling of the events gives a centroid depth of ~8-9 km, with slip extending 3-4 km

below that [*Elliott et al., 2010*; *Ryder et al., in press*]. If the centroid depth lies just above the brittle-ductile transition, as is commonly inferred [e.g., *Sibson, 1983*; *Ellis and Stöckhert, 2004*], then temperatures may be ~350 degrees at that depth, which is well in agreement with our model away from the detachment footwall where the geotherm is elevated due to ongoing exhumation (Figure 15).

Evidence for high crustal temperatures from outside the Lunggar region is widespread. We observed geysers near Raka, along the Indus-Yarlung Suture Zone, at approximately 29.60˚ N, 85.75˚ E. *Franchetau et al.* [*1984*] estimated high heat flow from elevated temperatures in lake sediment boreholes in south-central Tibet, south of the Indus-Yarlung Suture Zone. Thermo-barometry in the Nyainqentanglha Rift [*J. Kapp et al., 2005*] indicates temperatures within error of our pre-extensional geotherms (Figure 14). *Mechie et al.* [*2004*] located the α-β transition in quartz at ~17 km in the Qiangtang block through seismic methods, indicating an elevated geo-therm there (mean geothermal gradient 39 ˚C km^{-1}), although in the Lhasa block, they found more typical temperatures (mean geothermal gradient 25 ˚C km^{-1}). *Hu et al.* [*2000*] interpolated heat flow observations over the plateau and found very high values (>350 mW m^{-2}) in the Yadong-Gulu rift and moderately high values to the west, although observations are sparse; a similar study by *Wang* [*2001*] showed the plateau to have a high mean heatflow of ~80 mW m^{-2}. The same argu-ment outlined above for elevated temperatures evidenced by shallow seismicity holds for the entire plateau [e.g., *Molnar and Chen, 1987*; *Molnar and Lyon-Caen, 1989*; *Priestley et al., 2008*; *Wei et al., 2010*], and is supported by the short wavelength of rift-flank uplifts indicating a long-term effective elastic thickness of only 2-4 km [*Masek et al., 1994*]. Elevated heatflow is a necessary condition for large-scale lower-crustal flow, which has been commonly inferred to explain flat topography and extension within the plateau itself [e.g., *Cook and Royden, 2008*], ductile injec-tion into eastern Tibet [e.g., *Clark and Royden, 2000*] and extrusion through the Himalaya [e.g., *Beaumont et al., 2001*; *Nelson, et al., 1996*]. Evidence consistent with partial melt in the crust is given by seismic reflections [e.g., *Nelson et al., 1996*], low Vp/Vs ratios [e.g., *Hirn et al., 1995*] and widespread leucogranite magmatism [*J. Kapp et al., 2005*; *Kapp et al., 2008*; *Sanchez et al.,*

in review; this study].

A hot and mobile middle to lower crust may be a necessary condition for the formation of metamorphic core complexes [e.g., *Buck, 1988*], and is very likely to be responsible for the lack of a major regional lowering of topography around the Lunggar Rift, despite large amounts of crustal thinning and extension [*Block and Royden, 1990*]. The mobile crust would be able to flow laterally into the extending region to mitigate the gravitational potential energy contrasts that would be produced by the steep topographic gradients from the crustal thinning. That said, the relatively high number of large lakes, both near the rift and within rift basins bound by moderate to high angle normal faults (but not the supradetachment basins [*Kapp et al., 2008*]), may be indicative of minor regional subsidence, as nearby crust is drawn into the actively-uplifting core complex footwalls. This phenomenon, on a larger scale, has been suggested to explain subsidence of the Zhada basin in the Indian Himalaya between the Leo Pargil and Gurla Mandhata core complexes [*Saylor et al., 2010*].

6.4 Implications for rift and detachment fault development

The SLD is unlike many rift detachment faults in that core-complex type deformation is a relatively localized phenomenon; the western range-bounding normal fault in the central and southern Lunggar rift is ~70-80 km north-south (not taking into account curves in the fault trace), though the SLD and core complex are only about 15 km N-S. However, despite the relatively restricted areal extent of the SLD, it has accommodated greater and more rapid extension and exhumation than any other fault in the SLR. Additionally, faulting along the western rangefront transitions from a typical moderate to high angle normal fault geometry in the south, to low angle, and then back to high angle in the north. Most of the mapped detachment faults in the western US and elsewhere remain at low angle along strike, and are either buried or truncated by other faults on their ends, so the transition from low to high angle is not observed. Some analogs exist: the North Lunggar rift [*Kapp et al., 2008*], the Dixie Valley fault (Nevada) [*Caskey et al., 1996*], the Cañada David detachment, Baja, Mexico [*Axen et al., 2000; Fletcher and Spelz, 2009*], possibly the Mount

Suckling--Dayman Dome metamorphic core complex [*Daczko et al., 2011*], and segments of the Kenya rift [*Morley, 1999*] show an along-strike transition from high to low angle normal faulting, with along-strike widths of low angle faulting similar to the SLD. All of these, including the SLD, are associated with magmatism during or immediately preceding extension. However, magmatism may not be exclusive to the region of detachment faulting; certainly in the SLR, two dated samples are insufficient to fully constrain the extent of Miocene magmatism. These observations show that LANF and core complex development is not a distinct mode of rifting, nor that it will be the dominant extensional mode in a certain geodynamic environment (such as rapid extension in hot, thick crust). Instead, it is an end-member in the spectrum of rifting, but one that is generally associated with high magnitudes of extension and exhumation [e.g., *Abers, 2001; Forsyth, 1992*], as well as synkinematic magmatism [*Parsons and Thompson, 1993*].

The large along-strike variation in uplift and extension over fairly short distances in the SLR (Figure 16) is striking, but is well constrained by the structural and thermochronological observations and modeling. This extension gradient must be accommodated by deformation of the hanging wall, though no suitable structures were observed. A zone of distributed dextral shear to the northwest of the SLD may be present, but difficult to observe due to the cover of water, thick moraine and alluvium.

6.5 Timing and rates of Tibetan extension

Our results in the SLR suggest a minimum age for the onset of extension in southwestern Tibet of ~16-12 Ma (Figures 12 and 13). Furthermore, we find evidence of a rapid increase in extension rate at ~8 Ma in the northern part of the rift, as slip on the SLD began. These results are consistent with, and may reconcile, the few other studies of rifting within the Tibetan plateau. The modeled age of rift initiation here is similar to the results of *Blisniuk et al.* [*2001*] which uses cross-cutting relationships to provide a minimum age of the onset of rifting in central Tibet. Our results give a similar regional minimum, in that activity may have begun earlier on a nearby rift. However, our combination of thermal and structural constraints (limiting maximum extension)

provides both upper and lower bounds on initiation of the SLR itself. Our suggestions of rapid extension related to slip on the SLD are also consistent with work on the Nyainqentanghla segment of the Yadong-Gulu rift indicating a phase of rifting beginning at 8 Ma [*Harrison et al., 1995; J. Kapp et al., 2005*]. The thermal histories of samples in the footwall of the Nyainqentanghla detachment show a rapid latest Miocene to early Pliocene cooling event related to exhumation of the range due to slip on a high-angle normal fault [*Harrison et al., 1995*] or on the detachment itself [*J. Kapp et al., 2005*]; the more recent interpretation is supported by seismic imaging of the rift showing the detachment to continue uncut and at a low angle below the supradetachment basin, and to project to active fault scarps at the rangefront [*Cogan et al., 1998*]. However, evidence of higher-temperature cooling (>300 ˚C) in the middle Miocene is seen in their thermochronology data as well, and the footwall rocks would have had to have cooled through 350 ˚C in the middle Miocene if the mylonitic shear zone was formed during the current extensional phase. A scenario involving slow deformation beginning in the mid-Miocene followed by acceleration, involving slip on large-magnitude detachment faults, at ~8 Ma is consistent with all datasets. While there is no compelling reason to assume *a priori* that extension in the SLR and Nyainqentanglha should be contemporaneous, the larger dataset and more thorough thermal modeling from the SLR show how an earlier and slower phase of extension preceding an acceleration could be masked due to sparse sampling and the restricted thermal modeling limited by older computing technology.

The structural and thermochronological data from the footwalls of the SLD, North Lung-gar detachment [*Kapp et al., 2008*], and Nyainqentanglha detachment [*Harrison et al., 1995; J. Kapp et al., 2005*] involve an earlier phase of ductile deformation with superposed brittle deformation. *Ratschbacher et al.* [*2011*] combine evidence of Miocene ductile deformation and Pliocene-present brittle deformation from throughout the orogen and suggest that two distinct deformational events occurred in Tibet, and that the earlier, ductile event is not necessarily related to crustal extension. However, given that the normal-sense ductile shear occurs in detachment footwalls of rifts showing evidence of active extensional deformation (e.g. seismicity, Quaternary fault scarps with at least 10s of meters of throw), we prefer the interpretation that the change from ductile

to brittle deformation is a consequence of progressive exhumation and cooling of the footwall. Similar interpretations have been made for the North Lunggar detachment [*Kapp et al., 2008*], the Nyainqentanglha detachment [*J. Kapp et al., 2005*], Ama Drime detachment [*Langille et al., 2010*] and for many detachment faults in the Basin and Range [e.g., *Wernicke, 1981; Davis, 1983*], the Aegean [e.g., *Lee and Lister, 1992*], and Peru [e.g., *McNulty and Farber, 2002*].

6.6 Contribution to the Tibetan strain budget

As discussed in Section 1.2.2, some estimates have been made for net extension in Tibet. Given ~20 km extension for the SLR and about 10 km for the Pum Qu-Xainza and Tangra Yum Co rifts, and assuming small (~1 km) contribution from the various smaller rifts in the Lhasa block at the latitude of the SLR, we may broadly estimate net extension at 50-70 km. However, our results from the SLR show that along-strike variation can be significant, and therefore that applying a single or narrow range of values for Tibetan extension may be problematic.

Extension rates across the plateau are better constrained over the decadal scale by GPS geodesy. *Zhang et al.* [*2004*] measured 21.6 ± 2.5 mm a^{-1} extension between 79˚ and 95˚ E longitude, or roughly the area showing N-trending rifts. The sites SHIQ and TCOQ are located ~400 and ~150 km to the west and east of the SLR, respectively, and have an 100˚ component of 1.0 ± 1.3 and 4.6 ± 3.5 mm a^{-1}, yielding 3.6 ± 4.8 mm a^{-1} extension across the western Lhasa block [*Zhang et al., 2004*]. Though this figure is very imprecise, it gives a most probable value that is about 1 mm a^{-1} higher than extension across the SLR, suggesting that the Lunggar rift is the dominant extensional structure in the western Lhasa block. Interestingly, it also suggests that extension rates are considerably higher in the eastern Lhasa block; this is supported by the analysis of *Gan et al.* [*2007*] using GPS data from throughout the orogen. These comparisons assume that deformation rates may be compared from the 10 year scale to the 10^6 year scale; our modeling is not sufficient (or intended) to resolve high-frequency changes in slip rate due to the earthquake cycle, fault interaction, or other processes.

Support for both block-type [e.g., *Meade, 2007; Thatcher, 2007*] and continuum deforma-

tion [e.g. *England and Houseman, 1989; Cook and Royden, 2008*] can be found in the results from the SLR. Block-type deformation is supported by the results that the SLR has accommodated ~10-20 km of localized extension, which is of regional significance, and likely the majority of the extension that has occurred at that latitude in the western Lhasa block; therefore, the SLR bounds regions that are deforming at a much lower rate. However, the rapid along-strike variation in rates and magnitudes of extension are possibly accounted for by extension on neighboring normal faults (known or not), or diffuse deformation within the adjacent crust; in this case, extensional strain would be penetrative at a regional scale. Therefore, extensional strain is present throughout the western Lhasa block, but concentrated at the Lunggar Rift; essentially, strain is localized at rift zones instead of individual faults. This is in contrast to the preferred model of *Loveless and Meade* [*2011*], who consider the western Lhasa block to be essentially undeforming. However, given the lack of published slip rates across the Lunggar rift at the time that study was performed, the omission is understandable. The specific results here are consistent with the more general conclusion of *Loveless and Meade* [*2011*] that deformation type is spatially variable, with different areas occupying different positions on the continuum-rigid block spectrum. The observed distributed extension from the SLD through the Lopukangri Rift and to the smaller graben to the east [*Murphy et al., 2010*] is consistent with studies predicting or observing wide zones of extension in areas of hot and weak crust [*Buck, 1988; Kogan et al., 2012*].

6.7 Causes for Tibetan extension

Extension in Tibet has been attributed to a variety of causes. Thorough reviews of many of these have been published recently (*Lee et al., 2011; Ratschbacher et al., 2011*), and we will not attempt to replicate these efforts, as our results are from a small area and are in broad agreement with published work. However, we will discuss the implications of our results with respect to several prominent models that involve timing constraints.

Convective removal of mantle lithosphere is commonly inferred to explain the elevation and extension of the plateau (e.g., *Molnar et al., 1993; England and Houseman, 1988*). This

hypothesis is generally supported by geophysical studies indicating a hot upper mantle under the Qiantang block with low Vp/Vs and Poisson's ratios [e.g., *Owens and Zandt, 1997*]; colder mantle lithosphere under southern and far northern Tibet is quite reasonably explained as post-removal underthrusting of Indian and Tarim lithosphere. The timing of convective removal was earlier considered to occur at ~8 Ma, largely due to the work of *Molnar et al.* [*1993*], *Pan and Kidd* [*1992*] and *Harrison et al.* [*1995*]; more recently this date has been allowed to be pushed back by several million years to explain the Miocene deceleration of Indo-Asian convergence rate [*Molnar and Stock, 2009*]. Recent studies of mantle xenoliths in south Tibetan ultrapotassic rocks [e.g., *Liu et al., 2011*] show that the upper mantle was very hot and metasomatized by ~17 Ma, strongly suggesting that removal of mantle lithosphere was underway by this time. Therefore, an increase in elevation (and excess gravitational potential energy) shortly after this time may explain the middle Miocene onset of extension in central and western Tibet [*Blisniuk et al., 2001*; this study] and in the Nyainqentanglha rift [*Harrison et al., 1995*] should an early phase of extension have occurred. However, if convective removal occurred in the early-middle Miocene and explains extension and Indo-Asian convergence rate reduction [*Molnar and Stock, 2009*], then it cannot explain rapid extension beginning at 8 Ma [*Harrison et al., 1995; J. Kapp et al., 2005*; this study].

Yin [*2000*] suggested that the synchronous onset of extension from southern Tibet and the Himalaya north through Lake Baikal resulted from a sub-continental scale change in boundary conditions, which he attributed to rollback of the Pacific slab subducting below Eurasia. This timing was later revised to ~15 Ma, in accordance with the observed cessation of backarc seafloor spreading in the East China Sea [*Yin, 2010*]. This hypothesis is consistent with the onset of Tibetan extension, although the ability of the crust to transmit extensional stresses over >1000 km (from the Pacific coast across China to Tibet) is questionable, given the low theoretical tensile strength of the crust [*England et al., 1985*]; stress transmission may be aided by east-directed compression on the South and East Chinese cratons due to the Tibetan plateau's excess gravitational potential energy [*Kong and Bird, 1998*]. Furthermore, the change from tension to compression across the western Pacific subduction zones in the late Miocene indicates that another mechanism, such as

east-directed asthenospheric flow from beneath the Tibetan plateau is responsible [*Yin, 2010; Yin and Taylor, 2011*], although estimates for the initiation of this flow have not yet been made.

In their work considering various changes to Tibetan geodynamics that may induce extension, *England and Houseman* [*1988*] discuss how a reduction in Indo-Asian convergence rate could lead to extension; essentially, N-S compressional stress is linearly related to convergence rate, and a reduction in the former would lead to a reduction in the latter. Though they discount this possibility on the grounds that their models show the decrease would have to be far more drastic than the contemporaneous data allowed for, we suggest otherwise. The presence of both normal and strike-slip faulting, both accommodating E-W extension, indicate that the N-S compressional stress and vertical compressional stress are close to equal, whereas the E-W stress is the minimum compressive stress [*Molnar and Lyon-Caen, 1988*]; the change between normal faulting and strike-slip faulting may be related to modest changes in vertical stress related to local variations in elevation [*Elliott et al., 2010; Styron et al., 2011b*]. This modern near-equilibrium between N-S and vertical stress suggests that a decrease in N-S stress in the middle Miocene due to convergence deceleration may be sufficient to initiate extension. Coeval with the mid-Miocene onset of extension on the high plateau is a change from N-S thrusting to strike-slip faulting along E-W striking faults in northern Tibet [*Lease et al., 2011*], also consistent with a decrease in N-S compression (or an increase in vertical stress). However, middle Miocene Indo-Asian convergence rate decrease does not explain the extensional acceleration at 8 Ma, either.

It should be noted that none of these models are mutually exclusive, and some of them may be linked, such as the hypothesis that delamination and uplift caused the Indo-Asian convergence deceleration [*Molnar and Stock, 2009*]. Additionally, because the estimates of timing and rates of Tibetan extension are constrained by sparse data of different types, testing of these models for Tibetan extension may not be possible with sufficient resolution to falsify any of them. However, none of these models explain the observed rapid extension at 8 Ma. As this is based on only two data points, it is unclear whether this is a local signal relating to (for example) detachment fault evolution, or whether it represents a regionally extensive signal.

7 Conclusions

We provide the first geologic mapping and zircon U-Pb geochronology and zircon (U-Th)/He thermochronology of the South Lunggar rift in western Tibet. The SLR is a large N-S trending active rift and is the southern segment of the Lunggar Rift, likely the major extensional structure in southwestern Tibet. Robust thermokinematic modeling with Pecube (~25,000 simulations) indicates that extension initiated in the middle Miocene (16-12 Ma) and accelerated in the late Miocene (~8 Ma). Significant along-strike variation exists in deformation rates; horizontal extension rates are ~1 mm a^{-1} in the south and 2.5 mm a^{-1} in the north, and net extension is between ~10 and 21 km, respectively. The lower rates and magnitudes of extension in the southern SLR correlate with higher-angle normal faulting, while the higher rates and magnitudes correlate with the South Lunggar Detachment, a fairly narrow (~15 km along-strike) low-angle normal fault that has exhumed a metamorphic core complex. Testing of multiple fault geometries indicates that an antilistric geometry of the upper SLD (shallowing to sub-horizontal; i.e. the upper hinge of a rolling-hinge) is necessary to reproduce the zHe cooling age distribution; although several subsurface geometries are permissible, the best fit was provided by a detachment geometry that steepens to moderate angles at depth. Our results also show that the Tibetan crust is very hot; pre-extensional geothermal gradients are ~40 ˚C km^{-1} in the upper several km of the crust, and currently higher within the footwall of the SLD. Though several geodynamic models may explain the timing of rift initiation in the SLR in the early to middle Miocene, none so far explain the onset of rapid extension at 8 Ma.

111

in pushing us to test between magma emplacement and faulting as the cause of mylonitization.

References

Abers, G. A. (2001), Evidence for seismogenic normal faults at shallow dips in continental rifts, *Geological Society, London, Special Publications*, 187(1), 305-318, doi:10.1144/GSL. SP.2001.187.01.15.

Abers, G. A., A. Ferris, M. Craig, H. Davies, A. L. Lerner-Lam, J. C. Mutter, and B. Taylor (2002), Mantle compensation of active metamorphic core complexes at Woodlark rift in Papua New Guinea., *Nature*, 418(6900), 862-5, doi:10.1038/nature00990.

Andersen, T. (2002), Correction of common lead in U – Pb analyses that do not report 204 Pb, Chemical Geology, 192, 59 - 79.

Armijo, R., P. Tapponnier, J. L. Mercier, and H. Tong-Lin (1986), Quaternary extension in southern Tibet: Field observations and tectonic implications, *Journal of Geophysical Research*, 91, 13803-13872.

Armstrong, R., and P. Ward (1991), Geographic patterns of Cenozoic magmatism in the North American Cordillera: The temporal and spatial association of magmatism and metamorphic core complexes, *Journal of Geophysical Research*, 96(B8), 13,201-13,224.

Axen, G. J., M. Grove, A. Rothstein, M. Fletcher, and L. Abbott (2000), Thermal evolution of Monte Blanco dome: Low-angle normal faulting during the Gulf of California rifting and late Eocene denudation of the eastern Pensinsular Ranges, *Tectonics*, 19(2), 197-212.

Axen, G. J., and J. M. Bartley (1997), Field tests of rolling hinges: Existence, mechanical types, and implications for extensional tectonics, *Journal of Geophysical Research*, 102(B9), 20515–20.

Beaumont, C., R. Jamieson, M. H. Nguyen, and B. Lee (2001), Himalayan tectonics explained by extrusion of a low-viscosity crustal channel coupled to focused surface denudation., *Nature*, 414(6865), 738-742, doi:10.1038/414738a.

Bendick, R., and L. Flesch (2007), Reconciling lithospheric deformation and lower crustal flow beneath central Tibet, *Geology*, 35(10), 895, doi:10.1130/G23714A.1.

Blisniuk, P. M., B. R. Hacker, J. Glodny, L. Ratschbacher, S. Bi, Z. Wu, M. O. McWilliams, and

a Calvert (2001), Normal faulting in central Tibet since at least 13.5 Myr ago., *Nature*, 412(6847), 628-32, doi:10.1038/35088045.

Block, L., and L. H. Royden (1990), Core complex geometries and regional scale flow in the lower crust, *Tectonics*, 9(4), 557–567

Bosworth, W. (1985), Geometry of propagating continental rifts, *Nature*, 316(6029), 625-627, doi:10.1038/316625a0.

Braun, J. (2003), Pecube: a new finite-element code to solve the 3D heat transport equation including the effects of a time-varying, finite amplitude surface topography, *Computers & Geosciences*, 29(6), 787-794, doi:10.1016/S0098-3004(03)00052-9.

Brun, J., D. Sokoutis, and J. Van Den Driessche (1994), Analogue modeling of detachment fault systems and core complexes, *Geology*, 22(5), 319-322.

Buck, W. R. (1988), Flexural rotation of normal faults, *Tectonics*, 7(5), 959–973.

Buck, W. R. (1991), Modes of continental lithospheric extension, *Journal of Geophysical Research*, 96 (B12), 20161–20.

Burchfiel, B., and L. H. Royden (1985), North-south extension within the convergent Himalayan region, *Geology*, 13(10), 679-682.

Burg, J. P., A. Leyreloup, J. Girardeau, and G. M. Chen (1987), Structure and metamorphism of a tectonically thickened continental crust: the Yalu Tsangpo suture zone (Tibet), *Philosophical Transactions of the Royal Society of London. Series A, Mathematical and Physical Sciences*, 321 (1557), 67–86.

Burg, J. P., and G. M. Chen (1984), Tectonics and structural zonation of southern Tibet, China, *Nature*, 311, 219-223.

Campani, M., F. Herman, and N. Mancktelow (2010), Two-and three-dimensional thermal modeling of a low-angle detachment: Exhumation history of the Simplon Fault Zone, central Alps, *Journal of Geophysical Research*, 115 (B10), B10420, doi:10.1029/2009JB007036.

Caskey, S., S. Wesnousky, P. Zhang, and D. Slemmons (1996), Surface faulting of the 1954 Fairview Peak (Ms 7.2) and Dixie Valley (Mw 6.8) earthquakes, central Nevada, *Bulletin*

of the Seismological Society of America, 86(3), 761–787.

Clark, M. K., and L. H. Royden (2000), Topographic ooze: Building the eastern margin of Tibet by lower crustal flow, *Geology*, 28(8), 703-706, doi:10.1130/0091-7613(2000)28<703.

Cogan, M. J. et al. (1998), Shallow structure of the Yadong-Gulu rift, southern Tibet, from refraction analysis of Project INDEPTH common midpoint data, *Tectonics*, 17(1), 46–61.

Cook, K. L., and L. H. Royden (2008), The role of crustal strength variations in shaping orogenic plateaus, with application to Tibet, *Journal of Geophysical Research*, 113(B8), B08407, doi:10.1029/2007JB005457.

Copley, A., J.-P. Avouac, and B. P. Wernicke (2011), Evidence for mechanical coupling and strong Indian lower crust beneath southern Tibet, *Nature*, 472(7341), 79-81, doi:10.1038/nature09926.

Copley, A., and D. McKenzie (2007), Models of crustal flow in the India-Asia collision zone, *Geophysical Journal International*, 169, 683-698.

Crittenden, M. D., Jr., P. J. Coney, and G. H Davis, eds. (1980), Cordilleran metamorphic core complexes, *Geological Society of America Memoir 153*, 490 p.

Daoudene, Y., D. Gapais, G. Ruffet, E. Gloaguen, A. Cocherie, and P. Ledru (2012), Syn-thinning pluton emplacement during Mesozoic extension in eastern Mongolia, *Tectonics*, 31, TC3001, doi:10.1029/2011TC002926.

Daczko, N. R., P. Caffi, and P. Mann (2011), Structural evolution of the Dayman dome metamorphic core complex, eastern Papua New Guinea, *Geological Society of America Bulletin*, 123(11-12), 2335-2351, doi:10.1130/B30326.1.

Davis, G. H. (1983), Shear-zone model for the origin of metamorphic core complexes, *Geology*, 11(6), 342-347, doi:10.1130/0091-7613(1983)11<342.

DeCelles, P. G., P. Kapp, J. Quade, and G. E. Gehrels (2011), Oligocene-Miocene Kailas basin, southwestern Tibet: Record of postcollisional upper-plate extension in the Indus-Yarlung suture zone, *Geological Society of America Bulletin*, 123(7-8), 1337-1362, doi:10.1130/B30258.1.

DeCelles, P. G., D. M. Robinson, and G. Zandt (2002), Implications of shortening in the Himalayan fold-thrust belt for uplift of the Tibetan Plateau, *Tectonics*, 21(6), 1062, doi:10.1029/2001TC001322.

Dewane, T. J., D. F. Stockli, C. Hager, M. Taylor, L. Ding, J. Lee, and S. Wallis (2006), Timing of Cenozoic E-W extension in the Tangra Yum Co-Kung rift, south-central Tibet, *Eos Trans. AGU*, 87(52), Fall Meet. Suppl., Abstract T34C-04.

Dewey, J. (1988), Extensional collapse of orogens, *Tectonics*, 7(6), 1123-1139.

Dewey, J. F., R. M. Shackleton, C. Chengfa, and S. Yiyin (1988), The tectonic evolution of the Tibetan Plateau, *Philosophical Transactions of the Royal Society of London. Series A, Mathematical and Physical Sciences*, 327(1594), 379.

Ding, L., P. Kapp, D. Zhong, and W. Deng (2003), Cenozoic volcanism in Tibet: Evidence for a transition from oceanic to continental subduction, *Journal of Petrology*, 44(10), 1833-1865, doi:10.1093/petrology/egg061.

Ding, L., P. Kapp, and X. Wan (2005), Paleocene-Eocene record of ophiolite obduction and initial India-Asia collision, south central Tibet, *Tectonics*, 24(3), 1–18, doi:10.1029/2004TC001729.

Dodson, M. (1973), Closure temperature in cooling geochronological and petrological systems, *Contributions to Mineralogy and Petrology*, 17(8), 444, doi:10.2307/495689.

Duebendorfer, E.M., Faulds, J.E., and Fryxell, J.E. (2010), The South Virgin–White Hills detachment fault, southeastern Nevada and northwestern Arizona: Significance, displacement gradient, and corrugation formation, in Umhoefer, P.J., et al., eds., *Miocene tectonics of the Lake Mead region, central Basin and Range: Geological Society of America Special Paper 463*, p. 275–287, doi: 10.1130/2010.2463(12).

Edwards, M., and L. Ratschbacher (2005), Seismic and aseismic weakening effects in transtension: field and microstructural observations on the mechanics and architecture of a large fault zone in SE Tibet, *Geological Society, London, Special Publications*, 245(1), 109-141.

Ehlers, T. A. (2005), Crustal thermal processes and the interpretation of thermochronometer data, *Reviews in Mineralogy and Geochemistry*, 58(1), 315, doi:10.2138/rmg.2005.58.12.

Ehlers, T. A., P. A. Armstrong, and D. S. Chapman (2001), Normal fault thermal regimes and the interpretation of low-temperature thermochronometers, *Physics of the Earth and Planetary Interiors*, 126(3), 179–194.

Elliott, J., R. Walters, P. England, J. A. Jackson, Z. Li, and B. Parsons (2010), Extension on the Tibetan plateau: recent normal faulting measured by InSAR and body wave seismology, *Geophysical Journal International*, 183, 503-535, doi:10.1111/j.1365-246X.2010.04754.x.

Ellis, S., and B. Stöckhert (2004), Elevated stresses and creep rates beneath the brittle-ductile transition caused by seismic faulting in the upper crust, *Journal of Geophysical Research*, 109(B5), 1-10, doi:10.1029/2003JB002744.

England, P., and G. Houseman (1988), The mechanics of the Tibetan Plateau, *Philosophical Transactions of the Royal Society of London. Series A, Mathematical and Physical Sciences*, 326, 301–320.

Fitzgerald, P. G., E. M. Duebendorfer, J. E. Faulds, and P. O'Sullivan (2009), South Virgin–White Hills detachment fault system of SE Nevada and NW Arizona: Applying apatite fission track thermochronology to constrain the tectonic evolution of a major continental detachment fault, *Tectonics*, 28(2), 1-31, doi:10.1029/2007TC002194.

Fletcher, J. M., and R. M. Spelz (2009), Patterns of Quaternary deformation and rupture propagation associated with an active low-angle normal fault, Laguna Salada, Mexico: Evidence of a rolling hinge?, *Geosphere*, 5(4), 385-407, doi:10.1130/GES00206.1.

Förster, A., and H.-J. Förster (2000), Crustal composition and mantle heat flow: Implications from surface heat flow and radiogenic heat production in the Variscan Erzgebirge (Germany), *Journal of Geophysical Research.*, 105, 27,917–27,938.

Forsyth, D. W. (1992), Finite extension and low-angle normal faulting, *Geology*, 20(1), 27-30, doi:10.1130/0091-7613(1992)020<0027.

Francheteau, J., C. Jaupart, S. X. Jie, K. Wen-Hua, L. De-Lu, B. Jia-Chi, W. Hung-Pin, and D. Hsia-Yeu (1984), High heat flow in southern Tibet, *Nature*, 307(5), 32-36.

Friedmann, S. J., and D. W. Burbank (1995), Rift basins and supradetachment basins: intraconti-

nental extensional end-members, *Basin Research*, 7(2), 109–127.

Gan, W., P. Zhang, Z.-K. Shen, Z. Niu, M. Wang, Y. Wan, D. Zhou, and J. Cheng (2007), Present-day crustal motion within the Tibetan Plateau inferred from GPS measurements, *Journal of Geophysical Research*, 112(B08416), 1-14, doi:10.1029/2005JB004120.

Garzione, C. N., P. G. DeCelles, D. G. Hodkinson, T. P. Ojha, and B. N. Upreti (2003), East-west extension and Miocene environmental change in the southern Tibetan plateau: Thakkhola graben, central Nepal, *Bulletin of the Geological Society of America*, 115(1), 3-20.

Hager, C., Stockli, D., Dewane, T., Ding, L., Taylor, M., and Lee, J., 2006, Episodic Mio-Pliocene rifting in south-centralTibet. Thermochronometric constraints from the Xainza rift, *Eos Trans., AGU*, 87(52), Fall Meeting Supplement, abs. T34C–02.

Harrison, T., P. Copeland, and W. Kidd (1995), Activation of the Nyainqentanghla shear zone: Implications for uplift of the southern Tibetan Plateau, *Tectonics*, 14(3), 658-676.

Hedin, S. A. (1909), Trans-Himalaya: Discoveries and Adventures in Tibet, Macmillan, London.

Hirn, A., M. Jiang, M. Sapin, J. Diaz, and A. Nercessian (1995), Seismic anisotropy as an indicator of mantle flow beneath the Himalayas and Tibet, *Nature*, 375, 571-574.

Hreinsdottir, S., and R. A. Bennett (2009), Active aseismic creep on the Alto Tiberina low-angle normal fault, Italy, *Geology*, 37(8), 683-686, doi:10.1130/G30194A.1.

Hu, S., L. He, and J. Wang (2000), Heat flow in the continental area of China: a new data set, *Earth and Planetary Science Letters*, 179.

Jackson, S. E., N. J. Pearson, W. L. Griffin, and E. a. Belousova (2004), The application of laser ablation-inductively coupled plasma-mass spectrometry to in situ U–Pb zircon geochronology, *Chemical Geology*, 211(1-2), 47-69, doi:10.1016/j.chemgeo.2004.06.017.

Jaupart, C., S. Labrosse, and J.-C. Marechal (2007), Temperatures, Heat and Energy in the Mantle of the Earth, in *Treatise on Geophysics*, edited by G. Schubert and D. Bercovici, pp. 253-303, Elsevier.

Jessup, M. J., D. L. Newell, J. M. Cottle, A. L. Berger, and J. A. Spotila (2008), Orogen-parallel extension and exhumation enhanced by denudation in the trans-Himalayan Arun River

gorge, Ama Drime Massif, Tibet-Nepal, *Geology*, 36(7), 587, doi:10.1130/G24722A.1.

John, B. E., (1987), Geometry and evolution of a mid-crustal extensional fault system: Chemehu-evi Mountains, southeastern California, in Continenta Extension Tectonics, M. P. Coward, J. F. Dewey, and P. L. Hancock, *Geol. Soc. Spec. Publ. London*, 28, 313-335.

Kapp, J., T. Harrison, P. Kapp, M. Grove, O. M. Lovera, and L. Ding (2005), Nyainqentanglha Shan: A window into the tectonic, thermal, and geochemical evolution of the Lhasa block, southern Tibet, *Journal of Geophysical Research*, 110(B8), B08413, doi:10.1029/2004JB003330.

Kapp, P., P. DeCelles, G. Gehrels, M. Heizler, and L. Ding (2007), Geological records of the Lhasa-Qiangtang and Indo-Asian collisions in the Nima area of central Tibet, *Geological Society of America Bulletin*, 119(7-8), 917, doi:10.1130/B26033.1.d J. Guo (2003),

Kapp, P., M.A. Murphy, A. Yin, T. M. Harrison, L. Ding, and J. Guo, (2003) Mesozoic and Cenozoic tectonic evolution of the Shiquanhe area of western Tibet, *Tectonics*, 22(4), 1029, doi:10.1029/2001TC001332.

Kapp, P. A., M.H. Taylor, and D.F. Stockli (2008), Development of active low-angle normal fault systems during orogenic collapse: Insight from Tibet, *Geology*, 36(1), 7-10, doi:10.1130/G24054A.1.

Kapp, P., A. Yin, T. M. Harrison, and L. Ding (2005), Cretaceous-Tertiary shortening, basin development, and volcanism in central Tibet, *Geological Society of America Bulletin*, 117(7/8), 865, doi:10.1130/B25595.1.

Ketcham, R.A (1996), Thermal models of core-complex evolution in Arizona and New Guinea: Implications for ancient cooling paths and present-day heat flow, *Tectonics*, 15(5), 933-951.

Ketcham, R. A. (2005), Forward and Inverse Modeling of Low-Temperature Thermochronometry Data, *Reviews in Mineralogy*, 58, 275-314, doi:10.2138/rmg.2005.58.11.

Klootwijk, C., P. Conaghan, and C. M. A. Powell (1985), The Himalayan Arc: large-scale continental subduction, oroclinal bending and back-arc spreading, *Earth and Planetary Science Letters*, 75(2-3), 167–183.

Kogan, L., S. Fisseha, R. Bendick, R. E. Reilinger, S. McClusky, B. King, and T. Solomon (2012), Lithospheric strength and strain localization in continental extension from observations of the East African Rift, *Journal of Geophysical Research*, 117(b03402), 1-16, doi:10.1029/2011JB008516.

Kong, X., and P. Bird (1996), Neotectonics of Asia: thin-shell finite-element models with faults, in: *The tectonic evolution of Asia*, A. Yin and T. M. Harrison (eds), Cambridge UNiversity Press, p. 18-34.

Lacassin, R. et al. (2004), Large-scale geometry, offset and kinematic evolution of the Karakorum fault, Tibet, *Earth and Planetary Science Letters*, 219(3-4), 255–269, doi:10.1016/S0012-821X(04)00006-8.

Langille, J. M., M. J. Jessup, J. M. Cottle, D. Newell, and G. Seward (2010), Kinematic evolution of the Ama Drime detachment: insights into orogen-parallel extension and exhumation of the Ama Drime Massif, Tibet-Nepal, *Journal of Structural Geology*, 32(7), 900–919, doi:10.1016/j.jsg.2010.04.005.

Lease, R. O., D. W. Burbank, M. K. Clark, K. a. Farley, D. Zheng, and H. Zhang (2011), Middle Miocene reorganization of deformation along the northeastern Tibetan Plateau, *Geology*, 39(4), 359-362, doi:10.1130/G31356.1.

Lee, J., C. Hager, S. R. Wallis, D. F. Stockli, M. J. Whitehouse, M. Aoya, and Y. Wang (2011), Middle to late Miocene extremely rapid exhumation and thermal reequilibration in the Kung Co rift, southern Tibet, *Tectonics*, 30(2), 1-26, doi:10.1029/2010TC002745.

Lee, J., E. L. Miller, and J. F. Sutter (1987), Ductile strain and metamorphism in an extensional tectonic setting: a case study from the northern Snake Range, Nevada, USA, in *Continental Extensional Tectonics*, edited by M. P. Coward, J. F. Dewey, and P. L. Hancock, pp. 267-298.

Lee, J., and G. S. Lister (1992), Late Miocene ductile extension and detachment faulting, Mykonos, Greece, *Geology*, 20(2), 121-124.

Lister, G. S., and G. A. Davis (1989), The origin of metamorphic core complexes and detachment

faults formed during Tertiary continental extension in the northern Colorado River region, USA, *Journal of Structural Geology*, 11(1-2), 65–94.

Liu, C.-Z., F.-Y. Wu, S.-L. Chung, and Z.-D. Zhao (2011), Fragments of hot and metasomatized mantle lithosphere in Middle Miocene ultrapotassic lavas, southern Tibet, *Geology*, 39(10), 923-926, doi:10.1130/G32172.1.

Loveless, J. P., and B. J. Meade (2011), Partitioning of localized and diffuse deformation in the Tibetan Plateau from joint inversions of geologic and geodetic observations TS AT, *Earth and Planetary Science Letters*, 303(1-2), 11-24, doi:10.1016/j.epsl.2010.12.014.

Mahéo, G., P. H. Leloup, F. Valli, R. Lacassin, N. Arnaud, and J. Paquette (2007), Post 4 Ma initiation of normal faulting in southern Tibet . Constraints from the Kung Co half graben, *Earth and Planetary Science Letters*, 256, 233 - 243, doi:10.1016/j.epsl.2007.01.029.

Masek, J. G., B. L. Isacks, E. J. Fielding, and J. Browaeys (1994), Rift flank uplift in Tibet: Evidence for a viscous lower crust, *Tectonics*, 13(3), 659–667.

McNulty, B., and D. Farber (2002), Active detachment faulting above the Peruvian flat slab, *Geology*, 30(6), 567.

Meade, B. J. (2007), Present-day kinematics at the India-Asia collision zone, *Geology*, 35, 81-84.

Mechie, J., S. V. Sobolev, L. Ratschbacher, a. Y. Babeyko, G. Bock, a. G. Jones, K. D. Nelson, K. D. Solon, L. D. Brown, and W. Zhao (2004), Precise temperature estimation in the Tibetan crust from seismic detection of the α-β quartz transition, *Geology*, 32(7), 601, doi:10.1130/G20367.1.

Meigs, A. J., D. W. Burbank, and R. A. Beck (1995), Middle-late Miocene (>10 Ma) formation of the Main Boundary thrust in the western Himalaya, *Geology*, 23(5), 423-426, doi:10.1130/0091-7613(1995)023<0423.

Molnar, P., P. England, and J. Martinod (1993), Mantle dynamics, uplift of the Tibetan Plateau, and the Indian monsoon, *Reviews of Geophysics*, 31(4), 357–396.

Molnar, P., and W.-P. Chen (1983), Focal depths and fault plane solutions of earthquakes under the Tibetan plateau, *Journal of Geophysical Research*, 88(B2), 1180-1196.

Molnar, P., and H. Lyon-Caen (1989), Fault plane solutions of earthquakes and active tectonics of the Tibetan Plateau and its margins, *Geophysical Journal International*, 99, 123-153. onvergence with Eurasia since 20 Ma and its implications for Tibetan mantle dynamics, Tectonics, 28(TC3001), 1-11, doi:10.1029/2008TC002271.

Molnar, P., and J. M. Stock (2009), Slowing of India's convergence with Eurasia since 20 Ma and its implications for Tibetan mantle dynamics, *Tectonics*, 28(TC3001), 1-11, doi:10.1029/2008TC002271.

Molnar, P., and P. Tapponnier (1975), Cenozoic tectonics of Asia: effects of a continental collision, *Science*, 189(4201), 419–426.

Morley, C. K. (1999), Marked along-strike variations in dip of normal faults-the Lokichar fault, N. Kenya rift: a possible cause for metamorphic core complexes, *Journal of Structural Geology*, 21, 479-492.

Morley, C. K. (2009), Geometry and evolution of low-angle normal faults (LANF) within a Cenozoic high-angle rift system, Thailand: Implications for sedimentology and the mechanisms of LANF development, *Tectonics*, 28(5), 1-30, doi:10.1029/2007TC002202.

Murphy, M. (2007), Isotopic characteristics of the Gurla Mandhata metamorphic core complex: Implications for the architecture of the Himalayan orogen, *Geology*, doi:10.1130/G23774A.1.

Murphy, M. A., A. Yin, P. Kapp, T. M. Harrison, C. E. Manning, F. J. Ryerson, D. Lin, and G. Jinghui (2002), Structural evolution of the Gurla Mandhata detachment system, southwest Tibet: Implications for the eastward extent of the Karakoram fault system, *Geological Society of America Bulletin*, 114(4), 428-447.

Murphy, M., V. Sanchez, and M. Taylor (2010), Syncollisional extension along the India-Asia suture zone, south-central Tibet: Implications for crustal deformation of Tibet, *Earth and Planetary Science Letters*, 290(3-4), 233–243, doi:10.1016/j.epsl.2009.11.046.

Murphy, M., A. Yin, T. Harrison, S. Dürr, Z. Chen, F. J. Ryerson, W. S. F. Kidd, X. Wang, and X. Zhou (1997), Did the Indo-Asian collision alone create the Tibetan plateau?, *Geology*,

25(8), 719-722.

Nelson, K. D. et al. (1996), Partially molten middle crust beneath southern Tibet: Synthesis of project INDEPTH results, *Science*, 274(5293), 1684-1688.

Niemi, N. A, B. P. Wernicke, A. M. Friedrich, M. Simons, R. A. Bennett, and J. L. Davis (2004), BARGEN continuous GPS data across the eastern Basin and Range province, and implications for fault system dynamics, *Geophysical Journal International*, 159(3), 842-862, doi:10.1111/j.1365-246X.2004.02454.x.

Nábelek, J., G. Hetényi, J. Vergne, S. Sapkota, B. Kafle, M. Jiang, H. Su, J. Chen, and B.-S. Huang (2009), Underplating in the Himalaya-Tibet collision zone revealed by the Hi-CLIMB experiment., *Science*, 325(5946), 1371-1374, doi:10.1126/science.1167719.

Owens, T. J., and G. Zandt (1997), Implications of crustal property variations for models of Tibetan plateau evolution, *Nature*, 387(6628), 37–43.

Pan, Y., and W. Kidd (1992), Nyainqentanglha shear zone: A late Miocene extensional detachment in the southern Tibetan Plateau, *Geology*, 20(9), 775-778, doi:10.1130/0091-7613(1992)020<0775.

Parsons, T., and G. A. Thompson (1993), Does magmatism influence low-angle normal faulting? *Geology*, 21(3), 247-250.

Paton, C., J. Hellstrom, B. Paul, J. Woodhead, and J. Hergt (2011), Iolite: Freeware for the visualisation and processing of mass spectrometric data, *Journal of Analytical Atomic Spectrometry*, 2508-2518, doi:10.1039/c1ja10172b.

Petrus, J. A. and Kamber, B. S. (2012), VizualAge: A Novel Approach to Laser Ablation ICP-MS U-Pb Geochronology Data Reduction. *Geostandards and Geoanalytical Research*. doi: 10.1111/j.1751-908X.2012.00158.x

Priestley, K., J. Jackson, and D. Mckenzie (2008), Lithospheric structure and deep earthquakes beneath India, the Himalaya and southern Tibet, *Geophysical Journal International*, 172, 345-362, doi:10.1111/j.1365-246X.2007.03636.x.

Ratschbacher, L., I. Krumrei, M. Blumenwitz, M. Staiger, R. Gloaguen, B. V. Miller, S. D. Sam-

son, M. A. Edwards, and E. Appel (2011), Rifting and strike-slip shear in central Tibet and the geometry, age and kinematics of upper crustal extension in Tibet, *Geological Society, London, Special Publications*, 353(1), 127-163, doi:10.1144/SP353.8.

Reiners, P. (2005), Zircon (U-Th)/He thermochronometry, *Reviews in Mineralogy and Geochemistry*, 58(1936), 151-179, doi:10.2138/rmg.2005.58.6.

Rey, P., C. Teyssier, and D. Whitney (2009), The role of partial melting and extensional strain rates in the development of metamorphic core complexes, *Tectonophysics*, 477(3-4), 135–144, doi:10.1016/j.tecto.2009.03.010.

Robinson, A.C., Yin, A., Manning, C.E., Harrison, T.M., Zhang, S.-hong, and Wang, X.F. (2004), Tectonic evolution of the northeastern Pamir: Constraints from the northern portion of the Cenozoic Kongur Shan extensional system, western China: *Geological Society of America Bulletin*, v. 116, no. 7-8, p. 953, doi: 10.1130/B25375.1.

Robinson, A. C., A. Yin, and O. M. Lovera (2010), The role of footwall deformation and denudation in controlling cooling age patterns of detachment systems: An application to the Kongur Shan extensional system in the Eastern Pamir, China, *Tectonophysics*, 496(1-4), 28-43, doi:10.1016/j.tecto.2010.10.003.

Robinson, D. M., P. G. DeCelles, and P. Copeland (2006), Tectonic evolution of the Himalayan thrust belt in western Nepal: Implications for channel flow models, *Geological Society of America Bulletin*, 118(7/8), 865-885.

Ryder, I., R. Bürgmann, and E. J. Fielding, *in press,* Static stress interactions in extensional earthquake sequences: an example from the South Lunggar Rift, Tibet, *Journal of Geophysical Research,* doi:10.1029/2012JB009365.

Saylor, J., P. DeCelles, G. Gehrels, M. Murphy, R. Zhang, and P. Kapp (2010), Basin formation in the High Himalaya by arc-parallel extension and tectonic damming: Zhada basin, southwestern Tibet, *Tectonics*, 29(1-24), TC1004, doi:10.1029/2008TC002390.

Searle, M. P., J. R. Elliott, and R. J. Phillips (2011), Lithospheric structure and continental extrusion of Tibet, *Journal of the Geological Society, London*, 168, 633-672, doi:10.1144/0016-

76492010-139.

Sibson, R. H. (1983), Continental fault structure and the shallow earthquake source, *Journal of the Geological Society*, 140(5), 741–767.

Spencer, J. (2010), Structural analysis of three extensional detachment faults with data from the 2000 Space-Shuttle Radar Topography Mission, *GSA Today*, (8), 4-10, doi:10.1130/GSAT-G59A.1.

Spencer, J. E. (1984), Role of tectonic denudation in warping and uplift of low-angle normal faults, *Geology*, 12(2), 95-98.

Stockli, D. F. (2005), Application of Low-Temperature Thermochronometry to Extensional Tectonic Settings, *Reviews in Mineralogy and Geochemistry*, 58, 411-448, doi:10.2138/rmg.2005.58.16.

Stockli, D. F., B. E. Surpless, T. A. Dumitru, and K. A. Farley (2002), Thermochronological constraints on the timing and magnitude of Miocene and Pliocene extension in the central Wassuk Range, western Nevada, *Tectonics*, 21(4), 1028-1038.

Styron, R. H., M. H. Taylor, and M. A. Murphy (2011a), Oblique convergence, arc-parallel extension, and the role of strike-slip faulting in the High Himalaya, *Geosphere*, 7(2), 582-596, doi:10.1130/GES00606.1.

Styron, R., Taylor, M., Sundell, K., Stockli, D., McCallister, A., Liu, D., Ding, L., (2011b), Variations in extensional style in the Lunggar Rift, Southern Tibet, through a change in extensional driving forces, *Eos Trans. AGU*, 92 (52), Fall Meet Suppl., T43F-2457.

Styron, R., M. Taylor, and K. Okoronkwo (2010), Database of active structures from the Indo-Asian Collision, *Eos Trans. AGU*, 91(20), 0-1, doi:10.1130/GES00217.1.Wessel.

Sundell, K., Taylor, M., Styron, R., Stockli, D., Kapp, P., Liu, D., Ding, L (2011), Late Miocene – Pliocene development of the North Lunggar Rift: Implications for the onset of strike-slip faulting and constrictional strain in central Tibet, *Eos Trans. AGU*, 92 (52), Fall Meet Suppl., T43F, 2458.

Taylor, M., A. Yin, F. J. Ryerson, P. Kapp, and L. Ding (2003), Conjugate strike-slip faulting

along the Bangong-Nujiang suture zone accommodates coeval east-west extension and north-south shortening in the interior of the Tibetan Plateau, *Tectonics*, 22(4), 1-18, doi:10.1029/2002TC001361.

Thatcher, W. (2007), Microplate model for the present-day deformation of Tibet, *Journal of Geophysical Research*, 112(B01401), 1-13, doi:10.1029/2005JB004244.

Thiede, R. C., J. R. Arrowsmith, B. Bookhagen, M. McWilliams, E. R. Sobel, and M. R. Strecker (2006), Dome formation and extension in the Tethyan Himalaya, Leo Pargil, northwest India, *Bulletin of the Geological Society of America*, 118(5-6), 635, doi:10.1130/B25872.1.

Tirel, C., J.-P. Brun, and E. Burov (2008), Dynamics and structural development of metamorphic core complexes, *Journal of Geophysical Research*, 113(B4), 1-25, doi:10.1029/2005JB003694.

Volkmer, J. E., P. Kapp, J. H. Guynn, and Q. Lai (2007), Cretaceous-Tertiary structural evolution of the north central Lhasa terrane, Tibet, *Tectonics*, 26(6), TC6007, doi:10.1029/2005TC001832.

Wang, Y. (2001), Heat flow pattern and lateral variations of lithosphere strength in China mainland: constraints on active deformation, *Physics of the Earth and Planetary Interiors*, 126(3-4), 121-146, doi:10.1016/S0031-9201(01)00251-5.

Wei, S. et al. (2010), Regional earthquakes in northern Tibetan Plateau: Implications for lithospheric strength in Tibet, *Geophysical Research Letters*, 37(19), L19307, doi:10.1029/2010GL044800.

Wdowinski, S., and Axen, G.J. (1992), Isostatic rebound due to tectonic denudaton: A viscous flow model of a layered lithosphere, *Tectonics*, 11 (2), p. 303-315.

Wernicke, B. (1981), Low-angle normal faults in the Basin and Range Province: nappe tectonics in an extending orogen, *Nature*, 291, 645–648.

Wernicke, B. (1995), Low-angle normal faults and seismicity: A review, *Journal of Geophysical Research*, 100(B10), 20,159–20,174.

Wernicke, B., and G. J. Axen (1988), On the role of isostasy in the evolution of normal fault sys-

tems, *Geology*, 16, 848-851.

Whittington, A. G., A. M. Hofmeister, and P. I. Nabelek (2009), Temperature-dependent thermal diffusivity of the Earth's crust and implications for magmatism., *Nature*, 458(7236), 319-21, doi:10.1038/nature07818.

Wolfe, M. R., and D. F. Stockli (2010), Zircon (U–Th)/He thermochronometry in the KTB drill hole, Germany, and its implications for bulk He diffusion kinetics in zircon, *Earth and Planetary Science Letters*, 295(1-2), 69-82, doi:10.1016/j.epsl.2010.03.025.

Yin, A. (2000), Mode of Cenozoic east-west extension in Tibet suggesting a common origin of rifts in Asia during the Indo-Asian collision, *Journal of Geophysical Research*, 105(B9), 21,745-21,759, doi:10.1029/2000jb900168.

Yin, A. (2010), Cenozoic tectonic evolution of Asia: A preliminary synthesis, *Tectonophysics*, 488(1-4), 293-325, doi:10.1016/j.tecto.2009.06.002.

Yin, A., T. Harrison, and F. Ryerson (1994), Tertiary structural evolution of the Gangdese thrust system, southeastern Tibet, *Journal of Geophysical Research*, 99(B9), 18,175-18,190.

Yin, A., and J. F. Dunn (1992), Structural and stratigraphic development of the Whipple-Chemehuevi detachment fault system, southeastern California: Implications for the geometrical evolution of domal and basinal low-angle normal faults, *Geological Society Of America Bulletin*, 104(6), 659-674, doi:10.1130/0016-7606(1992)104<0659.

Yin, A., and T. M. Harrison (2000), Geologic Evolution of the Himalayan-Tibetan Orogen, *Annual Review of Earth and Planetary Sciences*, 28(1), 211-280, doi:10.1146/annurev.earth.28.1.211.

Yin, A., and M. H. Taylor (2011), Mechanics of V-shaped conjugate strike-slip faults and the corresponding continuum mode of continental deformation, *Geological Society of America Bulletin*, 123(9-10), 1798–1821, doi:10.1130/B30159.1.

Zhang, P. Z., Z. Shen, M. Wang, W. Gan, R. Bürgmann, P. Molnar, Q. Wang, Z. Niu, J. Sun, and J. Wu (2004), Continuous deformation of the Tibetan Plateau from global positioning system data, *Geology*, 32(9), 809-812.

Zhang, R., M. A. Murphy, T. J. Lapen, V. Sanchez, and M. Heizler (2011), Late Eocene crustal thickening followed by Early-Late Oligocene extension along the India-Asia suture zone: Evidence for cyclicity in the Himalayan orogen, *Geosphere*, 7(5), 1249-1268, doi:10.1130/GES00643.1.

Figures and tables with captions
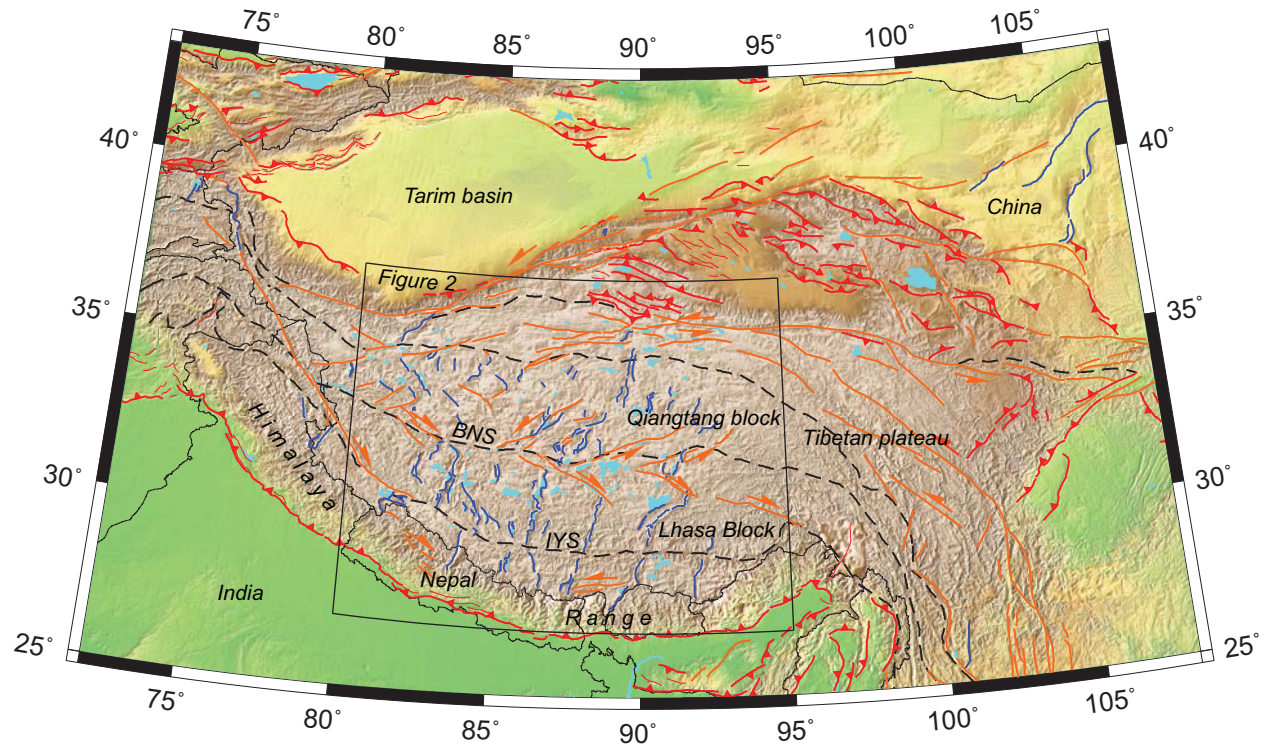
Figure 1: Active tectonic map of the Himalayan-Tibetan orogen. Structures are from HimaTi-betMap-1.1 [*Styron et al., 2010*]. Thick red structures = thrust faults. Thin red lines = fold axes. Blue lines = normal faults. Orange lines = strike-slip faults. Dashed black lines = suture zones. BNS = Bangong-Nujiang Suture Zone. IYS = Indus-Yarlung Suture Zone. Topography is from Shuttle Radar Topographic Mission. Lakes are from GSHHS [*Wessel and Smith, 1996*]. Black box indicates location of Figure 2.
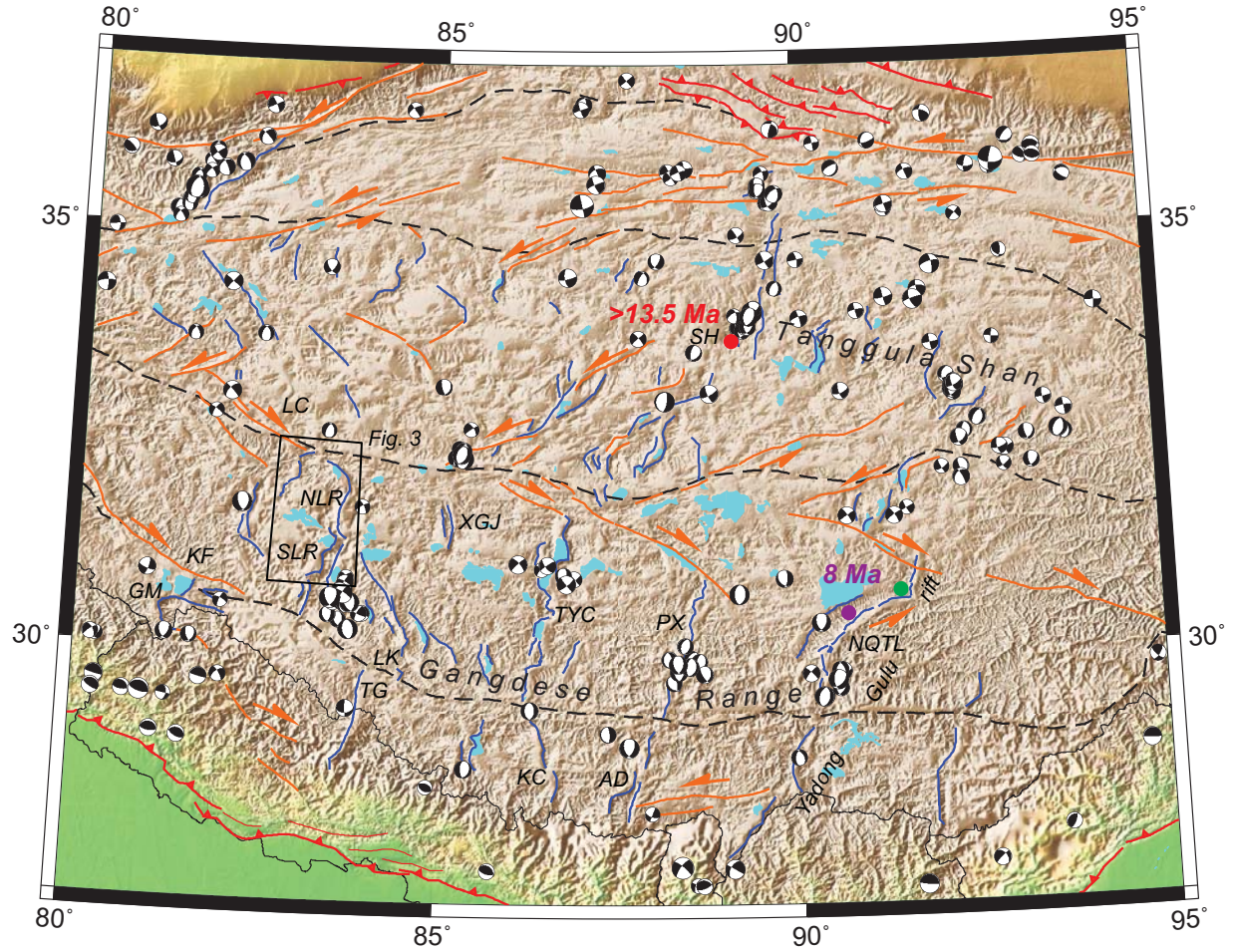
Figure 2: Active structures of central and southern Tibet. Map symbology is the same as in Figure 1. Earthquake focal mechanisms are from Global CMT (www.globalcmt.org) from 1 Jan 1976 to 20 Mar 2012 above 80 km depth. SH = Shuang Hu graben. LC = Lamu Co fault. NLR = North Lunggar rift. SLR = South Lunggar rift. XGJ = Xianggangjiang rift. LK = Lopukangri rift. TYC = Tangra Yum Co Rift. PX = Pumqu-Xainza rift. NQTL = Nyainqentanglha rift. KF = Karakoram fault. GM = Gurla Mandhata rift. TG = Thakkhola graben. KC = Kung Co rift. AD = Ama Drime rift. Purple circle marks study locations of *Pan and Kidd* [*1992*], *Harrison et al.* [*1995*] and *Kapp et al.* [*2005*]. Green circle marks study location of *Edwards and Ratschbacher* [*2005*]. Red circle marks study location of *Blisniuk et al.* [*2001*]. Black rectangle indicates location of our mapping in the Lunggar rift (Figure 3).

Map Units

ice	ice and snow
Qa	Quaternary alluvium
Qo	Quaternary alluvium (older)
Qsh	Quaternary shorelines
Qm	Quaternary moraine and outwash
N-Q	Neogene - Quaternary strata
myl	mylonites
gr	granite
v	volcanic rocks
K	Cretaceous strata and Tertiary volcanic rocks
Jr	Jurassic strata
Pz-Mz	Paleozoic-Mesozoic strata
ma	amphibolite-facies metamorphic rocks
mv	greenschist-facies volcanic rocks
	lake

Contacts

normal fault, active

normal fault, active, inferred

thrust fault, inferred

detachment fault, known

detachment fault, queried

right-slip fault

fault, inactive, buried

intrusive contact

intrusive contact, inferred or buried

depositional contact

0 3 6 12 18 24 km

Lamu Co fault

Qa

K

K

Qsh

Qa

Qa

Qo

Qa

Ngangla Ringco

Pz-Mz

Pz-Mz

Qsh

ice

Qm

Qm

gr

ice

ma

Pz-Mz

Qa

K

Qsh

ma

Pz-Mz

Pz-Mz

N-Q

N-Q

Qo

ma

NLD

Qo

N-Q

K

North Lunggar rift

Figure 4

Ringin-yubo Co

gr

gr

mv

Qo

Pz-Mz

South Lunggar rift

Qm

ma

myl

ice

mv

SLD

ice

Surla Range

Qm

A

B

A

PCF

B'

v

Qa

gr

mv

gr

Palung Co

ice

gr

Qa

Qsh

Gangdese Range

Figure 3: Bedrock and Quaternary geologic Map of the North and South Lunggar Rifts and Lamu Co fault. Mapping of North Lunggar Rift modified from *Kapp et al.* [*2008*] and our field observations. Mapping of Lamu Co fault modified from *Taylor et al.* [*2003*]. NLD = North Lunggar Detachment. SLD = South Lunggar Detachment. PCF = Palung Co fault. See Figure 2 for location. Cross-section lines A-A' and B-B' are also shown. Black box indicates location of Figure 4.
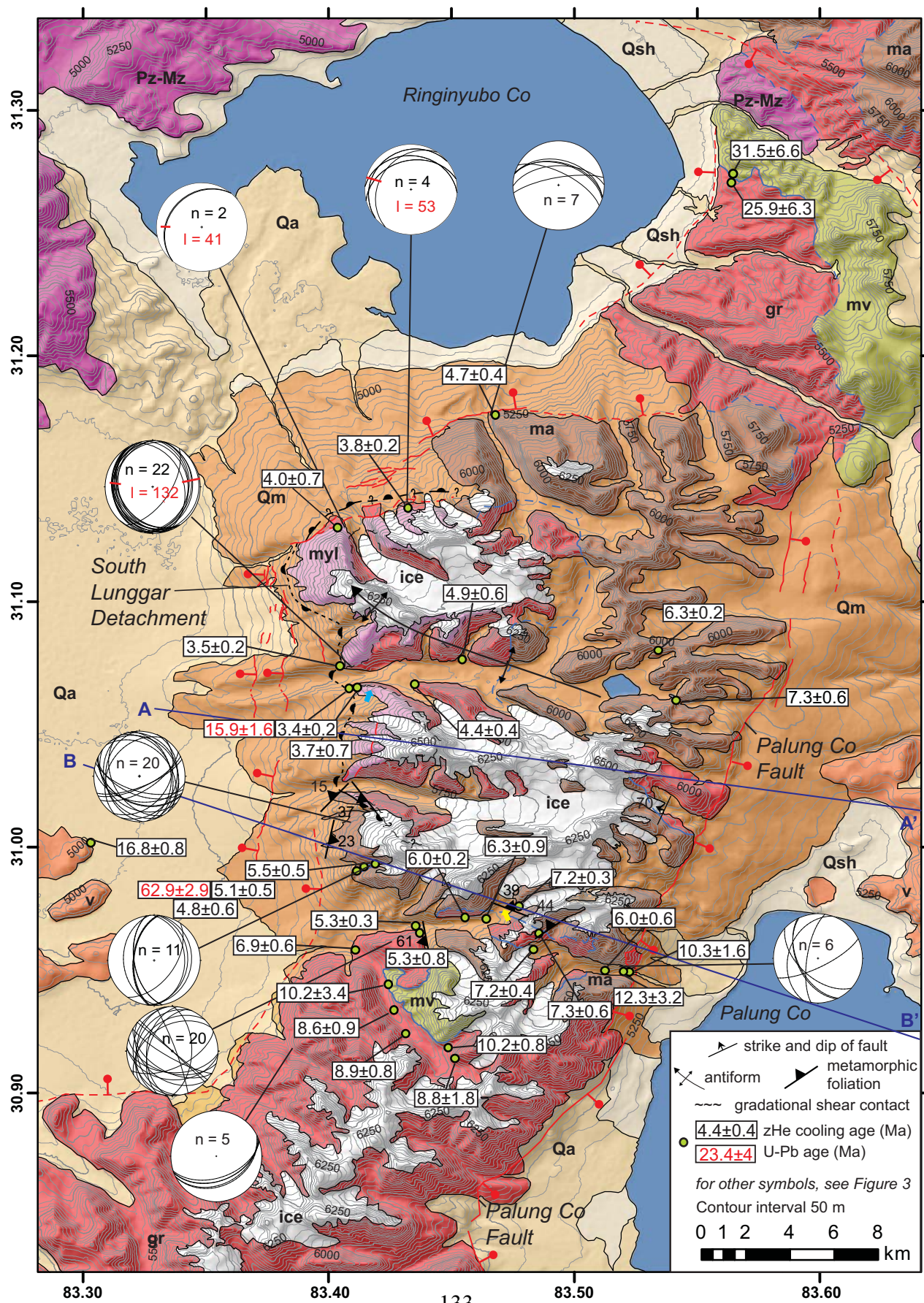
Figure 4: Geologic map of the South Lunggar Rift. See Figure 3 for location. Note that cross-section lines A-A' and B-B' extend off the map to the east; see Figure 3 for full extent. On stereo-nets, 'n' indicates the number of fault planes plotted, and 'l' indicates the number of fault striations or stretching lineations measured; red lines indicate average orientation of lineations. Small blue and yellow arrows indicate position and direction field photographs (Figures 5c and 6c) were taken at.
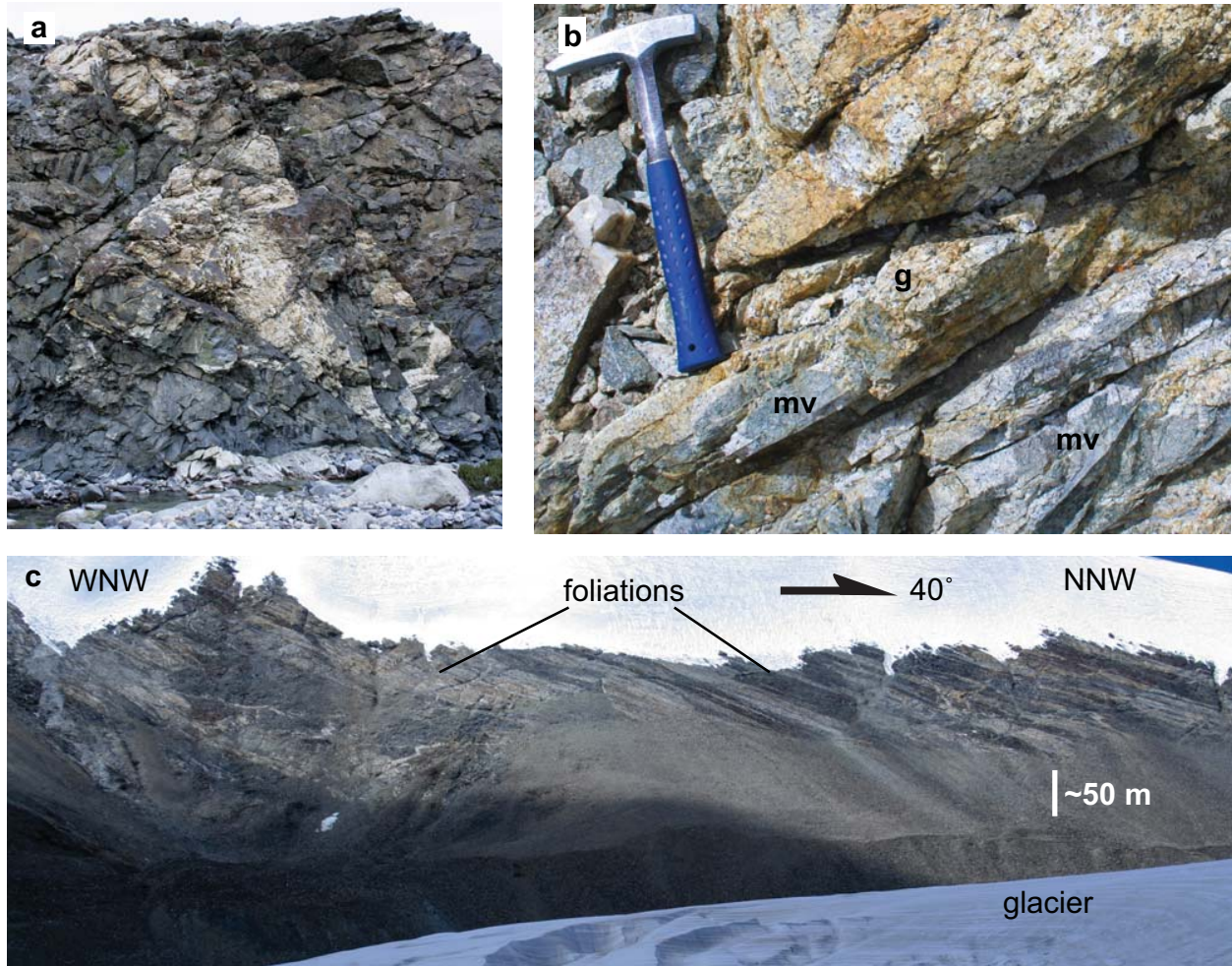
Figure 5: Field relationships in the southern Surla Range. (**a**): Undeformed leucogranites intruding pervasively fractured ampbibolite. Outcrop is approximately 3 m tall. (**b**) Leucogranite intruding greenschist-facies metavolcanic rocks. (**c**): Northwest looking view of moderately north-dipping gneissic foliation above glacier. Photograph taken from location and orientation indicated by yellow arrow in Figure 4; direction of view is perpendicular to arrow with trend shown.
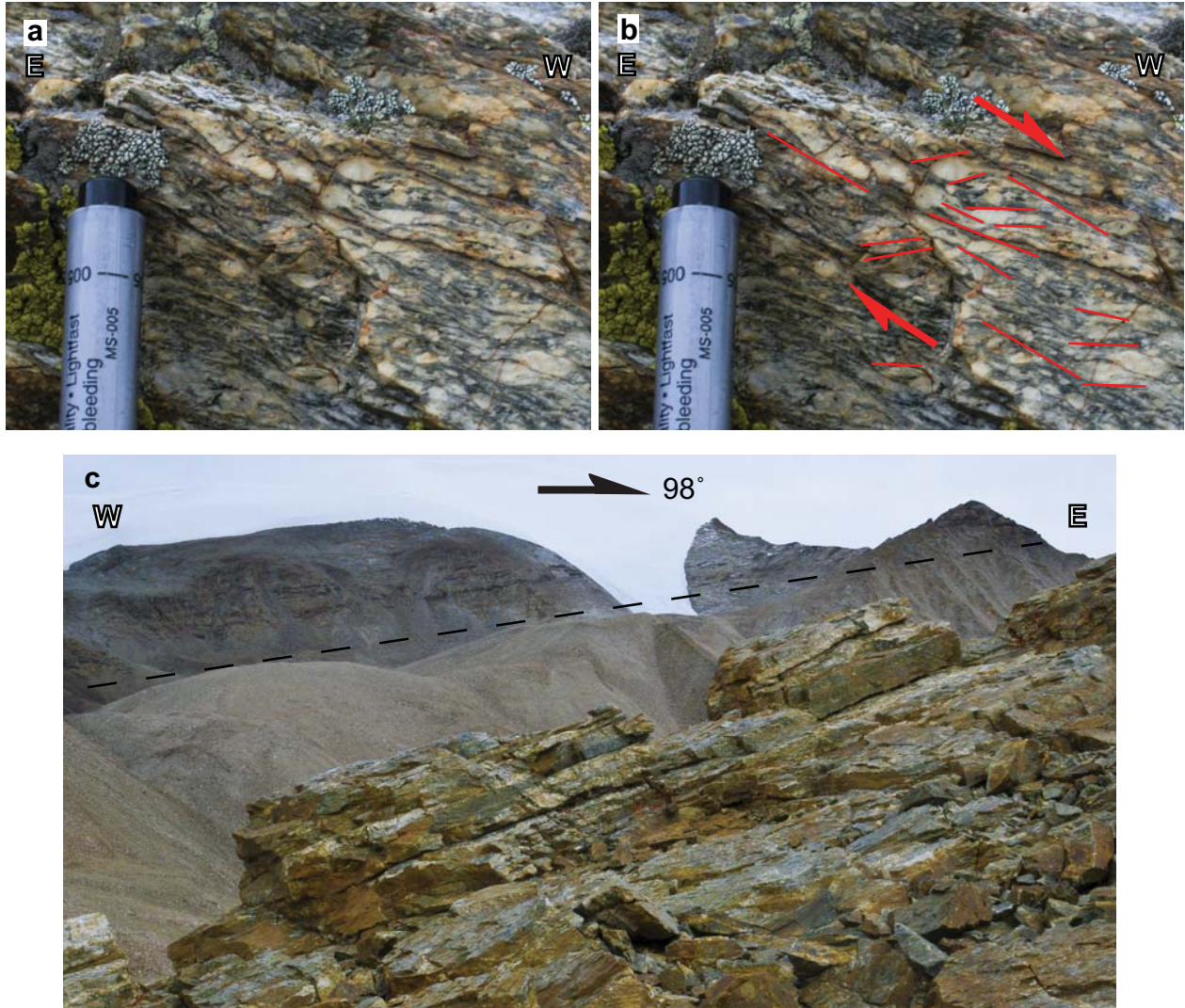
Figure 6: Field photographs of mylonitic shear zone near the detachment fault trace. (**a**) Uninterpreted close-up of mylonitic fabric. View is to the south. (b) Interpreted close-up of mylonite, showing S-C fabrics indicative of top down to the west, or normal-sense, shear. (c) North-northeast looking view of gently west-dipping mylonitic gneiss in foreground, and foliated rocks interpreted to be continuation of shear zone on the ridgeline in the background. Dashed line indicates bottom of mylonitic foliation; leucogranites below are essentially undeformed. Photograph taken from location and orientation indicated by blue arrow in Figure 4; direction of view is perpendicular to arrow with trend shown.
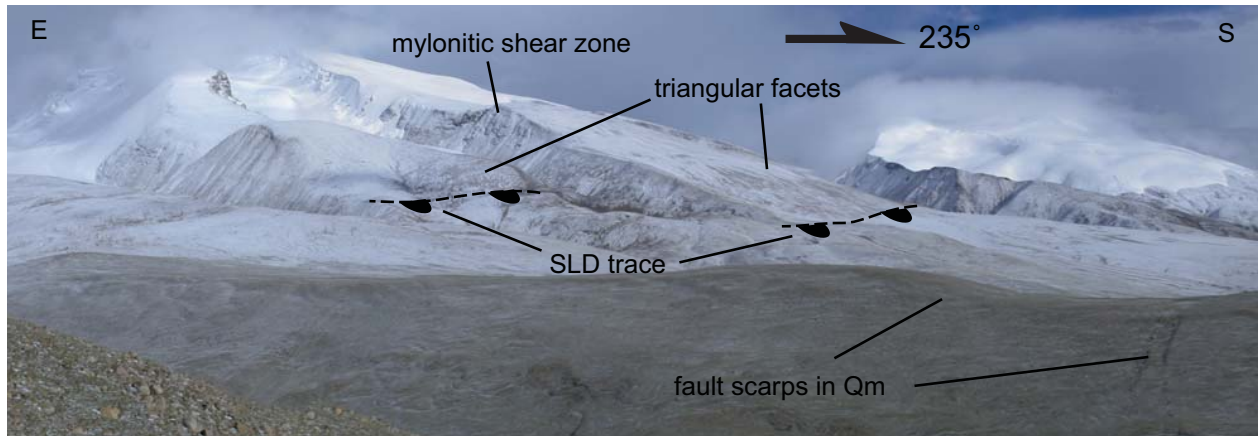
Figure 7: Southeast looking view of Surla Range showing triangular facets and mylonitic shear zone above the approximate trace of the SLD (here buried under **Qm**), as well as normal fault scarps (with different degrees of weathering) in Quaternary moraine extending past the rangefront. Direction of view is perpendicular to arrow with trend shown.
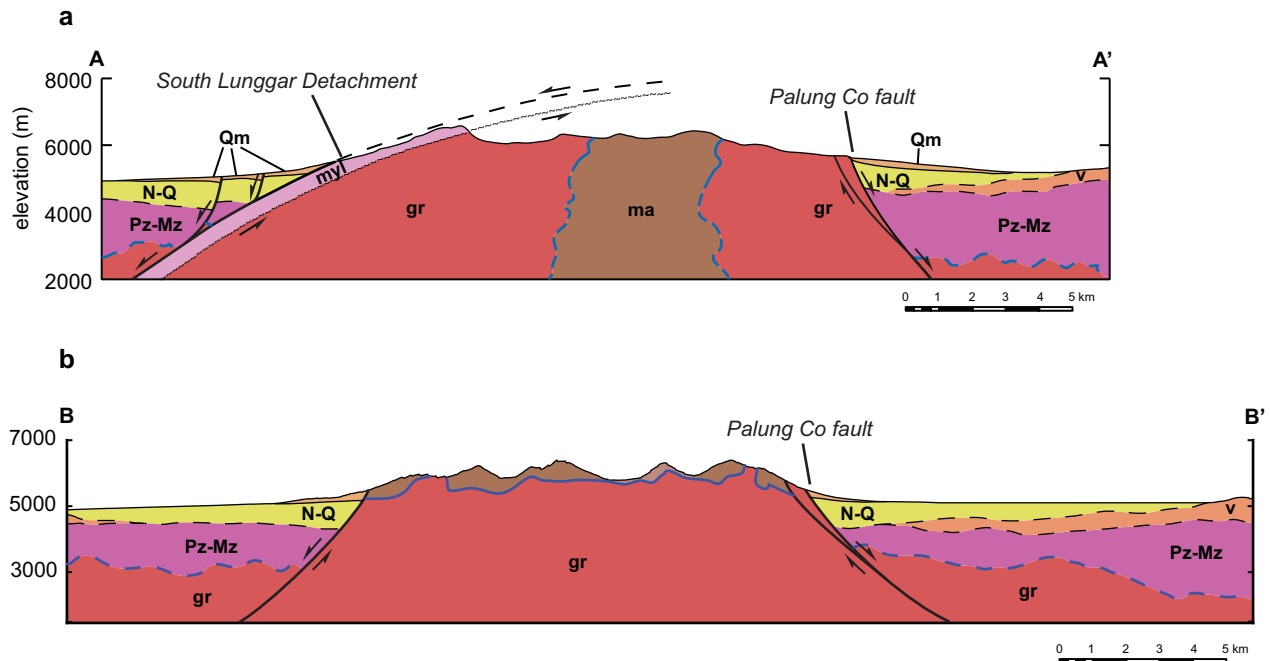
Figure 8: (a) Structural cross-section through the northern transect of the SLS (A-A' on Figure 4) showing low-angle South Lunggar Detachment and moderate-angle Palung Co fault. (b) Structural cross-section through the southern transect of the SLS (B-B' on Figure 4) showing moderately-dipping faults bounding the range.
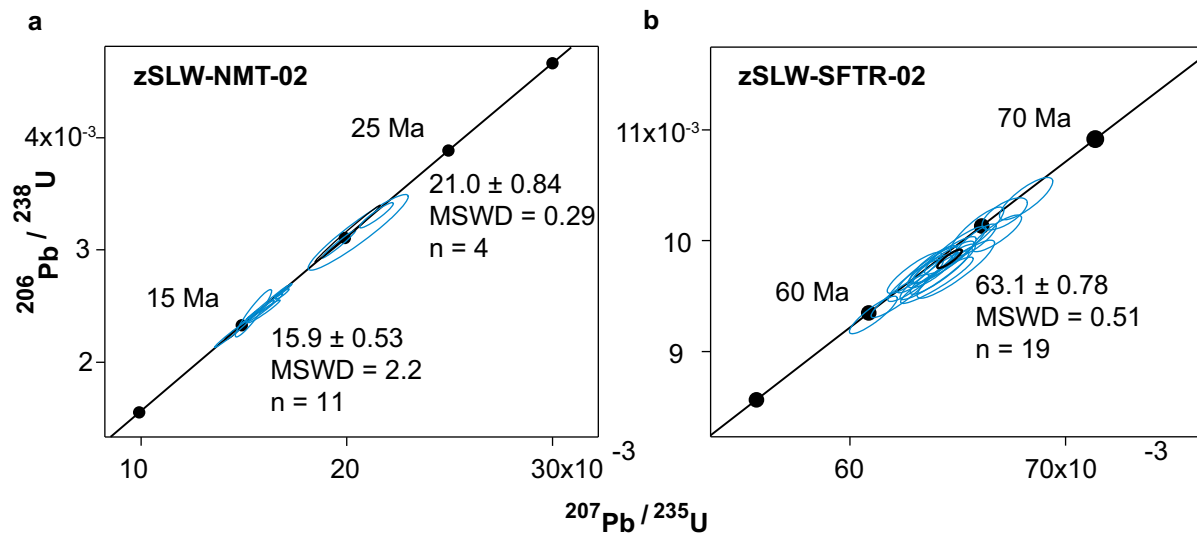
Figure 9: Concordia plots of zircon U-Pb ICP-MS rim analyses of two samples showing weighted mean $^{238}U/^{206}U$ ages. (a) Sample zSLW-NMT-02, mylonitized leucogranite from mylonite zone near SLD trace. Best-fit ellipse shown in black, with individual grain analyses shown in blue. Two populations are visible, one at ~15.9 Ma and one at ~21.0 Ma. (b) Sample zSLW-SFTR-02, ductilely deformed leucogranite from SLR footwall. Ages cluster at ~63 Ma, indicating Gangdese-age magmatism. See Figure 4 for sample locations.
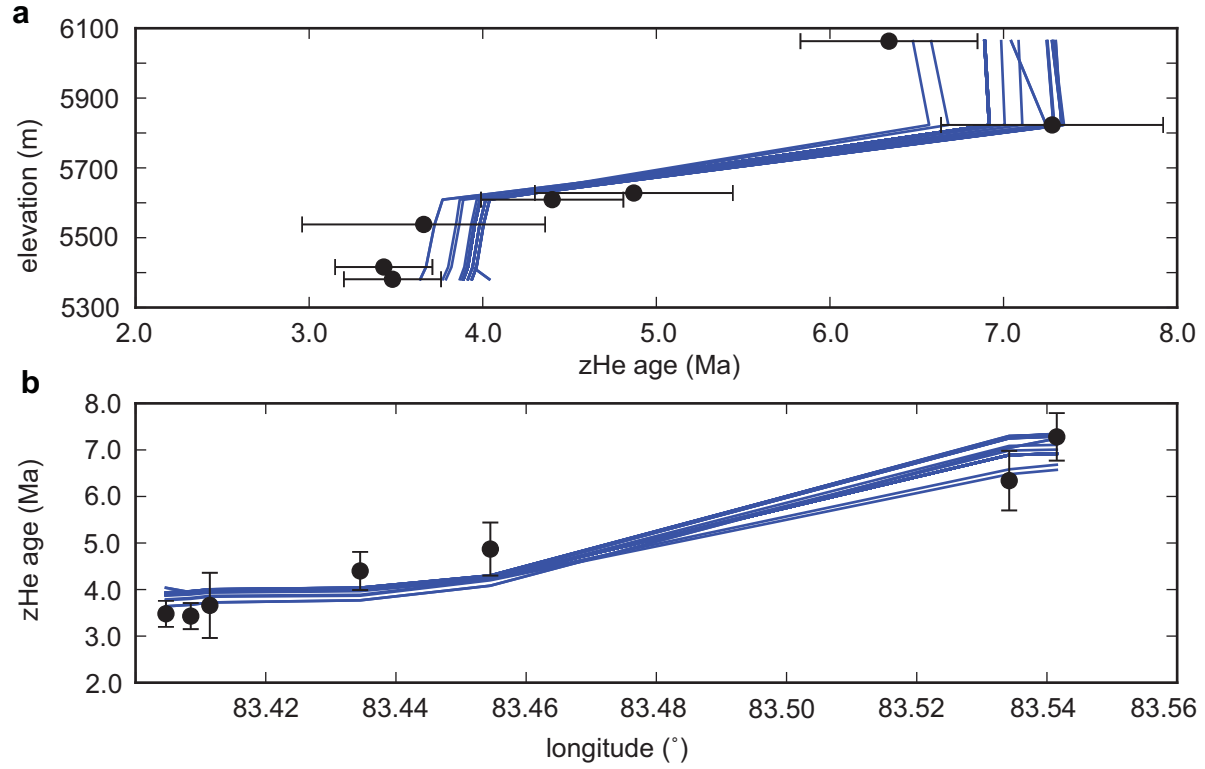
Figure 10: Pecube modeling results for north transect. (**a**) Age vs. elevation plot for observed data (black dots with 1σ errorbars) and model results. Blue lines indicate predicted ages at each sample location for runs where all ages fit the data within 2σ. (**b**) Age vs. longitude plot for same data and predicted ages. Symbology same as (**a**).
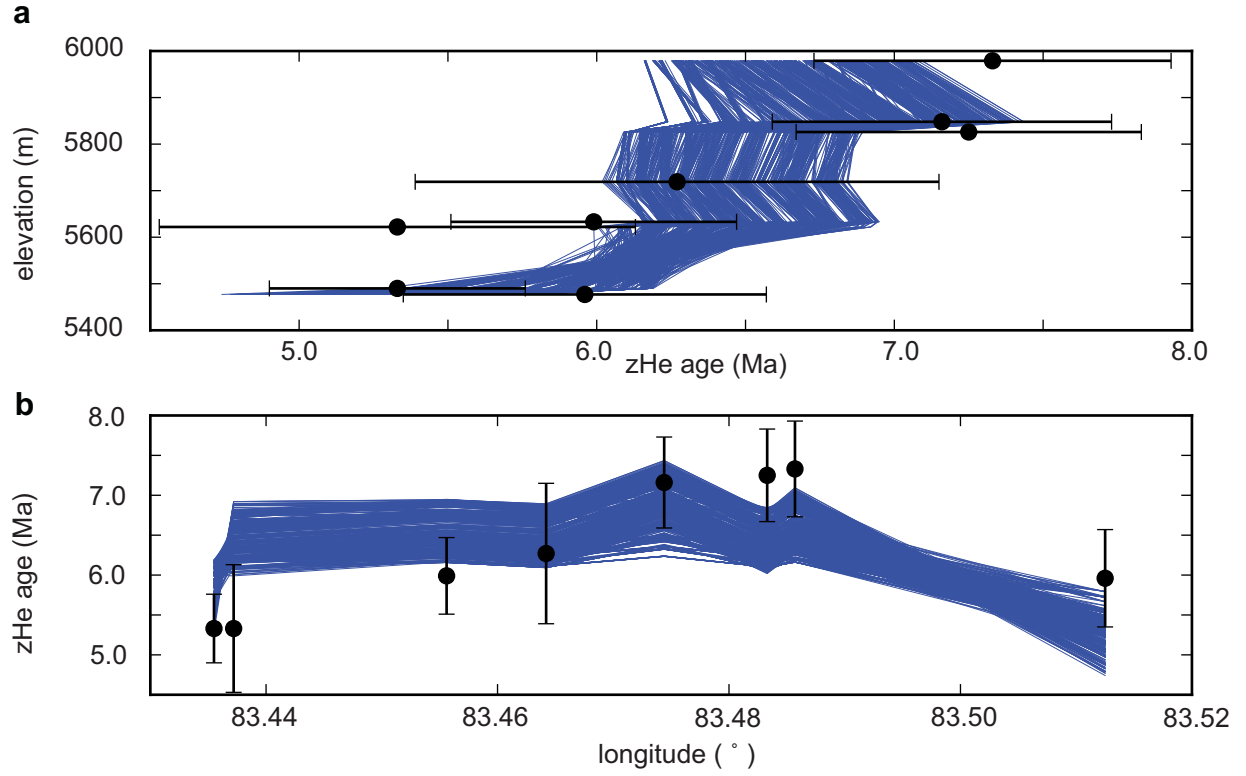
Figure 11: zHe data and Pecube model results for south transect. (**a**) Age vs. elevation plot for observed data (black dots with 1σ errorbars) and model results. Blue lines indicate predicted ages at each sample location for runs where all ages fit the data within 2σ. (**b**) Age vs. longitude plot for same data and predicted ages. Symbology same as (**a**).
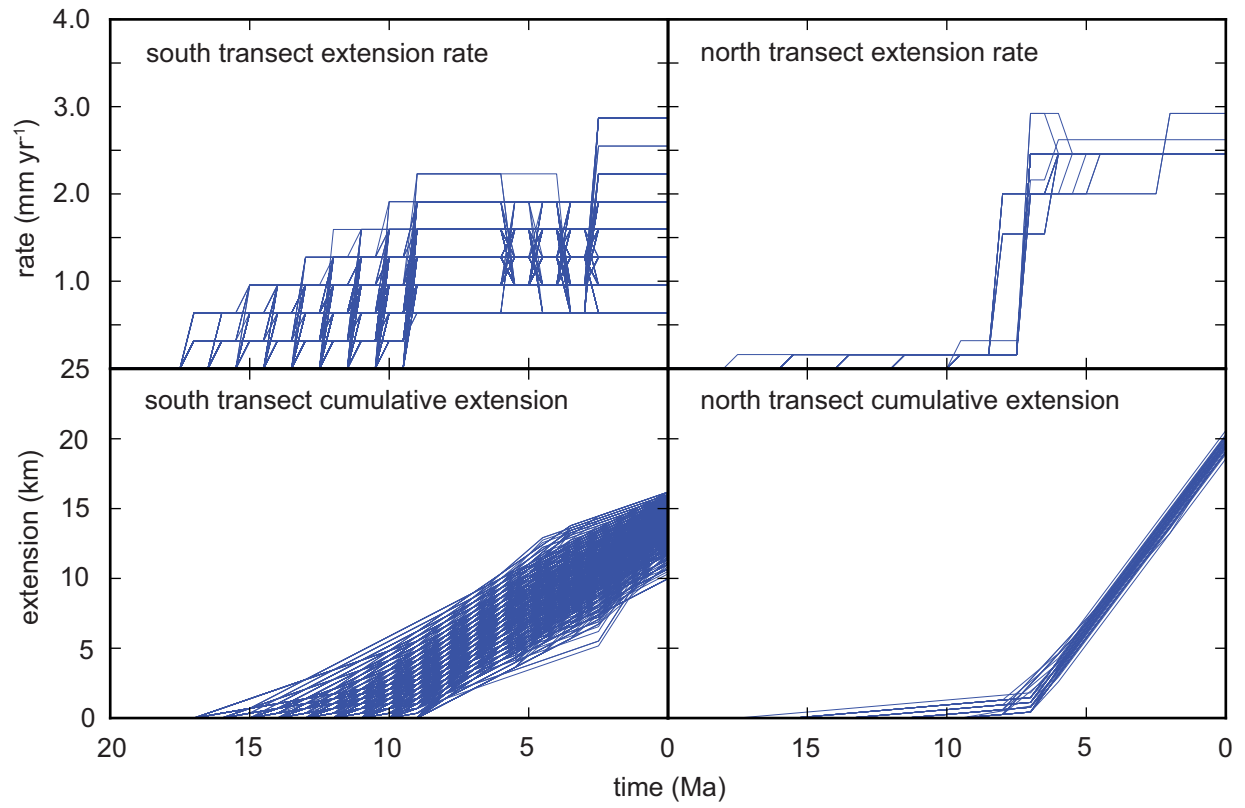
Figure 12: Extension rate and cumulative extension for north and south transect Pecube modeling results. Blue lines indicate model fits at 2σ.
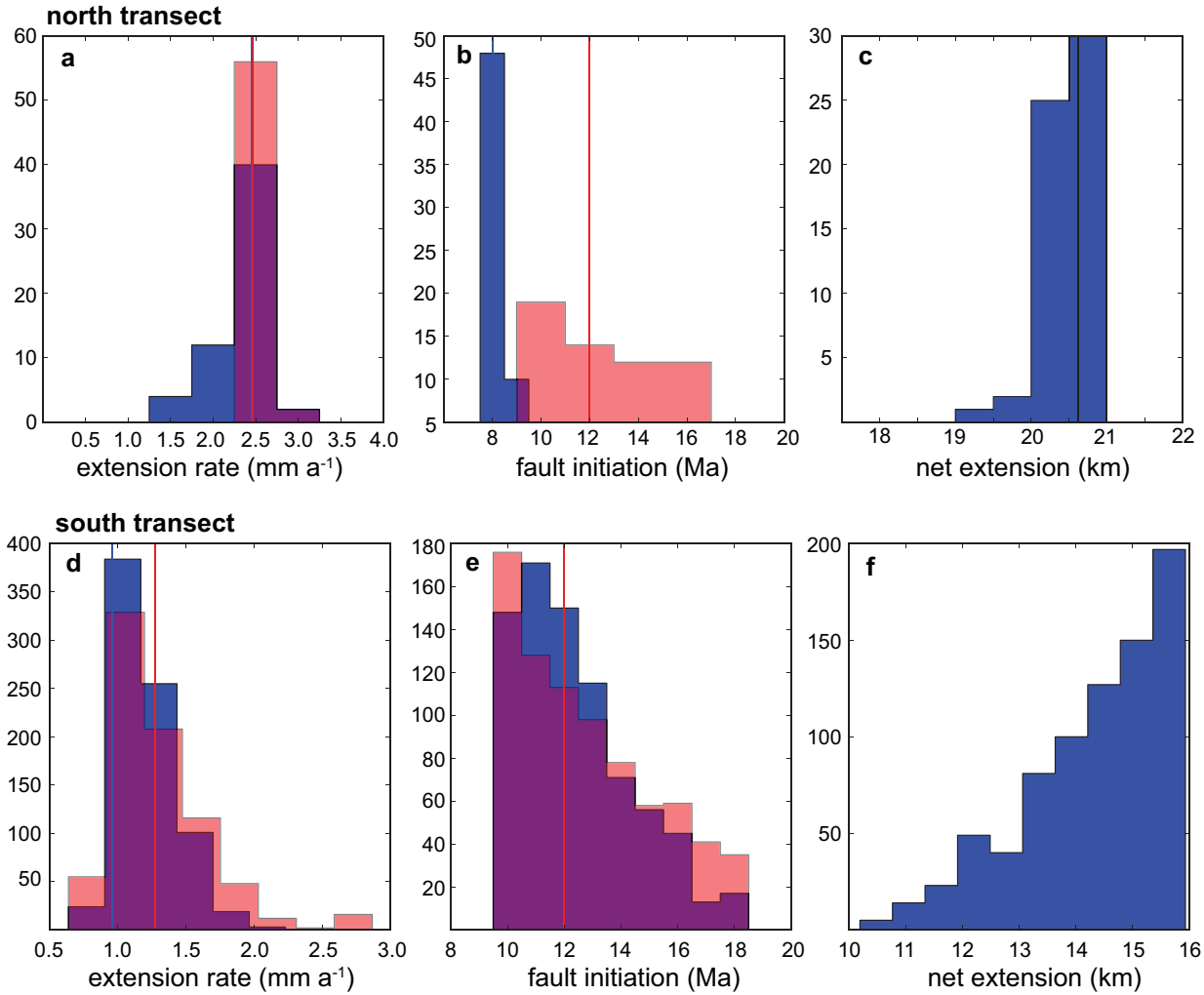
Figure 13: Histograms for model run results. **a**: Horizontal extension rate for the northern transect (A-A') before (blue) and after (red) a possible Pliocene acceleration for the northern transect. Purple in all graphs indicates overlap of red and blue histograms, and vertical lines indicate median values. **b**: Fault initation ages for the SLD (blue) and PCF (red). **c**: Net extension across the northern SLR. **d**: Horizontal exension rate for the southern transect (B-B') before (blue) and after (red) a possible Pliocene acceleration. **e**: Initiation ages for the western fault (blue) and PCF (red). **f**: Net extension across the southern SLR.
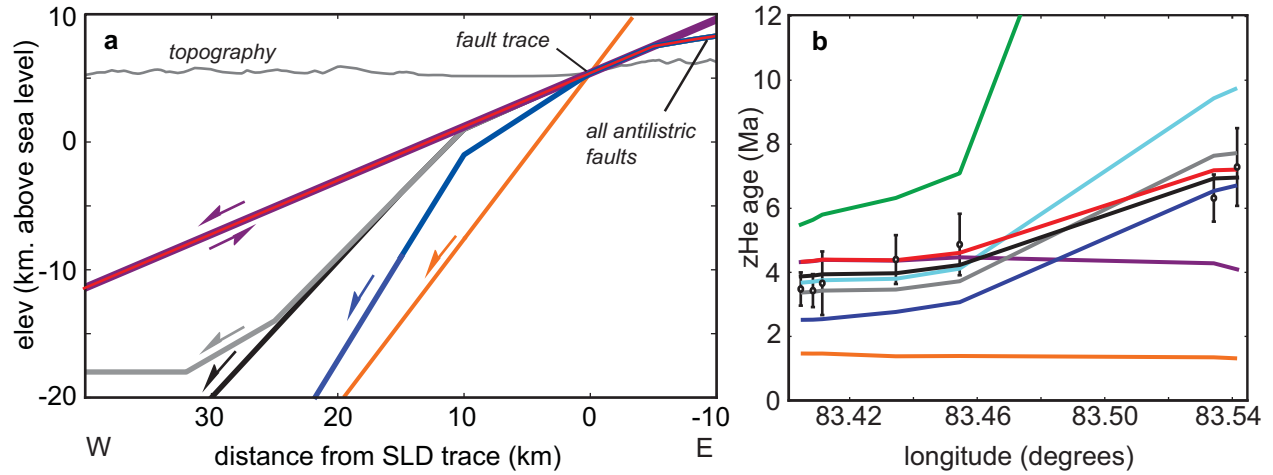
Figure 14: (**a**) SLD geometries tested during sensitivity testing. Orange = planar high-angle. Blue = steep antilistic. Grey = rolling hinge. Black = moderate antilistric (used in main models). Red = low-angle antilistric. Purple = planar low-angle. Red and purple faults have same subsurface geometry. All modeled faults daylight at mapped fault trace. No vertical exaggeration. (**b**) Results from sensitivity testing, presented as zHe age-longitude plot, with data as discrete points with 2-sigma errorbars, and model results as lines connecting modeled ages at data point locations. Green = 1/2 modeled crustal heat production. Light blue = lower (900 ˚C) Moho temperature. Other colors same as in (a).
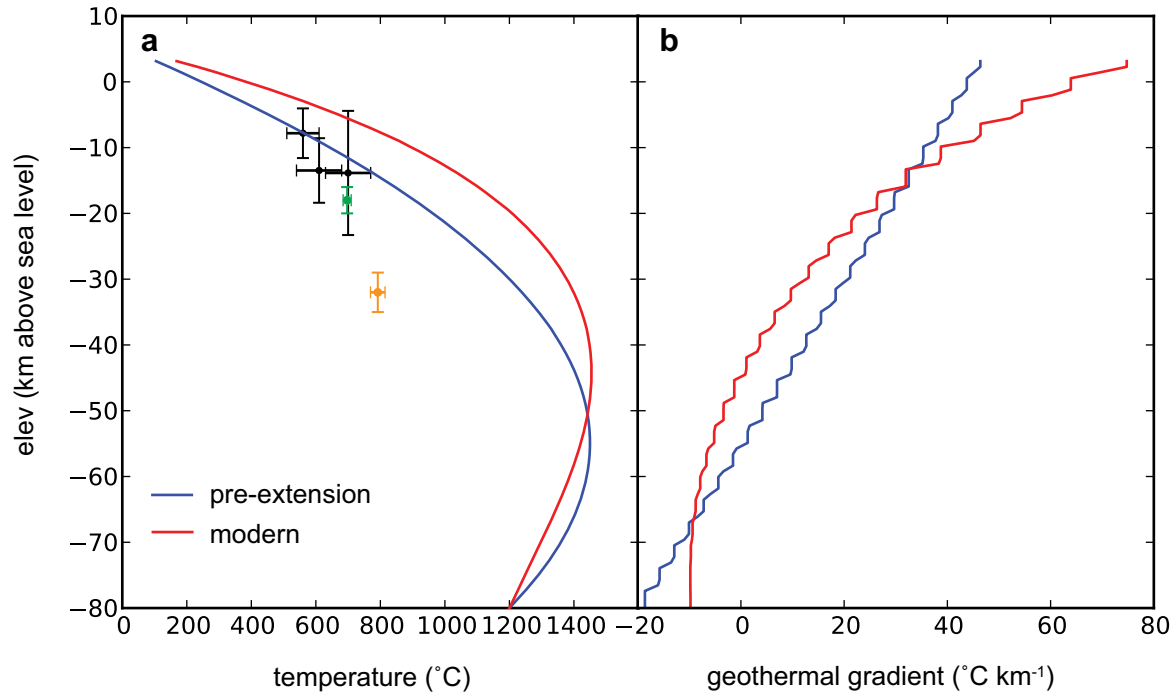
Figure 15: (**a**) Pre-extension and modern geotherm of the footwall of the SLD. Data points are other thermobarometric estimates. Black data are from petrologic studies in the Nyainqentanglha footwall [*J. Kapp et al., 2005*]. Green data point is from the α-β quartz transition in the Qiangtang block, and orange is the α-β quartz transition in the Lhasa block from seismic reflections [*Mechie et al., 2004*]. (**b**) Pre-extension and modern geothermal gradient from the same location as (a). Steps in geothermal gradient are an artefact of the model and indicate the depth resolution of the model.
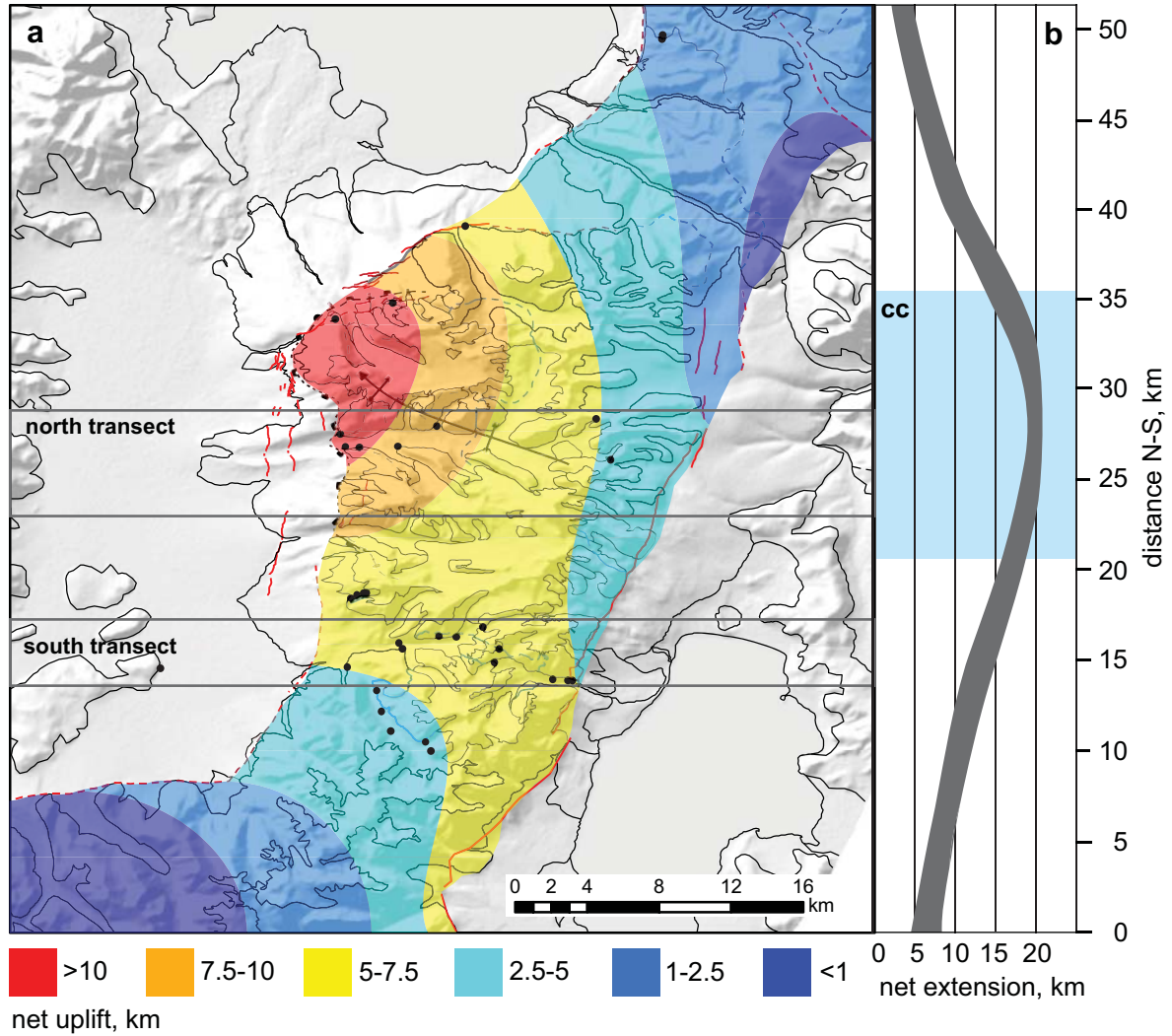
Figure 16: (**a**) Approximate contours of net uplift estimated from modeling results, zHe ages and structural mapping. Also shown are zHe sample locations (dark grey dots), geologic structures and contacts (see Figure 3 for symbology), and topography. Grey boxes show the width and location of the north and south transect Pecube models. Uncertainty in contour mapping is estimated at 2-5 km in both value and contour position based on variance in model results. (**b**) Net extension versus north-south distance from southern edge of map in (a); same scale as map. Dark grey band represents the 95% confidence interval, corresponding to the model results in Figures 12 and 13. Blue-grey box labeled 'cc' indicates along-strike extent of core complex, as judged by low-angle brittle and mylonitic fault fabrics and domal geometry.

146

Sample	Mean (Ma)	St. Dev. (Ma)	Age err. (Ma)	Latitude (°)	Longitude (°)	Altitude (m)
SLE-NMT-02	7.3	0.6	0.6	31.05958	83.54151	5823
SLE-NMT-03	6.3	0.2	0.5	31.08004	83.5342	6063
SLE-SCTR-01	9.4	0.8	0.7	30.94907	83.52237	5366
SLE-SCTR-02	11.8	1.5	0.9	30.94907	83.52237	5366
SLE-SCTR-03	12.3	3.2	1.0	30.94915	83.52008	5604
SLE-SCTR-05	6.0	0.6	0.5	30.94966	83.51246	5477
SLE-SCTR-06	7.2	0.4	0.6	30.95814	83.48333	5826
SLE-SCTR-07	7.3	0.6	0.6	30.96490	83.48569	5979
SLW-BSTR-01	10.2	3.4	0.8	30.94404	83.42437	5450
SLW-BSTR-02	8.6	0.9	0.7	30.93364	83.42674	5478
SLW-BSTR-03	8.9	0.8	0.7	30.92383	83.43140	5641
SLW-BSTR-05	8.8	1.8	0.7	30.91829	83.44883	5873
SLW-BSTR-06a	10.2	0.8	0.8	30.91379	83.45148	5874
SLW-CCTR-03	5.3	0.8	0.4	30.96502	83.43724	5622
SLW-CCTR-04	5.3	0.3	0.4	30.96790	83.43554	5490
SLW-CCTR-05	6.0	0.2	0.5	30.97127	83.45555	5663
SLW-CCTR-06	6.3	0.9	0.5	30.97082	83.46420	5719
SLW-CCTR-07	7.2	0.3	0.6	30.97590	83.47744	5848
SLW-HW-01	16.8	0.8	1.3	31.00171	83.30310	4960
SLW-LK-01	25.9	6.3	2.1	31.27406	83.56464	5010
SLW-LK-02	31.5	6.6	2.5	31.27406	83.56464	5010
SLW-NC-02	4.8	0.4	0.4	31.17597	83.46808	5201
SLW-NFT-01	3.8	0.2	0.3	31.13807	83.43247	5811
SLW-NMT-01	3.5	0.2	0.3	31.07366	83.40467	5381
SLW-NMT-02	3.4	0.2	0.3	31.07363	83.40496	5416
SLW-NMT-03	3.7	0.7	0.3	31.06495	83.41171	5538
SLW-NMT-04	4.4	0.4	0.4	31.06623	83.43498	5609
SLW-NMT-05	4.9	0.6	0.4	31.07644	83.4545	5628
SLW-NWC-01	4.0	0.7	0.3	31.13001	83.40368	5701
SLW-SFTR-01	4.8	0.6	0.4	30.99023	83.41145	5676
SLW-SFTR-02	5.1	0.5	0.4	30.99191	83.41448	5724
SLW-SFTR-04	5.5	0.5	0.4	30.99297	83.41912	5810
SLW-STR-01	6.9	0.6	0.6	30.95806	83.41096	5275

Table 1: Zircon (U-Th)/He sample summary. Individual aliquot analyses shown in the data repository (Table S2). Age error is 8% 2σ laboratory analytical error (see text for discussion).

North Transect fault parameter	Range	Step	Unit
SLD initiation	8 - 18	1	Ma
SLD initial slip rate	0.25 - 3.0	0.25 - 0.5	mm a^{-1}
SLD acceleration	2 - 6.5	0.5	Ma
SLD post-acceleration slip rate	1.5 - 4.5	0.5	mm a^{-1}
PCF initiation	10 - 18	2	Ma
PCF slip rate	0.25 - 1.5	0.25 - 0.5	mm a^{-1}

South Transect fault parameter	Range	Step	Unit
PCF initiation	10 - 18	2	Ma
PCF initial slip rate	0.5 - 2.0	0.5 - 1	mm a^{-1}
western fault initiation	10 - 18	2	Ma
western fault initial slip rate	0.5 - 2.0	0.5 - 1	mm a^{-1}
fault acceleration (of both faults)	3 - 6	1	Ma
PCF post-acceleration slip rate	0.5 - 3.0	0.5 - 1	mm a^{-1}
western fault post-acceleration slip rate	0.5 - 3.0	0.5 - 1	mm a^{-1}

Table 2: Parameters for rates and timing of faulting for Pecube modeling of the north and south zHe sampling transects.
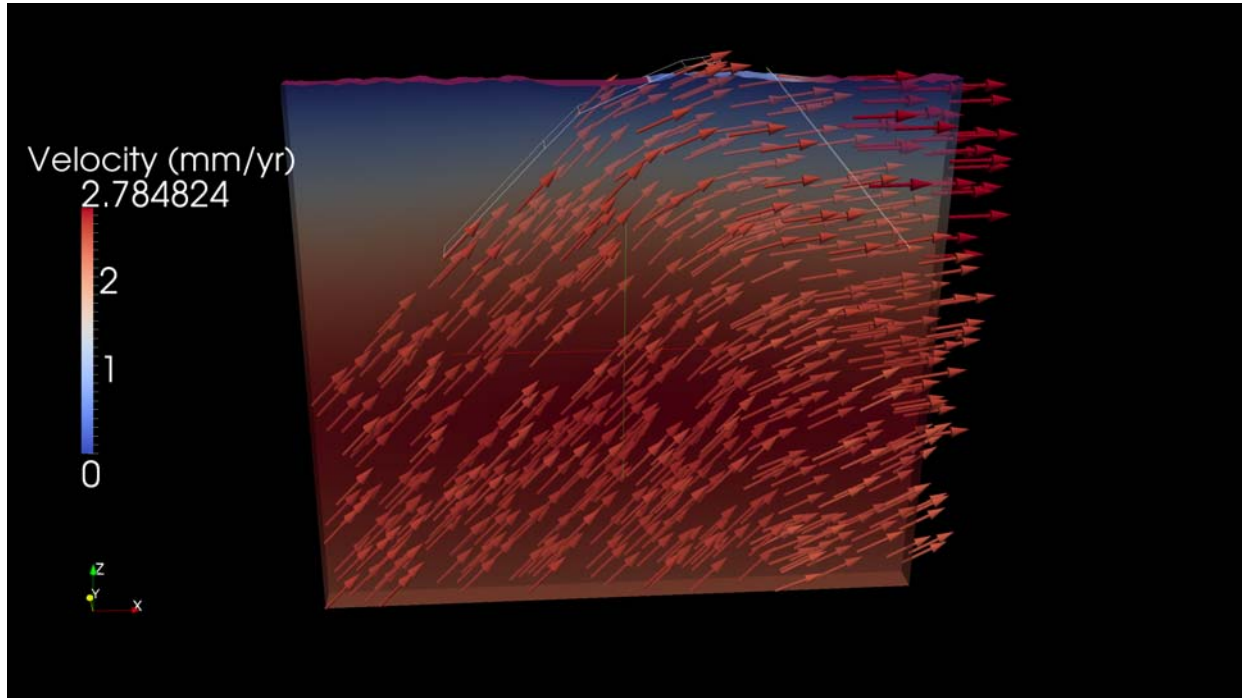
Figure S1: Pecube FEM model of the northern transect showing fault geometry and velocity vectors relative to the western (left) hanging wall. Color of the model indicates temperature.
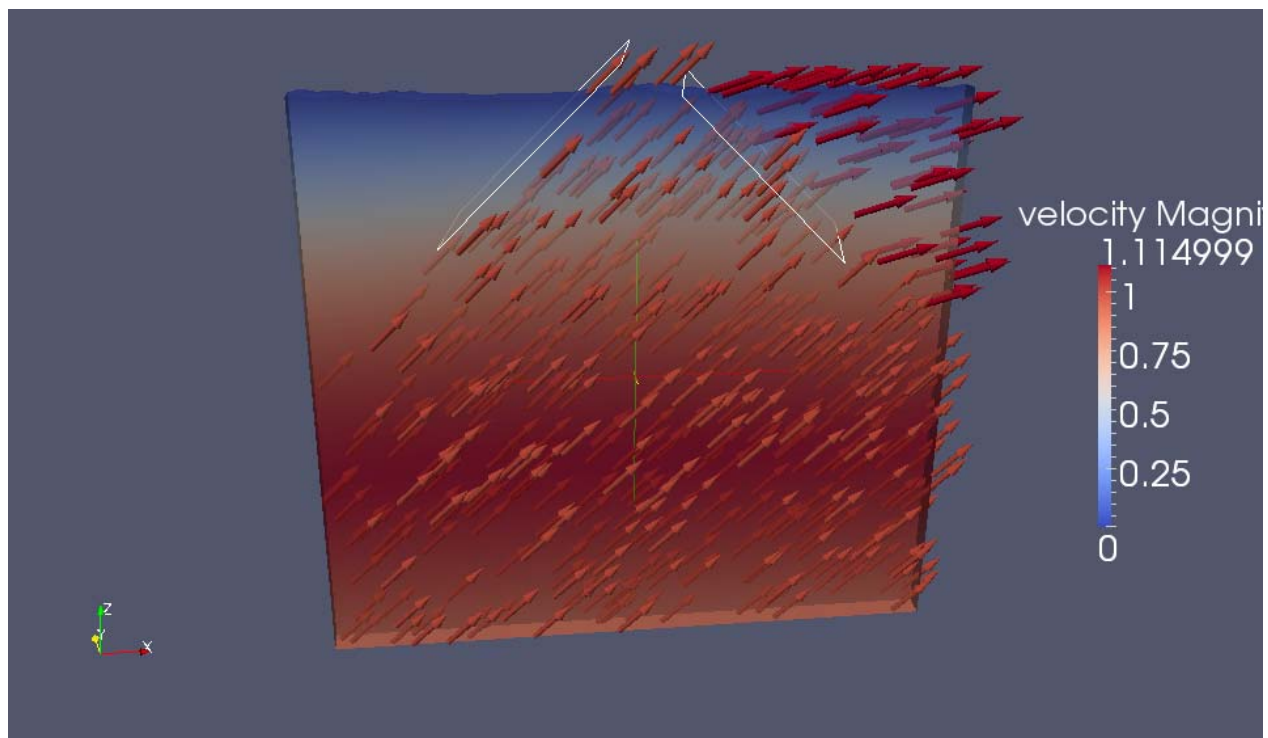
Figure S2: Pecube FEM model of the southern transect showing fault geometry and velocity vectors relative to the western (left) hanging wall. Color of the model indicates temperature.

Table S1: Zircon (U-Pb) results

sample	Age 206Pb/238Uc (Ma)	206Pb/238Uc error (2SD) (m.y.)	[U] (ppm)	[U]err (ppm)	[Th] (ppm)	[Th]err (ppm)	[U]/[Th]	[U]/[Th]err	Ratios (corrected for downhole and mass fra 207Pb/235U	207Pb/235U err, 2 sigma	206Pb/238U
SLW_SFTR_02_1	66.7	1.2	292	15	224.8	9.6	1.306	0.03	0.0686	0.0016	0.01036
SLW_SFTR_02_2	65.68	0.92	800	16	508	24	1.637	0.088	0.0666	0.001	0.01024
SLW_SFTR_02_3	63.6	1.4	308	13	236	16	1.308	0.039	0.0659	0.0017	0.00987
SLW_SFTR_02_4	62.9	1.2	593	13	452	13	1.363	0.04	0.0642	0.0012	0.00983
SLW_SFTR_02_5	62.37	0.94	841	17	463	23	1.884	0.08	0.0638	0.0011	0.00973
SLW_SFTR_02_6	62.5	1.7	344	12	269	10	1.293	0.023	0.066	0.0022	0.00976
SLW_SFTR_02_7	60.9	1.2	585	14	355	14	1.69	0.11	0.0677	0.0023	0.00958
SLW_SFTR_02_8	62.4	1.3	505	15	443	21	1.18	0.047	0.0671	0.0018	0.00978
SLW_SFTR_02_9	64.17	0.91	452	13	372	11	1.225	0.014	0.0671	0.0014	0.01002
SLW_SFTR_02_10	62.3	1.2	485.3	8.3	366	16	1.53	0.15	0.0634	0.0013	0.00972
SLW_SFTR_02_11	61.8	1.2	268.8	4.1	169.3	2.8	1.596	0.032	0.0653	0.0015	0.00966
SLW_SFTR_02_12	64.7	1.4	822	69	436	53	2.51	0.45	0.0659	0.0012	0.0101
SLW_SFTR_02_13	62.3	1.2	583	33	463	17	1.225	0.042	0.0637	0.0014	0.00971
SLW_SFTR_02_14	62.3	1.6	460	19	158	15	3.25	0.17	0.0664	0.0018	0.00975
SLW_SFTR_02_15	62.8	1.1	721	19	560	17	1.276	0.021	0.0649	0.0012	0.00977
SLW_SFTR_02_16	63	1.3	634	21	485	14	1.37	0.047	0.0648	0.0015	0.00984
SLW_SFTR_02_17	60	1.1	485	16	107.2	5.1	4.79	0.11	0.0622	0.0012	0.00934
SLW_SFTR_02_18	61.8	1.3	249.5	3.8	205	15	1.3	0.098	0.0704	0.0019	0.00971
SLW_SFTR_02_19	64.6	1.1	525	16	387	17	1.44	0.038	0.0662	0.0013	0.01007
SLW_NMT_02_1	20.3	2.2	803	57	290	45	2.93	0.55	0.0234	0.0015	0.00318
SLW_NMT_02_2	16.07	0.35	1231	62	524	22	2.5	0.19	0.0178	0.00061	0.002518
SLW_NMT_02_3	14.51	0.36	3250	310	1310	140	2.676	0.097	0.01543	0.0004	0.002259
SLW_NMT_02_4	19.65	0.8	874	98	590	100	1.519	0.092	0.0241	0.0015	0.00309
SLW_NMT_02_5	20.2	1.6	607	34	176	37	4.09	0.7	0.0262	0.0022	0.00321
SLW_NMT_02_6	15.8	0.65	754	31	453	45	1.8	0.14	0.0194	0.00096	0.00249
SLW_NMT_02_7	21.3	0.72	1770	220	78.9	9.7	25.6	2.2	0.02448	0.00058	0.00334
SLW_NMT_02_8	16.98	0.4	573	45	508	55	1.207	0.042	0.0244	0.0016	0.002748
SLW_NMT_02_9	16.79	0.3	779	12	488	11	1.624	0.034	0.01905	0.00056	0.002628
SLW_NMT_02_10	14.49	0.76	416	46	126	15	3.31	0.16	0.0308	0.0064	0.00242
SLW_NMT_02_11	16.31	0.93	794	64	388	37	2.04	0.28	0.0238	0.0013	0.00261
SLW_NMT_02_12	15.64	0.3	770	34	735	32	1.022	0.05	0.0277	0.0013	0.002542
SLW_NMT_02_13	16.02	0.78	1096	82	108	11	11.07	0.92	0.01803	0.00074	0.00251
SLW_NMT_02_14	15.38	0.4	619	32	484	55	1.52	0.33	0.0329	0.0012	0.002555
SLW_NMT_02_15	15.7	1.4	1526	79	221	14	6.57	0.27	0.0162	0.0011	0.00244

206Pb/238U err, 2 sigma	207Pb/206Pb	207Pb/206Pb err, 2 sigma	207Pb/235Uc	207Pb/235Uc err 2 sigma	206Pb/238Uc	206Pb/238Uc err 2 sigma	207Pb/206Pbc	207Pb/206Pbc err 2 sigma
0.00019	0.04814	0.00094	0.0677	0.0012	0.0104	0.00019	0.04812	0.0005
0.00014	0.04745	0.00065	0.0669	0.001	0.01024	0.00014	0.04752	0.0003
0.00022	0.048	0.0012	0.0645	0.0015	0.00991	0.00022	0.04758	0.00043
0.00018	0.04779	0.00081	0.0639	0.0014	0.0098	0.00019	0.04765	0.00036
0.00015	0.04801	0.00065	0.06334	0.00099	0.00972	0.00015	0.04788	0.00034
0.00026	0.0498	0.0014	0.064	0.0017	0.00974	0.00026	0.0485	0.00072
0.00019	0.0515	0.0019	0.0616	0.0014	0.0095	0.00019	0.04718	0.00042
0.00021	0.0496	0.0011	0.063	0.0014	0.00973	0.00021	0.04763	0.0004
0.00014	0.04887	0.00089	0.06538	0.00094	0.01	0.00014	0.04786	0.0004
0.00018	0.04774	0.00074	0.0627	0.0013	0.00971	0.00018	0.04792	0.0004
0.00019	0.04842	0.00092	0.0627	0.0013	0.00964	0.00019	0.04763	0.0004
0.00021	0.0478	0.00066	0.0656	0.0013	0.01009	0.00021	0.04771	0.00031
0.00019	0.048	0.00093	0.0641	0.0013	0.00971	0.00019	0.04792	0.0004
0.00024	0.0491	0.0012	0.0636	0.0018	0.00972	0.00025	0.04776	0.00042
0.00017	0.04782	0.00072	0.0637	0.0012	0.00978	0.00017	0.04772	0.00033
0.00021	0.04767	0.00081	0.0641	0.0015	0.00983	0.00021	0.04772	0.00037
0.00017	0.04806	0.00085	0.0608	0.0011	0.00935	0.00017	0.04774	0.00039
0.0002	0.0525	0.0015	0.0635	0.0018	0.00964	0.00021	0.04785	0.00068
0.00016	0.04788	0.00084	0.0663	0.0011	0.01007	0.00016	0.04804	0.0004
0.00033	0.0541	0.0038	0.0205	0.0024	0.00316	0.00034	0.0468	0.0014
0.000052	0.0525	0.002	0.01608	0.00038	0.002497	0.000054	0.04721	0.0004
0.000055	0.0496	0.0012	0.01443	0.00037	0.002254	0.000056	0.04717	0.00032
0.00012	0.0556	0.0023	0.0196	0.00082	0.00305	0.00012	0.04663	0.00075
0.00024	0.0588	0.0074	0.02	0.0016	0.00315	0.00025	0.04635	0.00051
0.0001	0.0561	0.0026	0.01597	0.00077	0.00245	0.0001	0.04739	0.0008
0.00011	0.0535	0.0017	0.02143	0.00082	0.00331	0.00011	0.04743	0.00069
0.00007	0.0648	0.0039	0.0169	0.00043	0.002638	0.000063	0.04713	0.00053
0.000045	0.0525	0.0014	0.01685	0.00033	0.002608	0.000046	0.04758	0.00054
0.00013	0.093	0.016	0.01438	0.00082	0.00225	0.00012	0.0460834	0.000003
0.00014	0.0676	0.0044	0.01615	0.00095	0.00253	0.00015	0.0460876	0.0000043
0.000051	0.0804	0.0037	0.01541	0.0003	0.002429	0.000046	0.0460847	0.0000015
0.00012	0.0537	0.0021	0.01605	0.00082	0.00249	0.00012	0.04751	0.00096
0.000063	0.0951	0.0034	0.01517	0.0004	0.002388	0.000062	0.04608475	0.00000099
0.00021	0.0487	0.0037	0.01545	0.00088	0.00244	0.00021	0.04625	0.00034

Table S2: zircon (U-Th)/He individual aliquot analytical results

Sample	Age (Ma)	U (ppm)	Th (ppm)	^{147}Sm (ppm)	[U]e	Th/U	He (nmol/g)	mass (ug)	Ft[a]	ESR[b]
SLE-NMT-01-1	12.54[c]	1361.1	864.3	2.0	1560.1	0.64	77.2	3.81	0.73	43.56
SLE-NMT-01-2	7.15	620.5	557.7	1.8	748.9	0.90	21.0	3.55	0.73	43.24
SLE-NMT-01-3	6.57	850.7	503.4	1.6	966.6	0.59	26.7	6.89	0.78	53.96
SLE-NMT-02-1	8.18	150.2	295.1	0.5	218.1	1.97	7.4	6.13	0.77	52.02
SLE-NMT-02-2	7.63	306.0	530.6	0.7	428.2	1.73	13.4	4.83	0.76	47.28
SLE-NMT-02-3	6.84	223.6	197.8	0.4	269.1	0.88	7.5	6.76	0.76	51.18
SLE-NMT-03-1	6.34	382.3	238.4	1.1	437.2	0.62	12.8	27.86	0.86	84.16
SLE-NMT-03-2	6.11	548.2	223.0	0.6	599.5	0.41	16.1	11.07	0.82	64.50
SLE-NMT-03-3	6.58	312.3	211.3	0.8	360.9	0.68	10.5	13.95	0.82	65.63
SLE-NMT-06-1	7.64	840.5	1918.7	0.5	1282.1	2.28	43.2	14.15	0.81	66.90
SLE-NMT-06-3	5.88	685.0	202.6	0.2	731.6	0.30	19.0	13.30	0.82	65.86
SLE-SCTR-01-1	9.56	992.9	512.1	0.5	1110.8	0.52	43.6	5.93	0.76	48.91
SLE-SCTR-01-2	8.02	294.7	171.9	0.0	334.3	0.58	11.6	9.99	0.80	60.64
SLE-SCTR-01-3	9.84	302.5	186.8	0.7	345.5	0.62	14.5	8.15	0.79	56.75
SLE-SCTR-01-4	10.10	458.8	258.3	2.2	518.2	0.56	21.4	5.41	0.76	48.59
SLE-SCTR-01-5	9.31	779.7	445.7	1.8	882.3	0.57	33.8	5.49	0.76	49.19
SLE-SCTR-02-1	13.47	128.2	118.3	2.0	155.4	0.92	8.7	5.84	0.76	50.71
SLE-SCTR-02-2	10.70	297.3	231.5	0.3	350.6	0.78	14.9	3.83	0.73	43.89
SLE-SCTR-02-3	11.24	431.4	348.1	0.9	511.5	0.81	23.8	6.49	0.77	50.69
SLE-SCTR-03-1	10.97	370.8	355.2	2.3	452.6	0.96	20.7	6.58	0.77	52.32
SLE-SCTR-03-2	41.15[c]	103.4	119.4	1.9	130.9	1.15	23.1	9.90	0.79	57.19
SLE-SCTR-03-3	10.11	371.2	266.8	2.4	432.6	0.72	18.6	8.49	0.79	56.08
SLE-SCTR-03-4	10.60	215.6	248.9	4.2	272.9	1.15	12.3	8.23	0.78	55.82
SLE-SCTR-03-5	14.03	427.2	873.5	1.6	628.2	2.04	35.0	4.74	0.73	44.49
SLE-SCTR-03-6	10.43	143.5	182.1	2.2	185.5	1.27	7.8	4.66	0.74	45.76
SLE-SCTR-04-1	18.89	1003.8	259.8	-0.6	1063.6	0.26	82.0	4.61	0.76	47.14
SLE-SCTR-04-3	10.80	1755.8	991.4	-0.2	1984.1	0.56	85.9	4.68	0.74	45.18
SLE-SCTR-05-1	5.30	503.9	78.1	-0.3	521.9	0.15	12.1	10.27	0.81	61.15
SLE-SCTR-05-2	6.48	780.0	372.8	-0.5	865.8	0.48	22.2	3.72	0.73	43.40
SLE-SCTR-05-3	6.11	2623.7	766.2	1.1	2800.1	0.29	70.6	5.26	0.76	49.16
SLE-SCTR-06-1	7.36	1376.6	768.4	-0.6	1553.4	0.56	46.5	4.90	0.75	47.40
SLE-SCTR-06-2	6.81	2044.7	899.9	-0.8	2251.8	0.44	61.0	4.65	0.74	43.87
SLE-SCTR-06-3	4.52[c]	430.7	2388.2	-0.4	980.5	5.55	18.1	5.22	0.74	48.15
SLE-SCTR-06-4	7.56	1541.6	360.2	1.3	1624.5	0.23	55.6	17.63	0.84	73.24
SLE-SCTR-07-1	7.55	1058.8	589.1	6.5	1194.5	0.56	36.1	4.59	0.74	44.79
SLE-SCTR-07-2	6.65	235.2	92.2	-0.4	256.4	0.39	7.0	5.21	0.76	47.48
SLE-SCTR-07-3	7.78	948.3	560.1	6.2	1077.3	0.59	34.5	5.90	0.76	49.23
SLW-BSTR-01-1	13.99	121.8	62.9	0.8	136.2	0.52	8.7	19.85	0.84	75.93
SLW-BSTR-01-2	9.09	383.6	231.4	1.7	436.9	0.60	17.8	18.44	0.83	70.79
SLW-BSTR-01-3	7.55	328.8	149.4	2.4	363.2	0.45	12.2	14.73	0.83	68.48
SLW-BSTR-02-1	9.59	294.9	170.7	1.5	334.2	0.58	14.3	16.21	0.82	67.99
SLW-BSTR-02-2	8.02	243.5	152.8	1.3	278.7	0.63	9.8	13.66	0.81	63.43
SLW-BSTR-02-3	8.23	213.0	177.7	1.5	253.9	0.83	8.9	8.87	0.79	56.75
SLW-BSTR-03-1	8.93	104.6	64.0	0.7	119.3	0.61	5.0	38.15	0.87	93.49
SLW-BSTR-03-2	9.71	679.7	348.5	2.1	760.0	0.51	35.0	47.85	0.88	99.85
SLW-BSTR-03-3	8.08	187.6	97.8	1.1	210.1	0.52	7.6	16.52	0.83	71.15
SLW-BSTR-05-1	7.38	681.2	341.8	2.0	759.9	0.50	23.8	7.48	0.78	54.94

SLW-BSTR-05-2	10.85	475.5	257.2	0.6	534.7	0.54	24.6	7.77	0.78	54.62
SLW-BSTR-05-3	8.10	548.6	277.1	2.2	612.4	0.51	21.4	9.74	0.80	59.19
SLW-BSTR-06a-1	10.11	186.8	117.7	1.1	213.9	0.63	9.6	12.84	0.82	66.92
SLW-BSTR-06a-2	9.42	249.9	151.5	2.8	284.8	0.61	11.9	15.87	0.82	67.23
SLW-BSTR-06a-3	11.03	410.0	247.7	3.5	467.1	0.60	22.6	12.17	0.81	63.13
SLW-CCTR-03-1	6.53	1527.0	540.0	-0.3	1651.3	0.35	42.7	3.68	0.73	43.08
SLW-CCTR-03-2	4.30	628.4	208.1	-0.5	676.3	0.33	11.6	3.79	0.74	44.29
SLW-CCTR-03-3	8.52[c]	893.0	260.2	-0.6	952.9	0.29	34.4	6.68	0.79	54.55
SLW-CCTR-03-4	5.36	555.5	210.1	0.4	603.9	0.38	13.9	7.70	0.79	57.28
SLW-CCTR-03-5	5.30	366.2	191.4	3.0	410.2	0.52	9.3	8.57	0.80	58.25
SLW-CCTR-03-6	5.18	614.1	208.4	1.2	662.0	0.34	14.4	6.84	0.78	53.23
SLW-CCTR-04-1	4.95	129.2	56.5	-0.6	142.2	0.44	2.9	5.95	0.77	50.02
SLW-CCTR-04-2	5.53	236.0	60.3	-0.1	249.9	0.26	6.1	12.52	0.82	65.47
SLW-CCTR-04-3	5.52	95.2	82.0	-0.9	114.1	0.86	2.5	4.37	0.74	45.70
SLW-CCTR-05-1	8.45[c]	1240.9	483.9	-1.6	1352.3	0.39	44.2	2.99	0.72	40.24
SLW-CCTR-05-2	5.83	499.1	181.6	-0.7	540.9	0.36	13.2	5.84	0.77	51.94
SLW-CCTR-05-3	5.96	655.4	277.6	-0.6	719.3	0.42	17.5	4.80	0.76	47.82
SLW-CCTR-05-4	6.18	875.0	934.8	1.9	1090.2	1.07	27.8	5.51	0.76	50.41
SLW-CCTR-06-1	6.72	265.9	299.5	-0.2	334.9	1.13	9.3	6.14	0.77	51.39
SLW-CCTR-06-2	5.25	567.4	530.0	-0.4	689.4	0.93	14.8	5.36	0.76	48.66
SLW-CCTR-06-3	6.84	445.7	356.6	1.2	527.8	0.80	15.1	7.36	0.77	52.43
SLW-CCTR-07-1	6.98	2841.1	475.6	-0.9	2950.5	0.17	80.7	3.34	0.73	41.28
SLW-CCTR-07-2	9.76[c]	1959.1	318.6	-0.7	2032.5	0.16	78.2	3.90	0.73	42.24
SLW-CCTR-07-3	7.49	392.5	279.2	1.8	456.8	0.71	15.1	12.71	0.82	66.16
SLW-CCTR-07-4	6.86	1951.2	705.8	1.2	2113.7	0.36	59.4	5.31	0.76	48.22
SLW-CCTR-07-5	7.30	1803.2	652.5	1.1	1953.4	0.36	59.0	5.99	0.77	49.86
SLW-HW-01-1	16.59	349.0	185.1	0.7	391.7	0.53	27.3	8.01	0.78	53.79
SLW-HW-01-2	16.13	341.8	174.4	3.0	382.0	0.51	25.5	6.15	0.77	50.59
SLW-HW-01-3	17.65	853.6	95.1	0.7	875.5	0.11	68.1	13.49	0.82	64.42
SLW-LK-01-1	26.93	238.1	157.7	2.3	274.4	0.66	28.5	2.97	0.72	40.84
SLW-LK-01-2	19.16	179.1	108.0	9.2	204.0	0.60	15.9	4.89	0.75	47.48
SLW-LK-01-3	31.65	601.0	239.8	14.0	656.2	0.40	84.7	5.60	0.76	47.87
SLW-LK-02-1	23.94	176.4	139.1	0.9	208.4	0.79	20.8	7.58	0.77	52.49
SLW-LK-02-2	35.54	262.5	196.6	2.0	307.8	0.75	45.3	7.63	0.77	50.98
SLW-LK-02-3	35.17	182.4	154.3	1.8	217.9	0.85	31.9	7.11	0.77	51.80
SLW-NC-02-1	5.04	113.3	77.6	0.6	131.1	0.69	2.8	7.77	0.79	55.67
SLW-NC-02-2	4.47	170.6	94.1	0.7	192.3	0.55	3.6	5.96	0.77	52.11
SLW-NFT-01-1	3.90	347.1	506.0	2.1	463.5	1.46	7.9	12.41	0.81	63.04
SLW-NFT-01-2	4.01	1757.5	314.6	1.4	1829.9	0.18	31.5	9.56	0.80	57.34
SLW-NFT-01-3	3.61	242.2	205.0	0.9	289.3	0.85	4.5	9.01	0.79	57.60
SLW-NMT-01-1	3.63	3592.8	263.4	0.9	3653.4	0.07	57.9	11.11	0.81	61.60
SLW-NMT-01-2	3.63	941.0	263.9	0.9	1001.7	0.28	14.8	5.95	0.76	47.16
SLW-NMT-01-3	3.21	3494.6	217.2	3.2	3544.6	0.06	47.3	6.98	0.77	50.34
SLW-NMT-02-1	3.65	400.0	268.8	0.0	461.9	0.67	7.1	6.86	0.77	52.71
SLW-NMT-02-2	3.47	561.8	305.5	0.7	632.1	0.54	8.8	4.21	0.74	45.02
SLW-NMT-02-3	3.18	146.4	93.0	-1.2	167.8	0.64	2.2	4.12	0.75	46.90
SLW-NMT-03-1	4.40	175.8	81.6	0.7	194.6	0.46	3.7	9.87	0.80	59.56
SLW-NMT-03-2	3.01	1112.9	112.9	0.5	1138.9	0.10	14.2	5.41	0.77	50.32
SLW-NMT-03-3	3.59	1078.8	481.5	1.2	1189.7	0.45	18.2	9.35	0.79	56.91
SLW-NMT-04-1	4.13	2705.4	1287.9	1.7	3001.9	0.48	52.6	11.35	0.79	55.92

SLW-NMT-04-2	4.23	799.9	140.8	0.3	832.3	0.18	14.7	7.06	0.78	51.52
SLW-NMT-04-3	4.89	2601.3	873.9	4.2	2802.4	0.34	58.4	8.47	0.79	56.50
SLW-NMT-05-1	5.28	322.7	95.5	1.5	344.7	0.30	8.3	22.20	0.85	80.24
SLW-NMT-05-2	4.23	508.7	71.4	0.6	525.1	0.14	10.5	35.71	0.88	95.73
SLW-NMT-05-3	5.14	617.9	166.7	0.5	656.2	0.27	14.9	13.85	0.82	65.67
SLW-NWC-01-1	3.99	704.3	387.8	0.6	793.6	0.55	12.7	4.50	0.74	45.69
SLW-NWC-01-2	3.25	607.2	436.9	1.1	707.8	0.72	9.3	5.87	0.75	47.42
SLW-NWC-01-3	4.61	984.8	490.0	1.0	1097.6	0.50	20.9	5.54	0.77	50.23
SLW-SFTR-01-1	4.20	384.6	154.6	2.2	420.2	0.40	7.9	15.44	0.82	67.61
SLW-SFTR-01-2	4.90	493.5	315.8	1.9	566.2	0.64	12.2	12.26	0.81	64.40
SLW-SFTR-01-3	5.44	557.9	380.4	3.2	645.5	0.68	15.7	16.15	0.83	69.89
SLW-SFTR-02-1	5.66	519.0	314.1	4.1	591.3	0.61	15.1	19.40	0.84	73.35
SLW-SFTR-02-2	4.86	540.2	380.5	6.3	627.9	0.70	13.7	17.98	0.83	71.91
SLW-SFTR-02-3	4.64	633.6	420.6	4.4	730.4	0.66	14.7	11.21	0.80	60.84
SLW-SFTR-04-1	5.18	680.7	264.7	1.2	741.7	0.39	15.7	5.09	0.75	47.37
SLW-SFTR-04-2	5.88	2173.8	376.4	10.9	2260.5	0.17	53.2	3.88	0.74	44.13
SLW-STR-01-1	6.63	288.9	213.8	1.5	338.1	0.74	9.3	6.21	0.77	51.78
SLW-STR-01-2	7.62	476.1	338.4	2.8	554.0	0.71	17.1	5.09	0.75	47.32
SLW-STR-01-3	6.41	567.7	373.7	1.3	653.8	0.66	16.5	3.59	0.73	42.80

[a]Alpha Ejection Correction

[b]Equivalent Spherical Radius

[c]Outlier rejected through Peirce's Criterion

Mike Taylor and Kurt Sundell at 5700 m on the North Lunggar Detachment footwall, suffering from cerebral edema and excessive happiness.

Chapter 5

Northward propagation of rapid east-directed extension in the Lunggar Rift, western Lhasa Terrane, Tibet: A consequence of Indian underthrusting?

Richard H. Styron, Michael H. Taylor and Kurt E. Sundell

Dept. of Geology, University of Kansas, 1475 Jayhawk Blvd, Lawrence, KS, 66045, USA

ABSTRACT

Extension of the Tibetan Plateau is often thought to result from gravitational collapse late in the Indo-Eurasian collision, resulting from a middle Miocene orogen-wide geodynamic change. Through thermokinematic modeling of 6 apatite and zircon (U-Th)/He bedrock transects in the Lunggar Rift, we show that though rifting initiated in the middle Miocene, most of the extension within the Lunggar rift has accumulated following a Mio-Pliocene increase in extension rate (from 0.25-1 mm/yr^{-1} to 3-5 mm/yr^{-1}). This wave of rapid extension propagated north at ~12 mm /yr^{-1}, similar in rate and location to the tip of the underthrusting Indian lower crust. We relate rapid extension and underthrusting in a conceptual model where mobile Tibetan middle to lower crust is forced eastward in response to thickening of the lowermost crust due to India underplating the Tibetan plateau, which is already at its maximum elevation.

INTRODUCTION

Active normal and strike-slip faulting of the Tibetan Plateau is ubiquitous throughout the elevated Tibetan plateau, accommodating north-south shortening and east-directed extension (e.g. Molnar and Tapponnier, 1978; Zhang et al., 2004) (Fig. 1). Normal faulting along north-trending rifts is dominant in the Lhasa terrane of southern Tibet (e.g., Armijo et al., 1986) and at the highest elevations elsewhere in the plateau (e.g., Molnar and Lyon-Caen, 1989; Elliott et al., 2010) while strike-slip faulting is dominant in central, northern and eastern Tibet (e.g., Armijo et al., 1989; Taylor et al., 2003); this partitioning of fault type may be related to differences in elevation (e.g., Elliott et al., 2010) or the location of the underthrust Indian plate below the southern plateau (e.g., Liu and Yang, 2003; Copley et al., 2011).

Because the plateau's high elevation gives it considerably more gravitational potential energy than its surrounding lowlands (Bird, 1991), extensional deformation of the plateau is commonly inferred to indicate gravitational collapse of the orogen (e.g., Dewey et al, 1988; Jade et al., 2004), which may have begun when the plateau rose to its modern elevation (e.g., Harrison et al., 1992; Molnar et al., 1993). The few extant studies constraining rift initiation within the plateau interior (Fig. 1) yield middle to late Miocene ages for the Nyainqentanglha Rift (Pan and Kidd, 1992; Harrison et al., 1995; Kapp et al., 2005), Damxung Shear Zone of the Yadong-Gulu Rift (Ratschbacher et al., 2011), Shuang Hu Rift (Blisniuk et al., 2001) and the Lunggar Rift (Styron et al., in review; Woodruff et al., in review). The broad simultaneity of these estimates lends credence to causal mechanisms for Tibetan extension applying to the whole orogen at once, such as a rapid convective removal of mantle lithosphere (e.g., England and Houseman, 1988) or rollback of western Pacific subducting slabs (e.g., Yin, 2000).

However, it is quite possible that Tibetan taphrogeny is a more dynamic process than is indicated by models focusing on gravitational collapse (e.g., Dewey et al., 1988), the onset of extension (e.g., Yin, 2000; Harrison et al., 1992) or the present plate configuration (e.g., Copley et al., 2011). DeCelles et al. (2002; 2011) and Lee et al. (2011) have suggested that progressive underthrusting of Indian lower crust beneath the southern plateau may cause a northward propagation of

rifting and higher topography above the Indian plate. India's penetration into Tibetan lithosphere may cause tectonic escape of the middle or lower Tibetan crust, forcing it eastward where it may inflate the crust of eastern Tibet (e.g., Royden et al., 1997). This is in apparent contradiction with observations suggesting a single age for the onset of rifting. However, recent work has indicated that normal fault slip rates have varied significantly over time (e.g., Lee et al., 2011; Styron et al., in review). Styron et al. (in review) showed that extension within the South Lunggar Rift rapidly increased at 8.5-8 Ma. This raises the possibility that temporal changes in extension rate are related to evolving orogenic configurations such as continued underthrusting of India. To test the hypothesis that India's penetration into or beneath Tibet causes an increase in the extension rate of south Tibetan rifts, we model 6 recently-collected apatite and zircon (U-Th)/He (aHe and zHe, respectively) bedrock transects from the footwalls of the Lunggar Rift to find evidence for or against a northward-propagating increase in extenion rate.

LUNGGAR RIFT

The Lunggar Rift is a major N-trending rift cutting across almost the entire Lhasa terrane from the IYS to the BNS (Fig. 1). In the north, it is linked to the Lamu Co right-lateral strike-slip fault, part of the central Tibetan V-shaped conjugate strike-slip fault zone (Taylor et al., 2003; Taylor and Peltzer, 2006). The rift has a distinct northern section (the North Lunggar rift) dominated by an east-dipping low-angle detachment fault, the North Lunggar detachment (Kapp et al., 2008; Woodruff et al., in review; Sundell et al., in prep.). Farther south, a relatively low-displacement accommodation zone is present between the North and South Lunggar rifts. The South Lunggar Rift consists of two graben bounding a central horst block. The dominant fault in the South Lunggar rift is a west-dipping low-angle detachment fault, the South Lunggar detachment, on the west side of the horst. The east side of the horst is bound by the moderately west-dipping Palung Co fault (Styron et al., in review). These latter two faults tip out in the Gangdese range, which is characterized here by many small N-trending graben (e.g., Yin, 2000). All of the faults named here show evidence for significant late Quaternary deformation, including fault scarps in Quaternary

160

sediments up to 10s of m high (Kapp et al., 2008; Styron et al., in review) and an earthquake swarm culminating in a Mw 6.8 event in 2008 (Elliott et al., 2010; Ryder et al., 2012).

Based on zHe data and thermokinematic modeling, Styron et al. (in review) show that rifting in the South Lunggar Rift began in the middle Miocene, and rapid extension initiated on the South Lunggar Detachment at 8.5-8 Ma, which continues through the present. Woodruff et al. (in review) used detrital aHe and zHe data from the North Lunggar superdetachment basin to infer the initiation of rifting at ~15 Ma. Sundell et al. (manuscript in preparation) use bedrock aHe and zHe results documenting Pliocene cooling of the North Lunggar Detachment footwall, potentially signaling an increase in footwall exhumation rate.

(U-TH)/HE THERMOCHRONOLOGY AND MODELING WITH PECUBE

(U-Th)/He thermochronology is a fairly recent but widely used tool for obtaining quantitative estimates of timing and rates of tectonic and erosional processes (e.g., Reiners et al., 2005). 46 bedrock thermochronological samples composing 6 fault-normal footwall transects spanning ~80 km along-strike in the Lunggar range were considered in this study (Fig. 2). The samples are from the larger datasets of Styron et al. (in review), Sundell et al (in prep) and Kapp et al. (2008) and are described more thoroughly therein. All samples were run for zircon and 14 were run for apatite. 2-5 (usually 3) aliquots were processed for each sample at the University of Kansas following the methods of Wolfe and Stockli (2010). All samples showed zHe cooling ages between ~7.5 and 2.5 Ma, and aHe ages ranged from ~4 to 0.5 Ma, indicating all samples were quickly exhumed from above the zircon thermal sensitivity window, ~200° C for rapidly cooled samples (Reiners et al., 2004) since the late Miocene.

The faulting and exhumational history of each transect was derived by 3-D thermokinematic modeling in Pecube v.3 (Braun, 2003)following the methods of Styron et al. (in review). The geometry of each model is based on topography and structural observations for the shallow surface and iterative testing of fault geometry and thermal parameters at depth, using (U-Th)/He ages and suitable parameters of nearby transects as criteria. Once each model was geometrically construct-

ed, thousands of forward modeling simulations of unique fault histories were run by incrementally changing fault parameters (timing of fault initiation and acceleration/deceleration, initial slip rate, final slip rate) for each fault in the model. The parameter space is very broad (Table DR1) but fully explored in a constrained grid search where a simulation is only run if the resulting total horizontal displacement is within an acceptable range determined by geologic mapping. Simulations were run on Ubuntu Linux environments on Amazon's EC2 servers via PiCloud (www.picloud.com), a Python-based interface. Simulations from the southern two transects are from Styron et al. (in review) though the results here are more precise due to an improved filtering algorithm.

The results of each simulation (predicted zHe and aHe ages) were tested against the data; if more predicted zHe or aHe ages fell outside the 2σ error of the corresponding observation than an allowable number of outliers for the transect (0-1 for zHe, 0-2 for aHe) that simulation was rejected. The remaining fault histories for each transect are then considered the possible histories for each transect.

MODEL RESULTS

Of the 50,801 total simulations, 88 acceptably fit the data. The fault histories for each transect are shown in Figure 2 as horizontal extension rate and cumulative horizontal extension through time. For each transect, the extensional history is precisely bracketed, especially since the Pliocene. Rift initation is constrained at 16-10 Ma in the South Lunggar Rift (Transects 5 and 6), 7-5 Ma for the accommodation zone (Transect 4) and 14-6 Ma in the North Lunggar Rift. These results are consistent with previous work on the Lunggar Rift (Kapp et al., 2008; Styron et al., in review; Sundell et al., in prep; Woodruff et al.; in review) and elsewhere in the Himalaya and Tibet. The results also show that extension rates have not been constant throughout the period of rifting. In particular, all transects show evidence for an increase in acceleration, though this change is greater in some transects than others, depending on whether there is a longer history of slow extension (<1 mm yr^{-1}) for that transect. Cumulative exhumation plots (Fig. 2B) show that most of the extension in the Lunggar rift has occured after this acceleration.

Strikingly, it is clear that the onset of rapid horizontal extension (>1 mm yr^{-1}) is progressively younger with distance north of the IYS (Figs 2B, 3), regardless of the age of rift initiation at that location. This suggests that accelerated rifting is related to the northward penetration of Indian lower crust into or beneath the crust of the Lhasa block.

If this hypothesis is correct, it is reasonable to predict that the rate of northward propagation of rapid extension is similar to the rate of India's underthrusting with respect to southern Tibet. We determine the rate of northward propagation of rapid extension by a Monte Carlo simulation. For each of 1,000,000 iterations, the onset of rapid extension at each transect is randomly sampled from the probability distribution for that parameter given by the Pecube modeling results. A linear regression line of age vs. distance is then fit to each sample set, the slope of which represents the rate of northward propagation. The Monte Carlo simulation yields values of northward propagation from 7 to 20 mm yr^{-1}, with a well-defined mode at ~12 mm yr^{-1} (Figure 3a). The minimum value for the rate of Indian underthrusting beneath the Lhasa block is the shortening rate across the Himalayan fold and thrust belt; this is estimated at 15-21 mm yr^{-1} since the late Miocene to present through balanced cross-section reconstructions (e.g., DeCelles et al., 2002), neotectonic studies (e.g., Lave and Avouac, 2000) and GPS geodesy (e.g, Ader et al., 2012; Banerjee et al., 2008). As no evidence of post- middle Miocene shortening structures between the Himalaya and northern Lhasa terrane are preesent in the prominent compilations (e.g., Taylor and Yin, 2009), Indo-Himalayan convergence rates likely equal Indo-Lhasa terrane convergence rates.

The northern tip of Indian lower crust has been recently located under the Lunggar Rift by Nabelek et al. (2009) through receiver function analysis; it is presently approximately under our transects in the North Lunggar Rift (though no uncertainty is given). If this location is correct, this indicates that the front of rapid rifting moves ahead of the Indian slab by about 50 km. This is shown in Fig. 3a with an ad-hoc modern uncertainty of 0.3° latitude.

DISCUSSION

We explain the spatial and temporal association of Indian underthrusting and rapid east-

directed Tibetan extension through a conceptual geodynamic model where the Indian slab displaces lower crust of the Lhasa terrane, forcing it to the east. Crustal thickening from the addition of India to the crustal column is partially limited by the maximum elevation of the Tibetan plateau, itself governed by the horizontal compressive stresses on the plateau (e.g. England and Houseman, 1988). We interpret this process to occur in an orogen that had reached its modern elevation (e.g. Quade et al., 2011) and begun extending at least 5-10 m.y. before the onset of rapid extension in the Lunggar rift (Blisniuk et al., 2001; Styron et al., in review; Woodruff et al., in review). Therefore, without increasing horizontal compressive stresses on the orogen (unlikely when convergence has been decreasing throughout collision; Molnar and Stock, 2009), elevation cannot increase, and middle to lower crust of the Tibetan plateau flows eastward, as the crustal geotherm is likely too high to allow for brittle, block-like deformation at depth. This flow is most rapid above and immediately in front of Indian lithosphere, which may be constricting the whole lithospheric column north of the slab and causing similar eastward extrusion (e.g., Yin and Taylor, 2011).

Geophysical data from central and southeastern Tibet support the hypothesis that the crust is anomalously weak and capable of flow. Magnetotellurimetric data from southern Tibet show low electrical resistivity, indicative of either fluids or partial melt (e.g., Unsworth et al., 2005); fluid-filled cracks can drastically lower the effective viscosity of rocks (e.g., O'Connell and Budianski, 1974). Central Tibet also displays seismic evidence of pervasive sub-horizontal rock fabric (Ozacar and Zandt, 2004) and radial anisotropy (Shapiro et al., 2004), thought to be evidence of crustal flow based on field and seismic observations and thermomechanical modeling (e.g., Dumond et al., 2010; Culshaw et al., 2006; Miessner et al., 2006). Anomalously low seismic wave speeds are found throughout southeastern Tibet, and large regions of extremely low shear wave velocities are found between the Sichuan basin and the eastern Himalaya (e.g., Yao et al., 2008; Wang et al., 2010), which may indicate thermally weakened crust capable of flow. However, these inferred low-strength regions are not continuous into the regions of moderate to low elevations southeast of Tibet.

The timing of these events is compatible with related events across the Tibetan-Himalayan

orogen. Based on stratigraphic and volcanic evidence, DeCelles et al. (2011) hypothesize that the Indian slab had penetrated as far north as the Qiangtang terrane by 32 Ma, after which it began to roll back. Following slab breakoff at 25-20 Ma, the new leading edge of the slab, now at the IYS at the longitude of the Lunggar rift, resumed northward underthrusting resumed at 20-15 Ma. Initial, slow east-directed extension of the Tibetan plateau began at this time, as did rapid arc-parallel extension in the Himalaya (e.g., Jessup et al., 2008; Thiede et al., 2006). Dramatic increases in the incision rates of southeastern Tibetan river gorges (Clark et al., 2005b) and erosion in their headwaters catchments (Duvall et al., 2012) at this time are potentially linked to crustal thickening in eastern Tibet due to lower crust flowing eastward from the high plateau (Clark et al., 2005a; Schoenbohm et al., 2006), likely forced out from in front of and above the Indian slab. Thus, rapid Tibetan extension does not seem to be the result of post-collisional orogenic collapse (e.g., Dewey et al., 1988) but instead is probably a consequence of ductile middle- to lower-crustal tectonic escape caused by continued convergence of India into an orogen at its maximum supportable elevation.

REFERENCES

Ader, T., Avouac, J.-P., Liu-Zeng, J., Lyon-Caen, H., Bollinger, L., Galetzka, J., Genrich, J., Thomas, M., Chanard, K., Sapkota, S.N., Rajaure, S., Shrestha, P., Ding, L., and Flouzat, M., 2012, Convergence rate across the Nepal Himalaya and interseismic coupling on the Main Himalayan Thrust: Implications for seismic hazard: Journal of Geophysical Research, v. 117, no. B4, p. 1–16, doi: 10.1029/2011JB009071.

Armijo, R., Tapponnier, P., Mercier, J.L., and Tong-Lin, H., 1986, Quaternary extension in southern Tibet: Field observations and tectonic implications: Journal of Geophysical Research, v. 91, p. 13803–13872.

Armijo, R., Tapponnier, P., and Tonglin, H., 1989, Late Cenozoic right-lateral strike-slip faulting in southern Tibet: Journal of Geophysical Research, v. 94, no. B3, p. 2787–2838.

Banerjee, P., Burgmann, R., Nagarajan, B., and Apel, E., 2008, Intraplate deformation of the Indian subcontinent: Geophysical Research Letters, v. 35, no. 18, p. L18301, doi: 10.1029/2008GL035468.

Bird, P., 1991, Lateral extrusion of lower crust from under high topography in the isostatic limit: Journal of Geophysical Research, v. 96, no. B6, p. 10,275–10,286.

Blisniuk, P.M., Hacker, B.R., Glodny, J., Ratschbacher, L., Bi, S., Wu, Z., McWilliams, M.O., and Calvert, a, 2001, Normal faulting in central Tibet since at least 13.5 Myr ago.: Nature, v. 412, no. 6847, p. 628–32, doi: 10.1038/35088045.

Braun, J., 2003, Pecube: a new finite-element code to solve the 3D heat transport equation including the effects of a time-varying, finite amplitude surface topography: Computers & Geosciences, v. 29, no. 6, p. 787–794, doi: 10.1016/S0098-3004(03)00052-9.

Clark, M. K., Bush, J. W. M., and Royden, L. H., 2005, Dynamic topography produced by lower crustal flow against rheological strength heterogeneities bordering the Tibetan Plateau: Geophysical Journal International, v. 162, p. 575-590, doi: 10.1111/j.1365-246X.2005.02580.x

Clark, M.K., House, M., Royden, L., Whipple, K., Burchfiel, B., Zhang, X., and Tang, W., 2005, Late Cenozoic uplift of southeastern Tibet: Geology, v. 33, no. 6, p. 525-528, doi: 10.1130/

G21265.1.

Copley, A., Avouac, J., and Wernicke, B.P., 2011, Evidence for mechanical coupling and strong Indian lower crust beneath southern Tibet: Nature, v. 472, no. 7341, p. 79–81, doi: 10.1038/ nature09926.

Culshaw, N.G., Beaumont, C., and Jamieson, R. a., 2006, The orogenic superstructure-infrastructure concept: Revisited, quantified, and revived: Geology, v. 34, no. 9, p. 733, doi: 10.1130/ G22793.1.

DeCelles, P.G., Kapp, P., Quade, J., and Gehrels, G.E., 2011, Oligocene-Miocene Kailas basin, southwestern Tibet: Record of postcollisional upper-plate extension in the Indus-Yarlung suture zone: Geological Society of America Bulletin, v. 123, no. 7-8, p. 1337–1362, doi: 10.1130/B30258.1.

DeCelles, P.G., Robinson, D.M., and Zandt, G., 2002, Implications of shortening in the Himalayan fold-thrust belt for uplift of the Tibetan Plateau: Tectonics, v. 21, no. 6, p. 1062, doi: 10.1029/2001TC001322.

Dewey, J.F., Shackleton, R.M., Chengfa, C., and Yiyin, S., 1988, The tectonic evolution of the Tibetan Plateau: Philosophical Transactions of the Royal Society of London. Series A, Mathematical and Physical Sciences, v. 327, no. 1594, p. 379.

Dumond, G., Goncalves, P., Williams, M.L., and Jercinovic, M.J., 2010, Subhorizontal fabric in exhumed continental lower crust and implications for lower crustal flow: Athabasca granulite terrane, western Canadian Shield: Tectonics, v. 29, no. 2, p. 1–32, doi: 10.1029/2009TC002514.

Duvall, A.R., Clark, M.K., Avdeev, B., Farley, K. a., and Chen, Z., 2012, Widespread late Cenozoic increase in erosion rates across the interior of eastern Tibet constrained by detrital low-temperature thermochronometry: Tectonics, v. 31, no. 3, p. 1–23, doi: 10.1029/2011TC002969.

Elliott, J., Walters, R., England, P., Jackson, J.A., Li, Z., and Parsons, B., 2010, Extension on the Tibetan plateau: recent normal faulting measured by InSAR and body wave seismology: Geophysical Journal International, v. 183, p. 503–535, doi: 10.1111/j.1365-

246X.2010.04754.x.

England, P., and Houseman, G., 1988, The Mechanics of the Tibetan Plateau: Philosophical Transactions of the Royal Society of London. Series A, Mathematical and Physical Sciences, v. 326, p. 301–320.

Harrison, T., Copeland, P., and Kidd, W., 1995, Activation of the Nyainqentanghla shear zone: Implications for uplift of the southern Tibetan Plateau: Tectonics, v. 14, no. 3, p. 658–676.

Harrison, T.M., Copeland, P., Kidd, W.S., and Yin, A., 1992, Raising Tibet: Science, v. 255, no. 5052, p. 1663–70, doi: 10.1126/science.255.5052.1663.

Jade, S., Bhatt, B., Yang, Z., Bendick, R., Gaur, V., Molnar, P., Anand, M., and Kumar, D., 2004, GPS measurements from the Ladakh Himalaya, India: preliminary tests of plate-like or continuous deformation in Tibet: Geological Society of America Bulletin, v. 116, no. 11-12, p. 1385–1391, doi: 10.1130/B25357.1.

Jessup, M.J., Newell, D.L., Cottle, J.M., Berger, A.L., and Spotila, J.A., 2008, Orogen-parallel extension and exhumation enhanced by denudation in the trans-Himalayan Arun River gorge, Ama Drime Massif, Tibet-Nepal: Geology, v. 36, no. 7, p. 587, doi: 10.1130/G24722A.1.

Kapp, J., Harrison, T., Kapp, P., Grove, M., Lovera, O.M., and Ding, L., 2005, Nyainqentanglha Shan: A window into the tectonic, thermal, and geochemical evolution of the Lhasa block, southern Tibet: Journal of Geophysical Research, v. 110, no. B8, p. B08413, doi: 10.1029/2004JB003330.

Kapp, P., Taylor, M., Stockli, D., and Ding, L., 2008, Development of active low-angle normal fault systems during orogenic collapse: Insight from Tibet: Geology, v. 36, no. 1, p. 7–10, doi: 10.1130/G24054A.1.

Lavé, J., and Avouac, J.P., 2000, Active folding of fluvial terraces across the Siwaliks Hills, Himalayas of central Nepal: Journal of Geophysical Research, v. 105, no. B3, p. 5735–5770.

Lee, J., Hager, C., Wallis, S.R., Stockli, D.F., Whitehouse, M.J., Aoya, M., and Wang, Y., 2011, Middle to late Miocene extremely rapid exhumation and thermal reequilibration in the Kung Co rift, southern Tibet: Tectonics, v. 30, no. 2, p. 1–26, doi: 10.1029/2010TC002745.

Liu, M., and Yang, Y., 2003, Extensional collapse of the Tibetan Plateau: Results of three-dimensional finite element modeling: Journal of Geophysical Research, v. 108, no. 8, p. 1–15, doi: 10.1029/2002JB002248.

Meissner, R., Rabbel, W., and Kern, H., 2006, Seismic lamination and anisotropy of the Lower Continental Crust: Tectonophysics, v. 416, no. 1-4, p. 81–99, doi: 10.1016/j.tecto.2005.11.013.

Molnar, P., England, P., and Martinod, J., 1993, Mantle dynamics, uplift of the Tibetan Plateau, and the Indian monsoon: Reviews of Geophysics, v. 31, no. 4, p. 357–396.

Molnar, P., and Lyon-Caen, H., 1989, Fault plane solutions of earthquakes and active tectonics of the Tibetan Plateau and its margins: Geophysical Journal International, v. 99, p. 123–153.

Molnar, P., and Stock, J.M., 2009, Slowing of India's convergence with Eurasia since 20 Ma and its implications for Tibetan mantle dynamics: Tectonics, v. 28, no. TC3001, p. 1–11, doi: 10.1029/2008TC002271.

Molnar, P., and Tapponnier, P., 1978, Active tectonics of Tibet: Journal of Geophysical Research, v. 83, no. B11, p. 5361–5375.

Nábelek, J., Hetényi, G., Vergne, J., Sapkota, S., Kafle, B., Jiang, M., Su, H., Chen, J., and Huang, B.-S., 2009, Underplating in the Himalaya-Tibet collision zone revealed by the Hi-CLIMB experiment.: Science, v. 325, no. 5946, p. 1371–1374, doi: 10.1126/science.1167719.

O'Connell, R. and Budiansky, B., 1974, Seismic velocities in dry and saturated cracked solids: Journal of Geophysical Research, v. 79, no. 35, p. 5412-5426

Ozacar, A.A., and Zandt, G., 2004, Crustal seismic anisotropy in central Tibet: Implications for deformational style and flow in the crust: Geophysical Research Letters, v. 31, no. L23601, p. 2–5, doi: 10.1029/2004GL021096.

Pan, Y., and Kidd, W., 1992, Nyainqentanglha shear zone: A late Miocene extensional detachment in the southern Tibetan Plateau: Geology, v. 20, no. 9, p. 775–778, doi: 10.1130/0091-7613(1992)020<0775.

Quade, J., Breecker, D.O., Daeron, M., and Eiler, J., 2011, The paleoaltimetry of Tibet: An isotopic perspective: American Journal of Science, v. 311, no. 2, p. 77–115, doi:

10.2475/02.2011.01.

Ratschbacher, L., Krumrei, I., Blumenwitz, M., Staiger, M., Gloaguen, R., Miller, B.V., Samson, S.D., Edwards, M.A., and Appel, E., 2011, Rifting and strike-slip shear in central Tibet and the geometry, age and kinematics of upper crustal extension in Tibet: Geological Society, London, Special Publications, v. 353, no. 1, p. 127–163, doi: 10.1144/SP353.8.

Reiners, P.W., Ehlers, T.A., and Zeitler, P.K., 2005, Past, Present, and Future of Thermochronology: Reviews in Mineralogy, v. 58, p. 1–18, doi: 10.2138/rmg.2005.58.1.

Reiners, P.W., Spell, T.L., Nicolescu, S., and Zanetti, K. a., 2004, Zircon (U-Th)/He thermochronometry: He diffusion and comparisons with 40Ar/39Ar dating: Geochimica et Cosmochimica Acta, v. 68, no. 8, p. 1857–1887, doi: 10.1016/j.gca.2003.10.021.

Royden, L.H., Burchfiel, B.C., King, R.W., Wang, E., Chen, Z., Shen, F., and Liu, Y., 1997, Surface deformation and lower crustal flow in eastern Tibet: Science, v. 276, p. 788–790.

Ryder, I., Burgmann, R., and Sun, J., 2012, Tandem afterslip on connected fault planes following the 2008 Nima-Gaize (Tibet) earthquake: Journal of Geophysical Research, v. 115, no. B03404, p. 1–16, doi: 10.1029/2009JB006423.

Schoenbohm, L., and Burchfiel, B., 2006, Propagation of surface uplift, lower crustal flow, and Cenozoic tectonics of the southeast margin of the Tibetan Plateau: Geology, , no. 10, p. 813–816, doi: 10.1130/G22679.1.

Shapiro, N. M., Ritzwoller, M. H., Molnar, P., and Levin, V. 2004, Thinning and flow of Tibetan crust constrained by seismic anisotropy. Science, v. 305, p. 233–236.

Styron, R., Taylor, M., and Okoronkwo, K., 2010, Database of active structures from the Indo-Asian Collision: Eos Trans. AGU, v. 91, no. 20, p. 0–1, doi: 10.1130/GES00217.1.Wessel.

Taylor, M., and Peltzer, G., 2006, Current slip rates on conjugate strike-slip faults in central Tibet using synthetic aperture radar interferometry: Journal of Geophysical Research, v. 111, no. B12402, p. 1–16.

Taylor, M., and Yin, A., 2009, Active structures of the Himalayan-Tibetan orogen and their relationships to earthquake distribution, contemporary strain field, and Cenozoic volcanism:

Geosphere, v. 5, no. 3, p. 199–214, doi: 10.1130/GES00217.1.

Taylor, M., Yin, A., Ryerson, F.J., Kapp, P., and Ding, L., 2003, Conjugate strike-slip faulting along the Bangong-Nujiang suture zone accommodates coeval east-west extension and north-south shortening in the interior of the Tibetan Plateau: Tectonics, v. 22, no. 4, p. 1–21, doi: 10.1029/2002TC001361.

Thiede, R.C., Arrowsmith, J.R., Bookhagen, B., McWilliams, M., Sobel, E.R., and Strecker, M.R., 2006, Dome formation and extension in the Tethyan Himalaya, Leo Pargil, northwest India: Bulletin of the Geological Society of America, v. 118, no. 5-6, p. 635, doi: 10.1130/B25872.1.

Unsworth, M.J., Jones, A.G., Wei, W., Marquis, G., Gokarn, S.G., Spratt, J.E., Bedrosian, P., Booker, J., Leshou, C., Clarke, G., Shenghui, L., Chanhong, L., Ming, D., Sheng, J., et al., 2005, Crustal rheology of the Himalaya and Southern Tibet inferred from magnetotelluric data.: Nature, v. 438, no. 7064, p. 78–81, doi: 10.1038/nature04154.

Wang, C.-Y., Lou, H., Silver, P.G., Zhu, L., and Chang, L., 2010, Crustal structure variation along 30°N in the eastern Tibetan Plateau and its tectonic implications: Earth and Planetary Science Letters, v. 289, no. 3-4, p. 367–376, doi: 10.1016/j.epsl.2009.11.026.

Wolfe, M.R., and Stockli, D.F., 2010, Zircon (U–Th)/He thermochronometry in the KTB drill hole, Germany, and its implications for bulk He diffusion kinetics in zircon: Earth and Planetary Science Letters, v. 295, no. 1-2, p. 69–82, doi: 10.1016/j.epsl.2010.03.025.

Yao, H., Beghein, C., and van der Hilst, R.D., 2008, Surface wave array tomography in SE Tibet from ambient seismic noise and two-station analysis - II. Crustal and upper-mantle structure: Geophysical Journal International, v. 173, no. 1, p. 205–219, doi: 10.1111/j.1365-246X.2007.03696.x.

Yin, A., 2000, Mode of Cenozoic east-west extension in Tibet suggesting a common origin of rifts in Asia during the Indo-Asian collision: Journal of Geophysical Research, v. 105, no. B9, p. 21,745–21,759, doi: 10.1029/2000jb900168.

Yin, A., and Taylor, M.H., 2011, Mechanics of V-shaped conjugate strike-slip faults and the cor-

responding continuum mode of continental deformation: Geological Society of America Bulletin, v. 123, no. 9-10, p. 1798–1821, doi: 10.1130/B30159.1.

Zhang, P.Z., Shen, Z., Wang, M., Gan, W., Bürgmann, R., Molnar, P., Wang, Q., Niu, Z., Sun, J., and Wu, J., 2004, Continuous deformation of the Tibetan Plateau from global positioning system data: Geology, v. 32, no. 9, p. 809–812.

Figures and tables with captions
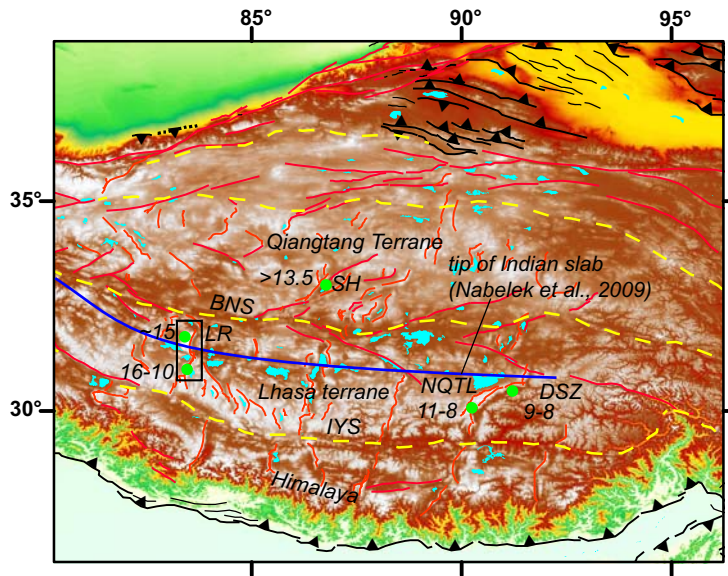
Figure 1: Map of central Tibet showing active normal faults (orange), strike-slip faults (red) and thrust faults (black) from Styron et al., 2010. Estimates for rift initation north of the IYS are shown by colored dots. SH = Shuang Hu graben. NQTL = Nyainqentanglha Rift. DSZ Damshung Shear Zone. LR = Lunggar Rift. IYS = Indus-Yarlung Suture. BNS= Bangong-Suture. Black box shows extent of Fig. 2A.
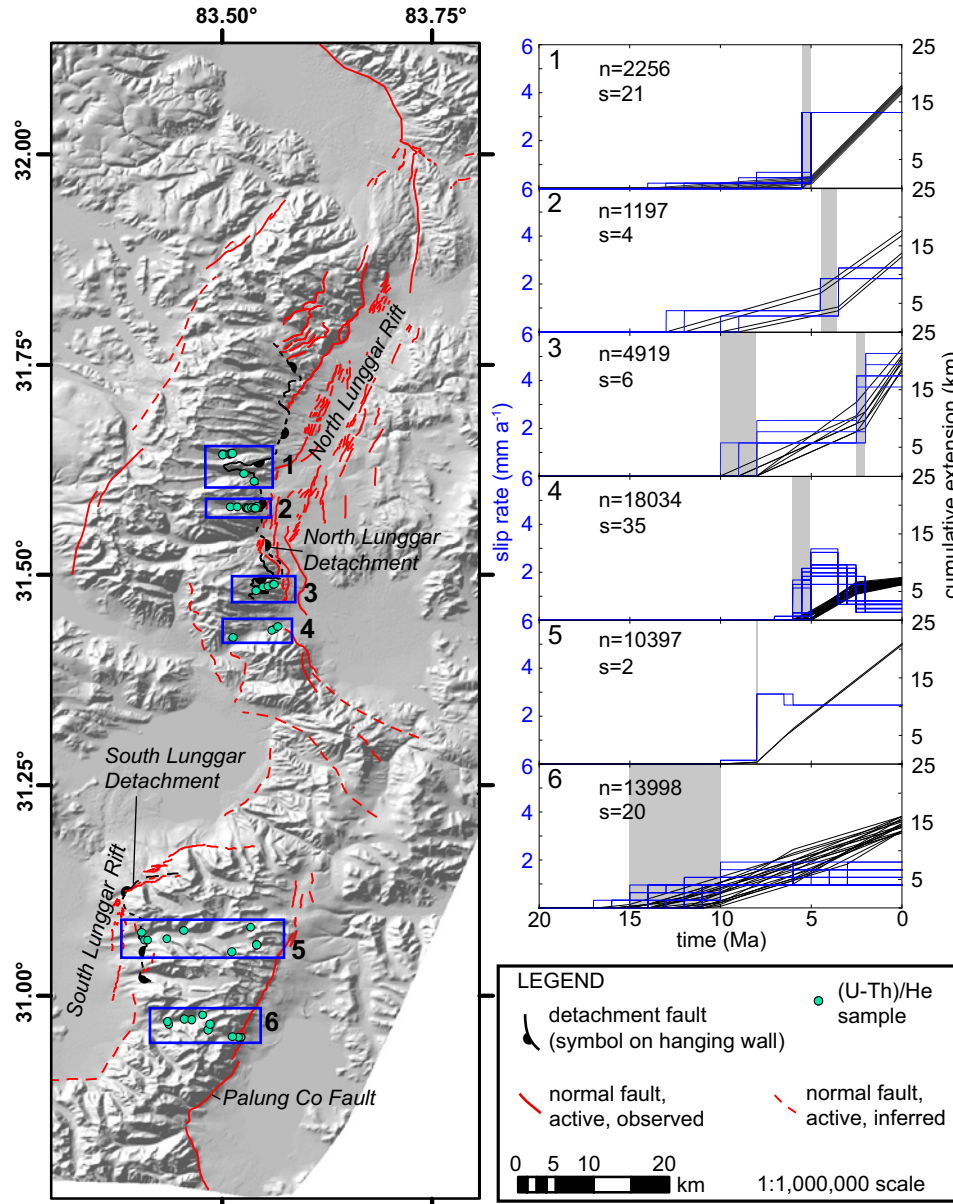
Figure 2. A: Topographic hillshade (from 90m SRTM topography) of the Lunggar rift showing extensional faults (from Styron et al., in review; Kapp et al., 2008) and the location of (U-Th)/He samples and transects. **B:** Results of Pecube thermokinematic modeling for each transect showing horizontal extension rate (blue) and cumulative extension (black). Grey boxes indicate periods of possible extensional acceleration. n= number of model runs. s = number of 'successful' runs fitting the data (shown).
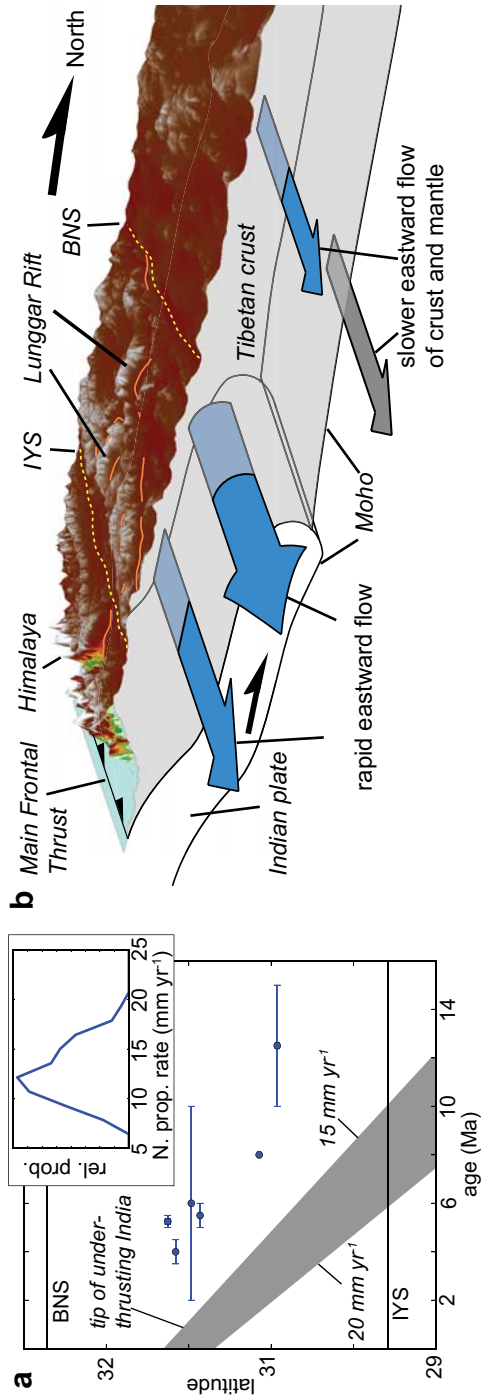
Figure 3. A: Plot of possible acceleration time intervals vs. latitude for the transects in the Lunggar rift. Grey region denotes location of the tip of the Indian slab, given a 0.3 deg error and a 15-20 mm yr-1 convergence rate. Inset shows probability distribution of the rate of northward propagation of rapid extension in the Lunggar rift. BNS = Bangong-Nujiang Suture. IYS = Indus-Yarlung Suture. **B**: Conceptual model illustrating accelerated eastward flow of Tibetan crust above the Indian slab. Surface colored by elevation. Suture zones shown in yellow. Active normal faults shown in orange.

Transect 1 fault parameter	Range	Step	Unit
NLD initiation	8 - 18	1	Ma
NLD initial slip rate	0 - 3.5	0.25 - 0.5	mm a^{-1}
NLD acceleration	2 - 7.5	0.5	Ma
NLD post-acceleration slip rate	0.5 - 5.5	0.25 - 0.5	mm a^{-1}
Horizontal extension	13 - 18	-	km

Transect 2 fault parameter	Range	Step	Unit
NLD initiation	8 - 18	1	Ma
NLD initial slip rate	0 - 3.5	0.25 - 0.5	mm a^{-1}
NLD acceleration	2 - 7.5	0.5	Ma
NLD post-acceleration slip rate	0.5 - 5.5	0.25 - 0.5	mm a^{-1}
Horizontal extension	13 - 18	-	km

Transect 3 fault parameter	Range	Step	Unit
NLD initiation	8 - 18	1	Ma
NLD initial slip rate	0 - 3.5	0.25 - 0.5	mm a^{-1}
NLD acceleration	2 - 7.5	0.5	Ma
NLD post-acceleration slip rate	0.5 - 5.5	0.25 - 0.5	mm a^{-1}
Horizontal extension	13 - 18	-	km

Transect 4 fault parameter	Range	Step	Unit
NLD initiation	5 - 14	0.5 - 1	Ma
NLD initial slip rate	0 - 4.0	0.25 – 0.5	mm a^{-1}
western fault initiation	5 - 14	0.5 - 1	Ma
western fault initial slip rate	0 - 1.0	0.25	mm a^{-1}
fault acceleration (of both faults)	2 – 5.5	0.5	Ma
NLD post-acceleration slip rate	0.25 - 4.0	0.25 – 0.5	mm a^{-1}
western fault post-acceleration slip rate	0.25 - 1.0	0.25	mm a^{-1}
Horizontal extension	10 - 16	-	km

Transect 5 fault parameter	Range	Step	Unit
SLD initiation	8 - 18	1	Ma
SLD initial slip rate	0.25 - 3.0	0.25 - 0.5	mm a^{-1}
SLD acceleration	2 - 6.5	0.5	Ma
SLD post-acceleration slip rate	1.5 - 4.5	0.5	mm a^{-1}
PCF initiation	10 - 18	2	Ma
PCF slip rate	0.25 - 1.5	0.25 - 0.5	mm a^{-1}
Horizontal extension	15 - 21	-	km

Transect 6 fault parameter	Range	Step	Unit
PCF initiation	10 - 18	2	Ma
PCF initial slip rate	0.5 - 2.0	0.5 - 1	mm a^{-1}
western fault initiation	10 - 18	2	Ma
western fault initial slip rate	0.5 - 2.0	0.5 - 1	mm a^{-1}
fault acceleration (of both faults)	3 - 6	1	Ma
PCF post-acceleration slip rate	0.5 - 3.0	0.5 - 1	mm a^{-1}
western fault post-acceleration slip rate	0.5 - 3.0	0.5 – 1	mm a^{-1}
Horizontal extension	10 - 16	-	km

Table DR1: Fault parameters for Pecube modeling for each transect.

Andrew McCallister, Dawa, Uncle and Kadup stopped for lunch on the road.

Chapter 6

An ongoing neotectonic slip rate study of the southeastern Karakoram Fault, Tibet

Richard Styron, Michael Taylor, Andrew McCallister, Guang Yang, John Gosse

Abstract

The Karakoram Fault, separating the northwestern Himalaya from western Tibet, is ~1000 km long right-lateral strike slip fault that may have an important role in the Himalayan-Tibetan orogeny. However, the type of role this fault plays is disputed. It may form an important structure accommodating lateral extrusion of Tibet eastward from in between India and the Himalaya, it may be a minor structure accommodating radial spreading of the Tibetan plateau, or it may accommodate northwest-directed transport and arc-parallel extension of the Himalaya against a relatively undeforming western Tibet. Each of these models calls for different predictions for net slip magnitudes and slip rates for the Karakoram fault, and these quantities may vary along strike. Though net (geologic) slip estimates have been made at many locations along the fault, and can test the models presented over 106 year timescales, late Quaternary slip rate studies are few. We have conducted field mapping and terrestrial cosmogenic nuclide sampling of a suitable site for a slip rate determination on the southeastern Karakoram fault, and constructed Monte Carlo-based computer modeling code to determine the late Quaternary slip history of the fault at this location. The code allows for full propagation of uncertainties from any type of probability distribution function in all parameters, and creates probability distributions for slip rate and accumulated offset at any time over the study period. Results of this study are awaiting analytical results of the samples, but hypothetical results using published age information is given for illustration.

Introduction

The Karakoram fault (KF) is a major intracontinental dextral strike-slip fault in the Himalayan-Tibetan orogen (Molnar and Tapponnier, 1975; Robinson, 2009) (Figure 1). The KF runs from the Kongur Shan Extensional System in the Pamir at least to the Gurla Mandhata Detachment in the Himalaya, a distance of 1000 km. The KF is generally collocated with the Indus-Yarlung Suture Zone, the suture formed by the Cretaceous-Paleogene collision of India and southern Eurasia (Yin and Harrison, 2000). Given its great extent and location near the modern India-Eurasia convergent plate boundary, the KF may play a major role in the Himalayan-Tibetan orogeny (Molnar and Tapponnier, 1975; Tapponnier et al., 1982; Searle, 1996; Styron et al., 2011), but the exact nature and magnitude of this role depends on the style of orogenesis. Different models of orogenic deformation call for different fault slip rates and magnitudes of net slip along the KF. But despite the importance of the KF to the Himalayan-Tibetan orogen, its deformational characteristics (rates, timing, magnitude) are still relatively unstudied, and the few extant studies are often highly discrepant in results (by a factor of 2-20) and consequent interpretation (Searle, 1996; Styron et al., 2011). This is true across the spectrum of methods: mapped geologic features predating and offset by the KF (e.g., batholiths or older thrust faults) have been interpreted to display horizontal separations ranging from ~1000 km (e.g., Peltzer and Tapponnier, 1988) to ~55 km (Murphy et al., 2000); similarly, late Quaternary slip rates have been estimated to be 4 mm a^{-1} (Brown et al., 2002) to 11 mm a^{-1} (Chevalier et al., 2005) based on Terrestrial Cosmogenic Nuclide (TCN) dating of offset geomorphic features such as moraines and debris flows; and space geodetic methods have estimated decadal slip rates of 1 mm a^{-1} (Wright et al., 2004) to 11 mm a^{-1} (Banerjee and Bürgmann, 2002).

More recent estimates of net slip and decadal slip rate have begun to converge. The lowest set of slip magnitudes range from 160 (Robinson, 2009) to 55 km (Murphy et al., 2000), and importantly, systematically decrease from northwest to southeast (Robinson, 2009; Styron et al., 2011), suggesting that the KF acts in some sense as a transform fault, accommodating different amounts of strain on either side of the fault (Styron et al., 2011). Additionally, the latest GPS stud-

ies show decadal slip rates of ~3.5 mm a-1 (Jade et al., 2004), which matches the most recent In-SAR study, with rates varying along strike between 6 and near 0 mm a[-1] (Wang and Wright, 2012). However, neotectonic studies still show very divergent results (Brown et al., 2002; Chevalier et al., 2005). We have located an optimal site near Menshi, Tibet, for a neotectonic slip rate study on the southeastern KF, and mapped and sampled offset alluvial and fluvial surfaces for Terrestrial Cosmogenic Nuclide (TCN) depth-profile exposure age dating (e.g. Gosse and Phillips, 2001) (Figure 2) during a field campaign to nearby rifts in September 2010. Three ^{36}Cl TCN pits were processed, and are awaiting isotope measurements at Purdue's PRIME Laboratory.

Incidentally, a study by Chevalier et al. (2012), referred to for brevity as C12, was very recently published; in their study they performed mapping and TCN dating of the same site, yielding a slip rate of $7.1 ^{+3.1}/_{-1.7}$ mm a^{-1}. This gives us an opportunity to compare our work to theirs. Reproduction of results is a foundation of science, though it is seldom done in field geologic studies. As discussed in more detail below, our mapping and that by C12 are generally correlative; however, we have significant differences in the favored reconstruction of fault offsets, in the TCN sampling and dating strategies, and the methods of slip rate derivations. As we do not yet have ages for our samples, we cannot tell if the results of C12 are reproducible. But given the importance of slip rate estimation of the KF to understanding Himalayan-Tibetan tectonics, the benefits to completing our study are great.

Models for Himalayan-Tibetan tectonics

Models of Himalayan-Tibetan orogenic dynamics require different roles for the KF. These roles may be parameterized by different slip rates on the KF, and therefore one may test these models through quantification of KF slip rates. Prominent, testable models for Himalayan-Tibetan deformation include the radial spreading model (e.g., Jade et al., 2004; Copley and McKenzie, 2007), the oblique convergence model (McCaffrey and Nabelek, 1998; Styron et al., 2011), and the lateral extrusion model (Tapponnier and Molnar, 1975; Lacassin et al., 2004). The specifics of these models will be outlined below. Furthermore, to varying degrees these differing hypotheses

underscore a more fundamental question in Tibetan geology and continental tectonics in general, which is the degree to which orogens deform in a plate-like (Avouac and Tapponnier, 1993; He and Chery, 2008) or continuous manner (Jade et al., 2004; Copley and McKenzie, 2007). In this sense, quantifying the fraction of strain in the Tibetan/Himalayan orogen that is accommodated on the KF, and its slip rate relative to the rates on smaller faults within the Tibetan interior (e.g., Taylor and Peltzer, 2006), is a primary objective for resolution of this debate.

Radial spreading

The radial spreading model of Tibetan deformation is motivated primarily by observations of widespread extension of the elevated plateau and its Himalayan rim, the radial GPS velocity field (e.g., velocities perpendicular to the arcuate Himalaya (Bendick and Bilham, 2001) and oriented outward) when viewed relative to India (e.g., Jade et al., 2004), the similarity of displacement vectors of thrust events on the Main Himalayan Thrust (Seeber and Pecher, 1998) to the GPS field, and the inference of an excess of gravitational potential energy implicit in the plateau's crust, which is 40-50 km thicker than the surrounding regions and stands ~5 km higher (e.g., England and Houseman, 1989). As typically imagined, this model is the continuum end-member on the continuum to block deformation spectrum of Tibetan tectonic models; one study states that Tibet spreads outward 'like honey on a dish' (Jade et al., 2004). Since this model holds that surface displacement vectors are oriented normal to the plateau's margins (Jade et al., 2004; Copley and McKenzie, 2007) and these vectors vary continuously, the role of a margin-parallel strike-slip fault such as the KF is very minor (Jade et al., 2004). Therefore, this model predicts that fault slip rates on the KF are only a small fraction of the 15-20 mm a^{-1} of strain north of the MHT. Though no papers make direct predictions, rates less than 3-4 mm a^{-1} are appropriate. Variations in slip rate along strike are not predicted. This model makes no explicit predictions on how KF fault slip is accommodated on its SE end.

Oblique convergence

The oblique convergence model of Himalayan-Tibetan deformation states that variations in convergence obliquity between the underthrusting Indian plate and the Himalaya (a necessary consequence of the margin geometry) cause differential margin-normal and margin-parallel basal shear stresses on the Himalaya. This results in margin-parallel translation of the Himalaya with respect to southern Tibet along the Karakoram fault; the velocity of this translation is higher in the NW than the SE, commensurate with the change in the margin-parallel component of convergence. This implies that the slip rates on the KF are faster in the NW than in the SE; GPS geodetic estimates of arc-parallel shear strain accumulation across the Himalaya and southwestern Tibet place a ceiling of 6-7 mm a^{-1} on this shear. The change in translation rate also requires margin-parallel extension throughout the Himalayan arc, which is accommodated by the many arc-parallel extensional structures in the Himalaya, such as the Leo Pargil dome (Thiede et al., 2006), the Gurla Mandhata Detachment (Murphy et al., 2002), the Thakkhola Graben (Hurtado et al., 2001), and the Ama Drime detachment (Jessup et al., 2008). Some studies supporting this model (Styron et al., 2011; C12) suggest that slip on the KF is transferred into the Himalaya at the Gurla Mandhata Detachment, an extensional stepover (Murphy and Copeland, 2005), and KF slip propagates toward the central Himalayan foreland along the Humla, Tibrikot and Bari Gad faults, likely at decreasing slip rates. Though these faults are known in the literature (e.g., Nakata, 1989), no slip rates have been determined for them over any time scale.

Lateral extrusion

The lateral extrusion model of Tibetan tectonics holds that Tibet is forced, or extruded, eastward as it is squeezed between the stronger India and central Asian cratons, due to India's impingement on southern Asia (Molnar and Tapponnier, 1975). This occurs along the plateau's marginal structures such as the KF, the Altyn Tagh fault, the Kunlun fault and the Indus-Yarlung suture. In this model, this process occurs relatively rapidly, and therefore rates and magnitudes of KF slip are high. These are predicted at 8-10 mm a^{-1} (Lacassin et al., 2004; Valli et al., 2008). Furthermore, this model explicitly calls for these rates to be constant along strike and to continue

eastward across the Indus-Yarlung Suture Zone.

Study site

The Menshi site on the KF is located at a transition between a restraining bend to the south-east of the Gar Basin and a broad, diffuse transtensional zone nearing Gurla Mandhata (Murphy and Burgess, 2006). The site was selected because here the KF is composed of only two fairly close strands (Figure 2) , in contrast to more complicated geometries along strike. The strands cut alluvial and fluvial deposits with reasonably clear offsets. The northern strand (Kailash Range Front Fault, or KKRF, as named by C12) displays dominantly right-lateral offsets (C12). These offsets are progressively larger for the older surfaces, consistent with right-lateral faulting through-out the depositional history of the surfaces. This strand is interpreted to be the main strand of the KF at this location. Most probable offsets on the KRRF were estimated to be ~25 m for the T1 (fluvial) surface, ~62 for the Qa1 (alluvial) surface, and ~122 m for the Qa2 (alluvial) surface (Figures 2, 3). Fig. 4 shows the Probability Distribution Functions (PDFs) for total offsets of these surfaces by the KF. Methods of error estimation are given below.

The southern strand (Darchen Fault, or DF, as named by C12) shows unambiguous signs of rupture, with clear disturbance of all surfaces other than the active (T0) channels. It also shows apparent right-lateral offsets of up to 150 m for the Qa1 surface and up to 220 m for the Qa2 (C12, Figure 2). However, in contrast to C12, our mapping of the fault trace suggests that this fault is a relatively steeply-dipping dip-slip fault with only minor (several m) displacement, based on these observations: Apparent right-lateral offsets are only found on the older surfaces in an area where they are unlikely to be preserved, and are not observed on the side of the stream that should be shielded from erosion, based on the assumed dextral slip sense and stream flow direction (e.g., Cowgill, 2007). No clear dextral offsets are observed in geomorphic features to either side of the apparent right-lateral offset, which are all very continuous across the anastomosing mapped ruptures. A several meter increase in the elevation of the older surfaces on the downstream side of the DF suggests that uplift of the downstream block deflected the stream to the right, creat-

183

ing an apparent, but false, right-lateral offset. The terrace riser on the upstream side of the DF is significantly sharper (less eroded) than on the downstream side of the fault, and small tributary stream channels on the upper (Qa1) surface are not incised to the level of the lower (T1) surface, as they are on the downstream side. This suggests that the stream has laterally eroded into the Qa1 surface, increasing the apparent displacement. Despite being ~7 m above the modern channel, the T1 risers show no displacement at all. A reconstruction of the Qa1 riser shows considerable (150+ m) offsets of all nearby contacts and geomorphic features (Figure 5). However, even though we view significant right-lateral slip on the DF as unlikely, our methods allow us to assign a low probability to it; this is represented by the long tail on the Qa and Qao PDFs in Fig. 4. Due to the laterally-eroded nature of the upstream riser, the reconstructed offset is viewed as a maximum with any lesser amount of tectonic offset possible.

We chose to sample at the DF site instead of the KRRF site because of better surface preservation at the former and the presence of nomads and livestock at the latter. The surfaces sampled were correlated across the map area field mapping, using the elevation relative to the streams, the sharpness of the terrace risers, and the amount of soil development and vegetation as indicators. Grain size is uniformly coarser to the north, as expected given its more proximal location to the Gangdese rangefront. The abandonment ages of the surfaces are assumed to be the same across the surface.

Discrepancies in mapping and reconstruction with C12

In general, our mapping and unit assignment is in agreement with C12. For clarity, our T0 and T1 units are named the same, and our Qa and Qao units are their T2 and T3 units (we interpret them as alluvial, not fluvial terrace, deposits). However, we have some differences that impact the reconstruction of fault offset. The largest is that we have some Qa in between the Qao and T1 surfaces on the KRRF site, leading us to assign smaller offset values. We also have two large differences in fault offset reconstruction (not mapping per se) that cause dramatic differences in net fault offset estimation. One is that C12 choose a restoration of a river and a T2/T3 contact to

the west of our common map area as the most likely reconstruction, which amounts to ~430 m of KRRF offset; this reconstruction clearly shows a left-lateral offset of ~300 m for contacts in our map area (C12 Fig. 6b). Additionally, they give a most likely value of ~188 m for the DF based on the discussed T2/Qa riser restoration, which also yields a left-lateral offset of almost 200 m on all neighboring contacts (Figure 5; C12 Fig. 6b). While we view the DF offset as unlikely, we incorporate it into our model (Fig. 4); however, as the ~430 m offset on the KKRF is incompatible with our mapping and reconstructions, we do not incorporate it.

C12 exposure age dating and slip rate derivation techniques

C12 use [10]Be TCN dating of surface cobbles to determine exposure ages of geomorphic features offset by the fault. In order to obtain the exposure age of a surface (not simply the individual cobbles) they reject outliers (based on undisclosed criteria) and choose the median value as the most probable, and the minimum and maximum unrejected cobble ages as the minimum and maximum values for the surface age; this range is about half of the median age for each of the two sampled surfaces (T1 and T3). In practice, exposure ages of individual clasts are a function of exposure age, 'inherited' TCN component accumulated prior to deposition, erosion rates of the surface, and the amount of bioturbation of the upper 10s of cm; these processes are almost certainly the cause for the variability in their observed ages. Because TCN inheritance yields older ages while erosion and bioturbation yield younger ages, it is not clear whether the net age bias (if any) is shifted towards older or younger ages. However, TCN depth profile techniques can determine these parameters with much greater accuracy.

C12 determined slip rates through straightforward division (offset / age), using the median values as most probable and the upper and lower bounds of each age and offset to obtain the upper and lower bounds for the slip rates. This process is independent for each offset/age pair and is not treated cumulatively. Then, all such slip rates intervals are compared and a value satisfying all measurements is taken as the most likely.

Methods

Our proposed methods involve the use of constructing Probability Density Functions (PDFs) for both the offset distance and the ages of geomorphic surfaces, and reconstructing slip and slip rate histories, incorporating all uncertainty through Monte Carlo methods. In contrast to many studies, we will use arbitrary PDFs with distributions completely constrained by the observations, instead of fitting functions that are familiar or mathematically convenient; this will give us the maximum rigor in error propagation and increase the accuracy of the result.

Offset reconstructions

Robustly accounting for uncertainty in the amount of fault offset of each surface is critical in neotectonics, as any uncertainty contributes directly to the uncertainty in slip rate estimates. Studies that do not assume a single fault offset value typically assume a uniform probability over some interval, or a Gaussian distribution. Presumably this is because of the mathematical simplicity involved in propagating errors with these distributions or the ease of reporting them, as they are both somewhat ill-suited to describing realistic probabilities for fault offsets. For a uniform (or boxcar) PDF, the probability jumps from 0 to a maximum value and back to 0 as a step function, but given the ambiguities in geomorphic mapping, it is difficult to understand geologically how such a line may be drawn; similarly, a Gaussian fault displacement PDF indicates that there is some real probability of offsets far larger or smaller than the favored value, including nearly infinite positive and negative values for displacement.

We have sidestepped this problem with a different method of reconstruction: The geologic map and 10 m SPOT satellite imagery were digitally separated along the fault trace, and reconstructions were performed in small spatial steps; for each step, the viability of the reconstruction was estimated (independent of other reconstructions) on a scale of 1-10 (10 being the most probable), including maximum and minimum estimates. Those points were then used to fit Green's function based tension splines (Wessel and Bercovici, 1998) to construct probability mass functions, which were then normalized to integrate to 1 to construct PDFs. These PDFs are shown

186

in Figure 4. The most obvious feature of the PDFs is that they highly skewed for the older two surfaces; this reflects the small but real probability that the apparent right-lateral offsets on the DF are actual tectonic displacements; the offset values given are therefore cumulative offsets for both faults.

^{36}Cl TCN Depth Profiling

TCN exposure age dating has proven to be a powerful method in neotectonic studies, but age determinations are functions of several site-specific variables, and failure to correctly deconvolve them may compromise the results based on inaccurate results. The relevant variables are exposure age, erosion rate, and TCN 'inheritance' (the component of TCN contained in a sample produced during events prior to the last depositional event). In neotectonic studies, the exposure age is typically the variable of interest, and the other two are often given prescribed values, estimated statistically (by the distribution in ages of samples and making causal assumptions), or ignored entirely. All previous neotectonics studies of the Karakoram fault have used some combination of these (Brown et al., 2002; Chevalier, et al., 2005; C12). However, the most successful method to solve for these three variables involves digging 'depth profiles', where 4-6 samples are taken from depths below the surface mixing zone (observed to be ~ 40 cm thickness in our pits) down to several meters depth. This method takes advantage of the quasi-exponential decrease in ^{36}Cl production with depth: the shape of the production vs. depth curve is uniquely sensitive to each of the three variables (Gosse and Phillips, 2001). Therefore, the equation for ^{36}Cl production as a function of depth, erosion rate and exposure age may be uniquely solved by constructing an overdetermined linear system, given more than three samples (observations). This gives it an epistemic advantage over the more common ^{10}Be dating, which may be measured more precisely, as the exponential ^{10}Be production curve is not uniquely sensitive to both erosion rate and exposure age; essentially, by using ^{36}Cl we have traded precision for accuracy.

The state of the art in TCN depth profile modeling is the MATLAB-based code of Hidy et al. (2010), which is a Monte Carlo simulator capable of incorporating uncertainty in the input

parameters (those associated with the TCN analytical uncertainty, production rates, etc.) as well as robust statistical output including PDFs for exposure age, erosion rate and inheritance, and Bayesian methods and importance sampling for reducing unintentional bias based on input parameter ranges.

Slip rate calculation

Most simply, fault slip rates are calculated as the offset of a feature divided by the age since the offset began. For the case of an active fault with multiple offset features and ages, each offset/age pair can be treated independently and these estimates may be averaged to get a single slip rate over the full time interval (e.g., Chevalier et al., 2012). Alternately the data pairs may be treated as points in a 'fault slip history' time series such that the older offset/age pairs are treated as cumulative, incorporating the slip rate information included in the younger measurements (e.g., Gold et al., 2010). With this latter method, an arbitrary function of net slip through time may be constructed by interpolating between the points, and the slip rate as a function through time is the first derivative of that function with respect to time. This is the approach that we choose, as it seems more reasonable to treat progressive offset/age pairs as cumulative; this approach also allows for more information to be extracted and essentially serves to remove the biasing of slip rate estimates from older age/offset pairs by younger pairs.

Our approach to slip history reconstruction with error propagation also involves Monte Carlo simulations. We have written Python code that performs the following tasks: First, the PDFs for the offsets and ages are constructed, as described above. Then, 100,000 samples are taken from each of those distributions through an inverse transform sampling algorithm, which for a large sample size ensures that the sample distribution represents the PDF (Downey, 2011). The set of one sample from each age and offset PDF is referred to as a 'run'. Runs containing offsets from older surfaces that are less than from younger surfaces, or containing ages from older surfaces that are less than ages from younger surfaces are removed; such a scenario would represent a highly-unlikely reversal in slip sense on the KF. Then, a 'fault slip history' for each run is made

by linear interpolation between each of the points, including a modern 0 offset and 0 age. Finally, this function is numerically differentiated to obtain the 'slip rate history', or slip rate as a function of time. After 100,000 iterations, robust probability distributions of cumulative offset for features of a given age and slip rate is obtained for every time step (e.g, every 500 years) over the period of study. This allows us to rigorously address not only the modern slip rate, but the possibility of slip rate variation through time (Figure 6).

Illustrative model results

Our reconstructions and estimates of offset features are shown in Fig. X. As an illustration of the results, we have run our simulation using our offset PDFs and age distributions based on the results of Chevalier et al. (2012) for those surfaces, using the most probable age ranges given as the mean and standard deviation for Gaussian age PDFs. The results are shown in Figure 6. The most probable results (modal values) show ~150 m of displacement over the past 150 ka (Figure 6a), leading to most probable slip rates of ~ 1 mm a-1 (Figure 6b). This rate is consistent with InSAR studies of the region (Wright et al., 2004; Wang and Wright 2012) which are capable of resolving slip rates across the KF itself, and lower than rates from GPS (Jade et al., 2004; Styron et al., 2011) which are upper limits as they represent total dextral shear between southwest Tibet and the Indian foreland. This value is significantly lower than the result of C12, although their results are comparable to our 95th percentile. This is unsurprising because the most likely values in our reconstructions show much less offset than in the reconstructions of C12.

However, we restate that these results are only illustrative, in that we do not have well-constrained surface exposure ages from TCN depth profiles. It is very possible that the ages given by C12 are too old due to TCN inheritance in the samples. If our TCN depth profile results give younger ages, our derived slip rates would be that commensurately faster, which may be more compatible with geologic and other neotectonic studies. This highlights the need to use TCN depth profiles to address exposure age, erosion and inheritance with the most rigor possible.

References

Avouac, J.P., and Tapponnier, P., 1993, Kinematic model of active deformation in central Asia: Geophysical Research Letters, v. 20, no. 10, p. 895–898.

Banerjee, P., Burgmann, R., Nagarajan, B., and Apel, E., 2008, Intraplate deformation of the Indian subcontinent: Geophysical Research Letters, v. 35, no. 18, p. L18301, doi: 10.1029/2008GL035468.

Bendick, R., and Bilham, R., 2001, How perfect is the Himalayan arc?: Geology, v. 29, no. 9, p. 791.

Brown, E.T., Bendick, R., Bourlès, D.L., Gaur, V., Molnar, P., Raisbeck, G.M., and Yiou, F., 2002, Slip rates of the Karakorum fault, Ladakh, India, determined using cosmic ray exposure dating of debris flows and moraines: J. Geophys. Res., v. 107, no. B9, p. 1-9, doi: 10.1029/2000jb000100.

Chevalier, M.-L., Ryerson, F.J., Tapponnier, P., Finkel, R.C., Van Der Woerd, J., Haibing, L., and Qing, L., 2005, Slip-Rate Measurements on the Karakorum Fault May Imply Secular Variations in Fault Motion: Science, v. 307, p. 411-414, doi: 10.1126/science.1105466.

Chevalier, M.-L., Tapponnier, P., Van der Woerd, J., Ryerson, F.J., Finkel, R.C., and Li, H., 2012, Spatially constant slip rate along the southern segment of the Karakorum fault since 200ka: Tectonophysics, v. 530-531, p. 152-179, doi: 10.1016/j.tecto.2011.12.014.

Copley, A., and McKenzie, D., 2007, Models of crustal flow in the India-Asia collision zone: Geophysical Journal International, v. 169, no. 2, p. 683-698, doi: 10.1111/j.1365-246X.2007.03343.x.

Cowgill, E., 2007, Impact of riser reconstructions on estimation of secular variation in rates of strike – slip faulting : Revisiting the Cherchen River site along the Altyn Tagh Fault , NW China: Earth and Planetary Science Letters, v. 254, p. 239 - 255, doi: 10.1016/j.epsl.2006.09.015.

Downey, A.B., 2011, Think Stats: Probability and Statistics for Programmers: Green Tea Press.

England, P., and Houseman, G., 1989, Extension during continental convergence, with application to the Tibetan Plateau: Journal of Geophysical Research, v. 94, no. B12, p. 17,561-

17,579.

Gold, R.D., and Cowgill, E.S., 2010, Deriving fault-slip histories to test for secular variation in slip, with examples from the Kunlun and Awatere faults: Earth and Planetary Science Letters, v. 301, no. 1-2, p. 52-64, doi: 10.1016/j.epsl.2010.10.011.

Gosse, J.C., and Phillips, F.M., 2001, Terrestrial in situ cosmogenic nuclides: theory and application: Quaternary Science Reviews, v. 20, p. 1475-1560.

He, J., and Chéry, J., 2008, Slip rates of the Altyn Tagh, Kunlun and Karakorum faults (Tibet) from 3D mechanical modeling: Earth and Planetary Science Letters, v. 274, no. 1-2, p. 50–58, doi: 10.1016/j.epsl.2008.06.049.

Hidy, A.J., Gosse, J.C., Pederson, J.L., Mattern, J.P., and Finkel, R.C., 2010, A geologically constrained Monte Carlo approach to modeling exposure ages from profiles of cosmogenic nuclides: An example from Lees Ferry, Arizona: Geochem. Geophys. Geosyst, v. 11, no. 9, p. 1-18, doi: 10.1029/2010GC003084.

Hurtado, J.M., Hodges, K.V., and Whipple, K.X., 2001, Neotectonics of the Thakkhola graben and implications for recent activity on the South Tibetan fault system in the central Nepal Himalaya: Geological Society of America Bulletin, v. 113, no. 2, p. 222.

Jade, S., Bhatt, B., Yang, Z., Bendick, R., Gaur, V., Molnar, P., Anand, M., and Kumar, D., 2004, GPS measurements from the Ladakh Himalaya, India: preliminary tests of plate-like or continuous deformation in Tibet: Geological Society of America Bulletin, v. 116, no. 11-12, p. 1385-1391, doi: 10.1130/B25357.1.

Lacassin, R., Valli, F., Arnaud, N., Leloup, P.H., Paquette, J.L., Haibing, L., Tapponnier, P., Chevalier, M.L., Guillot, S., Maheo, G., and others, 2004, Large-scale geometry, offset and kinematic evolution of the Karakorum fault, Tibet: Earth and Planetary Science Letters, v. 219, no. 3-4, p. 255–269, doi: 10.1016/S0012-821X(04)00006-8.

McCaffrey, R., and Nabelek, J., 1998, Role of oblique convergence in the active deformation of the Himalayas and southern Tibet plateau: Geology, v. 26, p. 691-694 ST - Role of oblique convergence in the a, doi: 10.1130/0091-7613(1998)026<0691:roocit>2.3.co;2.

Molnar, P., and Tapponnier, P., 1975, Cenozoic tectonics of Asia: effects of a continental collision: Science, v. 189, no. 4201, p. 419–426.

Murphy, M., and Burgess, W., 2006, Geometry, kinematics, and landscape characteristics of an active transtension zone, Karakoram fault system, Southwest Tibet: Journal of Structural Geology, v. 28, no. 2, p. 268-283, doi: 10.1016/j.jsg.2005.10.009.

Murphy, M.A., and Copeland, P., 2005, Transtensional deformation in the central Himalaya and its role in accommodating growth of the Himalayan orogen: Tectonics, v. 24, no. 4, p. TC4012, doi: 10.1029/2004tc001659.

Murphy, M., Yin, A., Kapp, P., Harrison, T., Lin, D., and Jinghui, G., 2000, Southward propagation of the Karakoram fault system, southwest Tibet: Timing and magnitude of slip: Geology, v. 28, no. 5, p. 451.

Nakata, T., 1989, Active faults of the Himalaya of India and Nepal: Tectonics of the western Himalayas: Geological Society of America Special Paper, v. 232, p. 243–264.

Peltzer, G., and Tapponnier, P., 1988, Formation and evolution of strike-slip faults, rifts, and basins during the India-Asia collision: An experimental approach: Journal of Geophysical Research, v. 93, no. B12, p. 15085–15.

Robinson, A.C., 2009, Geologic offsets across the northern Karakorum fault: Implications for its role and terrane correlations in the western Himalayan-Tibetan orogen: Earth and Planetary Science Letters, v. 279, no. 1-2, p. 123-130, doi: 10.1016/j.epsl.2008.12.039.

Searle, M., 1996, Geological evidence against large-scale pre-Holocene offsets along the Karakoram fault: Implications for the limited extrusion of the Tibetan Plateau: Tectonics, v. 15, no. 1, p. 171-186.

Seeber, L., and Pêcher, A., 1998, Strain partitioning along the Himalayan arc and the Nanga Parbat antiform: Geology, v. 26, no. 9, p. 791.

Styron, R.H., Taylor, M.H., and Murphy, M.A., 2011, Oblique convergence, arc-parallel extension, and the role of strike-slip faulting in the High Himalaya: Geosphere, v. 7, no. 2, p. 582-596, doi: 10.1130/GES00606.1.

Tapponnier, P., Peltzer, G., Le Dain, A.Y., Armijo, R., and Cobbold, P., 1982, Propagating extrusion tectonics in Asia: New insights from simple experiments with plasticine: Geology, v. 10, p. 611-616 ST - Propagating extrusion tectonics in A, doi: 10.1130/0091-7613(1982) 10<611:petian>2.0.co;2.

Taylor, M., and Peltzer, G., 2006, Current slip rates on conjugate strike-slip faults in central Tibet using synthetic aperture radar interferometry: Journal of Geophysical Research, v. 111, no. B12402, p. 1-16.

Thiede, R.C., Arrowsmith, J.R., Bookhagen, B., McWilliams, M., Sobel, E.R., and Strecker, M.R., 2006, Dome formation and extension in the Tethyan Himalaya, Leo Pargil, northwest India: Bulletin of the Geological Society of America, v. 118, no. 5-6, p. 635, doi: 10.1130/ B25872.1.

Valli, F., Herve, P., Paquette, J.-louis, Arnaud, N., Li, H., Tapponnier, P., Lacassin, R., and Liu, D., 2008, New U-Th/Pb constraints on timing of shearing and long-term slip-rate on the Karakorum fault: Tectonics, v. 27, no. TC5007, p. 1-33, doi: 10.1029/2007TC002184.

Wang, H., and Wright, T.J., 2012, Satellite geodetic imaging reveals internal deformation of western Tibet: Geophysical Research Letters, v. 39, no. 7, p. 1-5, doi: 10.1029/2012GL051222.

Wessel, P., and Bercovici, D., 1998, Interpolation with Splines in Tension : A Green's function approach: Computers & Geosciences, v. 30, no. 1, p. 77-93.

Wright, T., Parsons, B., and England, P., 2004, InSAR observations of low slip rates on the major faults of western Tibet: Science, v. 236, no. 2004, p. 236-239, doi: 10.1126/science.1096388.

Yin, A., and Harrison, T.M., 2000, Geologic evolution of the Himalayan-Tibetan orogen: Annual Review of Earth and Planetary Sciences, v. 28, no. 1, p. 211–280.

Figures with Captions

a: lateral extrusion

KF

Tibetan plateau

10

Himalaya

10

Range

b: radial spreading

3

KF

Tibetan plateau

3

Himalaya

Range

c: oblique convergence

KF

7

Tibetan plateau

3

Himalaya

Range

India
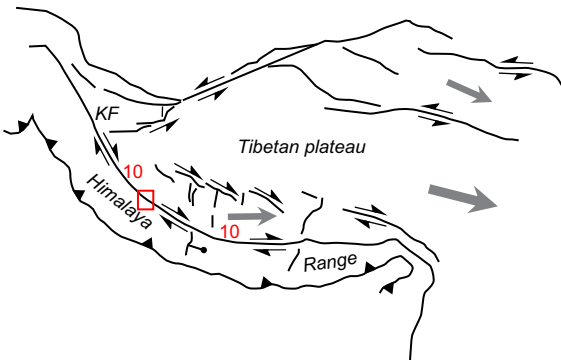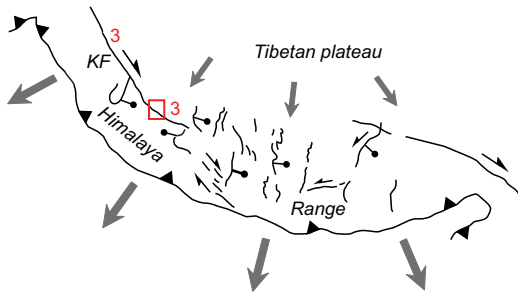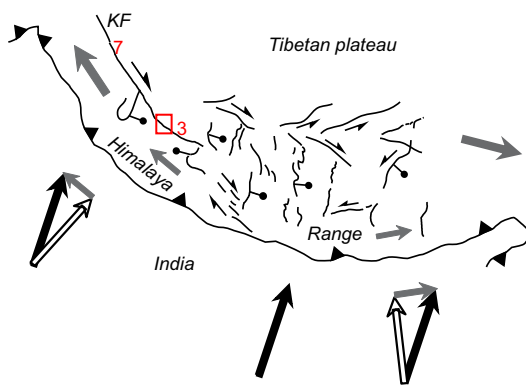
Figure. 1: Models for Himalayan and Tibetan deformation to be tested in this study. Grey arrows represent motion of the crust. The red box marks the location of our field site. Red numbers indicate the predicted slip rate for the KF at that location. In Fig. 1C, large black arrows show India's convergence direction. White and grey arrows show the respective range-normal and range-parallel velocity components. After Styron et al., (2011).
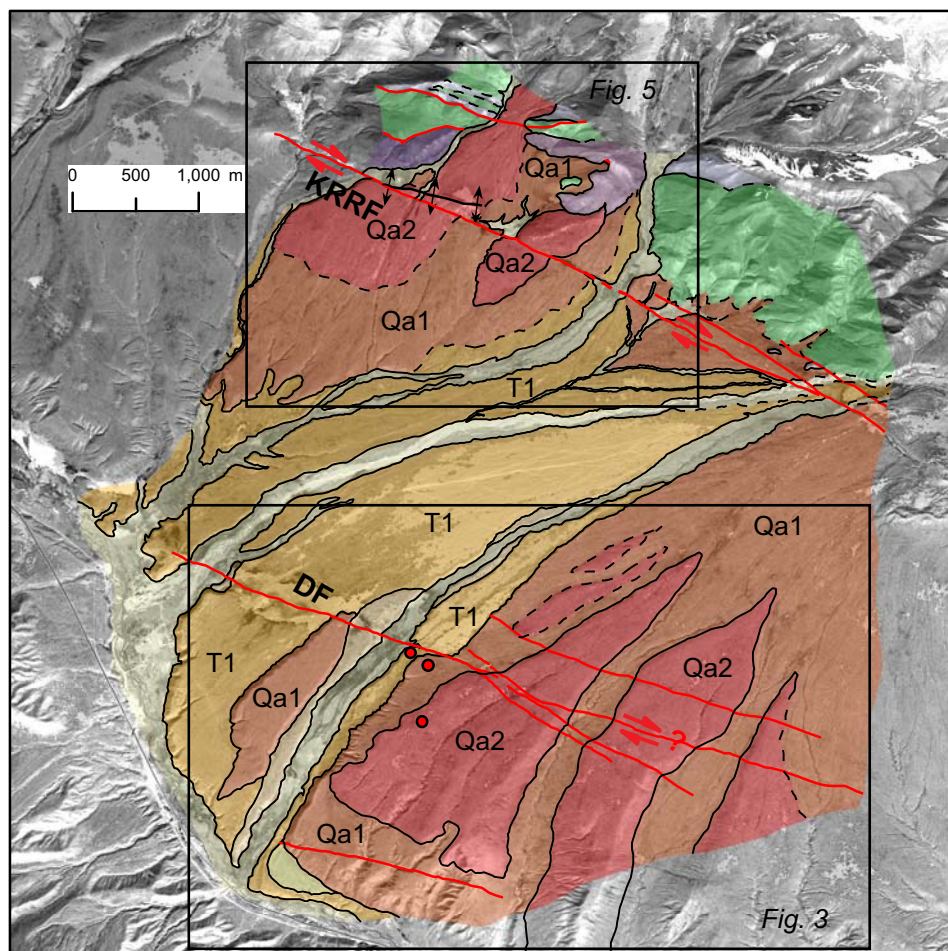
Fig ure 2: Neotectonic map of the Menshi site on the KF. KRRF = Kailash Range Front Fault.
DF=Darchen Fault. Red circles indicate TCN depth profile locations.

Fig ure 3: Terrace riser reconstruction of Qa1 (youngest riser) on the DF from C12. Note that after the reconstruction, the Qa2 (older) riser has an apparent left lateral offset implying the younger riser has accumulated more slip. See Figure 2 for location.
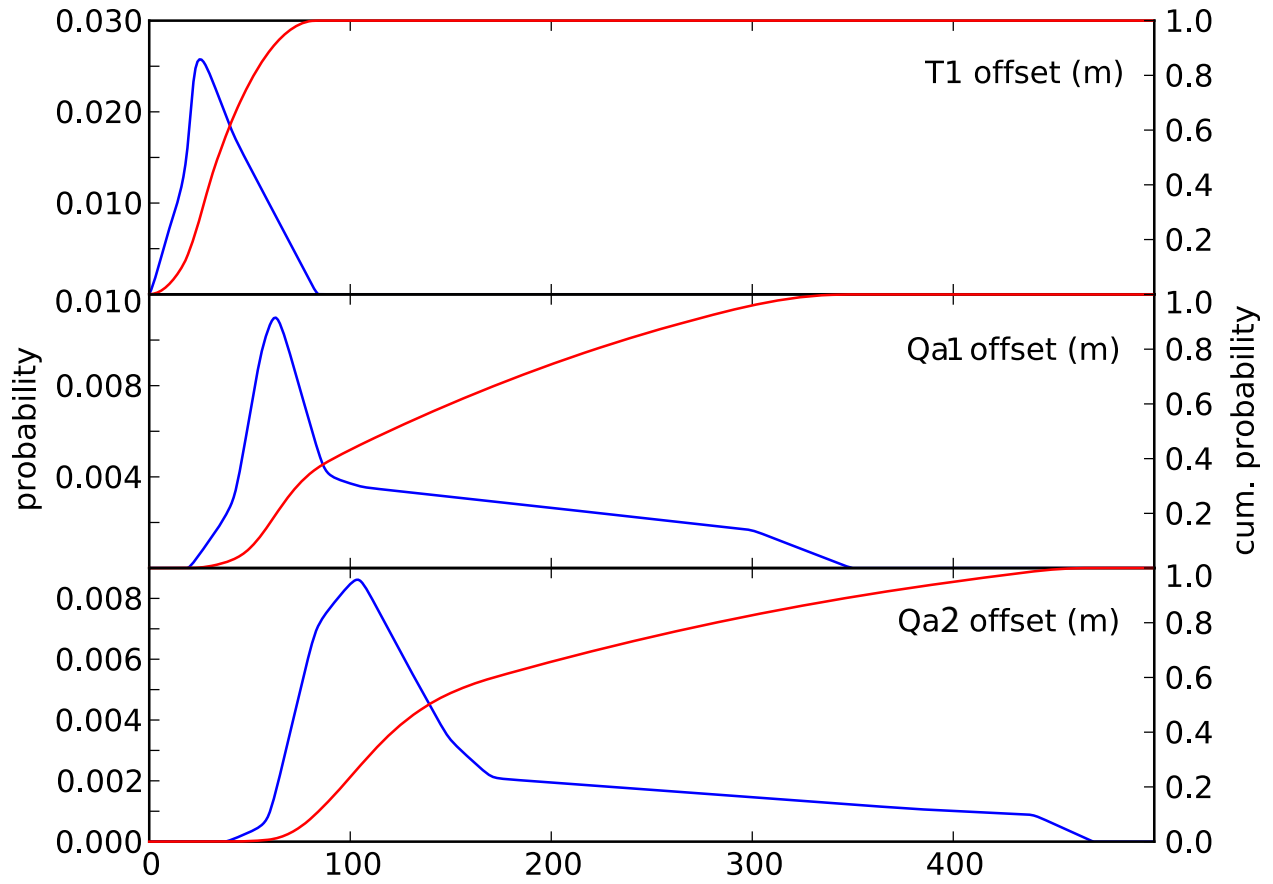
Figure 4: PDFs (blue) and CDFs (red) of fault offset at the Menshi site on the KF, incorporating both the KRRF and the DF offsets. Long tails on the Qa1 and Qa2 PDFs indicate the low-probability but high-magnitude large offsets on the DF.
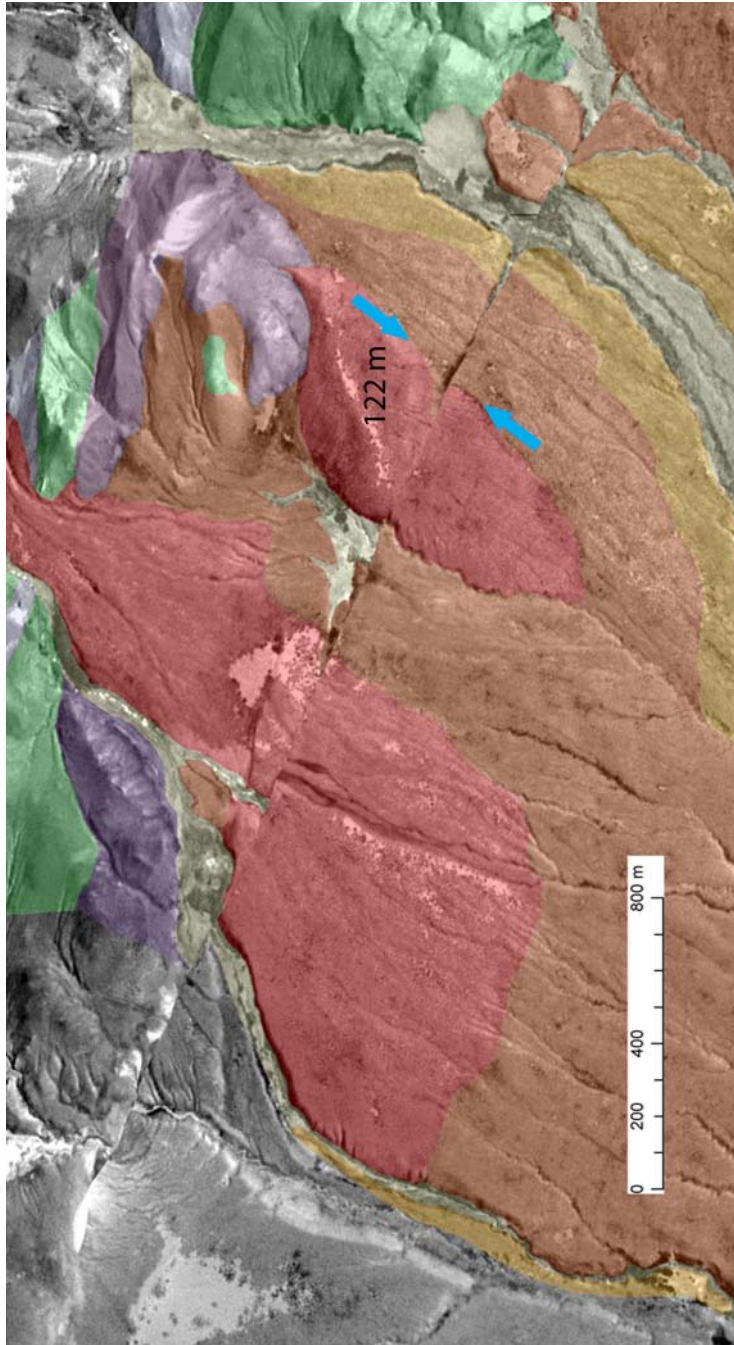
Figure 5: Highest-probability reconstruction of the oldest (Qa2) geomorphic surface on the KRRF, requiring 122 m of slip to restore. See Fig. 2 for location.
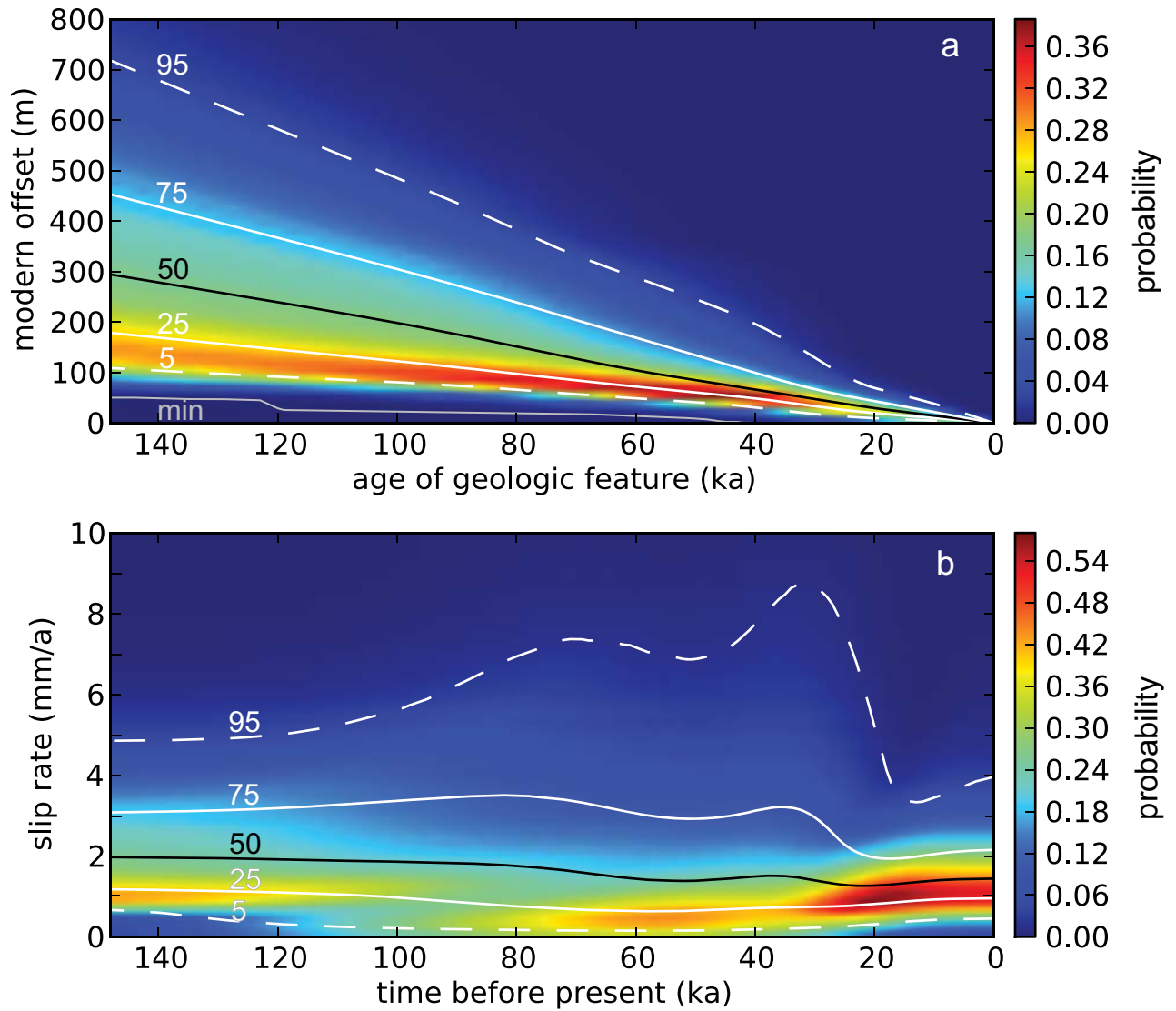
Figure 6: a) Probability through time of amount of modern offset of geologic features of a given age cut by the Karakoram Fault; this is essentially cumulative fault offset since a given time. Colors represent probability density, with warm colors being more probable than cool colors. Numbered lines represent the indicated percentiles, and the black line is the median value. b) Probability through time of slip rate on the Karakoram Fault. Symbology is the same as a. Note that for both distributions, the modal value (highest probability) is best approximated by the 25th percentile; this indicates that low values for cumulative slip and slip rate for the KF are much more likely, but there is some possibility of higher values.

The view from the northern Surla Range across Ringinyubo Co to the west side of the North Lunggar Range.

Chapter 7

Summary and Conclusions

The work presented in the previous four chapters concerns the determination of crustal deformation rates in southern Tibet and the Himalaya over 10 to 10^6 yr timescales. Although the methods used and the timescales considered vary drastically, the results show coherent patterns with regards to the rates, timing and style of deformation.

A picture of regional deformation

Tectonism in Tibet and the Himalaya displays particular patterns that are related to the boundary and body forces operating on the orogen, as well as the local rheology of the crust. Much (30-50%) of the deformation between India and stable Eurasia is taken up on the Main Himalayan Thrust, which is the megathrust separating Eurasia from India. This fault daylights as the Main Frontal Thrust (e.g., Lave and Avouac, 2000), the lowest-elevation and southernmost thrust in the Himalayan wedge, where most of the slip is concentrated. However, it has been suggested that faults farther into the wedge, in particular the Main Central Thrust, presently accommodate small amounts of deformation as well (e.g., Hodges et al., 2001).

Inboard and uphill of the Main Frontal Thrust, few thrust faults show evidence for activity. Instead, deformation is accommodated via strike-slip and normal faults that likely have relatively low slip rates (<5-6 mm yr^{-1}). These faults, which are often connected, generally accommodate extensional deformation of the orogen, though there is some regional variability. More precisely, extension may be subdivided into two overlapping domains, the Himalaya and Tibet.

Himalayan deformation

Active deformation in the Himalaya is characterized by thrusting at the base of the wedge, and strike-slip and normal faulting at higher elevations toward the hinterland of the wedge. These faults accommodate arc-parallel extension and translation of the Himalaya. This deformation

is considered in detail in Chapter 3, with the goal of quantifying deformation rates and testing deformational models. The results of that study indicate that over a 10 yr timescale, arc-parallel extension is quite significant, at a total of >30 mm yr^{-1}, though this extension is accommodated over many individual structures throughout the 1500 km long orogen. Large arc-parallel extensional structures include several metamorphic core complexes, namely the Leo Pargil (Thiede et al., 2006), Gurla Mandhata (Murphy et al., 2002) and Ama Drime (Jessup et al., 2008) domes; each of these has accommodated some 10s of km of extension and appears to be active. Furthermore, many smaller rifts (mostly hosting moderate to high-angle normal faults) are found throughout the Himalaya. These have been described mostly in the Nepalese central Himalaya, where extension is most rapid (Chapter 3), though this location may simply be more studied due to historical and geopolitical reasons.

Arc-parallel translation occurs on strike-slip faults with strikes parallel to the orogen. The major structure is the right-lateral Karakoram Fault (KF), which is located on the Indus-Yarlung Suture zone (IYS), marking the boundary between the Himalaya and Tibet. The KF shows decreasing magnitudes of net slip (over 10^7 yr timescales) to the southeast, ranging from ~165 km in the northwest (Robinson, 2009) to ~65 km in the southeast (Murphy et al., 2000). This slip gradient is interpreted to reflect arc-parallel extension in the Himalaya (to the southwest of the KF) that is not found in Tibet (to the northeast of the KF); northwest Himalayan crust translates more rapidly, and has translated greater distances, than crust to the southeast, and the KF accommodates that translation. Little arc-parallel translation is evident in the central Himalaya, though the east-central part of the range shows possible left-lateral arc-parallel faulting (Li and Yin, 2008), and the Yadong-Gulu rift, which is oblique to both the Himalaya and most south Tibetan rifts, has a left-lateral component (e.g., Armijo et al., 1986).

The organization of these faults and the geodetic velocity field is shown to be consistent with a model of variably oblique convergence between India and the Himalaya causing Himalayan arc-parallel extension and translation (Chapter 2). Specifically, observations of the arc-parallel

velocity field and the arc-parallel translation gradient match the model predictions, though these observations are in disagreement with other proposed models. The prediction of arc-parallel translation gradient along the KF is demonstrated for 10^7 yr scale geologic offsets, and is consistent with the geodetic data (though the uncertainty is very large).

However, lower KF slip rates in the southeast have not been demonstrated yet over the late Quaternary (timescales of 10^3-10^5 yr), which may provide the most accurate (though not necessarily most precise) estimates of 'modern' fault slip rates, because that time scale is longer than the seismic cycle and shorter than time scales for tectonic or geodynamic reorganizations. Published work (Brown et al., 2002; Chevalier et al., 2005, 2012) suggests the opposite, that slip rates increase to the southeast, though the two southeastern studies may be questionable (e.g., Brown et al., 2005; Chapter 6). Our ongoing work (Chapter 6) seeks to test this hypothesis with more thorough reconstructions and TCN dating methods. Though our work has significantly different offset reconstructions than that of Chevalier et al. 2012), if their ages for offset features are reasonably accurate, then a decrease in late Quaternary slip rate from the central KF (Brown et al., 2002) to the southeast (Chapter 6) is supported by the evidence.

Intriguingly, these rates, 1-3 mm yr^{-1}, are considerably lower than slip rates derived from offset, dated geologic features in similar locations (5-9 mm yr^{-1}; Murphy et al., 2000) but are consistent with geodetic studies (e.g., Chapter 2, Wright et al., 2004; Jade et al., 2004; Wang and Wright, 2012). A.M. McCallister (unpublished M.S. Thesis, University of Kansas, 2012) studied the Gurla Mandhata Rift, which is interpreted as an extensional stepover in the KF-Humla Fault system (Murphy and Copeland, 2005); his work shows that horizontal extension rates decreased from ~10 mm yr^{-1} to 1-3 mm yr^{-1} at some point since the late Miocene, though the uncertainty is large for all parameters. The oblique convergence hypothesis, which is supported by our work, holds that shear tractions in the direction of Indian plate motion are applied to the base of the Himalayan thrust wedge as India underthrusts the range. Because of the map-view curvature of the Himalaya (e.g., Bendick and Bilham, 2001), basal shear tractions have a spatially variable

ratio of their arc-normal to arc-parallel components. Arc-parallel shear tractions are near zero where convergence is normal to the arc, and increase progressively in either direction along strike, where the convergence becomes more oblique. The arc-parallel velocity of a given point in the Himalayan thrust wedge is proportional to and in the direction of the arc-parallel basal shear tractions. Arc-parallel extension, then, is the spatial rate of change of the arc-parallel velocity field along strike.

The success of the oblique convergence model in explaining Himalayan deformation highlights the role of the Indian plate in controlling Himalayan deformation. Though Indo-Himalayan or Indo-Eurasian convergence is the primary, if not the sole, cause of the Cenozoic Himalayan-Tibetan orogeny, the degree to which this first-order process controls second-order deformation is underestimated in many of the models seeking to explain deformation in the orogen (see Chapter 2 for a discussion of these models).

A key aspect of the configuration of rifts and arc-parallel strike-slip faults in the Himalaya is that where the Himalaya is bound by the KF, rifts do not penetrate north into Tibet. However, in the central and eastern Himalaya, rifts cross the IYS and appear to be linked to rifts in south Tibet.

Central and south Tibetan deformation

Deformation in south Tibet may be characterized as roughly east-west extension (more accurately E20˚S, or 110˚; this is normal to the Indo-Eurasian convergence direction) mostly accommodated on north-trending rifts. The rifts display a range of along-strike lengths and magnitudes of extension (where quantified or estimated). In the south, many small rifts occupy the high terrain of the Gangdese Range, but few extend north or south to lower elevations. Some notable rifts of 'moderate size' that are several 10s of km in length and contain high relief are the Lopukangri rift in the southwestern Lhasa terrane (e.g., Murphy et al., 2010) and the Xiagangjiang Rift (Volkmer et al., 2007), often spelled 'Shakangsham' in the literature of Tibetan exploration or

mountaineering, to the north-northeast of the Lopukangri Rift. There are arguably 5 main rifts in the Lhasa block; these cut across the Lhasa terrane from the Bangong-Nujiang Suture zone (BNS) in the north into the Gangdese Range in the south. Two of these, the Lunggar Rift in the west (Kapp et al, 2008; Chapters 3 and 4) and the Yadong-Gulu Rift, especially the Nyainqentanglha Rift segment (e.g., Pan and Kidd, 1992; Harrison et al., 1995; Kapp et al., 2005; Ratschbacher et al., 2011) have been studied in detail. The two rifts in between, the Tangra Yum Co and Pumqu-Xainza Rifts, have been studied (Dewane et al., 2006; Hager et al., 2006) but no research has been published on them, to the best of our knowledge. The fifth rift is to the west of the Lunggar Rift and contains the town of Yagra; it is currently unstudied.

All of the major South Tibetan rifts connect to southeast-striking right-lateral faults composing the southern half of the V-shaped conjugate strike-slip fault zone emanating from the BNS in central Tibet. Given the geometry of this fault system, deformation across it is mostly east-directed extension, although a smaller component of north-south will occur as well. Even though these faults are not optimally oriented to accommodate north-south shortening, they are essentially the only suitable structures on the elevated surface of the Tibetan Plateau capable of accommodating this strain, estimated at >10 mm yr^{-1} through GPS geodesy (Zhang et al., 2004). The member faults of this system have somewhat lower estimates of horizontal displacement than the most-developed parts of the Lunggar and Nyainquentanglha Rifts, ~12 km (Taylor et al., 2003) vs. 18-21 km (Chapters 3 and 4; Kapp et al., 2005), but are not incompatible given the observed variability in extension throughout the Lunggar Rift (Chapters 3 and 4). Slip rates for the strike-slip faults derived through geodesy (2-18 mm yr^{-1}; Taylor and Peltzer, 2006) are significantly higher than those estimated for the rifts through thermochronometry (1-4 mm yr^{-1}; Chapters 3 and 4; Kapp et al., 2005) except for the Lamu Co Fault which links with the Lunggar Rift. The slip rates for these two fault systems are virtually identical. The faster modern rates and lower displacements suggest that the majority of slip on the strike-slip faults has occurred later than on the rifts to the south; this supports the hypothesis developed in Chapter 5 of a northward propagation in rapid east-directed extension. However, it is not clear if these faults began contemporaneously with the

rifts and later accelerated or did not initiate until more recently.

Yin and Taylor (2011) have explained the non-Andersonian geometry and rapid slip rates of the V-shaped strike-slip faults as the brittle, upper crustal response to eastward flow of the crust and upper mantle. Based on the geometry of the faults, the geodetic velocity field, and mantle anisotropy data from seismic experiments, this flow appears to be a Pouseuille-type (parabolic) flow through a channel in between the underthrusting Indian and Eurasian lithospheres; the convergence of these two bodies squeezes the weaker Tibetan lithosphere and asthenosphere out to the east.

Time-variable slip rates and the role of the Indian plate

The work in this dissertation and the summarized information above contain two recurring themes: the temporal variability of fault slip rates, and the role of the underthrusting Indian plate. Furthermore, this work suggests that these themes are causally related: the changes in India's location and underthrusting rate beneath the orogen cause changes in the deformation rate at the surface. The dynamics of northward underthrusting or southward rollback of Indian lithosphere have been discussed by DeCelles et al. (2002; 2011), and appear to be temporally correlated with major shifts in the style of orogeny, such as the initiation or cessation of thrusting along the BNS or the Main Central Thrust. The work here shows that in addition to major changes in tectonic style, more subtle and progressive changes may result from India's changes in convergence style.

The onset of Himalayan extension in the middle Miocene (Chapter 2) occurs 5-10 m.y. after initiation of the Main Central Thrust and South Tibetan detachment and possibly immediately after their cessation. This change from north-south shortening and thickening of the High Himalaya to east-west extension and thinning is synchronous with the propagation of the active thrust front southward, with the formation of the Main Boundary Thrust (Meigs et al. 1995). It may be synchronous with the time the Tibetan Plateau reached its modern elevations as well (e.g., Quade et al., 2011); an increase in the 'backstop' height of a thrust wedge should cause the outward expansion of the wedge, and underplating at depth (e.g., Davis et al., 1983; DeCelles et al., 2009).

The timing of this corresponds to a renewal in the northward underthrusting (DeCelles et al., 2011). This synchronicity is well explained if the observed arc-parallel extension is caused by basal shear tractions due to India's underthrusting of the Himalaya.

The deceleration of fault slip on the KF and Gurla Mandhata detachment is a significant but unexplained development. Although this problem should be addressed in more detail, we suggest that basal shear stresses in the Himalayan hinterland are lower now than they were in the late Miocene and early Pliocene, when deformation rates appear to have been higher. As the oblique convergence hypothesis calls for arc-parallel extension and translation to relieve the arc-parallel shear tractions, it could be that these shear tractions have decreased in magnitude with time. Ader et al. (2012) use a geodetic and numerical approach to calculate interseismic coupling between India and the Himalaya along the Main Himalayan Thrust in Nepal and the adjacent Indian Himalaya. Their results show that coupling (leading to fault locking) on the MHT is high towards the foreland but has decreased to zero below Gurla Mandhata, indicating that slip between India and Tibet is completely ductile shear at this point. Studies (e.g., Bowman et al., 2003) have shown that slip partitioning of dip-slip and strike-slip strain in obliquely convergent or divergent situations is a process that occurs more frequently in the brittle realm, while ductile shear is commonly oblique. If this is the case, the southward propagation of thrusting on the MHT following middle Miocene thickening of the Himalayan crust may have lead to a situation where basal shear on the hinterlandward Himalaya is now ductile and can occur obliquely, therefore eliminating the need to relieve arc-parallel tractions through displacement independent of the arc-normal component. This hypothesis would predict that new structures accommodating arc-parallel extension and translation should develop closer to the tip of the Himalayan wedge; the Tibrikot and Bari Gad faults in Nepal (Chapter 2) may be examples of these.

The Tibetan Plateau began east-directed extension by the middle Miocene as well. Early extension appears to have been slow (e.g., Chapters 3 and 4), and little total extension was accumulated during this phase. Indeed, the isolation of many rifts far north of the Indian slab

to high elevations suggests that some extension is simply related to localized collapse of high topography. However, as India penetrated further and further into or underneath the Tibetan crust, rapid extension began close to the slab tip and continues above the slab. The hypothesis developed in Chapter 5 relates rapid extension to lateral (eastward) escape of crustal material above the slab. Essentially, this hypothesis is that India's underthrusting thickens the crust, but the surface of Tibet can extend no higher in altitude because its maximum altitude is determined by the horizontal compressive stresses supporting that elevation, so crust above the Indian slab extends eastward to compensate for crustal thickening at depth. We suggest that eastward advection of Lhasa terrane crust occurs through ductile flow in the middle to lower crust, where the high geotherm (Chapter 4) indicates that the crust is far too hot to deform by fracturing. Eastward flow from the high southern plateau may be tunneling into the crust of eastern Tibet, thickening the surface without visible shortening (Clark et al., 2005; Gan et al., 2007).

Extrapolation of geodetic slip rates back in time suggests that the observed offsets may have begun accumulating displacement at 3-2 Ma (Taylor and Peltzer, 2006) or even more recently if time-averaged rates are closer to the higher end of the slip rates estimated in that study. However, as discussed by Taylor and Peltzer (2006), fault slip rates may have begun slow and accelerated in the Pliocene, similar to our results for the Lunggar Rift. In either case, it is clear that rapid extension along the BNS is a relatively recent phenomenon, and probably later than in the North Lunggar Rift. The model of Yin and Taylor (2011) explaining deformation of the V-shaped conjugate strike-slip fault zone calls on India's constriction of the crust and upper mantle in between the Indian and Eurasian lithospheres. While the physical mechanism of extension (eastward extension and north-south shortening without changes in the thickness of any layer) is different from that suggested for the rifts to the south, the basic timing and cause (Indian underthrusting) is completely consistent between both cases. Since they are independent studies that do not rely on the same data or methods, they are mutually supportive.

References

Ader, T., Avouac, J.-P., Liu-Zeng, J., Lyon-Caen, H., Bollinger, L., Galetzka, J., Genrich, J., Thomas, M., Chanard, K., Sapkota, S.N., Rajaure, S., Shrestha, P., Ding, L., and Flouzat, M., 2012, Convergence rate across the Nepal Himalaya and interseismic coupling on the Main Himalayan Thrust: Implications for seismic hazard: Journal of Geophysical Research, v. 117, no. B04403, p. 1–16, doi: 10.1029/2011JB009071.

Armijo, R., Tapponnier, P., Mercier, J.L., and Tong-Lin, H., 1986, Quaternary extension in southern Tibet: Field observations and tectonic implications: Journal of Geophysical Research, v. 91, no. B14, p. 13803–13872.

Bendick, R., and Bilham, R., 2001, How perfect is the Himalayan arc?: Geology, v. 29, no. 9, p. 791–794, doi: 10.1130/0091-7613(2001)029<0791:HPITHA>2.0.CO;2.

Bowman, D., King, G., and Tapponnier, P., 2003, Slip partitioning by elastoplastic propagation of oblique slip at depth.: Science, v. 300, no. 5622, p. 1121–1123, doi: 10.1126/science.1082180.

Brown, E.T., Bendick, R., Bourles, D.L., Gaur, V., Molnar, P., Raisbeck, G.M., and Yiou, F., 2002, Slip rates of the Karakorum fault , Ladakh , India , determined using cosmic ray exposure dating of debris flows and moraines: Journal of Geophysical Research, v. 107, no. B9, p. 1–7, doi: 10.1029/2000JB000100.

Brown, E.T., Molnar, P., and Bourlés, D.L., 2005, Comment on "Slip-Rate Measurements on the Karakoram Fault May Imply Secular Variations in Fault Motion:" Science, v. 309, p. 1326b, doi: 10.1029/2000JB000100.

Chevalier, M.-L., Ryerson, F.J., Tapponnier, P., Finkel, R.C., Van Der Woerd, J., Haibing, L., and Qing, L., 2005, Slip-rate measurements on the Karakorum Fault may imply secular variations in fault motion.: Science, v. 307, no. 5708, p. 411–414, doi: 10.1126/science.1105466.

Chevalier, M.-L., Tapponnier, P., Van der Woerd, J., Ryerson, F.J., Finkel, R.C., and Li, H., 2012, Spatially constant slip rate along the southern segment of the Karakorum fault since 200ka:

Tectonophysics, v. 530-531, p. 152–179, doi: 10.1016/j.tecto.2011.12.014.

Clark, M.K., House, M.A., Royden, L.H., Whipple, K.X., Burchfiel, B.C., Zhang, X., and Tang, W., 2005, Late Cenozoic uplift of southeastern Tibet: Geology, v. 33, no. 6, p. 525–528, doi: 10.1130/G21265.1.

Davis, D., Suppe, J., and Dahlen, F.A., 1983, Mechanics of Fold-and-Thrust Belts and Accretionary Wedges: Journal of Geophysical Research, v. 88, no. B2, p. 1153–1172.

DeCelles, P.G., Ducea, M.N., Kapp, P., and Zandt, G., 2009, Cyclicity in Cordilleran orogenic systems: Nature Geoscience, v. 2, no. 4, p. 251–257, doi: 10.1038/ngeo469.

DeCelles, P.G., Kapp, P., Quade, J., and Gehrels, G.E., 2011, Oligocene-Miocene Kailas basin, southwestern Tibet: Record of postcollisional upper-plate extension in the Indus-Yarlung suture zone: Geological Society of America Bulletin, v. 123, no. 7-8, p. 1337–1362, doi: 10.1130/B30258.1.

DeCelles, P.G., Robinson, D.M., and Zandt, G., 2002, Implications of shortening in the Himalayan fold-thrust belt for uplift of the Tibetan Plateau: Tectonics, v. 21, no. 6, p. 1–12, doi: 10.1029/2001TC001322.

Gan, W., Zhang, P., Shen, Z.-K., Niu, Z., Wang, M., Wan, Y., Zhou, D., and Cheng, J., 2007, Present-day crustal motion within the Tibetan Plateau inferred from GPS measurements: Journal of Geophysical Research, v. 112, no. B08416, p. 1–14, doi: 10.1029/2005JB004120.

Harrison, T.M., Copeland, P., Kidd, W.S.F., and Lovera, O.M., 1995, Activation of the Nyainqentanghla Shear Zone: Implications for uplift of the southern Tibetan Plateau: Tectonics, v. 14, no. 3, p. 658–676.

Hodges, K.V., Hurtado, J.M., and Whipple, K.X., 2001, Southward extrusion of Tibetan crust and its effect on Himalayan tectonics: Tectonics, v. 20, no. 6, p. 799–809, doi: 10.1029/2001TC001281.

Jade, S., Bhatt, B.C., Yang, Z., Bendick, R., Gaur, V.K., Molnar, P., Anand, M.B., and Kumar, D., 2004, GPS measurements from the Ladakh Himalaya, India: Preliminary tests of plate-like or continuous deformation in Tibet: Geological Society of America Bulletin, v. 116, no.

11/12, p. 1385–1391, doi: 10.1130/B25357.1.

Jessup, M.J., Newell, D.L., Cottle, J.M., Berger, A.L., and Spotila, J. a., 2008, Orogen-parallel extension and exhumation enhanced by denudation in the trans-Himalayan Arun River gorge, Ama Drime Massif, Tibet-Nepal: Geology, v. 36, no. 7, p. 587–590, doi: 10.1130/G24722A.1.

Kapp, J., Harrison, T., Kapp, P., Grove, M., Lovera, O.M., and Ding, L., 2005, Nyainqentanglha Shan: A window into the tectonic, thermal, and geochemical evolution of the Lhasa block, southern Tibet: Journal of Geophysical Research, v. 110, no. B08413, p. 1–23, doi: 10.1029/2004JB003330.

Kapp, P., Taylor, M., Stockli, D., and Ding, L., 2008, Development of active low-angle normal fault systems during orogenic collapse: Insight from Tibet: Geology, v. 36, no. 1, p. 7–10, doi: 10.1130/G24054A.1.

Lave, J., and Avouac, J.-P., 2000, Active folding of fluvial terraces across the Siwaliks Hills, Himalayas of central Nepal Precambrian: Journal of Geophysical Research, v. 105, no. B3, p. 5735–5770.

Meigs, A., Burbank, D., and Beck, R., 1995, Middle-late Miocene (> 10 Ma) formation of the Main Boundary thrust in the western Himalaya: Geology, v. 23, no. 5, p. 423–426, doi: 10.1130/0091-7613(1995)023<0423.

Murphy, M.A., and Copeland, P., 2005, Transtensional deformation in the central Himalaya and its role in accommodating growth of the Himalayan orogen: Tectonics, v. 24, no. TC4012, p. 1–19, doi: 10.1029/2004TC001659.

Murphy, M. a., Sanchez, V., and Taylor, M.H., 2010, Syncollisional extension along the India–Asia suture zone, south-central Tibet: Implications for crustal deformation of Tibet: Earth and Planetary Science Letters, v. 290, no. 3-4, p. 233–243, doi: 10.1016/j.epsl.2009.11.046.

Murphy, M.A., Yin, A., Kapp, P., Harrison, T.M., Lin, D., and Jinghui, G., 1998, Southward propagation of the Karakoram fault system , southwest Tibet : Timing and magnitude of slip: Geology, v. 28, no. 5, p. 451–454.

Murphy, M. a., Yin, A., Kapp, P., Harrison, T.M., Manning, C.E., Ryerson, F.J., Lin, D., and Jinghui, G., 2002, Structural evolution of the Gurla Mandhata detachment system, southwest Tibet: Implications for the eastward extent of the Karakoram fault system: Geological Society of America Bulletin, v. 114, no. 4, p. 428–447, doi: 10.1130/0016-7606(2002)114<0 428:SEOTGM>2.0.CO;2.

Pan, Y., and Kidd, W.S.F., 1992, Nyainqentanglha shear zone: A late Miocene extensional detachment in the southern Tibetan Plateau: Geology, v. 20, no. 9, p. 775–778, doi: 10.1130/0091-7613(1992)020<0775.

Quade, J., Breecker, D.O., Daeron, M., and Eiler, J., 2011, The paleoaltimetry of Tibet: An isotopic perspective: American Journal of Science, v. 311, no. 2, p. 77–115, doi: 10.2475/02.2011.01.

Ratschbacher, L., Krumrei, I., Blumenwitz, M., Staiger, M., Gloaguen, R., Miller, B.V., Samson, S.D., Edwards, M. a., and Appel, E., 2011, Rifting and strike-slip shear in central Tibet and the geometry, age and kinematics of upper crustal extension in Tibet: Geological Society, London, Special Publications, v. 353, no. 1, p. 127–163, doi: 10.1144/SP353.8.

Robinson, A.C., 2009, Geologic offsets across the northern Karakorum fault: Implications for its role and terrane correlations in the western Himalayan-Tibetan orogen: Earth and Planetary Science Letters, v. 279, no. 1-2, p. 123–130, doi: 10.1016/j.epsl.2008.12.039.

Taylor, M., and Peltzer, G., 2006, Current slip rates on conjugate strike-slip faults in central Tibet using synthetic aperture radar interferometry: Journal of Geophysical Research, v. 111, no. B12402, p. 1–16.

Taylor, M., and Yin, a., 2009, Active structures of the Himalayan-Tibetan orogen and their relationships to earthquake distribution, contemporary strain field, and Cenozoic volcanism: Geosphere, v. 5, no. 3, p. 199–214, doi: 10.1130/GES00217.1.

Taylor, M., Yin, A., Ryerson, F.J., Kapp, P., and Ding, L., 2003, Conjugate strike-slip faulting along the Bangong-Nujiang suture zone accommodates coeval east-west extension and north-south shortening in the interior of the Tibetan Plateau: Tectonics, v. 22, no. 4, p.

1–18, doi: 10.1029/2002TC001361.

Thiede, R.C., Arrowsmith, J.R., Bookhagen, B., McWilliams, M., Sobel, E.R., and Strecker, M.R., 2006, Dome formation and extension in the Tethyan Himalaya, Leo Pargil, northwest India: Geological Society of America Bulletin, v. 118, no. 5-6, p. 635–650, doi: 10.1130/B25872.1.

Volkmer, J.E., Kapp, P., Guynn, J.H., and Lai, Q., 2007, Cretaceous-Tertiary structural evolution of the north central Lhasa terrane, Tibet: Tectonics, v. 26, no. 6, p. 1–18, doi: 10.1029/2005TC001832.

Wang, H., and Wright, T.J., 2012, Satellite geodetic imaging reveals internal deformation of western Tibet: Geophysical Research Letters, v. 39, no. 7, p. 1–5, doi: 10.1029/2012GL051222.

Wright, T.J., Parsons, B., England, P.C., and Fielding, E.J., 2004, InSAR observations of low slip rates on the major faults of western Tibet.: Science, v. 305, no. 5681, p. 236–239, doi: 10.1126/science.1096388.

Yin, A., and Taylor, M.H., 2011, Mechanics of V-shaped conjugate strike-slip faults and the corresponding continuum mode of continental deformation: Geological Society of America Bulletin, v. 123, no. 9-10, p. 1798–1821, doi: 10.1130/B30159.1.

Zhang, P.-Z., Shen, Z., Wang, M., Gan, W., Bürgmann, R., Molnar, P., Wang, Q., Niu, Z., Sun, J., Wu, J., Hanrong, S., and Xinzhao, Y., 2004, Continuous deformation of the Tibetan Plateau from global positioning system data: Geology, v. 32, no. 9, p. 809–812, doi: 10.1130/G20554.1.

Looking south at the western Surla Range and Palung Co, with the Gangdese range behind the storms.

Appendices

Appendix 1: Chapter 4 Pecube Input Files

cctr_thermo_data.txt

```
8
 83.48569    30.96490     5979   -9999 -9999 -9999 -9999 7.33  0.60   -9999 -9999
-9999 -9999 -9999 -9999 -9999 -9999 -9999 -9999 -1 -1 -1 -1 -1 -1 -1 -1 -1 -1
-1 -1 -1 -1 -1 -1 -1 -1 -1 -1 -1 -1 -1 -1 -1 -1 -1 -1 -1 -1 -1 -1

 83.47744    30.97590     5848   -9999 -9999 -9999 -9999 7.16  0.24   -9999 -9999
-9999 -9999 -9999 -9999 -9999 -9999 -9999 -9999 -1 -1 -1 -1 -1 -1 -1 -1 -1 -1
-1 -1 -1 -1 -1 -1 -1 -1 -1 -1 -1 -1 -1 -1 -1 -1 -1 -1 -1 -1 -1 -1

 83.48333    30.95814     5826   -9999 -9999 -9999 -9999 7.25  0.39   -9999 -9999
-9999 -9999 -9999 -9999 -9999 -9999 -9999 -9999 -1 -1 -1 -1 -1 -1 -1 -1 -1 -1
-1 -1 -1 -1 -1 -1 -1 -1 -1 -1 -1 -1 -1 -1 -1 -1 -1 -1 -1 -1 -1 -1

 83.46420    30.97082     5719   -9999 -9999 -9999 -9999 6.27  0.88   -9999 -9999
-9999 -9999 -9999 -9999 -9999 -9999 -9999 -9999 -1 -1 -1 -1 -1 -1 -1 -1 -1 -1
-1 -1 -1 -1 -1 -1 -1 -1 -1 -1 -1 -1 -1 -1 -1 -1 -1 -1 -1 -1 -1 -1

 83.45555    30.97127     5633   -9999 -9999 -9999 -9999 5.99  0.17   -9999 -9999
-9999 -9999 -9999 -9999 -9999 -9999 -9999 -9999 -1 -1 -1 -1 -1 -1 -1 -1 -1 -1
-1 -1 -1 -1 -1 -1 -1 -1 -1 -1 -1 -1 -1 -1 -1 -1 -1 -1 -1 -1 -1 -1

 83.43724    30.96502     5622   -9999 -9999 -9999 -9999 5.28  0.09   -9999 -9999
-9999 -9999 -9999 -9999 -9999 -9999 -9999 -9999 -1 -1 -1 -1 -1 -1 -1 -1 -1 -1
-1 -1 -1 -1 -1 -1 -1 -1 -1 -1 -1 -1 -1 -1 -1 -1 -1 -1 -1 -1 -1 -1

 83.43554    30.96790     5490   -9999 -9999 -9999 -9999 5.33  0.33   -9999 -9999
-9999 -9999 -9999 -9999 -9999 -9999 -9999 -9999 -1 -1 -1 -1 -1 -1 -1 -1 -1 -1
-1 -1 -1 -1 -1 -1 -1 -1 -1 -1 -1 -1 -1 -1 -1 -1 -1 -1 -1 -1 -1 -1

 83.51246    30.94966     5477   -9999 -9999 -9999 -9999 5.96  0.61   -9999 -9999
-9999 -9999 -9999 -9999 -9999 -9999 -9999 -9999 -1 -1 -1 -1 -1 -1 -1 -1 -1 -1
-1 -1 -1 -1 -1 -1 -1 -1 -1 -1 -1 -1 -1 -1 -1 -1 -1 -1 -1 -1 -1 -1
```

fault_parameters_cctrN.picloud

```
$ number of faults active at any time during the run
$1
2


$ fault 1
$ two points (in longitude-latitude) defining the y axis of the
$ coordinate system used to define the faults
$ the x-axis is to the right of the y-axis
83.42 31.08 83.385 30.90



$
$ number of points defining fault
2
$2

$ segment (x,y) coordinates
-5. 10.4
20. -15.4

$ number of time intervals to define its motion story
2


$ time interval (in geological time) and velocity
$ thrust is negative, normal is positive
13. 6. 0.5
6. 0. 1.


$$$$$$$$$$$$$$$$$$$$$$$$$$$$$$$$$$$$$$$$$$$$$$$$$$$$$$$$$$$$$$$$


$fault 2
$2
$ two points (in longitude-latitude) defining the y axis of the
$ coordinate system used to define the faults
$ the x-axis is to the right of the y-axis
$0.001 0.5 0. 0.5
$20. 0. 20.  0.

$
$ number of points defining fault
$
2

$ segment (x,y) coordinates
-13. 6.5
$0. 20
-35.5 -15.6
$-55. -35.

$ number of time intervals to define its motion story
2

$ time interval (in geological time) and velocity
$ thrust is negative, normal is positive
12. 6. 2.
6. 0. 0.5
```

topo_parameters.txt.cctrN_picloud

```
$ this is the input file for Pecube
$ you can add as many comment lines as you wish as long as they start with a
dollar sign
$
$ (1) the name of the run (also the name of the folder in which the solution
is stored)
$ should be 5 letter long
cctrN

$ (2) the name of the topography file used (if the name is Nil topo is assume
to be flat)
$      Otherwise the file should contain nx by ny points (see below) defining the
topography in meters
$      Note that the evolution of this topography (in amplitude and offset)
will be allowed to
$      change through time
$      If the name of the file ends with a slash "/", then Pecube will assume it
is a directory
$      in which a series of topo files (in meters) are to be stored (one per
time step), named topo0, topo1, etc
$      Pecube will also expect to find uplift rate files, named uplift0, uplift1,
etc in which an
$      uplift rate value (in km/Myr) will be stored for each location; similary
a set of surface
$      temperature files will be expected, named temp0, temp1, etc in °C
$      When this second option is activated, the topography amplification and
offset factors are not used
$      if the number of points in the longitude and latitude directions (next
input line)  are negative, the number of points in the
$      longitude direction (nx) will in fact correspond to the total number of
points; the points defining
$      the topography will be assumed to be randomly distributed (not on a
rectangular grid);
$      the number of points in the latitude direction (ny) will contain the
number of triangles connecting
$      the randomly distributed points.
$      the topography file should then contain nx triplets of longitude, lati-
tude and height of each point
$      followed by ny triplets of integer numbers between 1 and nx giving the
triangular connectivity
cctr_dem.dat

$ (3) the number of points in the longitude and latitude directions, respec-
tively
$      if they are negative, they correspond to the total number of points and
the number of triangles connecting them
1183 47

$ (4) the spacing in degrees of longitude and latitude, respectively
$      This is not used in case nx and ny are negative (random grid)
0.00083 0.00083

$ (5) a skipping factor (1 means all points of the topography are used; 2
means that
$      every second point is used etc). Note that nx, ny AND nskip define the
resolution of the
$      finite element grid in the horizontal directions
$      again this is not used in case nx and ny are negative (random grid)
10

$ (6) the longitude and latitude of the bottom left corner of the topo file
82.981666666667 30.946250096847
```

```
$ (7) the number of time steps in the tectonomorphic scenario
1

$ (8) the erosional time scale (exponential decay rate of topography)
0.

$ (9) for each time step +1:
$ (a) a starting time (in Myr in the past)
$ (b) an amplification factor for the topography
$ (c) an offset factor (in km),
$ (d) an output flag (for this time step: 0=no output / 1=output)
20. 1. 0. 1
$3.5 1. 0. 1
0. 1. 0. 1

$ (10) a flag for isostasy (1 isostasy on; 0 isostast off)
$ crustal density (in kg/m3), mantle density (kg/m3), Young modulus (in Pa),
poisson's
$ ratio, elastic plate thickness (in km), size of the FFT grid for elastic re-
bound
$ calculations (typically 1024 1024 but must be a power of 2)
0, 2700.,3200.,1.d11,0.25,28.8,1024,1024

$ (11) the model thickness (in km), number of points in the z direction, ther-
mal diffusivity in km2/Myr,
$ temperature at the base of the model (in C), temperature at z=0 (in C), at-
mospheric lapse rate (in
$ C/km), heat production in C/My
80.,25,25.,1200.,0.,0.,20.


$ (12) name of the file containing the thermochronological data
$ if Nil no date
$ otherwise it should contain the number of data points (locations)
$ for each location a line containing sample longitude, latitude, elevation
$ as well as Apatite He age, error in age, Apatite FT age, error in age
$ with a negative age corresponding to a non-existing age
cctr_thermo_data.txt


$ (13) the default age (in Myr) for rocks that never reach the closure tem-
perature, a flag to decide which
$ apatite FT routine to use (0 = van der Beek or 1 = Ketcham), a flag to decide
whether (flag=0) to use the absolute
$ age difference (between observed and predicted ages) to construct the misfit
function or (flag=1) the difference in
$ the slope of the age-elevation relationship (for each system), a flag to de-
cide whether (flag=0) the faults'geometry
$ is updated due to the movement on other faults or (flag=1) not, a friction
coefficient to use in the formula for shear heating
$ (friction=0 means no shear heating)
30. 0 0 0 0.

$ (14) a series of 9 flags to determine which age (system) has to be computed
from the thermal histories
$ computed in Pecube
0 1 0 0 0 0 0 0 0
$0 0 0 0 0 0 0 0 0
```

NMT_thermo_data.txt

```
7
 83.40467    31.07366     5381   -9999 -9999 -9999 -9999 3.48  0.24   -9999 -9999
-9999 -9999 -9999 -9999 -9999 -9999 -9999 -9999 -1 -1 -1 -1 -1 -1 -1 -1 -1 -1
-1 -1 -1 -1 -1 -1 -1 -1 -1 -1 -1 -1 -1 -1 -1 -1 -1 -1 -1 -1 -1 -1 -1 -1

 83.40848    31.06458     5416   -9999 -9999 -9999 -9999 3.43  0.24   -9999 -9999
-9999 -9999 -9999 -9999 -9999 -9999 -9999 -9999 -1 -1 -1 -1 -1 -1 -1 -1 -1 -1
-1 -1 -1 -1 -1 -1 -1 -1 -1 -1 -1 -1 -1 -1 -1 -1 -1 -1 -1 -1 -1 -1 -1 -1

 83.41171    31.06495     5538   -9999 -9999 -9999 -9999 3.66  0.70   -9999 -9999
-9999 -9999 -9999 -9999 -9999 -9999 -9999 -9999 -1 -1 -1 -1 -1 -1 -1 -1 -1 -1
-1 -1 -1 -1 -1 -1 -1 -1 -1 -1 -1 -1 -1 -1 -1 -1 -1 -1 -1 -1 -1 -1 -1 -1

 83.43498    31.06623     5609   -9999 -9999 -9999 -9999 4.40  0.41   -9999 -9999
-9999 -9999 -9999 -9999 -9999 -9999 -9999 -9999 -1 -1 -1 -1 -1 -1 -1 -1 -1 -1
-1 -1 -1 -1 -1 -1 -1 -1 -1 -1 -1 -1 -1 -1 -1 -1 -1 -1 -1 -1 -1 -1 -1 -1

 83.4545     31.07644     5628   -9999 -9999 -9999 -9999 4.87  0.57   -9999 -9999
-9999 -9999 -9999 -9999 -9999 -9999 -9999 -9999 -1 -1 -1 -1 -1 -1 -1 -1 -1 -1
-1 -1 -1 -1 -1 -1 -1 -1 -1 -1 -1 -1 -1 -1 -1 -1 -1 -1 -1 -1 -1 -1 -1 -1

 83.54151    31.05958     5823   -9999 -9999 -9999 -9999 7.29  0.63   -9999 -9999
-9999 -9999 -9999 -9999 -9999 -9999 -9999 -9999 -1 -1 -1 -1 -1 -1 -1 -1 -1 -1
-1 -1 -1 -1 -1 -1 -1 -1 -1 -1 -1 -1 -1 -1 -1 -1 -1 -1 -1 -1 -1 -1 -1 -1

 83.5342     31.08004     6063   -9999 -9999 -9999 -9999 6.32  0.23   -9999 -9999
-9999 -9999 -9999 -9999 -9999 -9999 -9999 -9999 -1 -1 -1 -1 -1 -1 -1 -1 -1 -1
-1 -1 -1 -1 -1 -1 -1 -1 -1 -1 -1 -1 -1 -1 -1 -1 -1 -1 -1 -1 -1 -1 -1 -1
```

fault_parameters.nmt.pecube

```
$ number of faults active at any time during the run
2

$ fault 1
$ two points (in longitude-latitude) defining the y axis of the
$ coordinate system used to define the faults
$ the x-axis is to the right of the y-axis

$0. 0.8 0.002 0.8
83.39 31.083 83.39 31.035

$ number of points defining fault
7


$ segment (x,y) coordinates


-10 8.3
-8. 8.
-5. 7.5
0. 5.4
10. 1.
15. -4.
30. -20.



$ number of time intervals to define its motion story
2


$ time interval (in geological time) and velocity
$ thrust is negative, normal is positive
8.8 4.0 1.5
4.0 0. 3.0


$$$$$$$$$$$$$$$$$$$$$$$$$$$$$$$$$$$$$$$$$$$$$$$$$$$$$$$$$$$$$$$$$$

$fault 2

$ number of points defining fault
2

$ segment (x,y) coordinates
-17.5 6.5
-40. -20.


$ number of time intervals to define its motion story

1

$ time interval (in geological time) and velocity
$ thrust is negative, normal is positive
12. 0. 0.5
```

topo_parameters.txt.nmt

```
$ this is the input file for Pecube
$ you can add as many comment lines as you wish as long as they start with a
dollar sign
$
$ (1) the name of the run (also the name of the folder in which the solution
is stored)
$ should be 5 letter long
nmtN5

$ (2) the name of the topography file used (if the name is Nil topo is assume
to be flat)
$     Otherwise the file should contain nx by ny points (see below) defining the
topography in meters
$     Note that the evolution of this topography (in amplitude and offset)
will be allowed to
$     change through time
$     If the name of the file ends with a slash "/", then Pecube will assume it
is a directory
$     in which a series of topo files (in meters) are to be stored (one per
time step), named topo0, topo1, etc
$     Pecube will also expect to find uplift rate files, named uplift0, uplift1,
etc in which an
$     uplift rate value (in km/Myr) will be stored for each location; similary
a set of surface
$     temperature files will be expected, named temp0, temp1, etc in °C
$     When this second option is activated, the topography amplification and
offset factors are not used
$     if the number of points in the longitude and latitude directions (next
input line)  are negative, the number of points in the
$     longitude direction (nx) will in fact correspond to the total number of
points; the points defining
$     the topography will be assumed to be randomly distributed (not on a
rectangular grid);
$     the number of points in the latitude direction (ny) will contain the
number of triangles connecting
$     the randomly distributed points.
$     the topography file should then contain nx triplets of longitude, lati-
tude and height of each point
$     followed by ny triplets of integer numbers between 1 and nx giving the
triangular connectivity
NMT_dem.dat

$ (3) the number of points in the longitude and latitude directions, respec-
tively
$     if they are negative, they correspond to the total number of points and
the number of triangles connecting them
1239 55

$ (4) the spacing in degrees of longitude and latitude, respectively
$     This is not used in case nx and ny are negative (random grid)
0.00083 0.00083

$ (5) a skipping factor (1 means all points of the topography are used; 2
means that
$     every second point is used etc). Note that nx, ny AND nskip define the
resolution of the
$     finite element grid in the horizontal directions
$     again this is not used in case nx and ny are negative (random grid)
10

$ (6) the longitude and latitude of the bottom left corner of the topo file
82.845 31.037916763514
```

```
$ (7) the number of time steps in the tectonomorphic scenario
1

$ (8) the erosional time scale (exponential decay rate of topography)
0.

$ (9) for each time step +1:
$ (a) a starting time (in Myr in the past)
$ (b) an amplification factor for the topography
$ (c) an offset factor (in km),
$ (d) an output flag (for this time step: 0=no output / 1=output)
20. 1. 0. 1
$3.5 1. 0. 1
0. 1. 0. 1

$ (10) a flag for isostasy (1 isostasy on; 0 isostast off)
$ crustal density (in kg/m3), mantle density (kg/m3), Young modulus (in Pa),
poisson's
$ ratio, elastic plate thickness (in km), size of the FFT grid for elastic re-
bound
$ calculations (typically 1024 1024 but must be a power of 2)
0, 2700.,3200.,1.d11,0.25,28.8,1024,1024

$ (11) the model thickness (in km), number of points in the z direction, ther-
mal diffusivity in km2/Myr,
$ temperature at the base of the model (in C), temperature at z=0 (in C), at-
mospheric lapse rate (in
$ C/km), heat production in C/My
80.,25,25.,1200.,0.,0.,20.

$ (12) name of the file containing the thermochronological data
$ if Nil no date
$ otherwise it should contain the number of data points (locations)
$ for each location a line containing sample longitude, latitude, elevation
$ as well as Apatite He age, error in age, Apatite FT age, error in age
$ with a negative age corresponding to a non-existing age
NMT_thermo_data.txt

$ (13) the default age (in Myr) for rocks that never reach the closure tem-
perature, a flag to decide which
$ apatite FT routine to use (0 = van der Beek or 1 = Ketcham), a flag to decide
whether (flag=0) to use the absolute
$ age difference (between observed and predicted ages) to construct the misfit
function or (flag=1) the difference in
$ the slope of the age-elevation relationship (for each system), a flag to de-
cide whether (flag=0) the faults'geometry
$ is updated due to the movement on other faults or (flag=1) not, a friction
coefficient to use in the formula for shear heating
$ (friction=0 means no shear heating)
30. 0 0 0 0.

$ (14) a series of 9 flags to determine which age (system) has to be computed
from the thermal histories
$ computed in Pecube
0 1 0 0 0 0 0 0 0
$0 0 0 0 0 0 0 0 0
```

Appendix 2: Chapter 4 Python files

calculate_weighted_means.py

```python
# -*- coding: utf-8 -*-
"""
Created on Mon Aug 13 09:43:45 2012
@author: Richard
"""

import numpy as nmp
import sys
sys.path.append('C://itchy//code_repos//geochron_stats')
import geochron_stats as gc


sftr_02_age = nmp.array([66.7, 65.68, 63.6, 62.9, 62.37, 62.5, 60.9, 62.4,

                        64.17, 62.3, 61.8, 64.7, 62.3, 62.3, 62.8, 63.0,
60.0,

                        61.8, 64.6])

sftr_02_err_2sd = nmp.array([1.2, 0.92, 1.4, 1.2, 0.94, 1.7, 1.2, 1.3, 0.91,

                            1.2, 1.2, 1.4, 1.2, 1.6, 1.1, 1.3, 1.1, 1.3, 1.1
])

sftr_02_err_sd = sftr_02_err_2sd / 2.

sftr_02_wm = gc.weighted_mean(sftr_02_age, sftr_02_err_sd)

sftr_02_mswd = gc.MSWD(sftr_02_age, sftr_02_err_sd, sftr_02_wm)

sftr_02_var = gc.weighted_variance(sftr_02_age, sftr_02_err_sd, sftr_02_wm)

sftr_02_1sd = gc.standard_error(sftr_02_var, len(sftr_02_age))

print 'SFTR 02 weighted mean=', sftr_02_wm, '+/-', sftr_02_1sd * 2, 'Ma'

print 'SFTR 02 MSWD =', sftr_02_mswd


nmt_02_age = nmp.array([21.3, 20.3, 20.2, 19.65, 16.98, 16.79, 16.31, 16.07,
                        16.02, 15.8, 15.7, 15.64, 15.38, 14.51, 14.49])

nmt_02_err_2sd = nmp.array([0.72, 2.2, 1.6, 0.8, 0.4, 0.3, 0.93, 0.35, 0.78,
                            0.65, 1.4, 0.3, 0.4, 0.36, 0.76])

nmt_02_err_sd = nmt_02_err_2sd / 2.

nmt_02_wm = gc.weighted_mean(nmt_02_age, nmt_02_err_sd)

nmt_02_mswd = gc.MSWD(nmt_02_age, nmt_02_err_sd, nmt_02_wm)

nmt_02_var = gc.weighted_variance(nmt_02_age, nmt_02_err_sd, nmt_02_wm)

nmt_02_1sd = gc.standard_error(nmt_02_var, len(nmt_02_age))

print 'NMT 02 weighted mean=', nmt_02_wm, '+/-', nmt_02_1sd * 2, 'Ma'

print 'NMT 02 MSWD =', nmt_02_mswd

nmt_02_old_age = nmt_02_age[0:3]

nmt_02_old_err_sd = nmt_02_err_sd[0:3]
```

226

```
nmt_02_old_wm = gc.weighted_mean(nmt_02_old_age, nmt_02_old_err_sd)

nmt_02_old_mswd = gc.MSWD(nmt_02_old_age, nmt_02_old_err_sd, nmt_02_old_wm)

nmt_02_old_var = gc.weighted_variance(nmt_02_old_age, nmt_02_old_err_sd,
                                      nmt_02_old_wm)

nmt_02_old_1sd = gc.standard_error(nmt_02_old_var, len(nmt_02_old_age))

print 'NMT 02 old weighted mean=', nmt_02_old_wm, '+/-', nmt_02_old_1sd * 2,
'Ma'

print 'NMT 02 old MSWD =', nmt_02_old_mswd

nmt_02_young_age = nmt_02_age[4:14]

nmt_02_young_err_sd = nmt_02_err_sd[4:14]

nmt_02_young_wm = gc.weighted_mean(nmt_02_young_age, nmt_02_young_err_sd)

nmt_02_young_mswd = gc.MSWD(nmt_02_young_age, nmt_02_young_err_sd,
                           nmt_02_young_wm)

nmt_02_young_var = gc.weighted_variance(nmt_02_young_age, nmt_02_young_err_sd,
                                        nmt_02_young_wm)

nmt_02_young_1sd = gc.standard_error(nmt_02_young_var, len(nmt_02_young_age))

print 'NMT 02 young weighted mean=', nmt_02_young_wm, '+/-', nmt_02_young_1sd
* 2, 'Ma'

print 'NMT 02 young MSWD =', nmt_02_young_mswd
```

geochron_stats.py

```python
# -*- coding: utf-8 -*-
"""
Created on Mon Aug 13 11:17:38 2012

@author: Richard
"""

import numpy as nmp

def weighted_mean(age_array, sd_array):
    sample_variance = sd_array ** 2

    w_mean_numerator = nmp.sum(age_array / sample_variance)

    w_mean_denominator = nmp.sum( 1 / sample_variance)

    weighted_mean = w_mean_numerator / w_mean_denominator

    return weighted_mean


def MSWD(age_array, sd_array, weighted_mean):
    sample_variance = sd_array **2
    x_bar = weighted_mean
    x = age_array
    w = 1/sample_variance
    w = w / nmp.sum(w)

    #term_1 = nmp.sum(w) / ( (nmp.sum(w))**2 - nmp.sum(w**2)  )
    term_1 = 1. / (len(w) - 1)
    term_2 = nmp.sum( (w * (x - x_bar)**2) / sample_variance )

    MSWD = term_1 * term_2

    return MSWD


def weighted_variance(age_array, sd_array, weighted_mean):
    sample_variance = sd_array **2
    x_bar = weighted_mean
    x = age_array
    w = 1/sample_variance
    w = w / nmp.sum(w)

    term_1 = nmp.sum(w) / ( (nmp.sum(w))**2 - nmp.sum(w**2)  )
    term_2 = nmp.sum(w * (x - x_bar)**2 )

    weighted_variance = term_1 * term_2

    return weighted_variance


def standard_error(weighted_variance, num_obs):
    standard_error = nmp.sqrt(weighted_variance) / nmp.sqrt(num_obs)

    return standard_error
```

228

cctr_filter_stdev.py

```
# -*- coding: utf-8 -*-
"""
Created on Fri Jan 27 08:53:34 2012

@author: Richard
"""

import numpy as nmp
import matplotlib.pyplot as plt

# observed values

# cooling age
sle_sctr_07_obs = 7.330

slw_cctr_07_obs = 7.160

sle_sctr_06_obs = 7.250

slw_cctr_06_obs = 6.270

slw_cctr_05_obs = 5.990

slw_cctr_03_obs = 5.330

slw_cctr_04_obs = 5.330

sle_sctr_05_obs = 5.960

# combine these
cctr_obs_age = nmp.array([sle_sctr_07_obs, slw_cctr_07_obs, sle_sctr_06_obs,
    slw_cctr_06_obs, slw_cctr_05_obs, slw_cctr_03_obs, slw_cctr_04_obs,
    sle_sctr_05_obs])

cctr_obs_age_lon = nmp.array([slw_cctr_04_obs, slw_cctr_03_obs, slw_cctr_05_
obs,
                               slw_cctr_06_obs, slw_cctr_07_obs, sle_sctr_06_
obs,
                               sle_sctr_07_obs, sle_sctr_05_obs])

# make max and min arrays at specified standard deviation
cctr_err_sd = nmp.array([0.6, 0.29, 0.39, 0.88, 0.17, 0.63, 0.33, 0.61])

#cctr_err = cctr_obs_age * 0.04 + cctr_err_sd

# larger of 1 sd or 8% analytical uncertainty
cctr_err = nmp.array([0.60, 0.57, 0.58, 0.88, 0.48, 0.80, 0.43, 0.61])

cctr_err_lon = nmp.array([0.43, 0.80, 0.48, 0.88, 0.57, 0.58, 0.60, 0.61])

#cctr_obs_age_err =

cctr_lo_1sd = cctr_obs_age - cctr_err

cctr_hi_1sd = cctr_obs_age + cctr_err

cctr_lo_2sd = cctr_obs_age - 2 * cctr_err

cctr_hi_2sd = cctr_obs_age + 2 * cctr_err


cctr_elev_obs = nmp.array([5979, 5848, 5826, 5719, 5633, 5622, 5490, 5477])
```

229

```python
cctr_elev_calc = nmp.array([5965, 5996, 5898, 5746, 5759, 5614, 5638, 5618])

cctr_lon = nmp.array([83.4355, 83.4372, 83.4556, 83.4642, 83.4744, 83.4833,
83.4857, 83.5125])

#######################

# load data

cctr_all_runs = nmp.loadtxt('cctr_all_runs.csv', delimiter=',')




#########################

# filter data


cctr_fits_1sd = nmp.zeros([20]) # create empty array to add to
cctr_fits_2sd = nmp.zeros([20]) # create empty array to add to


# Fits to data at 1 standard deviation

# loop to filter each calculated age with the observed age
for i in range(cctr_all_runs.shape[0]):
    if cctr_lo_1sd[0] <= cctr_all_runs[i,0] <= cctr_hi_1sd[0]\
    and cctr_lo_1sd[1] <= cctr_all_runs[i,1] <= cctr_hi_1sd[1]\
    and cctr_lo_1sd[2] <= cctr_all_runs[i,2] <= cctr_hi_1sd[2]\
    and cctr_lo_1sd[3] <= cctr_all_runs[i,3] <= cctr_hi_1sd[3]\
    and cctr_lo_1sd[4] <= cctr_all_runs[i,4] <= cctr_hi_1sd[4]\
    and cctr_lo_1sd[5] <= cctr_all_runs[i,5] <= cctr_hi_1sd[5]\
    and cctr_lo_1sd[6] <= cctr_all_runs[i,6] <= cctr_hi_1sd[6]\
    and cctr_lo_1sd[7] <= cctr_all_runs[i,7] <= cctr_hi_1sd[7]:
        cctr_fits_1sd = nmp.vstack((cctr_fits_1sd, cctr_all_runs[i,:]))

if cctr_fits_1sd.size > 20:
    cctr_fits_1sd = cctr_fits_1sd[1:,:] #remove first line (all zeros)


# if we want to save
#nmp.save('C:\\school\\tibet\\lunggar\\thermo\\pecube\\cctr_picloud_results\\
cctr_1sd_fits.npy', cctr_fits_1sd)

# name individual variables
    sle_sctr_07_1sd = cctr_fits_1sd[:,0]

    slw_cctr_07_1sd = cctr_fits_1sd[:,1]

    slw_cctr_06_1sd = cctr_fits_1sd[:,2]

    sle_sctr_06_1sd = cctr_fits_1sd[:,3]

    slw_cctr_05_1sd = cctr_fits_1sd[:,4]

    slw_cctr_03_1sd = cctr_fits_1sd[:,5]

    slw_cctr_04_1sd = cctr_fits_1sd[:,6]

    sle_sctr_05_1sd = cctr_fits_1sd[:,7]
```

230

```
    initA_1sd = cctr_fits_1sd[:,8]

    accel_1sd = cctr_fits_1sd[:,9]

    srA1_1sd = cctr_fits_1sd[:,10]

    srA2_1sd = cctr_fits_1sd[:,11]

    initB_1sd = cctr_fits_1sd[:,12]

    srB1_1sd = cctr_fits_1sd[:,13]

    srB2_1sd = cctr_fits_1sd[:,14]

    chi_sq_1sd = cctr_fits_1sd[:,15]

    net_ext_1sd = cctr_fits_1sd[:,16]

    exhumA_1sd = cctr_fits_1sd[:,17]

    exhumB_1sd = cctr_fits_1sd[:,18]

    tilt_1sd = cctr_fits_1sd[:,19]


    cctr_ages_1sd = nmp.transpose(cctr_fits_1sd[:,:8])
# Fits to data at 2 standard deviation

# loop to filter each calculated age with the observed age
for i in range(cctr_all_runs.shape[0]):
    if cctr_lo_2sd[0] <= cctr_all_runs[i,0] <= cctr_hi_2sd[0]\
    and cctr_lo_2sd[1] <= cctr_all_runs[i,1] <= cctr_hi_2sd[1]\
    and cctr_lo_2sd[2] <= cctr_all_runs[i,2] <= cctr_hi_2sd[2]\
    and cctr_lo_2sd[3] <= cctr_all_runs[i,3] <= cctr_hi_2sd[3]\
    and cctr_lo_2sd[4] <= cctr_all_runs[i,4] <= cctr_hi_2sd[4]\
    and cctr_lo_2sd[5] <= cctr_all_runs[i,5] <= cctr_hi_2sd[5]\
    and cctr_lo_2sd[6] <= cctr_all_runs[i,6] <= cctr_hi_2sd[6]\
    and cctr_lo_2sd[7] <= cctr_all_runs[i,7] <= cctr_hi_2sd[7]:
        cctr_fits_2sd = nmp.vstack((cctr_fits_2sd, cctr_all_runs[i,:]))
        #print cctr_all_runs[i,:]

cctr_fits_2sd = cctr_fits_2sd[1:,:]

# if we want to save
#nmp.save('C:\\school\\tibet\\lunggar\\thermo\\pecube\\cctr_picloud_results\\
cctr_1sd_fits.npy', cctr_fits_2sd)

# name individual variables
sle_sctr_07_2sd = cctr_fits_2sd[:,0]

slw_cctr_07_2sd = cctr_fits_2sd[:,1]

slw_cctr_06_2sd = cctr_fits_2sd[:,2]

sle_sctr_06_2sd = cctr_fits_2sd[:,3]

slw_cctr_05_2sd = cctr_fits_2sd[:,4]

slw_cctr_03_2sd = cctr_fits_2sd[:,5]

slw_cctr_04_2sd = cctr_fits_2sd[:,6]

sle_sctr_05_2sd = cctr_fits_2sd[:,7]
```

```
initA_2sd = cctr_fits_2sd[:,8]

accel_2sd = cctr_fits_2sd[:,9]

srA1_2sd = cctr_fits_2sd[:,10]

srA2_2sd = cctr_fits_2sd[:,11]

initB_2sd = cctr_fits_2sd[:,12]

srB1_2sd = cctr_fits_2sd[:,13]

srB2_2sd = cctr_fits_2sd[:,14]

chi_sq_2sd = cctr_fits_2sd[:,15]

net_ext_2sd = cctr_fits_2sd[:,16]

exhumA_2sd = cctr_fits_2sd[:,17]

exhumB_2sd = cctr_fits_2sd[:,18]

tilt_2sd = cctr_fits_2sd[:,19]


cctr_ages_2sd = nmp.transpose(cctr_fits_2sd[:,:8])

cctr_ages_2sd_lon = nmp.array([slw_cctr_04_2sd, slw_cctr_03_2sd, slw_
cctr_05_2sd,
                               slw_cctr_06_2sd, slw_cctr_07_2sd, sle_
sctr_06_2sd,
                               sle_sctr_07_2sd, sle_sctr_05_2sd])

#cctr_ages_2sd_lon = nmp.transpose(cctr_ages_2sd_lon)


#########################################################################
##
# slip rate through time calculations

# 1 standard deviation
times = 41

time_vector = nmp.linspace(0, 20, num=times)

if cctr_fits_1sd.size > 20:
    n_1sd = len(tilt_1sd)

    A_er_w_time_1sd = nmp.zeros((n_1sd, times))

    B_er_w_time_1sd = nmp.zeros((n_1sd, times))

    A_dip = 0.88

    B_dip = 0.88

    erA1_1sd = srA1_1sd * nmp.cos(A_dip)

    erA2_1sd = srA2_1sd * nmp.cos(A_dip)

    erB1_1sd = srB1_1sd * nmp.cos(B_dip)

    erB2_1sd = srB2_1sd * nmp.cos(B_dip)
```

```python
    for i in range(n_1sd):
        A_er_w_time_1sd[i, 0 : ((accel_1sd[i] * 2))] = erA2_1sd[i]

        A_er_w_time_1sd[i, (accel_1sd[i] * 2): (initA_1sd[i] * 2 -1)] =
erA1_1sd[i]

        B_er_w_time_1sd[i, 0 : ((accel_1sd[i] * 2))] = erB2_1sd[i]

        B_er_w_time_1sd[i, (accel_1sd[i] * 2): (initB_1sd[i] * 2 -1)] =
erB1_1sd[i]

    er_w_time_1sd = A_er_w_time_1sd + B_er_w_time_1sd

    net_ext_w_time_1sd = nmp.cumsum(er_w_time_1sd, axis=1)/1.85 # fix this hack
(?)

    cum_vector_1sd = net_ext_w_time_1sd[:,-1]

    cum_ext_w_time_1sd = nmp.zeros(nmp.shape(er_w_time_1sd))

    er_w_time_trans_1sd = nmp.transpose(er_w_time_1sd)

    for i in range(n_1sd):
        cum_ext_w_time_1sd[i,:] = cum_vector_1sd[i] - net_ext_w_time_1sd[i,:]

    cum_ext_w_time_trans_1sd = nmp.transpose(cum_ext_w_time_1sd)


###############

# 2 standard deviation

n_2sd = len(tilt_2sd)

A_er_w_time_2sd = nmp.zeros((n_2sd, times))

B_er_w_time_2sd = nmp.zeros((n_2sd, times))

A_dip = 0.88

B_dip = 0.88

erA1_2sd = srA1_2sd * nmp.cos(A_dip)

erA2_2sd = srA2_2sd * nmp.cos(A_dip)

erB1_2sd = srB1_2sd * nmp.cos(B_dip)

erB2_2sd = srB2_2sd * nmp.cos(B_dip)

for i in range(n_2sd):
        A_er_w_time_2sd[i, 0 : ((accel_2sd[i] * 2))] = erA2_2sd[i]

        A_er_w_time_2sd[i, (accel_2sd[i] * 2): (initA_2sd[i] * 2 -1)] =
erA1_2sd[i]

        B_er_w_time_2sd[i, 0 : ((accel_2sd[i] * 2))] = erB2_2sd[i]

        B_er_w_time_2sd[i, (accel_2sd[i] * 2): (initB_2sd[i] * 2 -1)] =
erB1_2sd[i]

er_w_time_2sd = A_er_w_time_2sd + B_er_w_time_2sd

net_ext_w_time_2sd = nmp.cumsum(er_w_time_2sd, axis=1)/1.85 # fix this hack (?)
```

```python
cum_vector_2sd = net_ext_w_time_2sd[:,-1]

cum_ext_w_time_2sd = nmp.zeros(nmp.shape(er_w_time_2sd))

er_w_time_trans_2sd = nmp.transpose(er_w_time_2sd)

for i in range(n_2sd):
    cum_ext_w_time_2sd[i,:] = cum_vector_2sd[i] - net_ext_w_time_2sd[i,:]

cum_ext_w_time_trans_2sd = nmp.transpose(cum_ext_w_time_2sd)

er1_2sd = erA1_2sd + erB1_2sd
er2_2sd = erA2_2sd + erB2_2sd

er1_2sd_median = nmp.median(er1_2sd)
er2_2sd_median = nmp.median(er2_2sd)

net_ext_2sd_median = nmp.median(net_ext_2sd)

initA_2sd_median = nmp.median(initA_2sd)
initB_2sd_median = nmp.median(initB_2sd)


print 'done with analysis'

################################################################################
###

plot_format = 'print'  # ppt or print

# slip rate and cumulative extension plots
if plot_format == 'ppt':
    fc1 = 'w'
    fc2 = 'r'

    # extension rate with time
    fig1 = plt.figure(1)
    ax1 = fig1.add_subplot(211, axisbg='black')
    ax1.plot(time_vector, er_w_time_trans_2sd, color=fc1, linewidth=0.75)
    ax1.plot(time_vector, er_w_time_trans_1sd, color=fc2, linewidth=1.5)
    #ax1.plot(time_vector, er_w_time_trans[:,0:9], color='blue', linewidth=2)
    plt.gca().invert_xaxis()
    plt.xlabel('Ma', color='white')
    plt.ylabel('extension, mm/yr', color='white')
    plt.title('CCTR extension rate through time', color='white')
    plt.xticks(color = 'white')
    plt.yticks(color = 'white')
    #plt.spine(color='white')


    # cumulative extension with time
    ax2 = fig1.add_subplot(212, axisbg='black')
    ax2.plot(time_vector, cum_ext_w_time_trans_2sd, color=fc1, linewidth=0.75)
    ax2.plot(time_vector, cum_ext_w_time_trans_1sd, color=fc2, linewidth=1.5)
    #ax2.plot(time_vector, cum_ext_w_time_trans[:,0:9], color='blue', lin-
ewidth=2)
    plt.gca().invert_xaxis()
    plt.xlabel('Ma', color='white')
    plt.ylabel('cum. extension, km', color='white')
    plt.title('CCTR cum. extension through time', color='white')
    plt.xticks(color = 'white')
    plt.yticks(color = 'white')

    for ax in [ax1, ax2]:
```

234

```
        for ticks in ax.xaxis.get_ticklines() + ax.yaxis.get_ticklines():
            ticks.set_color('w')
        for pos in ['top', 'bottom', 'left', 'right']:
            ax.spines[pos].set_edgecolor('w')


elif plot_format == 'print': #CHANGE
    fc1 = 'k'
    fc2 = 'r'

    # extension rate with time
    plt.figure(1)
    plt.subplot(121, axisbg='white')
    plt.plot(time_vector, er_w_time_trans_2sd, color=fc1, linewidth=0.5)
#    plt.plot(time_vector, er_w_time_trans_1sd, color=fc2, linewidth=1)
    #plt.plot(time_vector, er_w_time_trans[:,0:9], color='blue', linewidth=2)
    plt.gca().invert_xaxis()
    plt.xlabel('Ma', color='black')
    plt.ylabel('extension, mm/yr', color='black')
    plt.title('CCTR extension rate through time', color='black')

    # cumulative extension with time
    plt.subplot(122, axisbg='white')
    plt.plot(time_vector, cum_ext_w_time_trans_2sd, color=fc1, linewidth=0.5)
#    plt.plot(time_vector, cum_ext_w_time_trans_1sd, color=fc2, linewidth=1)
    #plt.plot(time_vector, cum_ext_w_time_trans[:,0:9], color='blue', lin-
ewidth=1)
    plt.gca().invert_xaxis()
    plt.xlabel('Ma', color='k')
    plt.ylabel('cum. extension, km', color='k')
    plt.title('CCTR cum. extension through time', color='k')


# histograms

if plot_format == 'ppt':
    fc1 = 'grey'
    fc2 = 'w'
    fig2 = plt.figure(2)
    # E fault init
    ax3= fig2.add_subplot(221, axisbg='black')
    bins = [9.5, 10.5, 11.5, 12.5, 13.5, 14.5, 15.5, 16.5, 17.5, 18.5]
    plt.hist(initA_2sd, bins, facecolor=fc1)
    plt.hist(initA_1sd, bins, facecolor=fc2)
    plt.title('E fault initiation vs chi square', color = 'w')
    plt.xlabel('E fault initiation, Ma', color = 'w')
    plt.xticks(color = 'w')
    plt.yticks(color = 'w')

    # E fault accel hist
    ax4 = fig2.add_subplot(222, axisbg='black')
    bins = [2.5, 3.5, 4.5, 5.5, 6.5]
    plt.hist(accel_2sd, bins, facecolor=fc1)
    plt.hist(accel_1sd, bins, facecolor=fc2)
    plt.title('E fault acceleration vs chi square', color = 'w')
    plt.xlabel('E fault acceleration, Ma',color = 'w')
    #plt.ylabel('chi square', color = 'w')
    plt.xticks(color = 'w')
    plt.yticks(color = 'w')

    # PCF initiation hist
    ax5 = fig2.add_subplot(223, axisbg='black')
    bins = [9.5, 10.5, 11.5, 12.5, 13.5, 14.5, 15.5, 16.5, 17.5, 18.5]
    plt.hist(initB_2sd, bins, facecolor=fc1)
    plt.hist(initB_1sd, bins, facecolor=fc2)
```

235

```python
        plt.title('PCF initiation vs chi square', color = 'w')
        plt.xlabel('PCF initiation, Ma', color = 'w')
        #plt.ylabel('chi square', color = 'w')
        plt.xticks(color = 'w')
        plt.yticks(color = 'w')

        # footwall tilt hist
        ax6 = fig2.add_subplot(224, axisbg='black')
        plt.hist(tilt_2sd, facecolor=fc1)
        plt.hist(tilt_1sd, facecolor=fc2)
        plt.title('Footwall tilt vs chi square', color = 'w')
        plt.xlabel('tilt (towards E), deg', color = 'w')
        #plt.ylabel('chi square', color = 'w')
        plt.xticks(color = 'w')
        plt.yticks(color = 'w')


        for ax in [ax3, ax4, ax5, ax6]:
          for ticks in ax.xaxis.get_ticklines() + ax.yaxis.get_ticklines():
              ticks.set_color('w')
          #for pos in ['top', 'bottom', 'left', 'right']:
          #    ax.spines[pos].set_edgecolor('w')


elif plot_format == 'print':
    fc1 = 'grey'
    fc2 = 'k'
    fc3 = 'w'
    fig2 = plt.figure(2)
    # E fault initiation hist
    ax3= fig2.add_subplot(241)
    bins = [9.5, 10.5, 11.5, 12.5, 13.5, 14.5, 15.5, 16.5, 17.5, 18.5]
    plt.hist(initA_2sd, bins, facecolor = fc1)
#    plt.hist(initA_1sd, bins, facecolor = fc2)
    #plt.hist(initA[0:9], bins, facecolor = fc3)
    #plt.axvline(x = w_mean_initA, color = fc3)
    plt.title('E fault initiation', color = 'k')
    plt.xlabel('E fault initiation, Ma', color = 'k')
    plt.xticks(color = 'k')
    plt.yticks(color = 'k')

    # E fault accel hist
    ax4 = fig2.add_subplot(242, axisbg='w')
    bins = [2.5, 3.5, 4.5, 5.5, 6.5]
    plt.hist(accel_2sd, bins, facecolor = fc1)
#    plt.hist(accel_1sd, bins, facecolor = fc2)
    #plt.hist(accel[0:9], bins, facecolor = fc3)
    #plt.axvline(x = w_mean_accel, color = fc3)
    plt.title('E fault acceleration', color = 'k')
    plt.xlabel('E fault acceleration, Ma',color = 'k')
    #plt.ylabel('chi square', color = 'w')
    plt.xticks(color = 'k')
    plt.yticks(color = 'k')

    # PCF initiation hist
    ax5 = fig2.add_subplot(243, axisbg='w')
    bins = [9.5, 10.5, 11.5, 12.5, 13.5, 14.5, 15.5, 16.5, 17.5, 18.5]
    plt.hist(initB_2sd, bins, facecolor = fc1)
#    plt.hist(initB_1sd, bins, facecolor = fc2)
    #plt.hist(initB[0:9], bins, facecolor = fc3)
    #plt.axvline(x = w_mean_initB, color = fc3)
    plt.title('PCF initiation vs chi square', color = 'k')
    plt.xlabel('PCF initiation, Ma', color = 'k')
    #plt.ylabel('chi square', color = 'w')
    plt.xticks(color = 'k')
```

```
    plt.yticks(color = 'k')

    # footwall tilt hist
    ax6 = fig2.add_subplot(244, axisbg='w')
    plt.hist(tilt_2sd, facecolor= fc1 )
#    plt.hist(tilt_1sd, facecolor= fc2 )
    #plt.hist(tilt[0:9], facecolor= fc3 )
    #plt.axvline(x = w_mean_tilt, color = fc3)
    plt.title('Footwall tilt vs chi square', color = 'k')
    plt.xlabel('tilt (towards E), deg', color = 'k')
    #plt.ylabel('chi square', color = 'w')
    plt.xticks(color = 'k')
    plt.yticks(color = 'k')

    # extension rates hist
    ax9 = fig2.add_subplot(245, axisbg='w')
    plt.hist(er1_2sd, bins = 6, color = 'blue', histtype = 'stepfilled', al-
pha=1)
    plt.hist(er2_2sd, bins = 8, color = 'red', alpha = 0.5, histtype = 'step-
filled')
    plt.axvline(x = er1_2sd_median, color='blue')
    plt.axvline(x = er2_2sd_median, color='red')
    plt.xlabel('extension rate (mm/yr)')



    ax11 = fig2.add_subplot(246, axisbg = 'w')
    plt.hist(initA_2sd, bins = [9.5, 10.5, 11.5, 12.5, 13.5, 14.5, 15.5, 16.5,
                              17.5, 18.5], color = 'blue',
histtype='stepfilled', alpha=1)
    plt.hist(initB_2sd, bins=bins, color='red', histtype='stepfilled', al-
pha=0.5)
    plt.axvline(x = initA_2sd_median, color='blue')
    plt.axvline(x = initB_2sd_median, color='red')
    plt.xlabel('fault initiation (Ma)')


    #fault init hist
    #ax11

    # net extension hist
    ax12 = fig2.add_subplot(247)
    plt.hist(net_ext_2sd, histtype='stepfilled', color='blue')
    plt.xlabel('net extension (km)')


if plot_format == 'ppt':
    fc1 = 'grey'
    fc2 = 'w'
    fc3 = 'r'
    fig3 = plt.figure(3)
    # age-elev plot
    ax7 = fig3.add_subplot(211, axisbg='k', figsize = (6,2))
    plt.plot(cctr_ages_2sd, cctr_elev_obs, 'b.')
#    plt.plot(cctr_ages_1sd, cctr_elev_obs, 'r.')
    plt.errorbar(cctr_obs_age, cctr_elev_obs, xerr = cctr_err, fmt='o',
color='w')
    plt.title('CCTR Age-Elev', color='w')
    plt.xlabel('zHe age, Ma', color='w')
    plt.ylabel('elev (m)', color='w')
    plt.xticks(color = 'w')
    plt.yticks(color='w')


    # age-lon plot
```

```python
    ax8 = fig3.add_subplot(212, axisbg='k', figsize = (6,2))
    plt.plot(cctr_lon, cctr_ages_2sd, 'b.')
#    plt.plot(cctr_lon, cctr_ages_1sd, 'r.')
    plt.errorbar(cctr_lon, cctr_obs_age, yerr = cctr_err, fmt='o', color='w')
    plt.title('CCTR Age-Lon', color='w')
    plt.xlabel('Lon, Degrees', color='w')
    plt.ylabel('zHe age, Ma', color='w')
    plt.xticks(color = 'w')
    plt.yticks(color='w')


    for ax in [ax3, ax4, ax5, ax6]:
        for ticks in ax.xaxis.get_ticklines() + ax.yaxis.get_ticklines():
            ticks.set_color('w')
        #for pos in ['top', 'bottom', 'left', 'right']:
            #ax.spines[pos].set_edgecolor('w')

if plot_format == 'print':  #CHANGE
    fc1 = 'grey'
    fc2 = 'w'
    fc3 = 'r'
    fig3 = plt.figure(3, figsize = (7,4))
    # age-elev plot
    ax7 = fig3.add_subplot(211, axisbg='w',)
    plt.plot(cctr_ages_2sd, cctr_elev_obs, 'b-')
#    plt.plot(cctr_ages_1sd, cctr_elev_calc, 'r-')
    plt.errorbar(cctr_obs_age, cctr_elev_obs, xerr = cctr_err, fmt='o',
color='k')
    plt.title('CCTR Age-Elev', color='k')
    plt.xlabel('zHe age, Ma', color='k')
    plt.ylabel('elev (m)', color='k')
    #plt.xticks(color = 'w')
    #plt.yticks(color='w')


    # age-lon plot
    ax8 = fig3.add_subplot(212, axisbg='w',)
    plt.plot(cctr_lon, cctr_ages_2sd_lon, 'b-')
#    plt.plot(cctr_lon, cctr_ages_1sd, 'r-')
    plt.errorbar(cctr_lon, cctr_obs_age_lon, yerr = cctr_err_lon, fmt='o',
color='k')
    plt.title('CCTR Age-Lon', color='k')
    plt.xlabel('Lon, Degrees', color='k')
    plt.ylabel('zHe age, Ma', color='k')
    #plt.xticks(color = 'w')
    #plt.yticks(color='w')


plt.show()
```

pecube_cloud_scripts_cctr.py

```python
#!/usr/bin/env python

import numpy as nmp
import subprocess, os, cloud


def calcNetExtension(initA, accel, srA1, srA2, dipFaultA, initB, srB1, srB2,
dipFaultB):
    """
    imports fault slip information and indicates whether net slip is
    under 25 km
    """
    # fault A extension
    slipA1 = (initA - accel) * srA1

    slipA2 = accel * srA2

    netSlipA = slipA1 + slipA2

    netExtensionA = netSlipA * nmp.cos(dipFaultA)

    #fault B extension
    slipB1 = (initB - accel) * srB1

    slipB2 = accel * srB2

    netSlipB = slipB1 + slipB2

    netExtensionB = netSlipB * nmp.cos(dipFaultB)


    # total extension

    netExtension = netExtensionA + netExtensionB

    return netExtension

###############################################################################
#########

def modifyInputFiles(initA, accel, srA1, srA2, initB, srB1, srB2, inputFile,
outputFile):
    """
    take Pecube input files and modify parameters based on
    the loop inputs from main script
    """
    #print 'writing input files'

    paramLineFaultA1 = 27  #line numbers for fault inputs

    paramLineFaultA2 = 28

    paramLineFaultB1 = 58

    paramLineFaultB2 = 59

    # modifications to fault A1
    datamod1 = '{} '.format(initA)
    datamod2 = '{} '.format(accel)
    datamod3 = '{} \n'.format(srA1)
```

239

```python
    # modifications to fault A2
    datamod4 = '{} '.format(accel)
    datamod5 = '0. '
    datamod6 = '{} \n'.format(srA2)

    # modifications to fault B
    datamod7 = '{} '.format(initB)
    datamod8 = '{} '.format(accel)
    datamod9 = '{} \n'.format(srB1)

    # modifications to fault B
    datamod10 = '{} '.format(accel)
    datamod11 = '0. '
    datamod12 = '{} \n'.format(srB2)


    start_point = 0    # start_point = len('-1.00 -1.00 -1.00 ')

    inputFile = open(inputFile, 'r')

    outputFile = open(outputFile, 'w+')

    lineno = 0                  # line tracker

    while 1:

        line = inputFile.readline()   # grab a line

        if not line: break       # end of file reached

        lineno = lineno + 1          # current working line

        if lineno == paramLineFaultA1:      # are we there yet?

            # here's the working bit that makes the sustitution.

            modifiedline = line[:start_point] + datamod1 + datamod2 + datamod3

            outputFile.write(modifiedline)

        elif lineno == paramLineFaultA2:

            modifiedline = line[:start_point] + datamod4 + datamod5 + datamod6

            outputFile.write(modifiedline)

        elif lineno == paramLineFaultB1:

            modifiedline = line[:start_point] + datamod7 + datamod8 + datamod9

            outputFile.write(modifiedline)

        elif lineno == paramLineFaultB2:

            modifiedline = line[:start_point] + datamod10 + datamod11 + data-
mod12

            outputFile.write(modifiedline)

        else:

            outputFile.write(line)      # copy line as it is into temp file
```

240

```
    inputFile.close()                        # done with it.

    outputFile.close()                       # rename afterward with the original
name

    #print 'done writing'

    #return(inputFile, outputFile)



############################################################################
#######

def renameFaultParams(inputFile, outputFile):
    """"
    replace old inputfile with new outputfile via calling bash
    """"
    #print 'replacing files'
    subprocess.call("cp {} {}".format(outputFile, inputFile), shell=True)
    #print 'done'


############################################################################
####

def runPecube():

    #print 'running Pecube'
    subprocess.call("bin/Pecube", shell=True)
    #print 'done with Pecube'


############################################################################
###


def save_output(comparison_file, initA, accel, srA1, srA2, initB, srB1, srB2):

    #print 'saving output'

    out_name = '/home/picloud/src/Pecube/cctrN/pred_{}_{}_{}_{}_{}_{}_{}.txt'.
format(initA,
        accel, srA1, srA2, initB, srB1, srB2)

    file_out = open(out_name, 'w+')

    comparison_file = open(comparison_file, 'r')

    lines = comparison_file.readlines()

    comparison_file.close()

    new_file = open('/home/picloud/src/Pecube/cctrN/new_file2.txt', 'w+')

    new_file.writelines([item for item in lines[1:]])

    new_file.close()

    new_file = open('/home/picloud/src/Pecube/cctrN/new_file2.txt', 'r')

    column = 9

    for line in new_file:
```

```python
        line = line.strip()
        sline = line.split()
        file_out.write(sline[column] + '\n')

    new_file.close()

    file_out.close()

    #print 'done'

    return out_name



##############################################################################
###


def calc_chi_square(obs, out_name):

    #print 'calculating chi square misfit'

    zHe_predicted = nmp.loadtxt(open(out_name))

    zHe_observed = nmp.loadtxt(open(obs))

    chi_square = sum((zHe_observed - zHe_predicted)**2 / zHe_observed) / 8

    #print 'done'

    return chi_square

##############################################################################
###


def append_info(out_name, chi_square, initA, accel, srA1, srA2, initB, srB1,
srB2, netExtension):

    #print 'making numpy matrices'

    in_array = nmp.loadtxt(open(out_name))

    out_array = '/home/picloud/src/Pecube/cctrN/run_{}_{}_{}_{}_{}_{}_{}.npy'.
format(initA,
        accel, srA1, srA2, initB, srB1, srB2)

    nmp.save(out_array, in_array)

    out_array_temp = nmp.load(out_array)

    out_array_temp = nmp.append(out_array_temp, [initA, accel, srA1, srA2,
initB, srB1, srB2, chi_square, netExtension])

    nmp.save(out_array, out_array_temp)

    cloud.files.put(out_array)

    return out_array

    #print 'done'

##############################################################################
###
```

```
def change_directory():
    subprocess.call("cd /home/picloud/src/Pecube", shell=True)
    directory = subprocess.call("pwd", shell=True)
    print directory


################################################################################
###

def change_dir_python():
    os.chdir('/home/picloud/src/Pecube')


################################################################################
###

def mkdir_test(test_dir):
    subprocess.call('mkdir {}'.format(test_dir), shell=True)



################################################################################
###

#def dir_list(natty_path):

def run_pecube_cloud():
    #os.chdir('/home/picloud/src/Pecube')
    pecube_print = subprocess.check_output("cd /home/picloud/src/Pecube &&
bin/Pecube", shell=True)
    return pecube_print

################################################################################
###

def dir_list():
    os.chdir('/home/picloud/src/Pecube/input/')
    dirlist = os.listdir(os.getcwd() )
    return dirlist
```

run_cctr_picloud.py

```python
#!/usr/bin/env python

import sys
sys.path.append('/home/itchy/python_scripts')
import os, cloud, subprocess, time
import pecube_cloud_scripts_cctr as psc
reload(psc)

# important files
inputFile = '/home/picloud/src/Pecube/input/fault_parameters.txt'

outputFile = '/home/picloud/src/Pecube/input/fault_parameters.txt.out'

comparison_file = '/home/picloud/src/Pecube/cctrN/Comparison.txt'

obs = '/home/picloud/src/Pecube/cctrN/obs.txt'

# fault parameters

initFaultAs = [10.0, 11.0, 12.0, 13.0, 14.0, 15.0, 16.0, 17.0, 18.0] #, 19.0,
20.0]

accelFaults = [3.0, 4.0, 5.0, 6.0]

slipRate1FaultAs = [0.5, 1.0, 1.5, 2.0]

slipRate2FaultAs = [0.5, 1.0, 1.5, 2.0, 3.0]

initFaultBs = [10.0, 11.0, 12.0, 13.0, 14.0, 15.0, 16.0, 17.0, 18.0] #, 19.0,
20.0]

slipRate1FaultBs = [0.5, 1.0, 1.5, 2.0]

slipRate2FaultBs = [0.5, 1.0, 1.5, 2.0, 3.0]

#accelFaultBs = [3.0, 4.0, 5.0, 6.0]


#       define constants (dipFaultA, dipFaultB)
dipFaultA = [0.88]

dipFaultB = [0.88]


#t0 = time.time()

#       define list of variable lists
faultParamsList = [[j, k, l, m, n, o, p] for j in initFaultAs for k in accel-
Faults for l in slipRate1FaultAs for m in slipRate2FaultAs for n in initFault-
Bs for o in slipRate1FaultBs for p in slipRate2FaultBs ]

#t1 = time.time()


#print t1-t0, 's to generate fault list'
# filter variables
faultParamsListFiltered = []

for faultParams in faultParamsList:

        [initA, accel, srA1, srA2, initB, srB1, srB2] = faultParams
```

```
        netExtension = psc.calcNetExtension(initA, accel, srA1, srA2, dipFaultA,
initB, srB1, srB2, dipFaultB)

#print netExtension

        if netExtension < 10.5:
                if netExtension >10:

                        faultParamsListFiltered.append(faultParams)

print len(faultParamsListFiltered)




def run_pecube_map(faultParamsListFiltered):
        [initA, accel, srA1, srA2, initB, srB1, srB2] = faultParamsListFiltered

        netExtension = psc.calcNetExtension(initA, accel, srA1, srA2, dipFaultA,
initB, srB1, srB2, dipFaultB)
#       test for amount of extension (maybe do this with a filter function
#       or something similar when making the variable list)

#       modify input files,
        psc.modifyInputFiles(initA, accel, srA1, srA2, initB, srB1, srB2, input-
File, outputFile)

        #rename fault parameters
        psc.renameFaultParams(inputFile, outputFile)

#       run pecube
        pecube_print = psc.run_pecube_cloud()

#       save output
        out_name = psc.save_output(comparison_file, initA, accel, srA1, srA2,
initB, srB1, srB2)

#       calculate chi square
        chi_square = psc.calc_chi_square(obs, out_name)

#       append results to results file(s)
        out_array = psc.append_info(out_name, chi_square, initA, accel, srA1,
srA2, initB, srB1, srB2, netExtension)

        #cloud.files.get(out_array, '/home/itchy/src/Pecube/picloud/results/
cctrN/{}'.format(out_array))

        return pecube_print


t0 = time.time()

pecube_cctr_105_10 = cloud.map(run_pecube_map, faultParamsListFiltered, _
env='natty_itchy_pecube')



cloud.result(pecube_cctr_105_10)

#numpy_results_list = cloud.files.list()


print 'Pecube took', time.time() - t0, 'seconds for',
len(faultParamsListFiltered), 'runs'

t1 = time.time()
```

```
for faultParams in faultParamsListFiltered:
    [initA, accel, srA1, srA2, initB, srB1, srB2] = faultParams
    filename = 'run_{}_{}_{}_{}_{}_{}_{}.npy'.format(initA,
      accel, srA1, srA2, initB, srB1, srB2)
    cloud.files.get(filename, '/home/itchy/src/Pecube/picloud/results/cctrN/
runs_16_15/{}'.format(filename))

print 'Done!  Picloud took', time.time()-t1, 'seconds to transfer files.'
```

nmt_param_test_results.py

```python
import numpy as nmp
import matplotlib.pyplot as plt

radiogenic = nmp.array([5.4906, 5.6409, 5.8025, 6.3244, 7.0934, 27.8018,
27.9307])


moho_900 = nmp.array([3.6772, 3.7084, 3.7533, 3.8001, 4.1168, 9.4353, 9.7520])

low_angle_all = nmp.array([4.3214, 4.3496, 4.3905, 4.3647, 4.4701, 4.2834,
4.0931])

rolling_hinge = nmp.array([3.3679, 3.3919, 3.4302, 3.4634, 3.7231, 7.6417,
7.7255])

steep_at_depth = nmp.array([2.5168, 2.5224, 2.5391, 2.7637, 3.0687, 6.5419,
6.7167])

low_angle_depth = nmp.array([4.3289, 4.3576, 4.3988, 4.3787, 4.6094, 7.1878,
7.2091])

hi_angle = nmp.array([1.4660, 1.4634, 1.4650, 1.3790, 1.3884, 1.3472, 1.3139])

best_model = nmp.array([3.8734, 3.8989, 3.9394, 3.9723, 4.2304, 6.9309,
6.9605])

nmt_obs_age = nmp.array([3.48, 3.43, 3.66, 4.40, 4.87, 6.32, 7.29])

nmt_err_sd = nmp.array([0.24, 0.24, 0.70, 0.41, 0.57, 0.23, 0.63])

nmt_err = 0.08 * nmt_obs_age + nmt_err_sd

nmt_elev_obs = nmp.array([5381, 5416, 5538, 5609, 5628, 6063, 5823])

nmt_lon = nmp.array([83.40467, 83.40848, 83.41141, 83.4345, 83.4545, 83.5342,
83.54151])


#####  make plots

fig1 = plt.figure(1)
ax1 = fig1.add_subplot(111, axisbg='k')
plt.plot(nmt_lon, radiogenic, 'g', nmt_lon, moho_900, 'c', nmt_lon, low_angle_
all, 'm', nmt_lon, rolling_hinge, 'y', nmt_lon, steep_at_depth, 'b', nmt_lon,
low_angle_depth, 'grey', nmt_lon, hi_angle, 'orange', nmt_lon, best_model,
'r')
plt.errorbar(nmt_lon, nmt_obs_age, yerr = nmt_err, fmt='o', color='w')
plt.xticks(color = 'white')
plt.yticks(color = 'white')

for ax in [ax1]:
    for ticks in ax.xaxis.get_ticklines() + ax.yaxis.get_ticklines():
        ticks.set_color('w')
    for pos in ['top', 'bottom', 'left', 'right']:
        ax.spines[pos].set_edgecolor('w')

plt.show()
```

247

nmt_filter_stdev.py

```python
# -*- coding: utf-8 -*-
"""
Created on Fri Jan 27 15:59:41 2012

@author: Richard
"""

import numpy as nmp
import matplotlib.pyplot as plt

nmt_obs_age = nmp.array([3.48, 3.43, 3.66, 4.40, 4.87, 7.28, 6.34])

#magmatic_correction = nmp.array([1.5, 1.5, 1.5, 1.0, 1.0, 0.75, 0.5])

#nmt_obs_age = nmt_obs_age + magmatic_correction

nmt_err_sd = nmp.array([0.24, 0.24, 0.70, 0.41, 0.57, 0.64, 0.24])

#nmt_err = nmt_obs_age * 0.04 + nmt_err_sd

nmt_obs_age_err = nmp.array([0.28, 0.28, 0.29, 0.35, 0.39, 0.58, 0.51])


# error is larger of standard deviation or lab error (std of FCT standard, or
8%)
nmt_err = nmp.array([0.28, 0.28, 0.70, 0.41, 0.57, 0.64, 0.51])

#nmt_err = nmt_err_sd

nmt_lo_1sd = nmt_obs_age - nmt_err

nmt_hi_1sd = nmt_obs_age + nmt_err

nmt_lo_2sd = nmt_obs_age - 2 * nmt_err

nmt_hi_2sd = nmt_obs_age + 2 * nmt_err

nmt_lo_3sd = nmt_obs_age - 3 * nmt_err

nmt_hi_3sd = nmt_obs_age + 3 * nmt_err

nmt_elev_obs = nmp.array([5381, 5416, 5538, 5609, 5628, 5823, 6063])

nmt_obs_age_lon = nmp.array([3.48, 3.43, 3.66, 4.40, 4.87, 6.34, 7.28])

nmt_lon = nmp.array([83.40467, 83.40848, 83.41141, 83.4345, 83.4545, 83.5342,
83.54151])

nmt_elev_calc = nmt_elev_obs # for now


###################################

# load data

nmt_all_runs = nmp.loadtxt('nmt_all_runs.csv', delimiter=',')

A_dip = 0.4

B_dip = 0.88
```

```python
initA = nmt_all_runs[:,7]

srA1 = nmt_all_runs[:,8]

accelA = nmt_all_runs[:,9]

srA2 = nmt_all_runs[:,10]

initB = nmt_all_runs[:,11]

srB = nmt_all_runs[:,12]

chi_sq = nmt_all_runs[:,13]

net_ext = nmt_all_runs[:,14]

exhumA = ((initA-accelA) * srA1 + accelA * srA2) * nmp.sin(A_dip)

#exhumA = nmp.transpose(exhumA)

exhumB = initB * srB * nmp.sin(B_dip)

#exhumB = nmp.transpose(exhumB)

tilt = nmp.degrees(nmp.arctan2((exhumA - exhumB), 20))

#exhumA = exhumA [nmp.newaxis]

#exhumB = exhumB [nmp.newaxis]

new_vecs = nmp.vstack((exhumA, exhumB, tilt))

new_vecs = nmp.transpose(new_vecs)


#tilt = tilt [nmp.newaxis]

#tilt = nmp.transpose(tilt)

nmt_all_runs = nmp.hstack((nmt_all_runs, new_vecs))


#########################

# filter data


nmt_fits_1sd = nmp.zeros([18]) # create empty array to add to
nmt_fits_2sd = nmp.zeros([18]) # create empty array to add to
nmt_fits_3sd = nmp.zeros([18]) # create empty array to add to

# Fits to data at 2 standard deviation

# loop to filter each calculated age with the observed age
for i in range(nmt_all_runs.shape[0]):
    if nmt_lo_2sd[0] <= nmt_all_runs[i,0] <= nmt_hi_2sd[0]\
    and nmt_lo_2sd[1] <= nmt_all_runs[i,1] <= nmt_hi_2sd[1]\
    and nmt_lo_2sd[2] <= nmt_all_runs[i,2] <= nmt_hi_2sd[2]\
    and nmt_lo_2sd[3] <= nmt_all_runs[i,3] <= nmt_hi_2sd[3]\
    and nmt_lo_2sd[4] <= nmt_all_runs[i,4] <= nmt_hi_2sd[4]\
    and nmt_lo_2sd[5] <= nmt_all_runs[i,5] <= nmt_hi_2sd[5]\
    and nmt_lo_2sd[6] <= nmt_all_runs[i,6] <= nmt_hi_2sd[6]:

        nmt_fits_2sd = nmp.vstack((nmt_fits_2sd, nmt_all_runs[i,:]))
        #print nmt_all_runs[i,:]
```

249

```
nmt_fits_2sd = nmt_fits_2sd[1:,:]

# if we want to save
#nmp.save('C:\\school\\tibet\\lunggar\\thermo\\pecube\\nmt_picloud_results\\
nmt_1sd_fits.npy', nmt_fits_2sd)

# name individual variables
slw_nmt_01_calc_2sd = nmt_fits_2sd[:,0]

slw_nmt_02_calc_2sd = nmt_fits_2sd[:,1]

slw_nmt_03_calc_2sd = nmt_fits_2sd[:,2]

slw_nmt_04_calc_2sd = nmt_fits_2sd[:,3]

slw_nmt_05_calc_2sd = nmt_fits_2sd[:,4]

sle_nmt_01_calc_2sd = nmt_fits_2sd[:,5]

sle_nmt_03_calc_2sd = nmt_fits_2sd[:,6]

initA_2sd = nmt_fits_2sd[:,7]

srA1_2sd = nmt_fits_2sd[:,8]

accelA_2sd = nmt_fits_2sd[:,9]

srA2_2sd = nmt_fits_2sd[:,10]

initB_2sd = nmt_fits_2sd[:,11]

srB_2sd = nmt_fits_2sd[:,12]

chi_sq_2sd = nmt_fits_2sd[:,13]

net_ext_2sd = nmt_fits_2sd[:,14]

exhumA_2sd = nmt_fits_2sd[:,15]

exhumB_2sd = nmt_fits_2sd[:,16]

tilt_2sd = nmt_fits_2sd[:,17]


nmt_ages_2sd = nmp.transpose(nmt_fits_2sd[:,:7])

nmt_ages_2sd_lon = nmp.array([slw_nmt_01_calc_2sd, slw_nmt_02_calc_2sd,
                              slw_nmt_03_calc_2sd, slw_nmt_04_calc_2sd,
                              slw_nmt_05_calc_2sd, sle_nmt_03_calc_2sd,
                              sle_nmt_01_calc_2sd])


# Fits to data at 1 standard deviation

# loop to filter each calculated age with the observed age
for i in range(nmt_all_runs.shape[0]):
    if nmt_lo_3sd[0] <= nmt_all_runs[i,0] <= nmt_hi_3sd[0]\
    and nmt_lo_3sd[1] <= nmt_all_runs[i,1] <= nmt_hi_3sd[1]\
    and nmt_lo_3sd[2] <= nmt_all_runs[i,2] <= nmt_hi_3sd[2]\
    and nmt_lo_3sd[3] <= nmt_all_runs[i,3] <= nmt_hi_3sd[3]\
    and nmt_lo_3sd[4] <= nmt_all_runs[i,4] <= nmt_hi_3sd[4]\
    and nmt_lo_3sd[5] <= nmt_all_runs[i,5] <= nmt_hi_3sd[5]\
    and nmt_lo_3sd[6] <= nmt_all_runs[i,6] <= nmt_hi_3sd[6]:
        nmt_fits_3sd = nmp.vstack((nmt_fits_3sd, nmt_all_runs[i,:]))
```

```python
if nmt_fits_3sd.size > 18:
    nmt_fits_3sd = nmt_fits_3sd[1:,:] #remove first line (all zeros)


# if we want to save
#nmp.save('C:\\school\\tibet\\lunggar\\thermo\\pecube\\nmt_picloud_results\\
nmt_3sd_fits.npy', nmt_fits_3sd)

# name individual variables

    slw_nmt_01_calc_3sd = nmt_fits_3sd[:,0]

    slw_nmt_02_calc_3sd = nmt_fits_3sd[:,1]

    slw_nmt_03_calc_3sd = nmt_fits_3sd[:,2]

    slw_nmt_04_calc_3sd = nmt_fits_3sd[:,3]

    slw_nmt_05_calc_3sd = nmt_fits_3sd[:,4]

    sle_nmt_01_calc_3sd = nmt_fits_3sd[:,5]

    sle_nmt_03_calc_3sd = nmt_fits_3sd[:,6]

    initA_3sd = nmt_fits_3sd[:,7]

    srA1_3sd = nmt_fits_3sd[:,8]

    accelA_3sd = nmt_fits_3sd[:,9]

    srA2_3sd = nmt_fits_3sd[:,10]

    initB_3sd = nmt_fits_3sd[:,11]

    srB_3sd = nmt_fits_3sd[:,12]

    chi_sq_3sd = nmt_fits_3sd[:,13]

    net_ext_3sd = nmt_fits_3sd[:,14]

    exhumA_3sd = nmt_fits_3sd[:,15]

    exhumB_3sd = nmt_fits_3sd[:,16]

    tilt_3sd = nmt_fits_3sd[:,17]


    nmt_ages_3sd = nmp.transpose(nmt_fits_3sd[:,:7])
################################################################################

# make histories out of the data

times = 41

time_vector = nmp.linspace(0, 20, num=times)

# 1 sd

if nmt_fits_3sd.size > 18:
    n_3sd = len(tilt_3sd)

    A_er_w_time_3sd = nmp.zeros((n_3sd, times))

    B_er_w_time_3sd = nmp.zeros((n_3sd, times))
```

251

```python
    erA1_3sd = srA1_3sd * nmp.cos(A_dip)

    erA2_3sd = srA2_3sd * nmp.cos(A_dip)

    erB_3sd = srB_3sd * nmp.cos(B_dip)

    for i in range(n_3sd):
        A_er_w_time_3sd[i, 0 : ((accelA_3sd[i] * 2))] = erA2_3sd[i]

        A_er_w_time_3sd[i, (accelA_3sd[i] * 2): (initA_3sd[i] * 2 -1)] =
erA1_3sd[i]

        B_er_w_time_3sd[i, 0: (initB_3sd[i] * 2)] = erB_3sd[i]

    er_w_time_3sd = A_er_w_time_3sd + B_er_w_time_3sd

    net_ext_w_time_3sd = nmp.cumsum(er_w_time_3sd, axis=1)/1.85 # fix this hack

    cum_vector_3sd = net_ext_w_time_3sd[:,-1]

    cum_ext_w_time_3sd = nmp.zeros(nmp.shape(er_w_time_3sd))

    er_w_time_trans_3sd = nmp.transpose(er_w_time_3sd)


    for i in range(n_3sd):
        cum_ext_w_time_3sd[i,:] = cum_vector_3sd[i] - net_ext_w_time_3sd[i,:]

    cum_ext_w_time_trans_3sd = nmp.transpose(cum_ext_w_time_3sd)

# 2 sd

n_2sd = len(tilt_2sd)

A_er_w_time_2sd = nmp.zeros((n_2sd, times))

B_er_w_time_2sd = nmp.zeros((n_2sd, times))

erA1_2sd = srA1_2sd * nmp.cos(A_dip)

erA2_2sd = srA2_2sd * nmp.cos(A_dip)

erB_2sd = srB_2sd * nmp.cos(B_dip)

for i in range(n_2sd):
    A_er_w_time_2sd[i, 0 : ((accelA_2sd[i] * 2))] = erA2_2sd[i]

    A_er_w_time_2sd[i, (accelA_2sd[i] * 2): (initA_2sd[i] * 2 -1)] =
erA1_2sd[i]

    B_er_w_time_2sd[i, 0: (initB_2sd[i] * 2)] = erB_2sd[i]

er_w_time_2sd = A_er_w_time_2sd + B_er_w_time_2sd

net_ext_w_time_2sd = nmp.cumsum(er_w_time_2sd, axis=1)/1.85 # fix this hack

cum_vector_2sd = net_ext_w_time_2sd[:,-1]

cum_ext_w_time_2sd = nmp.zeros(nmp.shape(er_w_time_2sd))

er_w_time_trans_2sd = nmp.transpose(er_w_time_2sd)
```

```
for i in range(n_2sd):
    cum_ext_w_time_2sd[i,:] = cum_vector_2sd[i] - net_ext_w_time_2sd[i,:]

cum_ext_w_time_trans_2sd = nmp.transpose(cum_ext_w_time_2sd)

############################################################################
###

plot_format = 'print'  # ppt or print

# slip rate and cumulative extension plots
if plot_format == 'ppt':
    fc1 = 'w'
    fc2 = 'r'

    # extension rate with time
    fig1 = plt.figure(1)
    ax1 = fig1.add_subplot(121, axisbg='black')
    ax1.plot(time_vector, er_w_time_trans_2sd, color=fc1, linewidth=0.75)
    ax1.plot(time_vector, er_w_time_trans_3sd, color=fc2, linewidth=1.5)
    #ax1.plot(time_vector, er_w_time_trans[:,0:9], color='blue', linewidth=2)
    plt.gca().invert_xaxis()
    plt.xlabel('Ma', color='white')
    plt.ylabel('extension, mm/yr', color='white')
    plt.title('NMT extension rate through time', color='white')
    plt.xticks(color = 'white')
    plt.yticks(color = 'white')
    #plt.spine(color='white')


    # cumulative extension with time
    ax2 = fig1.add_subplot(122, axisbg='black')
    ax2.plot(time_vector, cum_ext_w_time_trans_2sd, color=fc1, linewidth=0.75)
    ax2.plot(time_vector, cum_ext_w_time_trans_3sd, color=fc2, linewidth=1.5)
    #ax2.plot(time_vector, cum_ext_w_time_trans[:,0:9], color='blue', lin-
ewidth=2)
    plt.gca().invert_xaxis()
    plt.xlabel('Ma', color='white')
    plt.ylabel('cum. extension, km', color='white')
    plt.title('NMT cum. extension through time', color='white')
    plt.xticks(color = 'white')
    plt.yticks(color = 'white')

    for ax in [ax1, ax2]:
      for ticks in ax.xaxis.get_ticklines() + ax.yaxis.get_ticklines():
          ticks.set_color('w')
      for pos in ['top', 'bottom', 'left', 'right']:
          ax.spines[pos].set_edgecolor('w')


elif plot_format == 'print':
    fc1 = 'k'
    fc2 = 'r'

    # extension rate with time
    plt.figure(1)
    plt.subplot(121, axisbg='white')
    plt.plot(time_vector, er_w_time_trans_2sd, color=fc1, linewidth=0.5)
    #plt.plot(time_vector, er_w_time_trans_3sd, color=fc2, linewidth=1)
    #plt.plot(time_vector, er_w_time_trans[:,0:9], color='blue', linewidth=2)
    plt.gca().invert_xaxis()
    plt.xlabel('Ma', color='black')
```

253

```
    plt.ylabel('extension, mm/yr', color='black')
    plt.title('NMT extension rate through time', color='black')

    # cumulative extension with time
    plt.subplot(122, axisbg='white')
    plt.plot(time_vector, cum_ext_w_time_trans_2sd, color=fc1, linewidth=0.5)
    #plt.plot(time_vector, cum_ext_w_time_trans_3sd, color=fc2, linewidth=1)
    #plt.plot(time_vector, cum_ext_w_time_trans[:,0:9], color='blue', lin-
ewidth=1)
    plt.gca().invert_xaxis()
    plt.xlabel('Ma', color='k')
    plt.ylabel('cum. extension, km', color='k')
    plt.title('NMT cum. extension through time', color='k')


# histograms

if plot_format == 'ppt':
    fc1 = 'grey'
    fc2 = 'w'
    fig2 = plt.figure(2)
    # SLD init
    ax3= fig2.add_subplot(221, axisbg='black')
    bins = [7.5, 8.5, 9.5, 10.5, 11.5, 12.5, 13.5, 14.5, 15.5, 16.5, 17.5,
18.5]
    plt.hist(initA_2sd, bins, facecolor=fc1)
    plt.hist(initA_3sd, bins, facecolor=fc2)
    plt.title('SLD initiation vs chi square', color = 'w')
    plt.xlabel('SLD initiation, Ma', color = 'w')
    plt.xticks(color = 'w')
    plt.yticks(color = 'w')

    # SLD accel hist
    ax4 = fig2.add_subplot(222, axisbg='black')
    bins = [1.75, 2.25, 2.75, 3.25, 3.75, 4.25, 4.75, 5.25, 5.75, 6.25, 6.75]
    plt.hist(accelA_2sd, bins, facecolor=fc1)
    plt.hist(accelA_3sd, bins, facecolor=fc2)
    plt.title('SLD acceleration vs chi square', color = 'w')
    plt.xlabel('SLD acceleration, Ma',color = 'w')
    #plt.ylabel('chi square', color = 'w')
    plt.xticks(color = 'w')
    plt.yticks(color = 'w')

    # PCF initiation hist
    ax5 = fig2.add_subplot(223, axisbg='black')
    bins = [9, 11, 13, 15, 17, 19]
    plt.hist(initB_2sd, bins, facecolor=fc1)
    plt.hist(initB_3sd, bins, facecolor=fc2)
    plt.title('PCF initiation vs chi square', color = 'w')
    plt.xlabel('PCF initiation, Ma', color = 'w')
    #plt.ylabel('chi square', color = 'w')
    plt.xticks(color = 'w')
    plt.yticks(color = 'w')

    # footwall tilt hist
    ax6 = fig2.add_subplot(224, axisbg='black')
    plt.hist(tilt_2sd, facecolor=fc1)
    plt.hist(tilt_3sd, facecolor=fc2)
    plt.title('Footwall tilt vs chi square', color = 'w')
    plt.xlabel('tilt (towards E), deg', color = 'w')
    #plt.ylabel('chi square', color = 'w')
    plt.xticks(color = 'w')
    plt.yticks(color = 'w')
```

```
    for ax in [ax3, ax4, ax5, ax6]:
      for ticks in ax.xaxis.get_ticklines() + ax.yaxis.get_ticklines():
            ticks.set_color('w')
      #for pos in ['top', 'bottom', 'left', 'right']:
      #    ax.spines[pos].set_edgecolor('w')


elif plot_format == 'print':
    fc1 = 'grey'
    fc2 = 'k'
    fc3 = 'w'
    fig2 = plt.figure(2)
    # SLD initiation hist
    ax3= fig2.add_subplot(221)
    bins = [7.5, 8.5, 9.5, 10.5, 11.5, 12.5, 13.5, 14.5, 15.5, 16.5, 17.5,
18.5]
    plt.hist(initA_2sd, bins, facecolor = fc1)
    #plt.hist(initA_3sd, bins, facecolor = fc2)
    #plt.hist(initA[0:9], bins, facecolor = fc3)
    #plt.axvline(x = w_mean_initA, color = fc3)
    plt.title('SLD initiation', color = 'k')
    plt.xlabel('SLD initiation, Ma', color = 'k')
    plt.xticks(color = 'k')
    plt.yticks(color = 'k')

    # SLD accel hist
    ax4 = fig2.add_subplot(222, axisbg='w')
    bins = [1.75, 2.25, 2.75, 3.25, 3.75, 4.25, 4.75, 5.25, 5.75, 6.25, 6.75]
    plt.hist(accelA_2sd, bins, facecolor = fc1)
    #plt.hist(accelA_3sd, bins, facecolor = fc2)
    #plt.hist(accel[0:9], bins, facecolor = fc3)
    #plt.axvline(x = w_mean_accel, color = fc3)
    plt.title('SLD acceleration', color = 'k')
    plt.xlabel('SLD acceleration, Ma',color = 'k')
    #plt.ylabel('chi square', color = 'w')
    plt.xticks(color = 'k')
    plt.yticks(color = 'k')

    # PCF initiation hist
    ax5 = fig2.add_subplot(223, axisbg='w')
    bins = [9, 11, 13, 15, 17, 19]
    plt.hist(initB_2sd, bins, facecolor = fc1)
    #plt.hist(initB_3sd, bins, facecolor = fc2)
    #plt.hist(initB[0:9], bins, facecolor = fc3)
    #plt.axvline(x = w_mean_initB, color = fc3)
    plt.title('PCF initiation vs chi square', color = 'k')
    plt.xlabel('PCF initiation, Ma', color = 'k')
    #plt.ylabel('chi square', color = 'w')
    plt.xticks(color = 'k')
    plt.yticks(color = 'k')

    # footwall tilt hist
    ax6 = fig2.add_subplot(224, axisbg='w')
    #bins = [-25, -20, -15, -10, -5, 0, 5, 15, 25, 45]
    plt.hist(tilt_2sd, facecolor= fc1 )
    #plt.hist(tilt_3sd, facecolor= fc2 )
    #plt.hist(tilt[0:9], facecolor= fc3 )
    #plt.axvline(x = w_mean_tilt, color = fc3)
    plt.title('Footwall tilt vs chi square', color = 'k')
    plt.xlabel('tilt (towards E), deg', color = 'k')
    #plt.ylabel('chi square', color = 'w')
    plt.xticks(color = 'k')
    plt.yticks(color = 'k')
```

255

```
if plot_format == 'ppt':
    fc1 = 'grey'
    fc2 = 'w'
    fc3 = 'r'
    fig3 = plt.figure(3)
    # age-elev plot
    ax7 = fig3.add_subplot(211, axisbg='k')
    plt.plot(nmt_ages_2sd, nmt_elev_calc, 'b.')
    plt.plot(nmt_ages_3sd, nmt_elev_calc, 'r.')
    plt.errorbar(nmt_obs_age, nmt_elev_obs, xerr = nmt_err, fmt='o',
color='w')
    plt.title('NMT Age-Elev', color='w')
    plt.xlabel('zHe age, Ma', color='w')
    plt.ylabel('elev (m)', color='w')
    plt.xticks(color = 'w')
    plt.yticks(color='w')


    # age-lon plot
    ax8 = fig3.add_subplot(212, axisbg='k')
    plt.plot(nmt_lon, nmt_ages_2sd, 'b.')
    plt.plot(nmt_lon, nmt_ages_3sd, 'r.')
    plt.errorbar(nmt_lon, nmt_obs_age, yerr = nmt_err, fmt='o', color='w')
    plt.title('NMT Age-Lon', color='w')
    plt.xlabel('Lon, Degrees', color='w')
    plt.ylabel('zHe age, Ma', color='w')
    plt.xticks(color = 'w')
    plt.yticks(color='w')


    for ax in [ax7, ax8]:
        for ticks in ax.xaxis.get_ticklines() + ax.yaxis.get_ticklines():
            ticks.set_color('w')
        for pos in ['top', 'bottom', 'left', 'right']:
            ax.spines[pos].set_edgecolor('w')

if plot_format == 'print':
    fc1 = 'grey'
    fc2 = 'w'
    fc3 = 'r'
    fig3 = plt.figure(3, figsize = (7,4))
    # age-elev plot
    ax7 = fig3.add_subplot(211, axisbg='w')
    plt.plot(nmt_ages_2sd, nmt_elev_calc, 'b-')
    #plt.plot(nmt_ages_3sd, nmt_elev_calc, 'r-')
    plt.errorbar(nmt_obs_age, nmt_elev_obs, xerr = nmt_err, fmt='o',
color='k')
    plt.title('NMT Age-Elev', color='k')
    plt.xlabel('zHe age, Ma', color='k')
    plt.ylabel('elev (m)', color='k')
    #plt.xticks(color = 'w')
    #plt.yticks(color='w')


    # age-lon plot
    ax8 = fig3.add_subplot(212, axisbg='w')
    plt.plot(nmt_lon, nmt_ages_2sd_lon, 'b-')
    #plt.plot(nmt_lon, nmt_ages_3sd, 'r-')
    plt.errorbar(nmt_lon, nmt_obs_age_lon, yerr = nmt_err, fmt='o', color='k')
    plt.title('NMT Age-Lon', color='k')
    plt.xlabel('Lon, Degrees', color='k')
    plt.ylabel('zHe age, Ma', color='k')
    #plt.xticks(color = 'w')
```

```
    #plt.yticks(color='w')

plt.show()
```

pecube_cloud_scripts.py

```python
#!/usr/bin/env python

import numpy as nmp
import subprocess, os, cloud


def calcNetExtension(initA, srA1, accelA, srA2, dipFaultA, initB, srB, dip-
FaultB):
    """
    imports fault slip information and indicates whether net slip is
    under 25 km
    """
    # fault A extension
    slipA1 = (initA - accelA) * srA1

    slipA2 = accelA * srA2

    netSlipA = slipA1 + slipA2

    netExtensionA = netSlipA * nmp.cos(dipFaultA)

    #fault B extension
    netSlipB = initB * srB

    netExtensionB = netSlipB * nmp.cos(dipFaultB)

    # total extension
    netExtension = netExtensionA + netExtensionB

    return netExtension

###############################################################################
#########


def modifyInputFiles(initA, srA1, accelA, srA2, initB, srB, inputFile, output-
File):
    """
    take Pecube input files and modify parameters based on
    the loop inputs from main script
    """
    #print 'writing input files'

    paramLineFaultA1 = 35  #line numbers for fault inputs

    paramLineFaultA2 = 36

    paramLineFaultB = 58

    # modifications to fault A1
    datamod1 = '{} '.format(initA)
    datamod2 = '{} '.format(accelA)
    datamod3 = '{} \n'.format(srA1)

    # modifications to fault A2
    datamod4 = '{} '.format(accelA)
    datamod5 = '0. '
    datamod6 = '{} \n'.format(srA2)

    # modifications to fault B
    datamod7 = '{} '.format(initB)
    datamod8 = '0. '
```

258

```python
    datamod9 = '{} \n'.format(srB)


    start_point = 0    # start_point = len('-1.00 -1.00 -1.00 ')

    inputFile = open(inputFile, 'r')

    outputFile = open(outputFile, 'w+')

    lineno = 0                 # line tracker

    while 1:

        line = inputFile.readline()  # grab a line

        if not line: break      # end of file reached

        lineno = lineno + 1          # current working line

        if lineno == paramLineFaultA1:     # are we there yet?

            # here's the working bit that makes the sustitution.

            modifiedline = line[:start_point] + datamod1 + datamod2 + datamod3

            outputFile.write(modifiedline)

        elif lineno == paramLineFaultA2:

            modifiedline = line[:start_point] + datamod4 + datamod5 + datamod6

            outputFile.write(modifiedline)

        elif lineno == paramLineFaultB:

            modifiedline = line[:start_point] + datamod7 + datamod8 + datamod9

            outputFile.write(modifiedline)

        else:

            outputFile.write(line)       # copy line as it is into temp file


    inputFile.close()                    # done with it.

    outputFile.close()                   # rename afterward with the original
name

    #print 'done writing'

    #return(inputFile, outputFile)


#################################################################################
#######

def renameFaultParams(inputFile, outputFile):
    """
    replace old inputfile with new outputfile via calling bash
    """
    #print 'replacing files'
    subprocess.call("cp {} {}".format(outputFile, inputFile), shell=True)
```

```python
        #print 'done'


###########################################################################
####

def runPecube():

    #print 'running Pecube'
    subprocess.call("bin/Pecube", shell=True)
    #print 'done with Pecube'


###########################################################################
###

def save_output(comparison_file, initA, srA1, accelA, srA2, initB, srB):

    #print 'saving output'

    out_name = '/home/picloud/src/Pecube/nmtN5/pred_{}_{}_{}_{}_{}_{}.txt'.
format(initA,
        srA1, accelA, srA2, initB, srB)

    file_out = open(out_name, 'w+')

    comparison_file = open(comparison_file, 'r')

    lines = comparison_file.readlines()

    comparison_file.close()

    new_file = open('/home/picloud/src/Pecube/nmtN5/new_file2.txt', 'w+')

    new_file.writelines([item for item in lines[1:]])

    new_file.close()

    new_file = open('/home/picloud/src/Pecube/nmtN5/new_file2.txt', 'r')

    column = 9

    for line in new_file:

        line = line.strip()
        sline = line.split()
        file_out.write(sline[column] + '\n')

    new_file.close()

    file_out.close()

    #print 'done'

    return out_name



###########################################################################
###

def calc_chi_square(obs, out_name):
```

260

```python
    #print 'calculating chi square misfit'

    zHe_predicted = nmp.loadtxt(open(out_name))

    zHe_observed = nmp.loadtxt(open(obs))

    chi_square = sum((zHe_observed - zHe_predicted)**2 / zHe_observed) / 7

    #print 'done'

    return chi_square

###########################################################################
###


def append_info(out_name, chi_square, initA, srA1, accelA, srA2, initB, srB,
netExtension):

    #print 'making numpy matrices'

    in_array = nmp.loadtxt(open(out_name))

    out_array = '/home/picloud/src/Pecube/nmtN5/run_{}_{}_{}_{}_{}_{}.npy'.
format(initA,
        srA1, accelA, srA2, initB, srB)

    nmp.save(out_array, in_array)

    out_array_temp = nmp.load(out_array)

    out_array_temp = nmp.append(out_array_temp, [initA, srA1, accelA, srA2,
initB, srB, chi_square, netExtension])

    nmp.save(out_array, out_array_temp)

    cloud.files.put(out_array)

    return out_array

    #print 'done'

###########################################################################
###

def change_directory():
    subprocess.call("cd /home/picloud/src/Pecube", shell=True)
    directory = subprocess.call("pwd", shell=True)
    print directory


###########################################################################
###

def change_dir_python():
    os.chdir('/home/picloud/src/Pecube')


###########################################################################
###

def mkdir_test(test_dir):
    subprocess.call('mkdir {}'.format(test_dir), shell=True)
```

```
##########################################################################
###

#def dir_list(natty_path):

def run_pecube_cloud():
     #os.chdir('/home/picloud/src/Pecube')
     pecube_print = subprocess.check_output("cd /home/picloud/src/Pecube &&
bin/Pecube", shell=True)
     return pecube_print

##########################################################################
###

def dir_list():
     os.chdir('/home/picloud/src/Pecube/input/')
     dirlist = os.listdir(os.getcwd() )
     return dirlist
```

run_nmt_picloud.py

```python
#!/usr/bin/env python

import sys
sys.path.append('/home/itchy/python_scripts')
import os, cloud, subprocess, time
import pecube_cloud_scripts as psc
reload(psc)

# important files
inputFile = '/home/picloud/src/Pecube/input/fault_parameters.txt'

outputFile = '/home/picloud/src/Pecube/input/fault_parameters.txt.out'

comparison_file = '/home/picloud/src/Pecube/nmtN5/Comparison.txt'

obs = '/home/picloud/src/Pecube/nmtN5/obs.txt'

# fault parameters

initFaultAs = [9.0] #, 10.0, 11.0, 12.0, 13.0, 14.0, 15.0, 16.0, 17.0, 18.0,
19.0, 20.0]

#initFaultAs = [12.0, 9.0]

accelFaultAs = [2.0, 2.5, 3.0, 3.5, 4.0, 4.5, 5.0, 5.5, 6.0, 6.5]

#accelFaultAs = [2.0]

slipRate1FaultAs = [0.25, 0.5, 1.0, 1.5, 2.0, 2.5, 3.0, 3.5]

slipRate2FaultAs = [1.5, 2.0, 2.5, 3.0, 3.5, 4.0, 4.5, 5]

initFaultBs = [10.0, 12.0, 14.0, 16.0, 18.0, 20.0]

slipRateFaultBs = [0.5, 1.0, 1.5, 2.0]

# define constants (dipFaultA, dipFaultB)

dipFaultA = [0.4]

dipFaultB = [0.88]

#     define list of variable lists
faultParamsList = [[j, k, l, m, n, o] for j in initFaultAs for k in accelFaul-
tAs for l in slipRate1FaultAs for m in slipRate2FaultAs for n in initFaultBs
for o in slipRateFaultBs]


faultParamsListFiltered = []

for faultParams in faultParamsList:

    [initA, accelA, srA1, srA2, initB, srB] = faultParams

    netExtension = psc.calcNetExtension(initA, srA1, accelA, srA2, dip-
FaultA, initB, srB, dipFaultB)

#print netExtension

    if netExtension < 20:
        if netExtension > 12:
```

```
                faultParamsListFiltered.append(faultParams)

print len(faultParamsListFiltered)

def run_pecube_map(faultParamsListFiltered):
        [initA, accelA, srA1, srA2, initB, srB] = faultParamsListFiltered

        netExtension = psc.calcNetExtension(initA, srA1, accelA, srA2, dip-
FaultA, initB, srB, dipFaultB)
#       test for amount of extension (maybe do this with a filter function
#       or something similar when making the variable list)

#       modify input files,
        psc.modifyInputFiles(initA, srA1, accelA, srA2, initB, srB, inputFile,
outputFile)

        #rename fault parameters
        psc.renameFaultParams(inputFile, outputFile)

#       run pecube
        pecube_print = psc.run_pecube_cloud()

#       save output
        out_name = psc.save_output(comparison_file, initA, srA1, accelA, srA2,
initB, srB)

#       calculate chi square
        chi_square = psc.calc_chi_square(obs, out_name)

#       append results to results file(s)
        out_array = psc.append_info(out_name, chi_square, initA, srA1, accelA,
srA2, initB, srB, netExtension)

        #cloud.files.get(out_array, '/home/itchy/src/Pecube/picloud/results/
nmtN5/{}'.format(out_array))

        return pecube_print


t0 = time.time()

pecube_nmt_11 = cloud.map(run_pecube_map, faultParamsListFiltered, _
env='natty_itchy_pecube', _type='c2')



cloud.result(pecube_nmt_u20)

numpy_results_list = cloud.files.list()


print 'Pecube took', time.time() - t0, 'seconds for',
len(faultParamsListFiltered), 'runs'



for numpy_result in numpy_results_list:
        cloud.files.get(numpy_result, '/home/itchy/src/Pecube/picloud/results/
nmtN5/{}'.format(numpy_result))
```

Appendix 3: Chapter 5 Pecube input files

fault_parameters.txt.nlrT1

```
$ number of faults active at any time during the run
$2
1

$ fault 1
$ two points (in longitude-latitude) defining the y axis of the
$ coordinate system used to define the faults
$ the x-axis is to the right of the y-axis

$0. 0.8 0.002 0.8

83.5749 31.733 83.5525 31.5485


$ number of points defining fault
5

$ segment (x,y) coordinates
$-10 8.3
$-8. 8.
-30. -20.
-15. -4.
-10. 1.
0. 5.1
5. 5.85




$ number of time intervals to define its motion story
2


$ time interval (in geological time) and velocity
$ thrust is negative, normal is positive
18. 0.5 3.0
0.5 0. 4.0




$$$$$$$$$$$$$$$$$$$$$$$$$$$$$$$$$$$$$$$$$$$$$$$$$$$$$$$$$$$$$$$$$$$

$fault 2

$ number of points defining fault
$2

$ segment (x,y) coordinates
$-17.5 6.5
$-40. -20.


$ number of time intervals to define its motion story

$1

$ time interval (in geological time) and velocity
$ thrust is negative, normal is positive
$12. 0. 0.5
```

266

topo_parameters.txt.nlrT1

```
$ this is the input file for Pecube
$ you can add as many comment lines as you wish as long as they start with a
dollar sign
$
$ (1) the name of the run (also the name of the folder in which the solution
is stored)
$ should be 5 letter long
nlrT1

$ (2) the name of the topography file used (if the name is Nil topo is assume
to be flat)
$     Otherwise the file should contain nx by ny points (see below) defining the
topography in meters
$     Note that the evolution of this topography (in amplitude and offset)
will be allowed to
$     change through time
$     If the name of the file ends with a slash "/", then Pecube will assume it
is a directory
$     in which a series of topo files (in meters) are to be stored (one per
time step), named topo0, topo1, etc
$     Pecube will also expect to find uplift rate files, named uplift0, uplift1,
etc in which an
$     uplift rate value (in km/Myr) will be stored for each location; similary
a set of surface
$     temperature files will be expected, named temp0, temp1, etc in °C
$     When this second option is activated, the topography amplification and
offset factors are not used
$     if the number of points in the longitude and latitude directions (next
input line)  are negative, the number of points in the
$     longitude direction (nx) will in fact correspond to the total number of
points; the points defining
$     the topography will be assumed to be randomly distributed (not on a
rectangular grid);
$     the number of points in the latitude direction (ny) will contain the
number of triangles connecting
$     the randomly distributed points.
$     the topography file should then contain nx triplets of longitude, lati-
tude and height of each point
$     followed by ny triplets of integer numbers between 1 and nx giving the
triangular connectivity
nlrT1_dem.dat

$ (3) the number of points in the longitude and latitude directions, respec-
tively
$     if they are negative, they correspond to the total number of points and
the number of triangles connecting them
1501 49

$ (4) the spacing in degrees of longitude and latitude, respectively
$     This is not used in case nx and ny are negative (random grid)
0.00083 0.00083

$ (5) a skipping factor (1 means all points of the topography are used; 2
means that
$     every second point is used etc). Note that nx, ny AND nskip define the
resolution of the
$     finite element grid in the horizontal directions
$     again this is not used in case nx and ny are negative (random grid)
10

$ (6) the longitude and latitude of the bottom left corner of the topo file
82.999166666667 31.609583430181
```

```
$ (7) the number of time steps in the tectonomorphic scenario
1

$ (8) the erosional time scale (exponential decay rate of topography)
0.

$ (9) for each time step +1:
$ (a) a starting time (in Myr in the past)
$ (b) an amplification factor for the topography
$ (c) an offset factor (in km),
$ (d) an output flag (for this time step: 0=no output / 1=output)
$20. 1. 0. 1
20. 1. 0. 1
0. 1. 0. 1

$ (10) a flag for isostasy (1 isostasy on; 0 isostast off)
$ crustal density (in kg/m3), mantle density (kg/m3), Young modulus (in Pa),
poisson's
$ ratio, elastic plate thickness (in km), size of the FFT grid for elastic re-
bound
$ calculations (typically 1024 1024 but must be a power of 2)
0, 2700.,3200.,1.d11,0.25,28.8,1024,1024

$ (11) the model thickness (in km), number of points in the z direction, ther-
mal diffusivity in km2/Myr,
$ temperature at the base of the model (in C), temperature at z=0 (in C), at-
mospheric lapse rate (in
$ C/km), heat production in C/My
80.,25,25.,1200.,0.,0.,20.

$ (12) name of the file containing the thermochronological data
$ if Nil no date
$ otherwise it should contain the number of data points (locations)
$ for each location a line containing sample longitude, latitude, elevation
$ as well as Apatite He age, error in age, Apatite FT age, error in age
$ with a negative age corresponding to a non-existing age
nlrT1_thermo_data_prz.txt

$ (13) the default age (in Myr) for rocks that never reach the closure tem-
perature, a flag to decide which
$ apatite FT routine to use (0 = van der Beek or 1 = Ketcham), a flag to decide
whether (flag=0) to use the absolute
$ age difference (between observed and predicted ages) to construct the misfit
function or (flag=1) the difference in
$ the slope of the age-elevation relationship (for each system), a flag to de-
cide whether (flag=0) the faults'geometry
$ is updated due to the movement on other faults or (flag=1) not, a friction
coefficient to use in the formula for shear heating
$ (friction=0 means no shear heating)
30. 0 0 0 0.

$ (14) a series of 9 flags to determine which age (system) has to be computed
from the thermal histories
$ computed in Pecube
1 1 1 1 1 1 1 1 1
$0 0 0 0 0 0 0 0 0
```

nlrT1_thermo_data_prz.txt

```
10

83.50081    31.64325    5896  3.830 0.441 -9999 -9999 3.758 0.372 -9999 -9999
-9999 -9999 -9999 -9999 -9999 -9999 -9999 -9999 -1 -1 -1 -1 -1 -1 -1 -1 -1 -1
-1 -1 -1 -1 -1 -1 -1 -1 -1 -1 -1 -1 -1 -1 -1 -1 -1 -1 -1 -1 -1 -1
83.50126    31.64263    5800  3.789 0.769 -9999 -9999 5.557 1.177 -9999 -9999
-9999 -9999 -9999 -9999 -9999 -9999 -9999 -9999 -1 -1 -1 -1 -1 -1 -1 -1 -1 -1
-1 -1 -1 -1 -1 -1 -1 -1 -1 -1 -1 -1 -1 -1 -1 -1 -1 -1 -1 -1 -1 -1
83.50899    31.64332    5726  3.205 0.549 -9999 -9999 3.979 0.470 -9999 -9999
-9999 -9999 -9999 -9999 -9999 -9999 -9999 -9999 -1 -1 -1 -1 -1 -1 -1 -1 -1 -1
-1 -1 -1 -1 -1 -1 -1 -1 -1 -1 -1 -1 -1 -1 -1 -1 -1 -1 -1 -1 -1 -1
83.51051    31.64355    5708  2.717 0.434 -9999 -9999 4.376 0.350 -9999 -9999
-9999 -9999 -9999 -9999 -9999 -9999 -9999 -9999 -1 -1 -1 -1 -1 -1 -1 -1 -1 -1
-1 -1 -1 -1 -1 -1 -1 -1 -1 -1 -1 -1 -1 -1 -1 -1 -1 -1 -1 -1 -1 -1
83.51208    31.64389    5687  2.694 1.173 -9999 -9999 3.765 0.301 -9999 -9999
-9999 -9999 -9999 -9999 -9999 -9999 -9999 -9999 -1 -1 -1 -1 -1 -1 -1 -1 -1 -1
-1 -1 -1 -1 -1 -1 -1 -1 -1 -1 -1 -1 -1 -1 -1 -1 -1 -1 -1 -1 -1 -1
83.52605    31.61937    5386  -9999 -9999 -9999 -9999 3.923 0.322 -9999 -9999
-9999 -9999 -9999 -9999 -9999 -9999 -9999 -9999 -1 -1 -1 -1 -1 -1 -1 -1 -1 -1
-1 -1 -1 -1 -1 -1 -1 -1 -1 -1 -1 -1 -1 -1 -1 -1 -1 -1 -1 -1 -1 -1
83.53837    31.61040    5199  1.770 0.100 -9999 -9999 3.498 0.321 -9999 -9999
-9999 -9999 -9999 -9999 -9999 -9999 -9999 -9999 -1 -1 -1 -1 -1 -1 -1 -1 -1 -1
-1 -1 -1 -1 -1 -1 -1 -1 -1 -1 -1 -1 -1 -1 -1 -1 -1 -1 -1 -1 -1 -1
83.48471    31.62615    5842  -9999 -9999 -9999 -9999 -9999 -9999 -9999 -9999
-9999 -9999 -9999 -9999 -9999 -9999 -9999 -9999 -1 -1 -1 -1 -1 -1 -1 -1 -1 -1
-1 -1 -1 -1 -1 -1 -1 -1 -1 -1 -1 -1 -1 -1 -1 -1 -1 -1 -1 -1 -1 -1
83.47056    31.62710    6021  -9999 -9999 -9999 -9999 -9999 -9999 -9999 -9999
-9999 -9999 -9999 -9999 -9999 -9999 -9999 -9999 -1 -1 -1 -1 -1 -1 -1 -1 -1 -1
-1 -1 -1 -1 -1 -1 -1 -1 -1 -1 -1 -1 -1 -1 -1 -1 -1 -1 -1 -1 -1 -1
83.45203    31.63095    6222  -9999 -9999 -9999 -9999 -9999 -9999 -9999 -9999
-9999 -9999 -9999 -9999 -9999 -9999 -9999 -9999 -1 -1 -1 -1 -1 -1 -1 -1 -1 -1

-1 -1 -1 -1 -1 -1 -1 -1 -1 -1 -1 -1 -1 -1 -1 -1 -1 -1 -1 -1 -1 -1 -1
```

fault_parameters.txt.nlrT2

```
$ number of faults active at any time during the run
$2
1

$ fault 1
$ two points (in longitude-latitude) defining the y axis of the
$ coordinate system used to define the faults
$ the x-axis is to the right of the y-axis

$0. 0.8 0.002 0.8
83.54 31.596 83.54 31.56

$ number of points defining fault
6


$ segment (x,y) coordinates


$-10 8.3
$-8. 8.
-30. -21.
-12. -2.25
-5. 2.8
0. 5.35
5. 7.
5.1 7.


$ number of time intervals to define its motion story
2


$ time interval (in geological time) and velocity
$ thrust is negative, normal is positive
8.8 4.0 1.5
4.0 0. 3.0



$$$$$$$$$$$$$$$$$$$$$$$$$$$$$$$$$$$$$$$$$$$$$$$$$$$$$$$$$$$$$$$

$fault 2

$ number of points defining fault
$2

$ segment (x,y) coordinates
$-17.5 6.5
$-40. -20.


$ number of time intervals to define its motion story

$1

$ time interval (in geological time) and velocity
$ thrust is negative, normal is positive
$12. 0. 0.5
```

topo_parameters.txt.nlrT2

```
$ this is the input file for Pecube
$ you can add as many comment lines as you wish as long as they start with a
dollar sign
$
$ (1) the name of the run (also the name of the folder in which the solution
is stored)
$ should be 5 letter long
nlrT2

$ (2) the name of the topography file used (if the name is Nil topo is assume
to be flat)
$      Otherwise the file should contain nx by ny points (see below) defining the
topography in meters
$      Note that the evolution of this topography (in amplitude and offset)
will be allowed to
$      change through time
$      If the name of the file ends with a slash "/", then Pecube will assume it
is a directory
$      in which a series of topo files (in meters) are to be stored (one per
time step), named topo0, topo1, etc
$      Pecube will also expect to find uplift rate files, named uplift0, uplift1,
etc in which an
$      uplift rate value (in km/Myr) will be stored for each location; similary
a set of surface
$      temperature files will be expected, named temp0, temp1, etc in °C
$      When this second option is activated, the topography amplification and
offset factors are not used
$      if the number of points in the longitude and latitude directions (next
input line)  are negative, the number of points in the
$      longitude direction (nx) will in fact correspond to the total number of
points; the points defining
$      the topography will be assumed to be randomly distributed (not on a
rectangular grid);
$      the number of points in the latitude direction (ny) will contain the
number of triangles connecting
$      the randomly distributed points.
$      the topography file should then contain nx triplets of longitude, lati-
tude and height of each point
$      followed by ny triplets of integer numbers between 1 and nx giving the
triangular connectivity
nlrT2_dem.dat

$ (3) the number of points in the longitude and latitude directions, respec-
tively
$      if they are negative, they correspond to the total number of points and
the number of triangles connecting them
1501 41

$ (4) the spacing in degrees of longitude and latitude, respectively
$      This is not used in case nx and ny are negative (random grid)
0.00083 0.00083

$ (5) a skipping factor (1 means all points of the topography are used; 2
means that
$      every second point is used etc). Note that nx, ny AND nskip define the
resolution of the
$      finite element grid in the horizontal directions
$      again this is not used in case nx and ny are negative (random grid)
10

$ (6) the longitude and latitude of the bottom left corner of the topo file
82.999166666667 31.561250096847
```

```
$ (7) the number of time steps in the tectonomorphic scenario
1

$ (8) the erosional time scale (exponential decay rate of topography)
0.

$ (9) for each time step +1:
$ (a) a starting time (in Myr in the past)
$ (b) an amplification factor for the topography
$ (c) an offset factor (in km),
$ (d) an output flag (for this time step: 0=no output / 1=output)
$20. 1. 0. 1
12. 1. 0. 1
0. 1. 0. 1

$ (10) a flag for isostasy (1 isostasy on; 0 isostast off)
$ crustal density (in kg/m3), mantle density (kg/m3), Young modulus (in Pa),
poisson's
$ ratio, elastic plate thickness (in km), size of the FFT grid for elastic re-
bound
$ calculations (typically 1024 1024 but must be a power of 2)
0, 2700.,3200.,1.d11,0.25,28.8,1024,1024

$ (11) the model thickness (in km), number of points in the z direction, ther-
mal diffusivity in km2/Myr,
$ temperature at the base of the model (in C), temperature at z=0 (in C), at-
mospheric lapse rate (in
$ C/km), heat production in C/My
80.,25,25.,1200.,0.,0.,20.

$ (12) name of the file containing the thermochronological data
$ if Nil no date
$ otherwise it should contain the number of data points (locations)
$ for each location a line containing sample longitude, latitude, elevation
$ as well as Apatite He age, error in age, Apatite FT age, error in age
$ with a negative age corresponding to a non-existing age
nlrT2_thermo_data_prz.txt

$ (13) the default age (in Myr) for rocks that never reach the closure tem-
perature, a flag to decide which
$ apatite FT routine to use (0 = van der Beek or 1 = Ketcham), a flag to decide
whether (flag=0) to use the absolute
$ age difference (between observed and predicted ages) to construct the misfit
function or (flag=1) the difference in
$ the slope of the age-elevation relationship (for each system), a flag to de-
cide whether (flag=0) the faults'geometry
$ is updated due to the movement on other faults or (flag=1) not, a friction
coefficient to use in the formula for shear heating
$ (friction=0 means no shear heating)
30. 0 0 0 0.

$ (14) a series of 9 flags to determine which age (system) has to be computed
from the thermal histories
$ computed in Pecube
1 1 0 0 0 0 0 0 0
$0 0 0 0 0 0 0 0 0
```

nlrT2_thermo_data_prz.txt

18

```
83.53970     31.57835     5130  0.480 0.090 -9999 -9999 3.369 0.269 -9999 -9999
-9999 -9999 -9999 -9999 -9999 -9999 -9999 -9999 -1 -1 -1 -1 -1 -1 -1 -1 -1 -1
-1 -1 -1 -1 -1 -1 -1 -1 -1 -1 -1 -1 -1 -1 -1 -1 -1 -1 -1 -1 -1 -1
83.53848     31.57872     5147  0.640 0.100 -9999 -9999 4.774 1.710 -9999 -9999
-9999 -9999 -9999 -9999 -9999 -9999 -9999 -9999 -1 -1 -1 -1 -1 -1 -1 -1 -1 -1
-1 -1 -1 -1 -1 -1 -1 -1 -1 -1 -1 -1 -1 -1 -1 -1 -1 -1 -1 -1 -1 -1
83.53556     31.57888     5174  2.065 0.974 -9999 -9999 2.657 0.212 -9999 -9999
-9999 -9999 -9999 -9999 -9999 -9999 -9999 -9999 -1 -1 -1 -1 -1 -1 -1 -1 -1 -1
-1 -1 -1 -1 -1 -1 -1 -1 -1 -1 -1 -1 -1 -1 -1 -1 -1 -1 -1 -1 -1 -1
83.53150     31.57873     5217  0.000 0.000 -9999 -9999 3.322 0.681 -9999 -9999
-9999 -9999 -9999 -9999 -9999 -9999 -9999 -9999 -1 -1 -1 -1 -1 -1 -1 -1 -1 -1
-1 -1 -1 -1 -1 -1 -1 -1 -1 -1 -1 -1 -1 -1 -1 -1 -1 -1 -1 -1 -1 -1
83.54194     31.58077     5226  0.000 0.000 -9999 -9999 3.202 0.256 -9999 -9999
-9999 -9999 -9999 -9999 -9999 -9999 -9999 -9999 -1 -1 -1 -1 -1 -1 -1 -1 -1 -1
-1 -1 -1 -1 -1 -1 -1 -1 -1 -1 -1 -1 -1 -1 -1 -1 -1 -1 -1 -1 -1 -1
83.54046     31.57922     5235  0.000 0.000 -9999 -9999 3.441 0.275 -9999 -9999
-9999 -9999 -9999 -9999 -9999 -9999 -9999 -9999 -1 -1 -1 -1 -1 -1 -1 -1 -1 -1
-1 -1 -1 -1 -1 -1 -1 -1 -1 -1 -1 -1 -1 -1 -1 -1 -1 -1 -1 -1 -1 -1
83.54036     31.57914     5237  0.000 0.000 -9999 -9999 3.148 0.331 -9999 -9999
-9999 -9999 -9999 -9999 -9999 -9999 -9999 -9999 -1 -1 -1 -1 -1 -1 -1 -1 -1 -1
-1 -1 -1 -1 -1 -1 -1 -1 -1 -1 -1 -1 -1 -1 -1 -1 -1 -1 -1 -1 -1 -1
83.53745     31.57916     5267  0.000 0.000 -9999 -9999 2.819 0.750 -9999 -9999
-9999 -9999 -9999 -9999 -9999 -9999 -9999 -9999 -1 -1 -1 -1 -1 -1 -1 -1 -1 -1
-1 -1 -1 -1 -1 -1 -1 -1 -1 -1 -1 -1 -1 -1 -1 -1 -1 -1 -1 -1 -1 -1
83.53473     31.57905     5287  2.972 1.669 -9999 -9999 2.746 0.405 -9999 -9999
-9999 -9999 -9999 -9999 -9999 -9999 -9999 -9999 -1 -1 -1 -1 -1 -1 -1 -1 -1 -1
-1 -1 -1 -1 -1 -1 -1 -1 -1 -1 -1 -1 -1 -1 -1 -1 -1 -1 -1 -1 -1 -1
83.53054     31.57872     5377  0.000 0.000 -9999 -9999 3.417 1.153 -9999 -9999
-9999 -9999 -9999 -9999 -9999 -9999 -9999 -9999 -1 -1 -1 -1 -1 -1 -1 -1 -1 -1
-1 -1 -1 -1 -1 -1 -1 -1 -1 -1 -1 -1 -1 -1 -1 -1 -1 -1 -1 -1 -1 -1
83.53264     31.57869     5382  0.000 0.000 -9999 -9999 2.343 0.507 -9999 -9999
-9999 -9999 -9999 -9999 -9999 -9999 -9999 -9999 -1 -1 -1 -1 -1 -1 -1 -1 -1 -1
-1 -1 -1 -1 -1 -1 -1 -1 -1 -1 -1 -1 -1 -1 -1 -1 -1 -1 -1 -1 -1 -1
83.52932     31.57882     5389  0.000 0.000 -9999 -9999 3.032 0.599 -9999 -9999
-9999 -9999 -9999 -9999 -9999 -9999 -9999 -9999 -1 -1 -1 -1 -1 -1 -1 -1 -1 -1
-1 -1 -1 -1 -1 -1 -1 -1 -1 -1 -1 -1 -1 -1 -1 -1 -1 -1 -1 -1 -1 -1
83.51840     31.57966     5418  0.000 0.000 -9999 -9999 3.134 1.099 -9999 -9999
-9999 -9999 -9999 -9999 -9999 -9999 -9999 -9999 -1 -1 -1 -1 -1 -1 -1 -1 -1 -1
-1 -1 -1 -1 -1 -1 -1 -1 -1 -1 -1 -1 -1 -1 -1 -1 -1 -1 -1 -1 -1 -1
83.52893     31.57873     5420  0.000 0.000 -9999 -9999 3.069 0.245 -9999 -9999
-9999 -9999 -9999 -9999 -9999 -9999 -9999 -9999 -1 -1 -1 -1 -1 -1 -1 -1 -1 -1
-1 -1 -1 -1 -1 -1 -1 -1 -1 -1 -1 -1 -1 -1 -1 -1 -1 -1 -1 -1 -1 -1
83.51008     31.57996     5509  3.722 2.668 -9999 -9999 5.045 2.240 -9999 -9999
-9999 -9999 -9999 -9999 -9999 -9999 -9999 -9999 -1 -1 -1 -1 -1 -1 -1 -1 -1 -1
-1 -1 -1 -1 -1 -1 -1 -1 -1 -1 -1 -1 -1 -1 -1 -1 -1 -1 -1 -1 -1 -1
83.50900     31.58100     5688  0.000 0.000 -9999 -9999 6.500 3.000 -9999 -9999
-9999 -9999 -9999 -9999 -9999 -9999 -9999 -9999 -1 -1 -1 -1 -1 -1 -1 -1 -1 -1
-1 -1 -1 -1 -1 -1 -1 -1 -1 -1 -1 -1 -1 -1 -1 -1 -1 -1 -1 -1 -1 -1
83.50200     31.58400     5833  0.000 0.000 -9999 -9999 7.500 3.000 -9999 -9999
-9999 -9999 -9999 -9999 -9999 -9999 -9999 -9999 -1 -1 -1 -1 -1 -1 -1 -1 -1 -1
-1 -1 -1 -1 -1 -1 -1 -1 -1 -1 -1 -1 -1 -1 -1 -1 -1 -1 -1 -1 -1 -1
83.47600     31.58700     6198  0.000 0.000 -9999 -9999 9.500 3.500 -9999 -9999
-9999 -9999 -9999 -9999 -9999 -9999 -9999 -9999 -1 -1 -1 -1 -1 -1 -1 -1 -1 -1
-1 -1 -1 -1 -1 -1 -1 -1 -1 -1 -1 -1 -1 -1 -1 -1 -1 -1 -1 -1 -1 -1
```

fault_parameters.txt.nlrT3

```
$ number of faults active at any time during the run
$2
1

$ fault 1
$ two points (in longitude-latitude) defining the y axis of the
$ coordinate system used to define the faults
$ the x-axis is to the right of the y-axis

$0. 0.8 0.002 0.8
83.57 31.50 83.57 31.46


$ number of points defining fault
6

$ segment (x,y) coordinates
$-10 8.3
$-8. 8.
-30. -20.
-15. -4.
-10. 1.
0. 5.2
5.8 6.35
7.1 6.5




$ number of time intervals to define its motion story
2


$ time interval (in geological time) and velocity
$ thrust is negative, normal is positive
10. 3.5 0.5
3.5 0. 3.0



$$$$$$$$$$$$$$$$$$$$$$$$$$$$$$$$$$$$$$$$$$$$$$$$$$$$$$$$$$$$$$$$$$$

$fault 2

$ number of points defining fault
$2

$ segment (x,y) coordinates
$-17.5 6.5
$-40. -20.


$ number of time intervals to define its motion story

$1

$ time interval (in geological time) and velocity
$ thrust is negative, normal is positive
$12. 0. 0.5
```

topo_parameters.txt.nlrT3

```
$ this is the input file for Pecube
$ you can add as many comment lines as you wish as long as they start with a
dollar sign
$
$ (1) the name of the run (also the name of the folder in which the solution
is stored)
$ should be 5 letter long
nlrT3

$ (2) the name of the topography file used (if the name is Nil topo is assume
to be flat)
$     Otherwise the file should contain nx by ny points (see below) defining the
topography in meters
$     Note that the evolution of this topography (in amplitude and offset)
will be allowed to
$     change through time
$     If the name of the file ends with a slash "/", then Pecube will assume it
is a directory
$     in which a series of topo files (in meters) are to be stored (one per
time step), named topo0, topo1, etc
$     Pecube will also expect to find uplift rate files, named uplift0, uplift1,
etc in which an
$     uplift rate value (in km/Myr) will be stored for each location; similary
a set of surface
$     temperature files will be expected, named temp0, temp1, etc in °C
$     When this second option is activated, the topography amplification and
offset factors are not used
$     if the number of points in the longitude and latitude directions (next
input line)  are negative, the number of points in the
$     longitude direction (nx) will in fact correspond to the total number of
points; the points defining
$     the topography will be assumed to be randomly distributed (not on a
rectangular grid);
$     the number of points in the latitude direction (ny) will contain the
number of triangles connecting
$     the randomly distributed points.
$     the topography file should then contain nx triplets of longitude, lati-
tude and height of each point
$     followed by ny triplets of integer numbers between 1 and nx giving the
triangular connectivity
nlrT3_dem.dat

$ (3) the number of points in the longitude and latitude directions, respec-
tively
$     if they are negative, they correspond to the total number of points and
the number of triangles connecting them
1501 21

$ (4) the spacing in degrees of longitude and latitude, respectively
$     This is not used in case nx and ny are negative (random grid)
0.00083 0.00083

$ (5) a skipping factor (1 means all points of the topography are used; 2
means that
$     every second point is used etc). Note that nx, ny AND nskip define the
resolution of the
$     finite element grid in the horizontal directions
$     again this is not used in case nx and ny are negative (random grid)
10

$ (6) the longitude and latitude of the bottom left corner of the topo file
82.999166666667 31.474583430181
```

```
$ (7) the number of time steps in the tectonomorphic scenario
1

$ (8) the erosional time scale (exponential decay rate of topography)
0.

$ (9) for each time step +1:
$ (a) a starting time (in Myr in the past)
$ (b) an amplification factor for the topography
$ (c) an offset factor (in km),
$ (d) an output flag (for this time step: 0=no output / 1=output)
$20. 1. 0. 1
20. 1. 0. 1
0. 1. 0. 1

$ (10) a flag for isostasy (1 isostasy on; 0 isostast off)
$ crustal density (in kg/m3), mantle density (kg/m3), Young modulus (in Pa),
poisson's
$ ratio, elastic plate thickness (in km), size of the FFT grid for elastic re-
bound
$ calculations (typically 1024 1024 but must be a power of 2)
0, 2700.,3200.,1.d11,0.25,28.8,1024,1024

$ (11) the model thickness (in km), number of points in the z direction, ther-
mal diffusivity in km2/Myr,
$ temperature at the base of the model (in C), temperature at z=0 (in C), at-
mospheric lapse rate (in
$ C/km), heat production in C/My
80.,25,25.,1200.,0.,0.,20.

$ (12) name of the file containing the thermochronological data
$ if Nil no date
$ otherwise it should contain the number of data points (locations)
$ for each location a line containing sample longitude, latitude, elevation
$ as well as Apatite He age, error in age, Apatite FT age, error in age
$ with a negative age corresponding to a non-existing age
nlrT3_thermo_data_prz.txt

$ (13) the default age (in Myr) for rocks that never reach the closure tem-
perature, a flag to decide which
$ apatite FT routine to use (0 = van der Beek or 1 = Ketcham), a flag to decide
whether (flag=0) to use the absolute
$ age difference (between observed and predicted ages) to construct the misfit
function or (flag=1) the difference in
$ the slope of the age-elevation relationship (for each system), a flag to de-
cide whether (flag=0) the faults'geometry
$ is updated due to the movement on other faults or (flag=1) not, a friction
coefficient to use in the formula for shear heating
$ (friction=0 means no shear heating)
30. 0 0 0 0.

$ (14) a series of 9 flags to determine which age (system) has to be computed
from the thermal histories
$ computed in Pecube
1 1 0 0 0 0 0 0 0
$0 0 0 0 0 0 0 0 0
```

nlrT3_thermo_data.txt

7

```
83.54049      31.48035      5689   -9999 -9999 -9999 -9999 2.524354      0.231194
-9999 -9999 -9999 -9999 -9999 -9999 -9999 -9999 -9999 -9999 -1 -1 -1 -1 -1 -1
-1 -1 -1 -1 -1 -1 -1 -1 -1 -1 -1 -1 -1 -1 -1 -1 -1 -1 -1 -1
-1 -1
83.54921      31.48449      5436   -9999 -9999 -9999 -9999 3.22579      0.258063
-9999 -9999 -9999 -9999 -9999 -9999 -9999 -9999 -9999 -9999 -1 -1 -1 -1 -1 -1
-1 -1 -1 -1 -1 -1 -1 -1 -1 -1 -1 -1 -1 -1 -1 -1 -1 -1 -1 -1
-1 -1
83.55483      31.48523      5335   -9999 -9999 -9999 -9999 2.717082      0.217367
-9999 -9999 -9999 -9999 -9999 -9999 -9999 -9999 -9999 -9999 -1 -1 -1 -1 -1 -1
-1 -1 -1 -1 -1 -1 -1 -1 -1 -1 -1 -1 -1 -1 -1 -1 -1 -1 -1 -1
-1 -1
83.56088      31.48801      5197   -9999 -9999 -9999 -9999 2.791573      0.223326
-9999 -9999 -9999 -9999 -9999 -9999 -9999 -9999 -9999 -9999 -1 -1 -1 -1 -1 -1
-1 -1 -1 -1 -1 -1 -1 -1 -1 -1 -1 -1 -1 -1 -1 -1 -1 -1 -1 -1
-1 -1
83.562        31.48813      5172   -9999 -9999 -9999 -9999 3.524549
1.794247      -9999 -9999 -9999 -9999 -9999 -9999 -9999 -9999 -9999 -9999 -1 -1
-1 -1 -1 -1 -1 -1 -1 -1 -1 -1 -1 -1 -1 -1 -1 -1 -1 -1 -1 -1 -1 -1 -1 -1
-1 -1 -1 -1 -1 -1
83.525        31.482        6036   -9999 -9999 -9999 -9999 0.000 0.000 -9999 -9999
-9999 -9999 -9999 -9999 -9999 -9999 -9999 -9999 -1 -1 -1 -1 -1 -1 -1 -1 -1 -1
-1 -1 -1 -1 -1 -1 -1 -1 -1 -1 -1 -1 -1 -1 -1 -1 -1 -1 -1 -1 -1 -1
83.503        31.483        6309   -9999 -9999 -9999 -9999 0.000 0.000 -9999 -9999
-9999 -9999 -9999 -9999 -9999 -9999 -9999 -9999 -1 -1 -1 -1 -1 -1 -1 -1 -1 -1
-1 -1 -1 -1 -1 -1 -1 -1 -1 -1 -1 -1 -1 -1 -1 -1 -1 -1 -1 -1 -1 -1
```

fault_parameters.txt.nlrT4

```
$ number of faults active at any time during the run
2



$ fault 1
$ two points (in longitude-latitude) defining the y axis of the
$ coordinate system used to define the faults
$ the x-axis is to the right of the y-axis

$0. 0.8 0.002 0.8
83.366 31.630 83.796 31.228



$ number of points defining fault
3

$ segment (x,y) coordinates
$-10 8.3
$-8. 8.
-30. -35.
-15. -12.
$-10. 3.5
0. 4.9
$3. 6.4
$7.1 6.5




$ number of time intervals to define its motion story
2


$ time interval (in geological time) and velocity
$ thrust is negative, normal is positive
5.0 2.5 2.5
2.5 0. 0.5



$$$$$$$$$$$$$$$$$$$$$$$$$$$$$$$$$$$$$$$$$$$$$$$$$$$$$$$$$$$$$$$$

$fault 2

$ number of points defining fault
3

$ segment (x,y) coordinates
19. -10.
8. 4.9
7. 6.25454

$ number of time intervals to define its motion story

2

$ time interval (in geological time) and velocity
$ thrust is negative, normal is positive
10. 4.5 0.0
4.5 0. 0.05
```

278

topo_parameters.txt.nlrT4

```
$ this is the input file for Pecube
$ you can add as many comment lines as you wish as long as they start with a
dollar sign
$
$ (1) the name of the run (also the name of the folder in which the solution
is stored)
$ should be 5 letter long
nlrT4

$ (2) the name of the topography file used (if the name is Nil topo is assume
to be flat)
$     Otherwise the file should contain nx by ny points (see below) defining the
topography in meters
$     Note that the evolution of this topography (in amplitude and offset)
will be allowed to
$     change through time
$     If the name of the file ends with a slash "/", then Pecube will assume it
is a directory
$     in which a series of topo files (in meters) are to be stored (one per
time step), named topo0, topo1, etc
$     Pecube will also expect to find uplift rate files, named uplift0, uplift1,
etc in which an
$     uplift rate value (in km/Myr) will be stored for each location; similary
a set of surface
$     temperature files will be expected, named temp0, temp1, etc in °C
$     When this second option is activated, the topography amplification and
offset factors are not used
$     if the number of points in the longitude and latitude directions (next
input line)  are negative, the number of points in the
$     longitude direction (nx) will in fact correspond to the total number of
points; the points defining
$     the topography will be assumed to be randomly distributed (not on a
rectangular grid);
$     the number of points in the latitude direction (ny) will contain the
number of triangles connecting
$     the randomly distributed points.
$     the topography file should then contain nx triplets of longitude, lati-
tude and height of each point
$     followed by ny triplets of integer numbers between 1 and nx giving the
triangular connectivity
nlrT4_dem.dat

$ (3) the number of points in the longitude and latitude directions, respec-
tively
$     if they are negative, they correspond to the total number of points and
the number of triangles connecting them
1501 37

$ (4) the spacing in degrees of longitude and latitude, respectively
$     This is not used in case nx and ny are negative (random grid)
0.00083 0.00083

$ (5) a skipping factor (1 means all points of the topography are used; 2
means that
$     every second point is used etc). Note that nx, ny AND nskip define the
resolution of the
$     finite element grid in the horizontal directions
$     again this is not used in case nx and ny are negative (random grid)
10

$ (6) the longitude and latitude of the bottom left corner of the topo file
82.999166666667 31.414583430181
```

$ (7) the number of time steps in the tectonomorphic scenario
1

$ (8) the erosional time scale (exponential decay rate of topography)
0.

$ (9) for each time step +1:
$ (a) a starting time (in Myr in the past)
$ (b) an amplification factor for the topography
$ (c) an offset factor (in km),
$ (d) an output flag (for this time step: 0=no output / 1=output)
$20. 1. 0. 1
20. 1. 0. 1
0. 1. 0. 1

$ (10) a flag for isostasy (1 isostasy on; 0 isostast off)
$ crustal density (in kg/m3), mantle density (kg/m3), Young modulus (in Pa),
poisson's
$ ratio, elastic plate thickness (in km), size of the FFT grid for elastic re-
bound
$ calculations (typically 1024 1024 but must be a power of 2)
0, 2700.,3200.,1.d11,0.25,28.8,1024,1024

$ (11) the model thickness (in km), number of points in the z direction, ther-
mal diffusivity in km2/Myr,
$ temperature at the base of the model (in C), temperature at z=0 (in C), at-
mospheric lapse rate (in
$ C/km), heat production in C/My
80.,25,25.,1200.,0.,0.,20.

$ (12) name of the file containing the thermochronological data
$ if Nil no date
$ otherwise it should contain the number of data points (locations)
$ for each location a line containing sample longitude, latitude, elevation
$ as well as Apatite He age, error in age, Apatite FT age, error in age
$ with a negative age corresponding to a non-existing age
nlrT4_thermo_data.txt

$ (13) the default age (in Myr) for rocks that never reach the closure tem-
perature, a flag to decide which
$ apatite FT routine to use (0 = van der Beek or 1 = Ketcham), a flag to decide
whether (flag=0) to use the absolute
$ age difference (between observed and predicted ages) to construct the misfit
function or (flag=1) the difference in
$ the slope of the age-elevation relationship (for each system), a flag to de-
cide whether (flag=0) the faults'geometry
$ is updated due to the movement on other faults or (flag=1) not, a friction
coefficient to use in the formula for shear heating
$ (friction=0 means no shear heating)
30. 0 0 0 0.

$ (14) a series of 9 flags to determine which age (system) has to be computed
from the thermal histories
$ computed in Pecube
1 1 0 0 0 0 0 0 0
$0 0 0 0 0 0 0 0 0

nlrT4_thermo_data.txt

4

```
83.5131     31.4247     5336  3.974 0.238 -9999 -9999 4.637 0.371 -9999 -9999
-9999 -9999 -9999 -9999 -9999 -9999 -9999 -9999 -1 -1 -1 -1 -1 -1 -1 -1 -1 -1
-1 -1 -1 -1 -1 -1 -1 -1 -1 -1 -1 -1 -1 -1 -1 -1 -1 -1 -1 -1 -1 -1
83.5624     31.43495    4971  -9999 -9999 -9999 -9999 4.212 0.705 -9999 -9999
-9999 -9999 -9999 -9999 -9999 -9999 -9999 -9999 -1 -1 -1 -1 -1 -1 -1 -1 -1 -1
-1 -1 -1 -1 -1 -1 -1 -1 -1 -1 -1 -1 -1 -1 -1 -1 -1 -1 -1 -1 -1 -1
83.5598     31.43337    4942  2.912 0.175 -9999 -9999 3.521 0.282 -9999 -9999
-9999 -9999 -9999 -9999 -9999 -9999 -9999 -9999 -1 -1 -1 -1 -1 -1 -1 -1 -1 -1
-1 -1 -1 -1 -1 -1 -1 -1 -1 -1 -1 -1 -1 -1 -1 -1 -1 -1 -1 -1 -1 -1
83.5667     31.43743    4880  2.744 0.233 -9999 -9999 3.425 0.582 -9999 -9999
-9999 -9999 -9999 -9999 -9999 -9999 -9999 -9999 -1 -1 -1 -1 -1 -1 -1 -1 -1 -1
-1 -1 -1 -1 -1 -1 -1 -1 -1 -1 -1 -1 -1 -1 -1 -1 -1 -1 -1 -1 -1 -1
```

Appendix 4: Chapter 5 Python code

n_propagation_mc.py

```python
# -*- coding: utf-8 -*-
"""
Created on Sun Aug 26 22:24:57 2012

@author: Richard
"""

import numpy as nmp
import sys
sys.path.append('C:\\school\\stats\\thinkstats.code')
import Cdf
import matplotlib.pyplot as plt
#import statsmodels.api as sm
from scipy import stats

# values and counts from analysis
nlrT1_accel = dict({'5.':10, '5.5':11})

nlrT2_accel = dict({'3.5':2, '4.5':2})

nlrT3_accell = dict({'2.':3, '2.5':3})

nlrT3_init = dict({'8.':3, '9.':2, '10.':1})

nlrT3_accel = dict(list(nlrT3_accell.items()) + list(nlrT3_init.items()))

nlrT4_accel = dict({'5.':19, '5.5':12, '6.':4})

nmt_accel = dict({'8.':2})

cctr_accel = dict({'10.':7, '11.':6, '12':1, '13.':2, '14.':3, '15.':1})

accel_set = [nlrT1_accel, nlrT2_accel, nlrT3_accel, nlrT4_accel, nmt_accel,
             cctr_accel]
# latitude ranges
nlrT1_lat_range = nmp.array([31.6439, 31.6104])
nlrT1_lat = nmp.mean(nlrT1_lat_range)
nlrT1_lat_err = nmp.abs(nlrT1_lat_range[0] - nlrT1_lat)

nlrT2_lat_range = nmp.array([31.5808, 31.5784])
nlrT2_lat = nmp.mean(nlrT2_lat_range)
nlrT2_lat_err = nmp.abs(nlrT2_lat_range[0] - nlrT2_lat)

nlrT3_lat_range = nmp.array([31.4804, 31.4881])
nlrT3_lat = nmp.mean(nlrT3_lat_range)
nlrT3_lat_err = nmp.abs(nlrT3_lat_range[0] - nlrT3_lat)

nlrT4_lat_range = nmp.array([31.4247, 31.43743])
nlrT4_lat = nmp.mean(nlrT4_lat_range)
nlrT4_lat_err = nmp.abs(nlrT4_lat_range[0] - nlrT4_lat)

nmt_lat_range = nmp.array([31.08, 31.0646])
nmt_lat = nmp.mean(nmt_lat_range)
nmt_lat_err = nmp.abs(nmt_lat_range[0] - nmt_lat)

cctr_lat_range = nmp.array([30.9497, 30.9759])
cctr_lat = nmp.mean(cctr_lat_range)
cctr_lat_err = nmp.abs(cctr_lat_range[0] - cctr_lat)

lat_vec = nmp.array([nlrT1_lat, nlrT2_lat, nlrT3_lat, nlrT4_lat, nmt_lat,
                     cctr_lat])
```

```
lat_err = nmp.array([nlrT1_lat_err, nlrT2_lat_err, nlrT3_lat_err,
                     nlrT4_lat_err, nmt_lat_err, cctr_lat_err])

lat2km = 110.852

lat_km = (lat_vec - cctr_lat_range[0]) * lat2km

lat_km_err = lat_err * lat2km



lat_mat = nmp.vstack([lat_km, nmp.ones(len(lat_vec))]).T




# make cdfs
nlrT1_cdf = Cdf.MakeCdfFromDict(nlrT1_accel, 'nlrT1')
nlrT2_cdf = Cdf.MakeCdfFromDict(nlrT2_accel, 'nlrT2')
nlrT3_cdf = Cdf.MakeCdfFromDict(nlrT3_accel, 'nlrT3')
nlrT4_cdf = Cdf.MakeCdfFromDict(nlrT4_accel, 'nlrT4')
nmt_cdf = Cdf.MakeCdfFromDict(nmt_accel, 'nmt')
cctr_cdf = Cdf.MakeCdfFromDict(cctr_accel, 'cctr')


# monte carlo sampling

n = int(1e2)

# generate n random samples from accel distributions

nlrT1_sample = nmp.array([float(i) for i in nlrT1_cdf.Sample(n)])
nlrT2_sample = nmp.array([float(i) for i in nlrT2_cdf.Sample(n)])
nlrT3_sample = nmp.array([float(i) for i in nlrT3_cdf.Sample(n)])
nlrT4_sample = nmp.array([float(i) for i in nlrT4_cdf.Sample(n)])
nmt_sample = nmp.array([float(i) for i in nmt_cdf.Sample(n)])
cctr_sample = nmp.array([float(i) for i in cctr_cdf.Sample(n)])

accel_mat = nmp.vstack([nlrT1_sample, nlrT2_sample, nlrT3_sample,
                        nlrT4_sample, nmt_sample, cctr_sample])


M, B = nmp.linalg.lstsq(lat_mat, accel_mat)[0]

n_rate_km = (-1/M)# * lat2km

gkde = stats.gaussian_kde(n_rate_km)

pdf_pts = nmp.linspace(5,25, num=15)

n_rate_pdf = gkde.evaluate(pdf_pts)

# India stuff
india_times = nmp.arange(7) * 2

india_tip_now = 31.5

india_n_rate_km_hi = 20. #mm/a
india_n_rate_deg_hi = india_n_rate_km_hi / lat2km

india_n_rate_km_lo = 15. #mm/a
india_n_rate_deg_lo = india_n_rate_km_lo / lat2km
```

284

```python
#india_tip_times = india_tip_now - (india_times * india_n_rate_deg)
india_tip_err = nmp.ones(len(india_times)) * 0.3
india_err = 0.15

india_tip_hi = india_tip_now - (india_times * india_n_rate_deg_lo) + india_err

india_tip_lo = india_tip_now - (india_times * india_n_rate_deg_hi) - india_err


############
# plots

# array with all accel values

nlrT1_a = nmp.array([5., 5.5])
nlrT1_p = nmp.array([10., 11.])
nlrT1_p = nlrT1_p / sum(nlrT1_p)
nlrT1_l = nmp.array([nlrT1_lat, nlrT1_lat])

nlrT2_a = nmp.array([3.5, 4.5])
nlrT2_p = nmp.array([.5, .5])
nlrT2_l = nmp.array([nlrT2_lat, nlrT2_lat])

nlrT3_a = nmp.array([2., 2.5, 8., 9., 10.])
nlrT3_p = nmp.array([3., 3., 3., 2., 1.])
nlrT3_p = nlrT3_p / sum(nlrT3_p)
nlrT3_l = nmp.zeros(5) + nlrT3_lat

nlrT4_a = nmp.array([5., 5.5, 6.])
nlrT4_p = nmp.array([19., 12., 4.])
nlrT4_p = nlrT4_p / sum(nlrT4_p)
nlrT4_l = nmp.zeros(3) + nlrT4_lat

nmt_a = nmp.array([8.])
nmt_p = nmp.array([1.])
nmt_l = nmt_lat

cctr_a = nmp.array([10., 11., 12., 14., 15.])
cctr_p = nmp.array([7., 6., 1., 3., 1.])
cctr_p = cctr_p / sum(cctr_p)
cctr_l = nmp.zeros(5) + cctr_lat


accel_pts_vec = nmp.hstack([nlrT1_a, nlrT2_a, nlrT3_a, nlrT4_a, nmt_a,
cctr_a])
accel_pts_p = nmp.hstack([nlrT1_p, nlrT2_p, nlrT3_p, nlrT4_p, nmt_p, cctr_p])
accel_pts_l = nmp.hstack([nlrT1_l, nlrT2_l, nlrT3_l, nlrT4_l, nmt_l, cctr_l])


plt.figure(1)
#plt.scatter(accel_pts_vec, accel_pts_l, c=accel_pts_p, cmap=plt.cm.gray_r)
#plt.colorbar()
plt.fill_between(india_times, india_tip_hi, india_tip_lo, color='grey')
plt.errorbar(accel_vec, lat_vec, xerr = accel_err, yerr = lat_err, fmt='o',
            color='b')
#plt.errorbar(india_times, india_tip_times, yerr = india_tip_err, fmt='.',
#             color='g')
#plt.errorbar(2.5, 32.75, yerr = 0.5, xerr = 0.5, color='r')
plt.annotate(' o = start of rapid extension', (9.5, 32.15), color='b')
#plt.annotate(' . = India (just the tip)', (9.5, 32.), color='g')
plt.annotate('India (just the tip)', (8, 30.6),  color='grey')
plt.axhline(y=32.36, color='k')
plt.annotate('BNS',(2, 32.2),  color='k')
plt.axhline(y=30.29, color='k')
```

```
plt.annotate('IYS', (2, 30.3),  color='k')

#plt.plot(ww_n_rate * lat_km + ww_const, lat_km, 'r')
#plt.plot(ww_fit_lat, lat_vec, 'r')
plt.xlabel('age (Ma)')
plt.ylabel('latitude')
plt.title('Rapid extension and underthrusting in the western Lhasa block')

plt.figure(2)
plt.plot(pdf_pts, n_rate_pdf)


plt.show()
```

nlr_results_graphs.py

```python
# -*- coding: utf-8 -*-
"""
Created on Sun Aug 26 19:26:07 2012

@author: Richard
"""

import numpy as nmp
import matplotlib.pyplot as plt
#import statsmodels as sm

nlrT1_lat_range = nmp.array([31.6439, 31.6104])
nlrT1_lat = nmp.mean(nlrT1_lat_range)
nlrT1_lat_err = nmp.abs(nlrT1_lat_range[0] - nlrT1_lat)
nlrT1_accel_range = nmp.array([5.,5.5])
nlrT1_accel = nmp.mean(nlrT1_accel_range)
nlrT1_accel_err = nmp.abs(nlrT1_accel_range[0] - nlrT1_accel)
nlrT1_vel = nmp.array([3.15])




nlrT2_lat_range = nmp.array([31.5808, 31.5784])
nlrT2_lat = nmp.mean(nlrT2_lat_range)
nlrT2_lat_err = nmp.abs(nlrT2_lat_range[0] - nlrT2_lat)
nlrT2_accel_range = nmp.array([3.5, 4.5])
nlrT2_accel = nmp.mean(nlrT2_accel_range)
nlrT2_accel_err = nmp.abs(nlrT2_accel_range[0] - nlrT2_accel)
nlrT2_vel = nmp.array([2.5])




nlrT3_lat_range = nmp.array([31.4804, 31.4881])
nlrT3_lat = nmp.mean(nlrT3_lat_range)
nlrT3_lat_err = nmp.abs(nlrT3_lat_range[0] - nlrT3_lat)
nlrT3_accel_range = nmp.array([2.,10.])
nlrT3_accel = nmp.mean(nlrT3_accel_range)
nlrT3_accel_err = nmp.abs(nlrT3_accel_range[0] - nlrT3_accel)
nlrT3_vel = nmp.array([4.5])

nlrT4_lat_range = nmp.array([31.4247, 31.43743])
nlrT4_lat = nmp.mean(nlrT4_lat_range)
nlrT4_lat_err = nmp.abs(nlrT4_lat_range[0] - nlrT4_lat)
nlrT4_accel_range = nmp.array([5.,6.])
nlrT4_accel = nmp.mean(nlrT4_accel_range)
nlrT4_accel_err = nmp.abs(nlrT4_accel_range[0] - nlrT4_accel)
nlrT4_vel = nmp.array([1.8])




nmt_lat_range = nmp.array([31.08, 31.0646])
nmt_lat = nmp.mean(nmt_lat_range)
nmt_lat_err = nmp.abs(nmt_lat_range[0] - nmt_lat)
nmt_accel_range = nmp.array([8.,8.])
nmt_accel = nmp.mean(nmt_accel_range)
nmt_accel_err = nmp.abs(nmt_accel_range[0] - nmt_accel)
nmt_vel = nmp.array([2.8])

cctr_lat_range = nmp.array([30.9497, 30.9759])
cctr_lat = nmp.mean(cctr_lat_range)
cctr_lat_err = nmp.abs(cctr_lat_range[0] - cctr_lat)
cctr_accel_range = nmp.array([10.,15.])
cctr_accel = nmp.mean(cctr_accel_range)
```

```
cctr_accel_err = nmp.abs(cctr_accel_range[0] - cctr_accel)
cctr_vel = nmp.array([1.3])




accel_vec = nmp.array([nlrT1_accel, nlrT2_accel, nlrT3_accel, nlrT4_accel,
                       nmt_accel, cctr_accel])

accel_err = nmp.array([nlrT1_accel_err, nlrT2_accel_err, nlrT3_accel_err,
                       nlrT4_accel_err, nmt_accel_err, cctr_accel_err])

lat_vec = nmp.array([nlrT1_lat, nlrT2_lat, nlrT3_lat, nlrT4_lat, nmt_lat,
                     cctr_lat])

lat_err = nmp.array([nlrT1_lat_err, nlrT2_lat_err, nlrT3_lat_err,
                     nlrT4_lat_err, nmt_lat_err, cctr_lat_err])



lat2km = 110.852

lat_km = (lat_vec - cctr_lat_range[0]) * lat2km
lat_km_err = lat_err * lat2km

#lat_km_const = sm.add_constant(lat_km)
#lat_vec_const = sm.add_constant(lat_vec)

india_times = nmp.arange(7) * 2

india_tip_now = 31.5

india_n_rate_km_hi = 20. #mm/a
india_n_rate_deg_hi = india_n_rate_km_hi / lat2km

india_n_rate_km_lo = 15. #mm/a
india_n_rate_deg_lo = india_n_rate_km_lo / lat2km

#india_tip_times = india_tip_now - (india_times * india_n_rate_deg)
india_tip_err = nmp.ones(len(india_times)) * 0.3
india_err = 0.15

india_tip_hi = india_tip_now - (india_times * india_n_rate_deg_lo) + india_err

india_tip_lo = india_tip_now - (india_times * india_n_rate_deg_hi) - india_err

#accel_vs_lat_wwls = sm.WLS(accel_vec, lat_vec_const, weights=(1/accel_err))
#accel_vs_lat_wfit = accel_vs_lat_wwls.fit()
#ww_n_rate, ww_const = accel_vs_lat_wfit.params

#print ww_n_rate
#ww_n_rate_km = (-1/ww_n_rate) * lat2km

#print 'wwls rate of', ww_n_rate_km, 'mm/a'

#ww_fit_lat = ww_n_rate * lat_vec + ww_const


plt.figure(1)

plt.fill_between(india_times, india_tip_hi, india_tip_lo, color='grey')
plt.errorbar(accel_vec, lat_vec, xerr = accel_err, yerr = lat_err, fmt='o',
             color='b')
#plt.errorbar(india_times, india_tip_times, yerr = india_tip_err, fmt='.',
```

```
#               color='g')
#plt.errorbar(2.5, 32.75, yerr = 0.5, xerr = 0.5, color='r')
plt.annotate(' o = start of rapid extension', (9.5, 32.15), color='b')
#plt.annotate(' . = India (just the tip)', (9.5, 32.), color='g')
plt.annotate('India (just the tip)', (8, 30.6),  color='grey')
plt.axhline(y=32.36, color='k')
plt.annotate('BNS',(2, 32.2),  color='k')
plt.axhline(y=30.29, color='k')
plt.annotate('IYS', (2, 30.3),  color='k')

#plt.plot(ww_n_rate * lat_km + ww_const, lat_km, 'r')
#plt.plot(ww_fit_lat, lat_vec, 'r')
plt.xlabel('age (Ma)')
plt.ylabel('latitude')
plt.axis([0, 16, 30, 32.5])
plt.title('Rapid extension and underthrusting in the western Lhasa block')

plt.show()
```

pecube_scripts_nlrT1.py

```python
#!/usr/bin/env python

import numpy as nmp
import subprocess, os, cloud


def calcNetExtension(initA, accel, srA1, srA2, dipFaultA):
    """
    imports fault slip information and calculates net slip and extension
    """
    # fault A extension
    slipA1 = (initA - accel) * srA1

    slipA2 = accel * srA2

    netSlipA = slipA1 + slipA2

    netExtensionA = netSlipA * nmp.cos(dipFaultA)

    #fault B extension
    #slipB1 = (initB - accel) * srB1

    #slipB2 = accel * srB2

    #netSlipB = slipB1 + slipB2

    #netExtensionB = netSlipB * nmp.cos(dipFaultB)


    # total extension

    netExtension = netExtensionA # + netExtensionB

    return netExtension

#############################################################################
#########

def modifyInputFiles(initA, accel, srA1, srA2, inputFile, outputFile):
    """
    take Pecube input files and modify parameters based on
    the loop inputs from main script
    """
    #print 'writing input files'

    paramLineFaultA1 = 36  #line numbers for fault inputs

    paramLineFaultA2 = 37

    #paramLineFaultB1 = 58

    #paramLineFaultB2 = 59

    # modifications to fault A1
    datamod1 = '{} '.format(initA)
    datamod2 = '{} '.format(accel)
    datamod3 = '{} \n'.format(srA1)

    # modifications to fault A2
    datamod4 = '{} '.format(accel)
    datamod5 = '0. '
```

290

```python
    datamod6 = '{} \n'.format(srA2)

    # modifications to fault B
    #datamod7 = '{} '.format(initB)
    #datamod8 = '{} '.format(accel)
    #datamod9 = '{} \n'.format(srB1)

    # modifications to fault B
    #datamod10 = '{} '.format(accel)
    #datamod11 = '0. '
    #datamod12 = '{} \n'.format(srB2)


    start_point = 0   # start_point = len('-1.00 -1.00 -1.00 ')

    inputFile = open(inputFile, 'r')

    outputFile = open(outputFile, 'w+')

    lineno = 0              # line tracker

    while 1:

        line = inputFile.readline()  # grab a line

        if not line: break     # end of file reached

        lineno = lineno + 1        # current working line

        if lineno == paramLineFaultA1:     # are we there yet?

            # here's the working bit that makes the sustitution.

            modifiedline = line[:start_point] + datamod1 + datamod2 + datamod3

            outputFile.write(modifiedline)

        elif lineno == paramLineFaultA2:

            modifiedline = line[:start_point] + datamod4 + datamod5 + datamod6

            outputFile.write(modifiedline)
#        elif lineno == paramLineFaultB1:

#            modifiedline = line[:start_point] + datamod7 + datamod8 + datamod9

#            outputFile.write(modifiedline)

#        elif lineno == paramLineFaultB2:

#            modifiedline = line[:start_point] + datamod10 + datamod11 + data-
mod12

#            outputFile.write(modifiedline)

        else:

            outputFile.write(line)       # copy line as it is into temp file


    inputFile.close()                  # done with it.

    outputFile.close()                  # rename afterward with the original
```

291

```
name

    #print 'done writing'

    #return(inputFile, outputFile)



###############################################################################
#######
def renameFaultParams(inputFile, outputFile):
    """"
    replace old inputfile with new outputfile via calling bash
    """"
    #print 'replacing files'
    subprocess.call("cp {} {}".format(outputFile, inputFile), shell=True)
    #print 'done'


###############################################################################
####

def save_output(comparison_file, initA, accel, srA1, srA2):

    #print 'saving output'

    out_name = '/home/picloud/src/Pecube/nlrT1/nlrT1_{}_{}_{}_{}.txt'.
format(initA,
        accel, srA1, srA2)

    file_out = open(out_name, 'w+')

    comparison_file = open(comparison_file, 'r')

    lines = comparison_file.readlines()

    comparison_file.close()

    new_file = open('/home/picloud/src/Pecube/nlrT1/new_file2.txt', 'w+')

    new_file.writelines([item for item in lines[1:]])

    new_file.close()

    new_file = open('/home/picloud/src/Pecube/nlrT1/new_file2.txt', 'r')

    column_zHe = 9 # modified to add thermochronometer type

    column_aHe = 5 # new

    for line in new_file:

        line = line.strip()
        sline = line.split()
        file_out.write(sline[column_aHe] + '\n') # modified to specify thermo-
chronometer
        file_out.write(sline[column_zHe] + '\n') # new


    new_file.close()

    file_out.close()

    #print 'done'
```

```python
    return out_name



###############################################################################
###


def calc_chi_square(obs, out_name):

    #print 'calculating chi square misfit'

    zHe_predicted = nmp.loadtxt(open(out_name))

    zHe_observed = nmp.loadtxt(open(obs))

    chi_square = sum((zHe_observed - zHe_predicted)**2 / zHe_observed) / 8

    #print 'done'

    return chi_square

###############################################################################
###


def append_info(out_name, initA, accel, srA1, srA2, netExtension):

    #print 'making numpy matrices'

    in_array = nmp.loadtxt(open(out_name))

    out_array = '/home/picloud/src/Pecube/nlrT1/nlrT1_{}_{}_{}_{}.npy'.
format(initA,
        accel, srA1, srA2)

    nmp.save(out_array, in_array)

    out_array_temp = nmp.load(out_array)

    out_array_temp = nmp.append(out_array_temp, [initA, accel, srA1, srA2, ne-
tExtension])

    nmp.save(out_array, out_array_temp)

    cloud.files.put(out_array)

    out_array_name = 'nlrT1_{}_{}_{}_{}.npy'.format(initA, accel, srA1, srA2)
    return out_array_name

    #print 'done'

###############################################################################
###

def change_directory():
    subprocess.call("cd /home/picloud/src/Pecube", shell=True)
    directory = subprocess.call("pwd", shell=True)
    print directory


###############################################################################
###
```

```python
def change_dir_python():
    os.chdir('/home/picloud/src/Pecube')


################################################################
###

def mkdir_test(test_dir):
    subprocess.call('mkdir {}'.format(test_dir), shell=True)

################################################################
#########

def run_pecube():
    pecube_print = subprocess.check_output("cd /home/itchy/src/Pecube && bin/
Pecube", shell=True)
    return pecube_print

################################################################
###

#def dir_list(natty_path):

def run_pecube_cloud():
    #os.chdir('/home/picloud/src/Pecube')
    pecube_print = subprocess.check_output("cd /home/picloud/src/Pecube &&
bin/Pecube", shell=True)
    return pecube_print

################################################################
###

def dir_list():
    os.chdir('/home/picloud/src/Pecube/input/')
    dirlist = os.listdir(os.getcwd() )
    return dirlist
```

pecube_scripts_nlrT2.py

```python
#!/usr/bin/env python

import numpy as nmp
import subprocess, os, cloud


def calcNetExtension(initA, accel, srA1, srA2, dipFaultA):
    """
    imports fault slip information and calculates net slip and extension
    """
    # fault A extension
    slipA1 = (initA - accel) * srA1

    slipA2 = accel * srA2

    netSlipA = slipA1 + slipA2

    netExtensionA = netSlipA * nmp.cos(dipFaultA)

    #fault B extension
    #slipB1 = (initB - accel) * srB1

    #slipB2 = accel * srB2

    #netSlipB = slipB1 + slipB2

    #netExtensionB = netSlipB * nmp.cos(dipFaultB)


    # total extension

    netExtension = netExtensionA # + netExtensionB

    return netExtension

##############################################################################
#########


def modifyInputFiles(initA, accel, srA1, srA2, inputFile, outputFile):
    """
    take Pecube input files and modify parameters based on
    the loop inputs from main script
    """
    #print 'writing input files'

    paramLineFaultA1 = 36  #line numbers for fault inputs

    paramLineFaultA2 = 37

    #paramLineFaultB1 = 58

    #paramLineFaultB2 = 59

    # modifications to fault A1
    datamod1 = '{} '.format(initA)
    datamod2 = '{} '.format(accel)
    datamod3 = '{} \n'.format(srA1)

    # modifications to fault A2
    datamod4 = '{} '.format(accel)
    datamod5 = '0. '
```

```python
    datamod6 = '{} \n'.format(srA2)

    # modifications to fault B
    #datamod7 = '{} '.format(initB)
    #datamod8 = '{} '.format(accel)
    #datamod9 = '{} \n'.format(srB1)

    # modifications to fault B
    #datamod10 = '{} '.format(accel)
    #datamod11 = '0. '
    #datamod12 = '{} \n'.format(srB2)


    start_point = 0    # start_point = len('-1.00 -1.00 -1.00 ')

    inputFile = open(inputFile, 'r')

    outputFile = open(outputFile, 'w+')

    lineno = 0                # line tracker

    while 1:

        line = inputFile.readline()  # grab a line

        if not line: break      # end of file reached

        lineno = lineno + 1         # current working line

        if lineno == paramLineFaultA1:     # are we there yet?

            # here's the working bit that makes the sustitution.

            modifiedline = line[:start_point] + datamod1 + datamod2 + datamod3

            outputFile.write(modifiedline)

        elif lineno == paramLineFaultA2:

            modifiedline = line[:start_point] + datamod4 + datamod5 + datamod6

            outputFile.write(modifiedline)

#        elif lineno == paramLineFaultB1:

#            modifiedline = line[:start_point] + datamod7 + datamod8 + datamod9

#            outputFile.write(modifiedline)

#        elif lineno == paramLineFaultB2:

#            modifiedline = line[:start_point] + datamod10 + datamod11 + data-
mod12

#            outputFile.write(modifiedline)

        else:

            outputFile.write(line)       # copy line as it is into temp file


    inputFile.close()                    # done with it.

    outputFile.close()                    # rename afterward with the original
```

296

```
name

    #print 'done writing'

    #return(inputFile, outputFile)



###########################################################################
#######

def renameFaultParams(inputFile, outputFile):
    """"
    replace old inputfile with new outputfile via calling bash
    """"
    #print 'replacing files'
    subprocess.call("cp {} {}".format(outputFile, inputFile), shell=True)
    #print 'done'


###########################################################################
####

def runPecube():

    #print 'running Pecube'
    subprocess.call("bin/Pecube", shell=True)
    #print 'done with Pecube'


###########################################################################
###


def save_output(comparison_file, initA, accel, srA1, srA2):

    #print 'saving output'

    out_name = '/home/picloud/src/Pecube/nlrT2/nlrT2_{}_{}_{}_{}.txt'.
format(initA,
        accel, srA1, srA2)

    file_out = open(out_name, 'w+')

    comparison_file = open(comparison_file, 'r')

    lines = comparison_file.readlines()

    comparison_file.close()

    new_file = open('/home/picloud/src/Pecube/nlrT2/new_file2.txt', 'w+')

    new_file.writelines([item for item in lines[1:]])

    new_file.close()

    new_file = open('/home/picloud/src/Pecube/nlrT2/new_file2.txt', 'r')

    column_zHe = 9 # modified to add thermochronometer type

    column_aHe = 5 # new

    for line in new_file:

        line = line.strip()
```

297

```
        sline = line.split()
        file_out.write(sline[column_aHe] + '\n') # modified to specify thermo-
chronometer
        file_out.write(sline[column_zHe] + '\n') # new


    new_file.close()

    file_out.close()

    #print 'done'

    return out_name



############################################################################
###


def calc_chi_square(obs, out_name):

    #print 'calculating chi square misfit'

    zHe_predicted = nmp.loadtxt(open(out_name))

    zHe_observed = nmp.loadtxt(open(obs))

    chi_square = sum((zHe_observed - zHe_predicted)**2 / zHe_observed) / 8

    #print 'done'

    return chi_square

############################################################################
###


def append_info(out_name, initA, accel, srA1, srA2, netExtension):

    #print 'making numpy matrices'

    in_array = nmp.loadtxt(open(out_name))

    out_array = '/home/picloud/src/Pecube/nlrT2/3nlrT2_{}_{}_{}_{}.npy'.
format(initA,
        accel, srA1, srA2)

    nmp.save(out_array, in_array)

    out_array_temp = nmp.load(out_array)

    out_array_temp = nmp.append(out_array_temp, [initA, accel, srA1, srA2,
                          netExtension])

    nmp.save(out_array, out_array_temp)

    cloud.files.put(out_array)

    out_array_name = '3nlrT2_{}_{}_{}_{}.npy'.format(initA, accel, srA1, srA2)
    return out_array_name

    #print 'done'

############################################################################
```

```
###

def change_directory():
    subprocess.call("cd /home/picloud/src/Pecube", shell=True)
    directory = subprocess.call("pwd", shell=True)
    print directory


##########################################################################
###

def change_dir_python():
    os.chdir('/home/picloud/src/Pecube')


##########################################################################
###

def mkdir_test(test_dir):
    subprocess.call('mkdir {}'.format(test_dir), shell=True)

##########################################################################
#########

def run_pecube():
    pecube_print = subprocess.check_output("cd /home/itchy/src/Pecube && bin/
Pecube", shell=True)
    return pecube_print

##########################################################################
###

#def dir_list(natty_path):

def run_pecube_cloud():
    #os.chdir('/home/picloud/src/Pecube')
    pecube_print = subprocess.check_output("cd /home/picloud/src/Pecube &&
bin/Pecube", shell=True)
    return pecube_print

##########################################################################
###

def dir_list():
    os.chdir('/home/picloud/src/Pecube/input/')
    dirlist = os.listdir(os.getcwd() )
    return dirlist
```

pecube_scripts_nlrT3.py

```python
#!/usr/bin/env python

import numpy as nmp
import subprocess, os, cloud


def calcNetExtension(initA, accel, srA1, srA2, dipFaultA):
    """
    imports fault slip information and calculates net slip and extension
    """
    # fault A extension
    slipA1 = (initA - accel) * srA1

    slipA2 = accel * srA2

    netSlipA = slipA1 + slipA2

    netExtensionA = netSlipA * nmp.cos(dipFaultA)

    #fault B extension
    #slipB1 = (initB - accel) * srB1

    #slipB2 = accel * srB2

    #netSlipB = slipB1 + slipB2

    #netExtensionB = netSlipB * nmp.cos(dipFaultB)


    # total extension

    netExtension = netExtensionA # + netExtensionB

    return netExtension

##############################################################################
#########

def modifyInputFiles(initA, accel, srA1, srA2, inputFile, outputFile):
    """
    take Pecube input files and modify parameters based on
    the loop inputs from main script
    """
    #print 'writing input files'

    paramLineFaultA1 = 37   #line numbers for fault inputs

    paramLineFaultA2 = 38

    #paramLineFaultB1 = 58

    #paramLineFaultB2 = 59

    # modifications to fault A1
    datamod1 = '{} '.format(initA)
    datamod2 = '{} '.format(accel)
    datamod3 = '{} \n'.format(srA1)

    # modifications to fault A2
    datamod4 = '{} '.format(accel)
    datamod5 = '0. '
```

300

```python
        datamod6 = '{} \n'.format(srA2)

        # modifications to fault B
        #datamod7 = '{} '.format(initB)
        #datamod8 = '{} '.format(accel)
        #datamod9 = '{} \n'.format(srB1)

        # modifications to fault B
        #datamod10 = '{} '.format(accel)
        #datamod11 = '0. '
        #datamod12 = '{} \n'.format(srB2)


        start_point = 0   # start_point = len('-1.00 -1.00 -1.00 ')

        inputFile = open(inputFile, 'r')

        outputFile = open(outputFile, 'w+')

        lineno = 0               # line tracker

        while 1:

            line = inputFile.readline()  # grab a line

            if not line: break     # end of file reached

            lineno = lineno + 1        # current working line

            if lineno == paramLineFaultA1:     # are we there yet?

                # here's the working bit that makes the sustitution.

                modifiedline = line[:start_point] + datamod1 + datamod2 + datamod3

                outputFile.write(modifiedline)

            elif lineno == paramLineFaultA2:

                modifiedline = line[:start_point] + datamod4 + datamod5 + datamod6

                outputFile.write(modifiedline)
#        elif lineno == paramLineFaultB1:

#             modifiedline = line[:start_point] + datamod7 + datamod8 + datamod9

#              outputFile.write(modifiedline)

#        elif lineno == paramLineFaultB2:

#             modifiedline = line[:start_point] + datamod10 + datamod11 + data-
mod12

#              outputFile.write(modifiedline)

            else:

                outputFile.write(line)      # copy line as it is into temp file


        inputFile.close()                    # done with it.

        outputFile.close()                   # rename afterward with the original
```

301

```
name

    #print 'done writing'

    #return(inputFile, outputFile)



###############################################################################
#######

def renameFaultParams(inputFile, outputFile):
    """"
    replace old inputfile with new outputfile via calling bash
    """"
    #print 'replacing files'
    subprocess.call("cp {} {}".format(outputFile, inputFile), shell=True)
    #print 'done'


###############################################################################
####

def runPecube():

    #print 'running Pecube'
    subprocess.call("bin/Pecube", shell=True)
    #print 'done with Pecube'


###############################################################################
###


def save_output(comparison_file, initA, accel, srA1, srA2):

    #print 'saving output'

    out_name = '/home/picloud/src/Pecube/nlrT3/nlrT3_{}_{}_{}_{}.txt'.
format(initA,
        accel, srA1, srA2)

    file_out = open(out_name, 'w+')

    comparison_file = open(comparison_file, 'r')

    lines = comparison_file.readlines()

    comparison_file.close()

    new_file = open('/home/picloud/src/Pecube/nlrT3/new_file2.txt', 'w+')

    new_file.writelines([item for item in lines[1:]])

    new_file.close()

    new_file = open('/home/picloud/src/Pecube/nlrT3/new_file2.txt', 'r')

    column_zHe = 9 # modified to add thermochronometer type

    column_aHe = 5 # new

    for line in new_file:

        line = line.strip()
```

```
        sline = line.split()
        file_out.write(sline[column_aHe] + '\n') # modified to specify thermo-
chronometer
        file_out.write(sline[column_zHe] + '\n') # new


    new_file.close()

    file_out.close()

    #print 'done'

    return out_name



################################################################################
###


def calc_chi_square(obs, out_name):

    #print 'calculating chi square misfit'

    zHe_predicted = nmp.loadtxt(open(out_name))

    zHe_observed = nmp.loadtxt(open(obs))

    chi_square = sum((zHe_observed - zHe_predicted)**2 / zHe_observed) / 8

    #print 'done'

    return chi_square

################################################################################
###


def append_info(out_name, initA, accel, srA1, srA2, netExtension):

    #print 'making numpy matrices'

    in_array = nmp.loadtxt(open(out_name))

    out_array = '/home/picloud/src/Pecube/nlrT3/nlrT3_{}_{}_{}_{}.npy'.
format(initA,
        accel, srA1, srA2)

    nmp.save(out_array, in_array)

    out_array_temp = nmp.load(out_array)

    out_array_temp = nmp.append(out_array_temp, [initA, accel, srA1, srA2,
                            netExtension])

    nmp.save(out_array, out_array_temp)

    cloud.files.put(out_array)

    out_array_name = 'nlrT3_{}_{}_{}_{}.npy'.format(initA, accel, srA1, srA2)
    return out_array_name

    #print 'done'

################################################################################
```

```
###

def change_directory():
    subprocess.call("cd /home/picloud/src/Pecube", shell=True)
    directory = subprocess.call("pwd", shell=True)
    print directory


############################################################################
###

def change_dir_python():
    os.chdir('/home/picloud/src/Pecube')


############################################################################
###

def mkdir_test(test_dir):
    subprocess.call('mkdir {}'.format(test_dir), shell=True)

############################################################################
#########

def run_pecube():
    pecube_print = subprocess.check_output("cd /home/itchy/src/Pecube && bin/
Pecube", shell=True)
    return pecube_print

############################################################################
###

#def dir_list(natty_path):

def run_pecube_cloud():
    #os.chdir('/home/picloud/src/Pecube')
    pecube_print = subprocess.check_output("cd /home/picloud/src/Pecube &&
bin/Pecube", shell=True)
    return pecube_print

############################################################################
###

def dir_list():
    os.chdir('/home/picloud/src/Pecube/input/')
    dirlist = os.listdir(os.getcwd() )
    return dirlist
```

pecube_scripts_nlrT4.py

```python
#!/usr/bin/env python

import numpy as nmp
import subprocess, os, cloud


def calcNetExtension(init, accel, sr1, sr2, dipFault):
    """
    imports fault slip information and calculates net slip and extension
    """
    # fault A extension
    slip1 = (init - accel) * sr1

    slip2 = accel * sr2

    netSlip = slip1 + slip2

    netExtension = netSlip * nmp.cos(dipFault)

    return netExtension

###############################################################################
#########


def modifyInputFiles(initA, initB, accel, srA1, srA2, srB1, srB2, inputFile,
                     outputFile):
    """
    take Pecube input files and modify parameters based on
    the loop inputs from main script
    """
    #print 'writing input files'

    paramLineFaultA1 = 36  #line numbers for fault inputs

    paramLineFaultA2 = 37

    paramLineFaultB1 = 59

    paramLineFaultB2 = 60

    # modifications to fault A1
    datamod1 = '{} '.format(initA)
    datamod2 = '{} '.format(accel)
    datamod3 = '{} \n'.format(srA1)

    # modifications to fault A2
    datamod4 = '{} '.format(accel)
    datamod5 = '0. '
    datamod6 = '{} \n'.format(srA2)

    # modifications to fault B
    datamod7 = '{} '.format(initB)
    datamod8 = '{} '.format(accel)
    datamod9 = '{} \n'.format(srB1)

    # modifications to fault B
    datamod10 = '{} '.format(accel)
    datamod11 = '0. '
    datamod12 = '{} \n'.format(srB2)
```

305

```python
    start_point = 0   # start_point = len('-1.00 -1.00 -1.00 ')

    inputFile = open(inputFile, 'r')

    outputFile = open(outputFile, 'w+')

    lineno = 0                # line tracker

    while 1:

        line = inputFile.readline()  # grab a line

        if not line: break     # end of file reached

        lineno = lineno + 1          # current working line

        if lineno == paramLineFaultA1:     # are we there yet?

            # here's the working bit that makes the sustitution.

            modifiedline = line[:start_point] + datamod1 + datamod2 + datamod3

            outputFile.write(modifiedline)

        elif lineno == paramLineFaultA2:

            modifiedline = line[:start_point] + datamod4 + datamod5 + datamod6

            outputFile.write(modifiedline)

        elif lineno == paramLineFaultB1:

            modifiedline = line[:start_point] + datamod7 + datamod8 + datamod9

            outputFile.write(modifiedline)

        elif lineno == paramLineFaultB2:

            modifiedline = line[:start_point] + datamod10 + datamod11 + data-
mod12

            outputFile.write(modifiedline)

        else:

            outputFile.write(line)     # copy line as it is into temp file


    inputFile.close()                  # done with it.
    outputFile.close()                 # rename afterward with the original
name

    #print 'done writing'

    #return(inputFile, outputFile)


##############################################################################
#######

def renameFaultParams(inputFile, outputFile):
    """
```

```python
        replace old inputfile with new outputfile via calling bash
        """
        #print 'replacing files'
        subprocess.call("cp {} {}".format(outputFile, inputFile), shell=True)
        #print 'done'


###########################################################################
####

def runPecube():

        #print 'running Pecube'
        subprocess.call("bin/Pecube", shell=True)
        #print 'done with Pecube'


###########################################################################
###

def save_output(comparison_file, initA, initB, accel, srA1, srA2, srB1, srB2,
                netextension):

        #print 'saving output'

        out_name = '/home/picloud/src/Pecube/nlrT4/nlrT4_{}_{}_{}_{}_{}_{}_
{}.txt'.format(initA, initB, accel, srA1, srA2, srB1, srB2)

        file_out = open(out_name, 'w+')

        comparison_file = open(comparison_file, 'r')

        lines = comparison_file.readlines()

        comparison_file.close()

        new_file = open('/home/picloud/src/Pecube/nlrT4/new_file2.txt', 'w+')

        new_file.writelines([item for item in lines[1:]])

        new_file.close()

        new_file = open('/home/picloud/src/Pecube/nlrT4/new_file2.txt', 'r')

        column_zHe = 9 # modified to add thermochronometer type

        column_aHe = 5 # new

        for line in new_file:

                line = line.strip()
                sline = line.split()
                file_out.write(sline[column_aHe] + '\n') # modified to specify thermo-
chronometer
                file_out.write(sline[column_zHe] + '\n') # new


        new_file.close()

        file_out.close()

        #print 'done'

        return out_name
```

307

```
##############################################################################
###


def calc_chi_square(obs, out_name):

    #print 'calculating chi square misfit'

    zHe_predicted = nmp.loadtxt(open(out_name))

    zHe_observed = nmp.loadtxt(open(obs))

    chi_square = sum((zHe_observed - zHe_predicted)**2 / zHe_observed) / 8

    #print 'done'

    return chi_square

##############################################################################
###


def append_info(out_name, initA, initB, accel, srA1, srA2, srB1, srB2, netEx-
tension):

    in_array = nmp.loadtxt(open(out_name))

    out_array = '/home/picloud/src/Pecube/nlrT4/nlrT4_{}_{}_{}_{}_{}_{}_
{}.npy'.format(initA, initB, accel, srA1, srA2, srB1, srB2)

    nmp.save(out_array, in_array)

    out_array_temp = nmp.load(out_array)

    out_array_temp = nmp.append(out_array_temp, [initA, initB, accel, srA1,
                            srA2, srB1, srB2, netExtension])

    nmp.save(out_array, out_array_temp)

    cloud.files.put(out_array)

    out_array_name = 'nlrT4_{}_{}_{}_{}_{}_{}_{}.npy'.format(initA, initB, ac-
cel, srA1, srA2, srB1, srB2)
    return out_array_name

    #print 'done'

##############################################################################
###

def change_directory():
    subprocess.call("cd /home/picloud/src/Pecube", shell=True)
    directory = subprocess.call("pwd", shell=True)
    print directory


##############################################################################
###

def change_dir_python():
    os.chdir('/home/picloud/src/Pecube')
```

```python
##########################################################################
###

def mkdir_test(test_dir):
    subprocess.call('mkdir {}'.format(test_dir), shell=True)

##########################################################################
#########

def run_pecube():
    pecube_print = subprocess.check_output("cd /home/itchy/src/Pecube && bin/
Pecube", shell=True)
    return pecube_print

##########################################################################
###

#def dir_list(natty_path):

def run_pecube_cloud():
    #os.chdir('/home/picloud/src/Pecube')
    pecube_print = subprocess.check_output("cd /home/picloud/src/Pecube &&
bin/Pecube", shell=True)
    return pecube_print

##########################################################################
###

def dir_list():
    os.chdir('/home/picloud/src/Pecube/input/')
    dirlist = os.listdir(os.getcwd() )
    return dirlist
```

run_nlrT1_cloud.py

```
import sys
sys.path.append('/home/itchy/python_scripts')
import cloud, time
import numpy as nmp
import pecube_scripts_nlrT1 as psc

inputFile = '/home/picloud/src/Pecube/input/fault_parameters.txt'
#inputFile = '/home/itchy/src/Pecube/input/fault_parameters.txt'

outputFile = '/home/picloud/src/Pecube/input/fault_parameters.txt.out'
#outputFile = '/home/itchy/src/Pecube/input/fault_parameters.txt.out'

comparison_file = '/home/picloud/src/Pecube/nlrT1/Comparison.txt'
#comparison_file = '/home/itchy/src/Pecube/nlrT1/Comparison.txt'

# fault parameters

initFaultAs = [8., 9., 10., 11., 12., 13., 14., 15., 16., 17., 18.]
#[11.0, 12.0]

#[8.0, 9.0]#, 10.0, [11.0], 12.0, 13.0, 14.0, 15.0, 16.0, 17.0, 18.0] #, 19.0,
20.0]

accelFaults = [2.0, 2.5, 3.0, 3.5, 4.0, 4.5, 5.0, 5.5, 6.0, 6.5, 7.0, 7.5]
#accelFaults = [3.0, 4.0, 5.0] #, 6.0, 7.0, 8.0]


slipRate1FaultAs = [0., 0.25, 0.5, 0.75, 1.0, 1.5, 2.0, 2.5, 3.0, 3.5]

slipRate2FaultAs = [0.5, 0.75, 1.0, 1.5, 2.0, 2.5, 3.0, 3.5, 4.0, 4.5, 5.0,
5.5]

dipFaultA = [0.434631204]

faultParamsList = [[j, k, l, m] for j in initFaultAs for k in accelFaults for
l in slipRate1FaultAs for m in slipRate2FaultAs]

faultParamsListFiltered = []

for faultParams in faultParamsList:

    [initA, accel, srA1, srA2] = faultParams
    netExtension = psc.calcNetExtension(initA, accel, srA1, srA2, dipFaultA)
    if netExtension < 18:
        if netExtension >13:
            faultParamsListFiltered.append(faultParams)


print len(faultParamsList), 'total params'

print len(faultParamsListFiltered), 'filtered params'

def run_pecube_map(faultParamsListFiltered):
    [initA, accel, srA1, srA2] = faultParamsListFiltered

    netExtension = psc.calcNetExtension(initA, accel, srA1, srA2, dipFaultA)

    psc.modifyInputFiles(initA, accel, srA1, srA2, inputFile, outputFile)

    psc.renameFaultParams(inputFile, outputFile)

    pecube_print = psc.run_pecube_cloud()
```

310

```
    out_name = psc.save_output(comparison_file, initA, accel, srA1, srA2)

    out_array_name = psc.append_info(out_name, initA, accel, srA1, srA2,
                              netExtension)

    #cloud.files.get(out_array_name, '/home/itchy/src/Pecube/nlrT1/picloud/{}'.
format(out_array_name))
    #cloud.files.get(out_array_name)

    return out_array_name




t0 = time.time()

#pecube_nlrT2_runs = map(run_pecube_map, faultParamsListFiltered)
nlrT1_cloud_fix = cloud.map(run_pecube_map, faultParamsListFiltered,
                          _env='nlr_pecube_clone2')

new_nlrT1_runs = cloud.result(nlrT1_cloud_fix)


t1 = time.time()

print 'Pecube took', time.time() - t0, 'seconds for',
len(faultParamsListFiltered), 'runs'

#nlrT1_files = cloud.map(get_files_map, faultParamsListFiltered)


#print 'Pecube took', t1 - t0, 'seconds for', len(faultParamsListFiltered),
'runs.  That is', (t1 - t0) / float(len(faultParamsListFiltered)), 'seconds per
run.'
```

run_nlrT2_cloud.py

```python
# -*- coding: utf-8 -*-
"""
Created on Wed Jun 20 22:11:56 2012

@author: itchy
"""

import sys
sys.path.append('/home/itchy/python_scripts')
import cloud, time
import numpy as nmp
import pecube_scripts_nlrT2 as psc

inputFile = '/home/picloud/src/Pecube/input/fault_parameters.txt'

outputFile = '/home/picloud/src/Pecube/input/fault_parameters.txt.out'

comparison_file = '/home/picloud/src/Pecube/nlrT2/Comparison.txt'


# fault parameters

initFaultAs = [8.0, 9.0, 10.0, 11.0, 12.0, 13.0, 14.0, 15.0, 16.0, 17.0, 18.0]
#, 19.0, 20.0]

accelFaults = [2.0, 2.5, 3.0, 3.5, 4.0, 4.5, 5.0, 5.5, 6.0, 6.5, 7.0, 7.5]
#accelFaults = [3.0, 4.0, 5.0] #, 6.0, 7.0, 8.0]


slipRate1FaultAs = [0., 0.25, 0.5, 0.75, 1.0, 1.5, 2.0, 2.5, 3.0, 3.5]

slipRate2FaultAs = [0.5, 0.75, 1.0, 1.5, 2.0, 2.5, 3.0, 3.5, 4.0, 4.5, 5.0,
5.5]

dipFaultA = [0.4716]

faultParamsList = [[j, k, l, m] for j in initFaultAs for k in accelFaults for
l in slipRate1FaultAs for m in slipRate2FaultAs]

faultParamsListFiltered = []

for faultParams in faultParamsList:

    [initA, accel, srA1, srA2] = faultParams
    netExtension = psc.calcNetExtension(initA, accel, srA1, srA2, dipFaultA)
    if netExtension < 18:
        if netExtension >13:
            faultParamsListFiltered.append(faultParams)


print len(faultParamsList), 'total params'

print len(faultParamsListFiltered), 'filtered params'

def run_pecube_map(faultParamsListFiltered):
    [initA, accel, srA1, srA2] = faultParamsListFiltered

    netExtension = psc.calcNetExtension(initA, accel, srA1, srA2, dipFaultA)

    psc.modifyInputFiles(initA, accel, srA1, srA2, inputFile, outputFile)

    psc.renameFaultParams(inputFile, outputFile)
```

312

```
    pecube_print = psc.run_pecube_cloud()

    out_name = psc.save_output(comparison_file, initA, accel, srA1, srA2)

    out_array_name = psc.append_info(out_name, initA, accel, srA1, srA2, ne-
tExtension)

    #cloud.files.get(out_array_name, '/home/itchy/src/Pecube/nlrT2/picloud/{}'.
format(out_array_name))
    #cloud.files.get(out_array_name)

    return out_array_name



t0 = time.time()

pecube_nlrT2_fixed_runs = cloud.map(run_pecube_map, faultParamsListFiltered,
                                    _env='nlr_pecube_clone2')

nlrT2_fixed_runs = cloud.result(pecube_nlrT2_fixed_runs)


print 'Pecube took', time.time() - t0, 'seconds for',
len(faultParamsListFiltered), 'runs'

#t1 = time.time()
#pecube_nlrT2_files = cloud.map(get_files_map, faultParamsListFiltered)
```

run_nlrT3_cloud.py

```python
# -*- coding: utf-8 -*-
"""
@author: itchy
"""

import sys
sys.path.append('/home/itchy/python_scripts')
import cloud, time
import numpy as nmp
import pecube_scripts_nlrT3 as psc

inputFile = '/home/picloud/src/Pecube/input/fault_parameters.txt'

outputFile = '/home/picloud/src/Pecube/input/fault_parameters.txt.out'

comparison_file = '/home/picloud/src/Pecube/nlrT3/Comparison.txt'


# fault parameters

initFaultAs = [8.0, 9.0, 10.0, 11.0, 12.0, 13.0, 14.0, 15.0, 16.0, 17.0, 18.0]
#, 19.0, 20.0]

accelFaults = [2.0, 2.5, 3.0, 3.5, 4.0, 4.5, 5.0, 5.5, 6.0, 6.5, 7.0, 7.5]
#accelFaults = [3.0, 4.0, 5.0] #, 6.0, 7.0, 8.0]


slipRate1FaultAs = [0., 0.25, 0.5, 0.75, 1.0, 1.5, 2.0, 2.5, 3.0, 3.5]

slipRate2FaultAs = [0.5, 0.75, 1.0, 1.5, 2.0, 2.5, 3.0, 3.5, 4.0, 4.5, 5.0,
5.5]

dipFaultA = [0.39]

faultParamsList = [[j, k, l, m] for j in initFaultAs for k in accelFaults for
l in slipRate1FaultAs for m in slipRate2FaultAs]

faultParamsListFiltered = []

for faultParams in faultParamsList:

    [initA, accel, srA1, srA2] = faultParams
    netExtension = psc.calcNetExtension(initA, accel, srA1, srA2, dipFaultA)
    if netExtension < 22:
        if netExtension >18:
            faultParamsListFiltered.append(faultParams)


print len(faultParamsList), 'total params'

print len(faultParamsListFiltered), 'filtered params'

def run_pecube_map(faultParamsListFiltered):
    [initA, accel, srA1, srA2] = faultParamsListFiltered

    netExtension = psc.calcNetExtension(initA, accel, srA1, srA2, dipFaultA)

    psc.modifyInputFiles(initA, accel, srA1, srA2, inputFile, outputFile)

    psc.renameFaultParams(inputFile, outputFile)

    pecube_print = psc.run_pecube_cloud()
```

314

```
    out_name = psc.save_output(comparison_file, initA, accel, srA1, srA2)

    out_array_name = psc.append_info(out_name, initA, accel, srA1, srA2, ne-
tExtension)

    #cloud.files.get(out_array_name, '/home/itchy/src/Pecube/nlrT2/picloud/{}'.
format(out_array_name))
    #cloud.files.get(out_array_name)

    return out_array_name



t0 = time.time()

nlrT3_fixed_runs2 = cloud.map(run_pecube_map, faultParamsListFiltered,
                             _env='nlr_pecube_clone2')

nlrT3_fixed = cloud.result(nlrT3_fixed_runs2)


print 'Pecube took', time.time() - t0, 'seconds for',
len(faultParamsListFiltered), 'runs'
```

run_nlrT4_cloud.py

```python
import sys
sys.path.append('/home/itchy/python_scripts')
import cloud, time
import numpy as nmp
import pecube_scripts_nlrT4 as psc

inputFile = '/home/picloud/src/Pecube/input/fault_parameters.txt'

outputFile = '/home/picloud/src/Pecube/input/fault_parameters.txt.out'

comparison_file = '/home/picloud/src/Pecube/nlrT4/Comparison.txt'


# fault parameters

initFaultAs = [5.0, 5.5, 6.0, 6.5, 7.0]
#[8.0, 9.0, 10.0, 12.0, 14.0]#, 16.0]#, 16.0, 17.0, 18.0]

initFaultBs = [5.0, 6.0, 7.0]
#[8.0, 9.0, 10.0, 12.0, 14.0]#, 16.0]#, 16.0, 17.0, 18.0]

accelFaults = [2.0, 2.5, 3.0, 3.5, 4.0, 4.5, 5.0, 5.5]#, 6.0]
#accelFaults = [3.0, 4.0, 5.0] #, 6.0, 7.0, 8.0]


slipRate1FaultAs = [0., 0.25, 0.5, 0.75, 1.0, 1.5, 2.0, 2.5, 3.0, 3.5, 4.0]#,
1.5, 2.0, 2.5, 3.0, 3.5]

slipRate2FaultAs = [0.25, 0.5, 0.75, 1.0, 1.5, 2.0, 2.5, 3.0, 3.5, 4.0]#, 5.0]

slipRate1FaultBs = [0., 0.25, 0.5, 0.75, 1.0]#, 1.5, 2.0, 2.5, 3.0, 3.5,
4.0]#, 1.5, 2.0, 2.5, 3.0, 3.5]

slipRate2FaultBs = [0.25, 0.5, 0.75, 1.0]#, 1.5, 2.0, 2.5, 3.0, 3.5, 4.0]#,
3.0]#, 4.0, 5.0]



dipFaultA = [0.84]

dipFaultB = [0.93]

t0 = time.time()

faultParamsList = [[j, k, l, m, n, o, p] for j in initFaultAs for k in init-
FaultBs for l in accelFaults for m in slipRate1FaultAs for n in slipRate2Faul-
tAs for o in slipRate1FaultBs for p in slipRate2FaultBs]

t1 = time.time()

print t1-t0, 's to generate fault list'
print len(faultParamsList)



# filter variables
faultParamsListFiltered = []
nlrT4_run_list = []

for faultParams in faultParamsList:
```

```
        [initA, initB, accel, srA1, srA2, srB1, srB2] = faultParams

        netExtensionA = psc.calcNetExtension(initA, accel, srA1, srA2, dip-
FaultA)

        netExtensionB = psc.calcNetExtension(initB, accel, srB1, srB2, dip-
FaultB)

        netExtension = netExtensionA + netExtensionB

#print netExtension

        if 5 < netExtension < 7.5 and initA > accel and initB > accel and srB1
== srB2:

            faultParamsListFiltered.append(faultParams)
            run_name = 'nlrT4_{}_{}_{}_{}_{}_{}_{}.npy'.format(initA, initB,
accel, srA1, srA2, srB1, srB2)
            nlrT4_run_list.append(run_name)


t2 = time.time()
print t2-t1, 's to cut list to', len(faultParamsListFiltered), 'items'

def run_pecube_map(faultParamsListFiltered):
    [initA, initB, accel, srA1, srA2, srB1, srB2] = faultParamsListFiltered

    #netExtension = psc.calcNetExtension(initA, accel, srA1, srA2, dipFaultA)
    netExtensionA = psc.calcNetExtension(initA, accel, srA1, srA2, dipFaultA)
    netExtensionB = psc.calcNetExtension(initB, accel, srB1, srB2, dipFaultB)
    netExtension = netExtensionA + netExtensionB

    psc.modifyInputFiles(initA, initB, accel, srA1, srA2, srB1, srB2, input-
File,
                         outputFile)

    psc.renameFaultParams(inputFile, outputFile)

    pecube_print = psc.run_pecube_cloud()

    out_name = psc.save_output(comparison_file, initA, initB, accel, srA1,
                               srA2, srB1, srB2, netExtension)

    out_array_name = psc.append_info(out_name, initA, initB, accel, srA1,
srA2,
                                     srB1, srB2, netExtension)


    return out_array_name


t3 = time.time()

#pecube_nlrT4_runs_decel = cloud.map(run_pecube_map, faultParamsListFiltered,
#                          _env='nlr_pecube_clone2')

#run_list = cloud.result(pecube_nlrT4_runs_decel)


print 'Pecube took', time.time() - t3, 'seconds for',
len(faultParamsListFiltered), 'runs'
```

pecube_tools.py

```
"""
module for filtering of Pecube/picloud data, making plots,
deformation histories, etc.

"""
import numpy as nmp
import matplotlib.pyplot as plt

# filtering functions
def max_errors(sd_err, lab_err):
    """Makes an error array composed of the larger of the lab error
    (from the standard deviation of the analytical standard) or the
    standard deviation of the individual aliquot ages for each sample

    Returns: error array
    """
    num_obs = len(sd_err)
    err_array = nmp.zeros(num_obs)

    for s in nmp.arange(num_obs):
        err_array[s] = nmp.maximum(sd_err[s], lab_err[s])

        # make very wide (1 Gy) error bars for no data (obs of 0)
        if err_array[s] == 0:
            err_array[s] = 10

    return err_array


def get_result_index(first_result, result_interval, num_obs):
    """Gets the indices of the thermochronometer of interest"""
    last_result = first_result + (num_obs -1) * result_interval
    stop_result = last_result + result_interval
    result_index = nmp.arange(first_result, stop_result, result_interval)

    return result_index


def check_fits(result_row, obs_age_lo, obs_age_hi, first_result,
               result_interval, num_obs):
    """Checks whether each modeled sample fits the observed age within error
    and returns array with 1 (True: fits) or 0 (False: doesn't fit) for each
    sample in the model
    """
    err_index = nmp.arange(num_obs)
    result_index = get_result_index(first_result, result_interval, num_obs)
    success_array = nmp.zeros(num_obs)

    for i in err_index:
        res = result_index[i]
        if obs_age_lo[i] <= result_row[res] <= obs_age_hi[i]:
            success_array[i] = 1

    return success_array


def filter_ages(results_array, obs_age_lo, obs_age_hi, first_result,
                result_interval, num_obs, num_outliers):
    """Takes results array and filters them, so that passing runs have
    (num_obs - num_outliers) successes.  A success means that for a sample,
    the model age is within error of the observed age
```

318

```python
    Returns: row indices for filtered (passing) rows
    """
    #TODO:  Make these args keyword args so that they are less confusing to
type

    num_rows = results_array.shape[0]
    enough_fits = num_obs - num_outliers
    successful_runs = list([])

    for i in range(num_rows):
        result_row = results_array[i,:]
        success_array = check_fits(result_row, obs_age_lo, obs_age_hi,
                                   first_result, result_interval, num_obs)

        if nmp.sum(success_array) >= enough_fits:
            successful_runs.append(i)

      #success_array = filter_results(results_array, successful_runs)

    return successful_runs


def combine_successful_runs(*args):
    """Takes 2 lists of successful runs (e.g. from two thermochronometers
    and finds common elements.  In the future will be updated to handle more
    thermochronometers, probably with a loop.

    Arguments: row indices for successful fits

    Returns: array containing row indices for successful runs with all
    thermochronometers.
    """
    if len(args) == 1:
        all_successful_runs = nmp.array(args[0])


    elif len(args) == 2:
        list0 = nmp.array(args[0])
        list1 = nmp.array(args[1])
        all_successful_runs = list0[nmp.in1d(list0, list1)]

    elif len(args) == 0:
        print 'This function needs some arguments!'

    else:
        print 'too many lists!  For now only 2 please.'

    return all_successful_runs


def filter_results(results_array, all_successful_runs):
    """Makes new array of only successful runs"""
    filtered_runs = results_array[all_successful_runs, :]
    return filtered_runs


def get_chronometer_results(result_array, result_index):
    """Returns array of only one chronometer from larger result array"""
    chron_results = result_array[:,result_index]
    return chron_results


def calc_chi_square(obs, pred, num_obs):
    """Calculates chi-quare"""
```

319

```python
        data_exists = obs != 0.
        obs_data = obs[data_exists]
        pred_data = pred[data_exists]
        chi_square = sum((obs_data - pred_data)**2 / obs_data) / num_obs

        return chi_square


#TODO: make function to filter results where slip rate is constant during accel


# fault history functions
def make_time_vector(time_start = 20., time_stop = 0., time_step = 0.01,
        decimals = 3):
    """Makes a vector of dates in the past.  Default is time range from 20 Ma
    to 0 Ma (present) with a 10 ky time step. Also rounds to specified decimals
    to avoid problems with floating point errors when indexing, default = 3.
    For shorter time steps, this should be changed.

    Returns time vector"""

        # make sure default args are floats
    time_start = nmp.float(time_start)
    time_stop = nmp.float(time_stop)
    time_step = nmp.float(time_step)

        # make vector of times (Ma)
    num = ( (time_start - time_stop) / time_step) + 1
    time_vector = nmp.linspace(time_start, time_stop, num=num)

    # Rounds to specified precision
    time_vector = nmp.around(time_vector, decimals = decimals)

    return time_vector


def make_slip_rate_w_time(init, accel, sr1, sr2, time_vector = 'None',
                          fault_stop = 0.):
    """Defines a slip rate history based on fault initiation, acceleration,
    and slip rate values.

    Returns vector of slip rates at specified time intervals.
    """

    # make a time vector with default values if one hasn't been made
    if time_vector == 'None':
    #print 'I am making a time vector for you but not giving it to you.'
        time_vector = make_time_vector()

    # get indexes from time vector for where the rates change
    init_index = nmp.where(time_vector == init)
    init_index = int(init_index[0])
    accel_index = nmp.where(time_vector == accel)
    accel_index = int(accel_index[0])
    fs_index = nmp.where(time_vector == fault_stop)
    fs_index = int(fs_index[0])

    # make empty sr w/ time vector and fill it with rates
    slip_rate_w_time = nmp.zeros(len(time_vector))
    slip_rate_w_time[init_index : accel_index] = sr1
    slip_rate_w_time[accel_index : fs_index + 1] = sr2

    return slip_rate_w_time
```

```python
def get_cum_vector(deform_rate_w_time, time_step = 0.01):
    """Makes vector of cumulative deformation.  Needs time step to normalize,
    defaults to 0.01 ka."""

    cum_vector = nmp.cumsum(deform_rate_w_time) * time_step
    cum_vector = nmp.hstack(([0.],cum_vector[:-1]))

    return cum_vector


def make_fault_params_array(input_array, init_col, accel_col, sr1_col,
                            sr2_col, stop_col = []):
    """Makes separate array of just the fault parameters for a single fault.
    Needs to be run for each fault.  These may then be concatenated.

    Indices:
    Init = 0
    accel = 1
    sr1 = 2
    sr2 = 3
    """

    #TODO: generalize for more changes in slip rate

    init_column = input_array[:,init_col]
    accel_column = input_array[:,accel_col]
    sr1_column = input_array[:,sr1_col]
    sr2_column = input_array[:,sr2_col]

    fault_params_array = nmp.hstack((init_column, accel_column, sr1_column,
                                     sr2_column))

    if stop_col != []:
      stop_column = input_array[:,stop_col]
      fault_params_array = nmp.hstack((fault_params_array, stop_column))

    return fault_params_array


#def make_cum_array(


# plotting functions
def make_fault_histograms(fig, final_array, init_col, sr1_col, accel_col, sr2_
col):
    fig = fig

    # initA
    ax1 = fig.add_subplot(221)
    bins = [7.5, 8.5, 9.5, 10.5, 11.5, 12.5, 13.5, 14.5, 15.5, 16.5, 17.5,
18.5]
    plt.hist(final_array[:,init_col], bins)
    plt.xlabel('initiation, Ma')

    # srA1
    ax2 = fig.add_subplot(222)
    bins = [-0.25, 0.25, 0.75, 1.25, 1.75, 2.25, 2.75, 3.25, 3.75, 4.25, 4.75,
            5.25, 5.75, 6.25, 6.75]
    plt.hist(final_array[:,sr1_col], bins)
    plt.xlabel('slip rate 1, mm/yr')

    # accel
    ax3 = fig.add_subplot(223)
    bins = [1.75, 2.25, 2.75, 3.25, 3.75, 4.25, 4.75, 5.25, 5.75, 6.25, 6.75]
```

```python
        plt.hist(final_array[:,accel_col], bins)
        plt.xlabel('acceleration, Ma')

        # srA2
        ax4 = fig.add_subplot(224)
        bins = [0.25, 0.75, 1.25, 1.75, 2.25, 2.75, 3.25, 3.75, 4.25, 4.75, 5.25,
                5.75, 6.25, 6.75]
        plt.hist(final_array[:,sr2_col], bins)
        plt.xlabel('slip rate 2, mm/yr')

        return fig


def make_ext_histories(fig, transect, time_vector, er_w_time_array,
                              cum_ext_w_time_array, lcolor='k', lwidth=0.5):
    """Makes plots of extension rate and cumulative extension through time"""

    lc = lcolor
    lw = lwidth
    fig = fig
    #plt.title('extension histories, {0} transect'.format(transect))
    plt.subplots_adjust(hspace = 0.0001)

    # ext rate w/ time plot
    ax1 = fig.add_subplot(211)
    plt.plot(time_vector, er_w_time_array, color = lc, linewidth=lw)
    plt.gca().invert_xaxis()
    plt.ylim([0, 6])
    #plt.xlabel('time, Ma')
    plt.ylabel('extension rate, mm/a')

    # cumulative extension plot
    ax2 = fig.add_subplot(212, sharex=ax1)
    plt.plot(time_vector, cum_ext_w_time_array, color = lc, linewidth=lw)
    #plt.gca().invert_xaxis()
    plt.ylim([0, 25])
    plt.xlabel('time, Ma')
    plt.ylabel('cumulative extension, km')

    xticklabels = ax1.get_xticklabels()
    plt.setp(xticklabels, visible=False)


    return fig


def lon_elev_plots(fig, pred_ages, obs_ages, obs_err,
                   lon, elev, symb_type = 'dot'):

    #red_ages = results_indices[results_array] #check on this

    fig.add_subplot(211)
    if symb_type == 'dot':
        plt.plot(lon, pred_ages, 'b.')
    elif symb_type == 'line':
      plt.plot(lon, pred_ages, color = 'b')
    else:
      print 'not a known plot type'

    plt.errorbar(lon, obs_ages, yerr = obs_err, fmt='o', color='k')
    plt.xlabel('longitude')
    plt.ylabel('Age (Ma)')


    fig.add_subplot(212)
```

```
if symb_type == 'dot':
    plt.plot(pred_ages, elev, 'b.')
elif symb_type == 'line':
  plt.plot(pred_ages, elev, color = 'b')
#else:
# print 'not a known plot type'

plt.errorbar(obs_ages, elev, xerr = obs_err, fmt='o', color='k')
plt.xlabel('Age (Ma)')
plt.ylabel('elev. (m)')

return fig
```

nlrT1_filter_tools.py

```python
import numpy as nmp
import pecube_tools as pt
import os
import matplotlib.pyplot as plt


if os.name == 'nt':
    results_array = nmp.load('C:\\itchy\\code_repos\\pt_working\\results\\
nlrT1_results.npy')
elif os.name == 'posix':
#    results_array = nmp.load('/media/4C307D4D22E94879/school/tibet/lunggar/
kurt/pecube/nlrT2/nlr_results.npy')
    results_array = nmp.load('/home/itchy/src/Pecube/nlrT1/picloud/new_runs/
nlrT1_results.npy')

#results_array = nmp.load('nlrT2_results.py')

# column indices for fault parameters
init_col = 20
accel_col = 21
sr1_col = 22
sr2_col = 23
net_extension_col = 24

fault_dip = 0.434631204


# input observations and error calculations (larger of analytical and lab er-
ror)

# last 3 observations are dummies based on Woodruff et al.
#aHe_obs = nmp.array([3.830, 3.789, 3.205, 2.717, 2.694, 0.0, 1.770, 4., 5.,
6.5])
aHe_obs = nmp.array([3.830, 3.789, 3.205, 2.717, 2.694, 0.0, 1.770])

#aHe_sd_err = nmp.array([0.441, 0.769, 0.549, 0.434, 1.173, 0.0, .01, 2.0, 2.,
2.0])
aHe_sd_err = nmp.array([0.441, 0.769, 0.549, 0.434, 1.173, 0.0, .01])
#,20.,20.,20.])


#zHe_obs = nmp.array([3.758, 5.557, 3.979, 4.376, 3.765, 3.923, 3.498, 6.5,
7.5, 9.5])
zHe_obs = nmp.array([3.758, 5.557, 3.979, 4.376, 3.765, 3.923, 3.498])


#zHe_sd_err = nmp.array([0.372, 1.177, 0.470, 0.350, 0.301, 0.322, 0.321, 2.,
2., 2.,])
zHe_sd_err = nmp.array([0.372, 1.177, 0.470, 0.350,0.301, 0.322, 0.321])

elev_obs = nmp.array([5896, 5800, 5726, 5708, 5687, 5386, 5199])#, 5842, 6021,
6222])

elev_pred = nmp.array([5826, 5816, 5660, 5620, 5576, 5416])#, 5194, 5978,
6263])

lon = nmp.array([83.5008, 83.5013, 83.5090, 83.5105, 83.5121, 83.5260,
83.5384]) #,83.4847, 83.4706, 83.4520])

num_obs = len(zHe_obs)
```

```
# filtering parameters

num_aHe_outliers = 0

num_zHe_outliers = 1

aHe_lab_err = 0.06 * aHe_obs

zHe_lab_err = 0.05 * zHe_obs

aHe_err = pt.max_errors(aHe_sd_err, aHe_lab_err)

zHe_err = pt.max_errors(zHe_sd_err, zHe_lab_err)

aHe_first_result = 0

zHe_first_result = 1

num_chronometers = 2

result_interval = num_chronometers

# error bounds
aHe_1sd_err_lo = aHe_obs - aHe_err
aHe_2sd_err_lo = aHe_obs - 2 * aHe_err
aHe_1sd_err_hi = aHe_obs + aHe_err
aHe_2sd_err_hi = aHe_obs + 2 * aHe_err

zHe_1sd_err_lo = zHe_obs - zHe_err
zHe_2sd_err_lo = zHe_obs - 2 * zHe_err
zHe_1sd_err_hi = zHe_obs + zHe_err
zHe_2sd_err_hi = zHe_obs + 2 * zHe_err


# zHe run variables
zHe_sigma = 2 #sigma, 1 or 2
if zHe_sigma == 1:
     obs_age_lo = zHe_1sd_err_lo
     obs_age_hi = zHe_1sd_err_hi

elif zHe_sigma == 2:
     obs_age_lo = zHe_2sd_err_lo
     obs_age_hi = zHe_2sd_err_hi

num_outliers = num_zHe_outliers
zHe_index = pt.get_result_index(zHe_first_result, result_interval, num_obs)

# filter zHe runs
zHe_successful_runs = pt.filter_ages(results_array, obs_age_lo, obs_age_hi,
                                     zHe_first_result, result_interval,
                                     num_obs, num_outliers)

# aHe run variables
aHe_sigma = 2 #sigma, 1 or 2
if aHe_sigma == 1:
     obs_age_lo = aHe_1sd_err_lo
     obs_age_hi = aHe_1sd_err_hi

elif aHe_sigma == 2:
     obs_age_lo = aHe_2sd_err_lo
     obs_age_hi = aHe_2sd_err_hi


num_outliers = num_aHe_outliers
```

```python
aHe_index = pt.get_result_index(aHe_first_result, result_interval, num_obs)
# filter aHe runs
aHe_successful_runs = pt.filter_ages(results_array, obs_age_lo, obs_age_hi,
                                     aHe_first_result, result_interval,
                                     num_obs, num_outliers)


all_successful_runs = pt.combine_successful_runs(zHe_successful_runs,
                                                 aHe_successful_runs)

filtered_runs = pt.filter_results(results_array, all_successful_runs)

num_filtered = filtered_runs.shape[0]

aHe_success_ages = pt.get_chronometer_results(filtered_runs, aHe_index)
zHe_success_ages = pt.get_chronometer_results(filtered_runs, zHe_index)
nlrT1_aHe_success = aHe_success_ages
nlrT1_zHe_success = zHe_success_ages

nlrT1_init = filtered_runs[:,init_col]
nlrT1_accel = filtered_runs[:,accel_col]
nlrT1_sr1 = filtered_runs[:,sr1_col]
nlrT1_sr2 = filtered_runs[:,sr2_col]
nlrT1_extension = filtered_runs[:,net_extension_col]

#nlrT1_lat = nmp.mean[lat]

print 'You got', results_array.shape[0], 'total runs.'
print 'You got', len(zHe_successful_runs), 'good zircon runs.'
print 'You got', len(aHe_successful_runs), 'good apatite runs.'
print 'You got', num_filtered, 'good total runs!'


# make histories
time_start = 20.
time_stop = 0.
time_step = 0.01

time_vector = pt.make_time_vector(time_start = time_start,
                                  time_stop = time_stop, time_step = time_
step,
                                  decimals = 3)
times = len(time_vector)

er_w_time_array = nmp.zeros((times, num_filtered))
cum_ext_w_time_array = nmp.zeros((times, num_filtered))

for i in range(num_filtered):
    init = filtered_runs[i,init_col]
    accel = filtered_runs[i,accel_col]
    er1 = filtered_runs[i,sr1_col] * nmp.cos(fault_dip)
    er2 = filtered_runs[i,sr2_col] * nmp.cos(fault_dip)

    er_w_time_array[:,i] = pt.make_slip_rate_w_time(init, accel, er1, er2,
                                                    time_vector = time_vector)

    cum_ext_w_time_array[:,i] = pt.get_cum_vector(er_w_time_array[:,i],
                                                  time_step)



fig1 = plt.figure(1)
#plt.title('NLR Transect 1')
pt.make_fault_histograms(fig1, filtered_runs, init_col, sr1_col, accel_col,
```

```
                              sr2_col)

fig2 = plt.figure(2)
pt.make_ext_histories(fig2, 'nlrT1', time_vector, er_w_time_array,
                              cum_ext_w_time_array)


fig3 = plt.figure(3)
pt.lon_elev_plots(fig3, zHe_success_ages.T, zHe_obs, zHe_err* 2, lon, elev_obs)

fig4 = plt.figure(4)
pt.lon_elev_plots(fig4, aHe_success_ages.T, aHe_obs, aHe_err* 2, lon, elev_obs)
#plt.title('NLR Transect 1')

plt.show()
```

nlrT2_filter_tools.py

```python
import numpy as nmp
import pecube_tools as pt
import os
import matplotlib.pyplot as plt


if os.name == 'nt':
    results_array = nmp.load('C:\\itchy\\code_repos\\pt_working\\results\\
nlrT2_results.npy')
elif os.name == 'posix':
#    results_array = nmp.load('/media/4C307D4D22E94879/school/tibet/lunggar/
kurt/pecube/nlrT2/nlr_results.npy')
    results_array = nmp.load('/home/itchy/src/Pecube/nlrT2/picloud/new_runs/
nlr_results.npy')

#results_array = nmp.load('nlrT2_results.py')

fault_dip = [0.47]

# column indices for fault parameters
init_col = 36
accel_col = 37
sr1_col = 38
sr2_col = 39
net_extension_col = 40


# input observations and error calculations (larger of analytical and lab er-
ror)

aHe_obs = nmp.array([0.48, 0.64, 2.065, 0., 0., 0., 0., 0., 2.972, 0., 0.,
                     0., 0., 0., 3.722])#, 0., 0., 0.])

aHe_sd_err = nmp.array([0.09, 0.1, 0.97, 0,0,0,0,0, 1.67,0,0,0,0,0, 2.67])#,
0., 0., 0.])

zHe_obs = nmp.array([3.369, 4.774, 2.657, 3.322, 3.202, 3.441, 3.148, 2.819,
                     2.746, 3.417, 2.343, 3.032, 3.134, 3.069, 5.045])#, 5.5,
8., 9.5])

zHe_sd_err = nmp.array([0.27, 1.71, 0.21, 0.68, 0.26, 0.28, 0.33, 0.75, 0.41,
                        1.15, 0.51, 0.60, 1.10, 0.25, 2.24])#, 3., 3., 3.])

elev_obs = nmp.array([5130, 5147, 5174, 5217, 5226, 5235, 5237, 5267, 5287,
                      5377, 5382, 5389, 5418, 5420, 5509])#, 5688, 5833,
6198])

elev_pred = nmp.array([5211, 5230, 5277, 5334, 5208, 5213, 5213, 5253, 5293,
                       5348, 5316, 5370, 5599, 5373, 5764])#, 5833, 6134,
6245])

num_obs = len(zHe_obs)


# filtering parameters

num_aHe_outliers = 2

num_zHe_outliers = 0

aHe_lab_err = 0.06 * aHe_obs
```

```
zHe_lab_err = 0.05 * zHe_obs

aHe_err = pt.max_errors(aHe_sd_err, aHe_lab_err)

zHe_err = pt.max_errors(zHe_sd_err, zHe_lab_err)

aHe_first_result = 0

zHe_first_result = 1

num_chronometers = 2

result_interval = num_chronometers

# error bounds
aHe_1sd_err_lo = aHe_obs - aHe_err
aHe_2sd_err_lo = aHe_obs - 2 * aHe_err
aHe_1sd_err_hi = aHe_obs + aHe_err
aHe_2sd_err_hi = aHe_obs + 2 * aHe_err

zHe_1sd_err_lo = zHe_obs - zHe_err
zHe_2sd_err_lo = zHe_obs - 2 * zHe_err
zHe_1sd_err_hi = zHe_obs + zHe_err
zHe_2sd_err_hi = zHe_obs + 2 * zHe_err

# zHe run variables
zHe_sigma = 2 #sigma, 1 or 2
if zHe_sigma == 1:
    obs_age_lo = zHe_1sd_err_lo
    obs_age_hi = zHe_1sd_err_hi

elif zHe_sigma == 2:
    obs_age_lo = zHe_2sd_err_lo
    obs_age_hi = zHe_2sd_err_hi


num_outliers = num_zHe_outliers
zHe_index = pt.get_result_index(zHe_first_result, result_interval, num_obs)
# filter zHe runs
zHe_successful_runs = pt.filter_ages(results_array, obs_age_lo, obs_age_hi,
                                     zHe_first_result, result_interval,
                                     num_obs, num_outliers)

# aHe run variables
aHe_sigma = 1 #sigma, 1 or 2
if aHe_sigma == 1:
    obs_age_lo = aHe_1sd_err_lo
    obs_age_hi = aHe_1sd_err_hi

elif aHe_sigma == 2:
    obs_age_lo = aHe_2sd_err_lo
    obs_age_hi = aHe_2sd_err_hi


num_outliers = num_aHe_outliers
aHe_index = pt.get_result_index(aHe_first_result, result_interval, num_obs)
# filter aHe runs
aHe_successful_runs = pt.filter_ages(results_array, obs_age_lo, obs_age_hi,
                                     aHe_first_result, result_interval,
                                     num_obs, num_outliers)


all_successful_runs = pt.combine_successful_runs(zHe_successful_runs,
                                                 aHe_successful_runs)
```

329

```
filtered_runs = pt.filter_results(results_array, all_successful_runs)

num_filtered = filtered_runs.shape[0]

aHe_success_ages = pt.get_chronometer_results(filtered_runs, aHe_index)
zHe_success_ages = pt.get_chronometer_results(filtered_runs, zHe_index)

nlrT2_aHe_success = aHe_success_ages
nlrT2_zHe_success = zHe_success_ages

nlrT2_init = filtered_runs[:,init_col]
nlrT2_accel = filtered_runs[:,accel_col]
nlrT2_sr1 = filtered_runs[:,sr1_col]
nlrT2_sr2 = filtered_runs[:,sr2_col]
nlrT2_extension = filtered_runs[:,net_extension_col]


print 'You got', results_array.shape[0], 'total runs.'
print 'You got', len(zHe_successful_runs), 'good zircon runs.'
print 'You got', len(aHe_successful_runs), 'good apatite runs.'
print 'You got', num_filtered, 'good total runs!'


# make histories
time_start = 20.
time_stop = 0.
time_step = 0.01

time_vector = pt.make_time_vector(time_start = time_start,
                                  time_stop = time_stop, time_step = time_
step,
                                  decimals = 3)
times = len(time_vector)

er_w_time_array = nmp.zeros((times, num_filtered))
cum_ext_w_time_array = nmp.zeros((times, num_filtered))

for i in range(num_filtered):
    init = filtered_runs[i,init_col]
    accel = filtered_runs[i,accel_col]
    er1 = filtered_runs[i,sr1_col] * nmp.cos(fault_dip)
    er2 = filtered_runs[i,sr2_col] * nmp.cos(fault_dip)

    er_w_time_array[:,i] = pt.make_slip_rate_w_time(init, accel, er1, er2,
                                                    time_vector = time_vector)

    cum_ext_w_time_array[:,i] = pt.get_cum_vector(er_w_time_array[:,i],
                                                  time_step)



fig1 = plt.figure(1)
pt.make_fault_histograms(fig1, filtered_runs, init_col, sr1_col, accel_col,
                         sr2_col)

fig2 = plt.figure(2)
pt.make_ext_histories(fig2, 'nlrT2', time_vector, er_w_time_array,
                      cum_ext_w_time_array)

plt.show()
```

nlrT3_filter_tools.py

```python
import numpy as nmp
import pecube_tools as pt
import os
import matplotlib.pyplot as plt


if os.name == 'nt':
    results_array = nmp.load('C:\\itchy\\code_repos\\pt_working\\results\\
nlrT3_results.npy')
elif os.name == 'posix':
#    results_array = nmp.load('/media/4C307D4D22E94879/school/tibet/lunggar/
kurt/pecube/nlrT2/nlr_results.npy')
    results_array = nmp.load('/home/itchy/src/Pecube/nlrT3/picloud/new_runs/
nlr_results.npy')

#results_array = nmp.load('nlrT2_results.py')

# column indices for fault parameters
init_col = 14
accel_col = 15
sr1_col = 16
sr2_col = 17
net_extension_col = 18

fault_dip = 0.37


# input observations and error calculations (larger of analytical and lab er-
ror)

# last 2 observations are dummies based on Woodruff et al.
aHe_obs = nmp.array([0.,0.,0.,0.,0.])#,0.,0.])

aHe_sd_err = nmp.array([30.,30.,30.,30.,30.])#,0.,0.])

#zHe_obs = nmp.array([2.524, 3.226, 2.717, 2.79, 3.524])#, 6.5, 9.5])
zHe_obs = nmp.array([3.524, 3.226, 2.717, 2.79, 3.524])#, 6.5, 9.5])

zHe_sd_err = nmp.array([0.231, 0.258, 0.217, 0.223, 1.794])#, 3.0, 4.0])
#zHe_sd_err = nmp.array([1.231, 0.258, 0.217, 0.223, 1.794])

elev_obs = nmp.array([5689, 5436, 5335, 5197, 5172])#, 6036, 6309])

elev_pred = nmp.array([5626, 5467, 5393, 5274, 5251])#, 5961, 6342])

num_obs = len(zHe_obs)


# filtering parameters

num_aHe_outliers = 0

num_zHe_outliers = 0

aHe_lab_err = 0.06 * aHe_obs

zHe_lab_err = 0.05 * zHe_obs

aHe_err = pt.max_errors(aHe_sd_err, aHe_lab_err)

zHe_err = pt.max_errors(zHe_sd_err, zHe_lab_err)
```

```python
aHe_first_obs = 0

zHe_first_obs = 1

num_chronometers = 2

obs_interval = num_chronometers

# error bounds
aHe_1sd_err_lo = aHe_obs - aHe_err
aHe_2sd_err_lo = aHe_obs - 2 * aHe_err
aHe_1sd_err_hi = aHe_obs + aHe_err
aHe_2sd_err_hi = aHe_obs + 2 * aHe_err

zHe_1sd_err_lo = zHe_obs - zHe_err
zHe_2sd_err_lo = zHe_obs - 2 * zHe_err
zHe_1sd_err_hi = zHe_obs + zHe_err
zHe_2sd_err_hi = zHe_obs + 2 * zHe_err


# zHe run variables
zHe_sigma = 2 #sigma, 1 or 2
if zHe_sigma == 1:
     obs_age_lo = zHe_1sd_err_lo
     obs_age_hi = zHe_1sd_err_hi

elif zHe_sigma == 2:
     obs_age_lo = zHe_2sd_err_lo
     obs_age_hi = zHe_2sd_err_hi

first_obs = zHe_first_obs
num_outliers = num_zHe_outliers

# filter zHe runs
zHe_successful_runs = pt.filter_ages(results_array, obs_age_lo, obs_age_hi,
                                     first_obs, obs_interval, num_obs,
                                     num_outliers)

# aHe run variables
aHe_sigma = 1 #sigma, 1 or 2
if aHe_sigma == 1:
     obs_age_lo = aHe_1sd_err_lo
     obs_age_hi = aHe_1sd_err_hi

elif aHe_sigma == 2:
     obs_age_lo = aHe_2sd_err_lo
     obs_age_hi = aHe_2sd_err_hi

first_obs = aHe_first_obs
num_outliers = num_aHe_outliers

# filter aHe runs
aHe_successful_runs = pt.filter_ages(results_array, obs_age_lo, obs_age_hi,
                                     first_obs, obs_interval, num_obs,
                                     num_outliers)


all_successful_runs = pt.combine_successful_runs(zHe_successful_runs,
                                                 aHe_successful_runs)

filtered_runs = pt.filter_results(results_array, all_successful_runs)


nlrT3_init = filtered_runs[:,init_col]
```

```
nlrT3_accel = filtered_runs[:,accel_col]
nlrT3_sr1 = filtered_runs[:,sr1_col]
nlrT3_sr2 = filtered_runs[:,sr2_col]
nlrT3_extension = filtered_runs[:,net_extension_col]

num_filtered = filtered_runs.shape[0]

print 'You got', results_array.shape[0], 'total runs.'
print 'You got', len(zHe_successful_runs), 'good zircon runs.'
print 'You got', len(aHe_successful_runs), 'good apatite runs.'
print 'You got', num_filtered, 'good total runs!'


# make histories
time_start = 20.
time_stop = 0.
time_step = 0.01

time_vector = pt.make_time_vector(time_start = time_start,
                                  time_stop = time_stop, time_step = time_
step,
                                  decimals = 3)
times = len(time_vector)

er_w_time_array = nmp.zeros((times, num_filtered))
cum_ext_w_time_array = nmp.zeros((times, num_filtered))

for i in range(num_filtered):
    init = filtered_runs[i,init_col]
    accel = filtered_runs[i,accel_col]
    er1 = filtered_runs[i,sr1_col] * nmp.cos(fault_dip)
    er2 = filtered_runs[i,sr2_col] * nmp.cos(fault_dip)

    er_w_time_array[:,i] = pt.make_slip_rate_w_time(init, accel, er1, er2,
                                          time_vector = time_vector)

    cum_ext_w_time_array[:,i] = pt.get_cum_vector(er_w_time_array[:,i],
                                          time_step)




fig1 = plt.figure(1)
pt.make_fault_histograms(fig1, filtered_runs, init_col, sr1_col, accel_col,
                         sr2_col)

fig2 = plt.figure(2)
pt.make_ext_histories(fig2, 'nlrT3', time_vector, er_w_time_array,
                      cum_ext_w_time_array)

plt.show()
```

nlrT4_filter_tools.py

```python
import numpy as nmp
import pecube_tools as pt
import os
import matplotlib.pyplot as plt


if os.name == 'nt':
    results_array = nmp.loadtxt('C:\\itchy\\code_repos\\pt_working\\re-
sults\\nlrT4_results.csv', delimiter=',')
elif os.name == 'posix':
#    results_array = nmp.load('/media/4C307D4D22E94879/school/tibet/lunggar/
kurt/pecube/nlrT2/nlr_results.npy')
    results_array = nmp.loadtxt('/home/itchy/src/Pecube/nlrT4/new_runs/nlr_
results.csv', delimiter=',')

#results_array = nmp.load('nlrT2_results.py')

# column indices for fault parameters
initA_col = 8
initB_col = 9
accel_col = 10
srA1_col = 11
srA2_col = 12
srB1_col = 13
srB2_col = 14
net_extension_col = 15

fault_A_dip = 0.84
fault_B_dip = 0.93

# input observations and error calculations (larger of analytical and lab er-
ror)

aHe_obs = nmp.array([3.974, 0., 2.912, 2.744])

aHe_sd_err = nmp.array([0.238, 0., 0.175, 0.233])

zHe_obs = nmp.array([4.637, 4.212, 3.521, 3.425])

zHe_sd_err = nmp.array([0.371, 0.705, 0.282, 0.581])

elev_obs = nmp.array([5336, 4971, 4942, 4880])

elev_pred = nmp.array([5317, 4987, 5022, 4898])

lon = nmp.array([83.5131, 83.5624, 83.5598, 83.5667])

num_obs = len(zHe_obs)


# filtering parameters

num_aHe_outliers = 1

num_zHe_outliers = 0

aHe_lab_err = 0.06 * aHe_obs

zHe_lab_err = 0.04 * zHe_obs
```

```
aHe_err = pt.max_errors(aHe_sd_err, aHe_lab_err)

zHe_err = pt.max_errors(zHe_sd_err, zHe_lab_err)

aHe_first_result = 0

zHe_first_result = 1

num_chronometers = 2

result_interval = num_chronometers

# error bounds
aHe_1sd_err_lo = aHe_obs - aHe_err
aHe_2sd_err_lo = aHe_obs - 2 * aHe_err
aHe_1sd_err_hi = aHe_obs + aHe_err
aHe_2sd_err_hi = aHe_obs + 2 * aHe_err

zHe_1sd_err_lo = zHe_obs - zHe_err
zHe_2sd_err_lo = zHe_obs - 2 * zHe_err
zHe_1sd_err_hi = zHe_obs + zHe_err
zHe_2sd_err_hi = zHe_obs + 2 * zHe_err


# zHe run variables
zHe_sigma = 2 #sigma, 1 or 2
if zHe_sigma == 1:
    obs_age_lo = zHe_1sd_err_lo
    obs_age_hi = zHe_1sd_err_hi

elif zHe_sigma == 2:
    obs_age_lo = zHe_2sd_err_lo
    obs_age_hi = zHe_2sd_err_hi

first_result = zHe_first_result
num_outliers = num_zHe_outliers
zHe_index = pt.get_result_index(zHe_first_result, result_interval, num_obs)

# filter zHe runs
zHe_successful_runs = pt.filter_ages(results_array, obs_age_lo, obs_age_hi,
                                     first_result, result_interval, num_obs,
                                     num_outliers)

# aHe run variables
aHe_sigma = 2 #sigma, 1 or 2
if aHe_sigma == 1:
    obs_age_lo = aHe_1sd_err_lo
    obs_age_hi = aHe_1sd_err_hi

elif aHe_sigma == 2:
    obs_age_lo = aHe_2sd_err_lo
    obs_age_hi = aHe_2sd_err_hi

first_result = aHe_first_result
num_outliers = num_aHe_outliers
aHe_index = pt.get_result_index(aHe_first_result, result_interval, num_obs)

# filter aHe runs
aHe_successful_runs = pt.filter_ages(results_array, obs_age_lo, obs_age_hi,
                                     first_result, result_interval, num_obs,
                                     num_outliers)


all_successful_runs = pt.combine_successful_runs(zHe_successful_runs,
                                                 aHe_successful_runs)
```

335

```
filtered_runs = pt.filter_results(results_array, all_successful_runs)

num_filtered = filtered_runs.shape[0]


aHe_success_ages = pt.get_chronometer_results(filtered_runs, aHe_index)
zHe_success_ages = pt.get_chronometer_results(filtered_runs, zHe_index)

nlrT4_initA = filtered_runs[:,initA_col]
nlrT4_initB = filtered_runs[:,initB_col]
nlrT4_accel = filtered_runs[:,accel_col]
nlrT4_srA1 = filtered_runs[:,srA1_col]
nlrT4_srA2 = filtered_runs[:,srA2_col]
nlrT4_srB = filtered_runs[:,srB1_col]
nlrT4_extension = filtered_runs[:,net_extension_col]

#aHe_err =

print 'You got', results_array.shape[0], 'total runs.'
print 'You got', len(zHe_successful_runs), 'good zircon runs.'
print 'You got', len(aHe_successful_runs), 'good apatite runs.'
print 'You got', num_filtered, 'good total runs!'




# make histories
time_start = 20.
time_stop = 0.
time_step = 0.01

time_vector = pt.make_time_vector(time_start = time_start,
                                  time_stop = time_stop, time_step = time_
step,
                                  decimals = 3)
times = len(time_vector)

er_w_time_array_A = nmp.zeros((times, num_filtered))
er_w_time_array_B = nmp.zeros((times, num_filtered))

cum_ext_w_time_array_A = nmp.zeros((times, num_filtered))
cum_ext_w_time_array_B = nmp.zeros((times, num_filtered))

for i in range(num_filtered):
    initA = filtered_runs[i,initA_col]
    initB = filtered_runs[i,initB_col]
    accel = filtered_runs[i,accel_col]
    erA1 = filtered_runs[i,srA1_col] * nmp.cos(fault_A_dip)
    erB1 = filtered_runs[i,srB1_col] * nmp.cos(fault_B_dip)
    #er1 = erA1 + erB1
    erA2 = filtered_runs[i,srA2_col] * nmp.cos(fault_A_dip)
    erB2 = filtered_runs[i,srB2_col] * nmp.cos(fault_B_dip)
    #er2 = erA2 + erB2

    er_w_time_array_A[:,i] = pt.make_slip_rate_w_time(initA, accel, erA1,
erA2,
                                            time_vector = time_vector)

    er_w_time_array_B[:,i] = pt.make_slip_rate_w_time(initB, accel, erB1,
erB2,
                                            time_vector = time_vector)

    cum_ext_w_time_array_A[:,i] = pt.get_cum_vector(er_w_time_array_A[:,i],
                                            time_step)
```

```
        cum_ext_w_time_array_B[:,i] = pt.get_cum_vector(er_w_time_array_B[:,i],
                                        time_step)

    er_w_time_array = er_w_time_array_A + er_w_time_array_B

    cum_ext_w_time_array = cum_ext_w_time_array_A + cum_ext_w_time_array_B
# make plots
fig1 = plt.figure(1)

pt.make_fault_histograms(fig1, filtered_runs, initA_col, srA1_col, accel_col,
                            srA2_col)
plt.title('Fault A')

fig2 = plt.figure(2)

pt.make_fault_histograms(fig2, filtered_runs, initB_col, srB1_col, accel_col,
                            srB2_col)
plt.title('Fault B')

fig3 = plt.figure(3)
pt.make_ext_histories(fig3, 'nlrT4', time_vector, er_w_time_array,
                            cum_ext_w_time_array)

fig4 = plt.figure(4)
pt.lon_elev_plots(fig4, aHe_success_ages.T, aHe_obs, aHe_err * 2, lon, elev_
obs)

plt.show()
```

nmt_filter_tools.py

```python
# -*- coding: utf-8 -*-
"""
Created on Sat Aug 25 15:37:30 2012

@author: Richard
"""

import numpy as nmp
import pecube_tools as pt
import os
import matplotlib.pyplot as plt

if os.name == 'nt':
    results_array = nmp.load('C:\\school\\tibet\\lunggar\\thermo\\pecube\\nmt_
picloud_results\\nmt_all_runs.npy')



# column indices for fault parameters
initA_col = 7
initB_col = 11
accel_col = 9
srA1_col = 8
srA2_col = 10
srB1_col = 12
srB2_col = 12
net_extension_col = 14

fault_A_dip = 0.4
fault_B_dip = 0.88


# input observations and error calculations (larger of analytical and lab er-
ror)

zHe_obs = nmp.array([3.48, 3.43, 3.66, 4.40, 4.87, 7.28, 6.34])

zHe_sd_err = nmp.array([0.24, 0.24, 0.70, 0.41, 0.57, 0.64, 0.24])

elev_obs = nmp.array([5381, 5416, 5538, 5609, 5628, 5823, 6063])

elev_pred = nmp.array([5381, 5416, 5538, 5609, 5628, 5823, 6063])

lon = nmp.array([83.40467, 83.40848, 83.41141, 83.4345, 83.4545, 83.5342,
83.54151])

num_obs = len(zHe_obs)


# filtering parameters

num_zHe_outliers = 0


zHe_lab_err = 0.05 * zHe_obs


zHe_err = pt.max_errors(zHe_sd_err, zHe_lab_err)

zHe_first_result = 0
```

```
num_chronometers = 1

result_interval = num_chronometers

# error bounds

zHe_1sd_err_lo = zHe_obs - zHe_err
zHe_2sd_err_lo = zHe_obs - 2 * zHe_err
zHe_1sd_err_hi = zHe_obs + zHe_err
zHe_2sd_err_hi = zHe_obs + 2 * zHe_err


# zHe run variables
zHe_sigma = 2 #sigma, 1 or 2
if zHe_sigma == 1:
        obs_age_lo = zHe_1sd_err_lo
        obs_age_hi = zHe_1sd_err_hi

elif zHe_sigma == 2:
        obs_age_lo = zHe_2sd_err_lo
        obs_age_hi = zHe_2sd_err_hi

first_result = zHe_first_result
num_outliers = num_zHe_outliers
zHe_index = pt.get_result_index(zHe_first_result, result_interval, num_obs)

# filter zHe runs
zHe_successful_runs = pt.filter_ages(results_array, obs_age_lo, obs_age_hi,
                                     first_result, result_interval, num_obs,
                                     num_outliers)



all_successful_runs = pt.combine_successful_runs(zHe_successful_runs)

filtered_runs = pt.filter_results(results_array, all_successful_runs)

num_filtered = filtered_runs.shape[0]

zHe_success_ages = pt.get_chronometer_results(filtered_runs, zHe_index)

#aHe_err =

print 'You got', results_array.shape[0], 'total runs.'
print 'You got', len(zHe_successful_runs), 'good zircon runs.'

print 'You got', num_filtered, 'good total runs!'



# make histories
time_start = 20.
time_stop = 0.
time_step = 0.01

time_vector = pt.make_time_vector(time_start = time_start,
                                  time_stop = time_stop, time_step = time_
step,
                                  decimals = 3)
times = len(time_vector)

er_w_time_array_A = nmp.zeros((times, num_filtered))
```

```
er_w_time_array_B = nmp.zeros((times, num_filtered))

cum_ext_w_time_array_A = nmp.zeros((times, num_filtered))
cum_ext_w_time_array_B = nmp.zeros((times, num_filtered))

for i in range(num_filtered):
    initA = filtered_runs[i,initA_col]
    initB = filtered_runs[i,initB_col]
    accel = filtered_runs[i,accel_col]
    erA1 = filtered_runs[i,srA1_col] * nmp.cos(fault_A_dip)
    erB1 = filtered_runs[i,srB1_col] * nmp.cos(fault_B_dip)
    #er1 = erA1 + erB1
    erA2 = filtered_runs[i,srA2_col] * nmp.cos(fault_A_dip)
    erB2 = filtered_runs[i,srB2_col] * nmp.cos(fault_B_dip)
    #er2 = erA2 + erB2

    er_w_time_array_A[:,i] = pt.make_slip_rate_w_time(initA, accel, erA1,
erA2,
                                           time_vector = time_vector)

    er_w_time_array_B[:,i] = pt.make_slip_rate_w_time(initB, accel, erB1,
erB2,
                                           time_vector = time_vector)

    cum_ext_w_time_array_A[:,i] = pt.get_cum_vector(er_w_time_array_A[:,i],
                                      time_step)

    cum_ext_w_time_array_B[:,i] = pt.get_cum_vector(er_w_time_array_B[:,i],
                                      time_step)

    er_w_time_array = er_w_time_array_A + er_w_time_array_B

    cum_ext_w_time_array = cum_ext_w_time_array_A + cum_ext_w_time_array_B

# make plots
fig1 = plt.figure(1)
pt.make_fault_histograms(fig1, filtered_runs, initA_col, srA1_col, accel_col,
                         srA2_col)


fig2 = plt.figure(2)
pt.make_fault_histograms(fig2, filtered_runs, initB_col, srB1_col, accel_col,
                         srB2_col)


fig3 = plt.figure(3)
pt.make_ext_histories(fig3, 'nlrT4', time_vector, er_w_time_array,
                         cum_ext_w_time_array)
```

cctr_filter_tools.py

```
# -*- coding: utf-8 -*-
"""
Created on Sat Aug 25 15:37:30 2012

@author: Richard
"""

import numpy as nmp
import pecube_tools as pt
import os
import matplotlib.pyplot as plt

if os.name == 'nt':
    results_array = nmp.load('C:\\school\\tibet\\lunggar\\thermo\\pecube\\
cctr_picloud_results\\cctr_all_runs.npy')



# column indices for fault parameters
initA_col = 8
initB_col = 12
accel_col = 9
srA1_col = 10
srA2_col = 11
srB1_col = 13
srB2_col = 14
net_extension_col = 16

fault_A_dip = 0.88
fault_B_dip = 0.88


# input observations and error calculations (larger of analytical and lab er-
ror)

zHe_obs = nmp.array([7.33, 7.16, 7.25, 6.27, 5.99, 5.33, 5.33, 5.96])

zHe_sd_err = nmp.array([0.6, 0.29, 0.39, 0.88, 0.17, 0.63, 0.33, 0.61])

elev_obs = nmp.array([5979, 5848, 5826, 5719, 5633, 5622, 5490, 5477])

elev_pred = nmp.array([5965, 5996, 5898, 5746, 5759, 5614, 5638, 5618])

lon = nmp.array([83.4355, 83.4372, 83.4556, 83.4642, 83.4744, 83.4833,
83.4857, 83.5125])

num_obs = len(zHe_obs)


# filtering parameters

num_zHe_outliers = 0


zHe_lab_err = 0.05 * zHe_obs


zHe_err = pt.max_errors(zHe_sd_err, zHe_lab_err)

zHe_first_result = 0
```

```
num_chronometers = 1

result_interval = num_chronometers

# error bounds

zHe_1sd_err_lo = zHe_obs - zHe_err
zHe_2sd_err_lo = zHe_obs - 2 * zHe_err
zHe_1sd_err_hi = zHe_obs + zHe_err
zHe_2sd_err_hi = zHe_obs + 2 * zHe_err


# zHe run variables
zHe_sigma = 2 #sigma, 1 or 2
if zHe_sigma == 1:
        obs_age_lo = zHe_1sd_err_lo
        obs_age_hi = zHe_1sd_err_hi

elif zHe_sigma == 2:
        obs_age_lo = zHe_2sd_err_lo
        obs_age_hi = zHe_2sd_err_hi

first_result = zHe_first_result
num_outliers = num_zHe_outliers
zHe_index = pt.get_result_index(zHe_first_result, result_interval, num_obs)

# filter zHe runs
zHe_successful_runs = pt.filter_ages(results_array, obs_age_lo, obs_age_hi,
                                     first_result, result_interval, num_obs,
                                     num_outliers)



all_successful_runs = pt.combine_successful_runs(zHe_successful_runs)

filtered_runs = pt.filter_results(results_array, all_successful_runs)

num_filtered = filtered_runs.shape[0]

zHe_success_ages = pt.get_chronometer_results(filtered_runs, zHe_index)

#aHe_err =

print 'You got', results_array.shape[0], 'total runs.'
print 'You got', len(zHe_successful_runs), 'good zircon runs.'

print 'You got', num_filtered, 'good total runs!'



# make histories
time_start = 20.
time_stop = 0.
time_step = 0.01

time_vector = pt.make_time_vector(time_start = time_start,
                                  time_stop = time_stop, time_step = time_
step,
                                  decimals = 3)
times = len(time_vector)

er_w_time_array_A = nmp.zeros((times, num_filtered))
```

```python
er_w_time_array_B = nmp.zeros((times, num_filtered))

cum_ext_w_time_array_A = nmp.zeros((times, num_filtered))
cum_ext_w_time_array_B = nmp.zeros((times, num_filtered))

for i in range(num_filtered):
    initA = filtered_runs[i,initA_col]
    initB = filtered_runs[i,initB_col]
    accel = filtered_runs[i,accel_col]
    erA1 = filtered_runs[i,srA1_col] * nmp.cos(fault_A_dip)
    erB1 = filtered_runs[i,srB1_col] * nmp.cos(fault_B_dip)
    #er1 = erA1 + erB1
    erA2 = filtered_runs[i,srA2_col] * nmp.cos(fault_A_dip)
    erB2 = filtered_runs[i,srB2_col] * nmp.cos(fault_B_dip)
    #er2 = erA2 + erB2

    er_w_time_array_A[:,i] = pt.make_slip_rate_w_time(initA, accel, erA1,
erA2,
                                        time_vector = time_vector)

    er_w_time_array_B[:,i] = pt.make_slip_rate_w_time(initB, accel, erB1,
erB2,
                                        time_vector = time_vector)

    cum_ext_w_time_array_A[:,i] = pt.get_cum_vector(er_w_time_array_A[:,i],
                                    time_step)

    cum_ext_w_time_array_B[:,i] = pt.get_cum_vector(er_w_time_array_B[:,i],
                                    time_step)

    er_w_time_array = er_w_time_array_A + er_w_time_array_B

    cum_ext_w_time_array = cum_ext_w_time_array_A + cum_ext_w_time_array_B

# make plots
fig1 = plt.figure(1)
pt.make_fault_histograms(fig1, filtered_runs, initA_col, srA1_col, accel_col,
                         srA2_col)


fig2 = plt.figure(2)
pt.make_fault_histograms(fig2, filtered_runs, initB_col, srB1_col, accel_col,
                         srB2_col)


fig3 = plt.figure(3)
pt.make_ext_histories(fig3, 'cctr', time_vector, er_w_time_array,
                      cum_ext_w_time_array)
```

Appendix 5: Chapter 6 TCN depth profile descriptions

KF Profile 1 description

8/17/2010
Location: Karakoram Pit #1 (High Terrace)
31.24953 N
80.70887 E
4622 m

Surface Description:
    Vegetation:
Small bushes ~20-30 cm high with 10cm-5m gaps between bushes and small clumps of grass inter-grown with the bushes. There are a lot of sheep, yak and horse imprints in the area showing high grazing traffic.

    Ground Surface:
Pebble to cobble clasts made of granite and volcanics. Dark red sandy clay making up the main body of the soil. Pebbles lying on top of the surface, could be lag remnants.

Pit Description:

Mixing zone is ~30 cm thick, top part is a very fine soil, little organics, fine sand to clay with gravel less then 5 cm, angular to sub angular, granite to intermediate with volcanics/metaseds. Some bioturbation evident by roots .7 cm thick, related to nearby bushes, 1.5 cm burrows.

Below the mixing zone there is evidence of minor bioturbation (1mm thick roots). The roots extend down 120 cm, very sporadic.

Coarse grained, cobble (biggest 20 cm) conglomerate, fine gravel to coarse sand lenses up to 4 cm thick, only evidence for bedding. Fine gravel are sub rounded meta sed clasts, sand is granitic. The entire thing is matrix supported, made of fine gravel to sand.

Sample Depths:

Sample 1: 192cm-186cm
Sample 2: 149cm-145cm
Sample 3: 137cm-131cm
Sample 4: 98cm-92cm
Sample 5: 75cm-70cm
Sample 6: 45cm-41cm

Photograph of the surface of Pit 1.

Photograph of upper part of Pit 1 showing well-developed soil mixing zone and bioturbation above less-modified sediment below

Photograph of interior of Pit 1 well below mixing zone, showing typical sediment characteristics of pit, as well as excavated sample horizon.

KF Profile 2 description

08/20/2010
Karakoram Pit #2 (Mid Terrace)
31.25353 N
80.70930 E
4607 m

Surface Description:
    Vegetation:
Small scrub bushes ~20 cm tall, 30-60 cm wide, with spacing between plants ranging from 5-120 cm covering ~35% of the surface. Small clumps of grasses ~10 cm wide, 5-15 cm tall covering <2% of the surface, higher densities of the grasses are seen near the small scrub bushes. Small fern-ish plants 2 cm tall 1-5 cm wide cover <1% of the ground surface. No other vegetation is seen in the area.

    Ground Surface:
Gravel-cobble (20cm) made of granites to intermediates with volcanics/metaseds. This lies on top of a dark brown sandy mud that makes up 80-90% of the non vegetated surface. The surface is fairly flat with a few fluvial incisions. This is the second highest terrace. There are two terraces further below this terrace. To the north and south are high mountans +6km away.
On the surface there is heavy signs of horse and yak presence. Scat and trails are abundant, horses have been spotted in the nearby river beds.

Pit Description:
Mixing zone is ~60-65 cm, dark brown fine sands with lots of clay. Minor gravel fraction, lots of roots <1 cm in diameter. Immediately below the mixing zone is a zone of cobbles, clast supported, matrix is a fine sand to clay mostly fine sand. Clasts: felsic to intermediate intrusives, volcanics and some quartzite, meta seds present at Pit #1 are not present here. Below the cobble layer is a matrix supported conglomerate, clasts up to 10 cm, clast composition is the same as described above, matrix is a clayey sand (medium), 3 cm lenses of coarse sand, small roots <1 cm in diameter are present to 1 m. Below the cobble layer other than the lenses there is no observable bedding.

Sample Depths:

Sample 1: 197cm-190cm
Sample 2: 160cm-157cm
Sample 3: 139cm-133cm
Sample 4: 115cm-112cm
Sample 5: 92cm-85cm
Sample 6: 70cm-62cm

Photograph of Pit 2 surface showing nearby vegetation.

Photograph of upper part of Pit 2 showing thick (~60 cm) soil mixing zone above conglomeratic layer interpreted as the top of the unmixed zone.

Photograph of the interior of Pit 2 showing typical sedimentary structure.

KF Profile 3 description

8/28/2010
Karakoram Fault Pit #3
31.25440 N
80.70806 E
4601 m

Surface Description:
    Vegetation:
-15-150 cm bushed up to 80 cm tall 30-200 cm spacing between bushes.
-Small clumps of grass, 15 cm in diameter up to 30 cm tall, mostly growing with the bushes.
-Small 1-3 cm leafy plants, roots go ~3 cm down, 1-20 spacing between plants.

    Ground Surface:
Gravel and pebble clasts sitting on the surface, clasts are complosed of volcanics, graites and intermediates with scattered cobbles. Most of the surface is a drak brown sandy clay.

Pit Description:
Mixing zone is up to 50 cm, brown (med), fine sand, clay and silt, some gravel- large cobbles (> 20 cm) below mixing zone, sediment consists of mostly fine gravel to boulder (>50 cm). Some sand is present but virtually no silt or clay. Most of the pit is a clast supported, some zones of gravel have no matrix, just pore space. Lithology dominantly granite with some intermediates and volcanics (very minor), the only sings of cementation are calcite veins on the bottom of clasts in the upper 90 cm of the pit. This pit was exceedingly loose and wall failures were ubiq-uitous during sampling. The potential for contamination of samples from overlying sediments is moderate. Roots are present throughout the depth of the pit especially where the is a lot of sand. I don't know whether this can cause mixing of sand.

Sample Depths:

Sample 3: 133cm-127cm
Sample 4: 86cm-80cm
Sample 5: 68cm-61cm
Sample 6: 58cm-51cm

Photograph of Pit 3 surface showing vegetation surrounding the pit.

Photograph of upper part of Pit 3 showing mixing zone and typical sedimentary structure below.

Photograph of Pit 3 below mixing zone showing conglomeratic nature of sediments.

Appendix 6: Chapter 6 Python codes

slip_rate_tools.py

```python
# -*- coding: utf-8 -*-
"""
Created on Thu Aug 30 14:00:54 2012

@author: Richard
"""

import numpy as nmp
#import Splines

class OffsetMarker:
    """Represents an offset geologic marker.

    Attributes:
        offsets: list of possible offset distances for the given marker.
            If offset_type = Gauss, offsets = [mean, sd]
        offset_probs: list of probabilities of corresponding offset distances
        offset_dist_type: offset prob. distribution (gauss, uniform, arbi-
trary)
        ages: list of possible ages for the given marker
        age_probs: list of probabilities of corresponding ages
        age_dist_type: age prob. distribution (gauss, uniform, arbitrary)
        source: Source for information (e.g., what article, field campaign)

    """
    def __init__(self, offsets='offsets', offset_probs = [],
                 offset_dist_type = 'offset_dist_type', ages = 'ages',
                 age_probs = [], age_dist_type = 'age_dist_type',
                 source='None'):
        self.offset_probs = offset_probs
        self.offset_dist_type = offset_dist_type
        if offset_dist_type == 'Gauss':
            self.offset_mean = offsets[0]
            self.offset_sd = offsets[1]
        elif offset_dist_type == 'Uniform':
            self.offset_mean = offsets[0]
            self.offset_err = offsets[1]
        else:
            self.offsets == offsets

        self.age_probs = age_probs
        self.age_dist_type = age_dist_type
        if age_dist_type == 'Gauss':
            self.age_mean = ages[0]
            self.age_sd = ages[1]
        elif age_dist_type == 'Uniform':
            self.age_mean = ages[0]
            self.age_err = ages[1]
        else:
            self.ages == ages

        self.source = source


    def append_age(self, new_age, new_age_prob=[]):
        """Add an offset/age pair to the marker.
        Maybe should be removed because it might cause problems"""
        self.ages.append(new_age)
        self.age_probs.append(new_age_prob)

    def generateProbs():
        pass
```

```python
    def sample_offset_from_gauss(self, n):
        """Generates n-length sample from Gaussian distribution of offsets"""
        offset_sample = self.offset_sd * nmp.random.randn(n) + self.offset_
mean
        offset_sample = offset_sample[offset_sample >= 0]

        return offset_sample

    def sample_offset_from_uniform(self, n):
        """Generates n-length sample from uniform distribution of ages"""
        offset_sample = ((nmp.random.rand(n) * 2 -1) * self.offset_err +
                         self.offset_mean)

        return offset_sample

    def sample_offset_from_arbitrary(self, n):
        """not supported yet"""
        pass

    def sample_offset(self, n):
        """Generates n-length array of samples from distribution"""
        if self.offset_dist_type == 'Gauss':
            offset_sample = self.sample_offset_from_gauss(n)

        elif self.offset_dist_type == 'Uniform':
            offset_sample = self.sample_offset_from_uniform(n)

        elif self.offset_dist_type == 'Arbitrary':
            offset_sample = self.sample_offset_from_arbitrary(n)

        else:
            print 'What is the offset distribution type?'

        return offset_sample

    def sample_age_from_gauss(self, n):
        """Generates n-length sample from Gaussian distribution of ages"""
        age_sample = self.age_sd * nmp.random.randn(n) + self.age_mean
        age_sample = age_sample[age_sample >= 0]

        return age_sample

    def sample_age_from_uniform(self, n):
        """Generates n-length sample from uniform distribution of ages"""
        age_sample = (nmp.random.rand(n) * 2 -1) * self.age_err + self.age_
mean

        return age_sample

    def sample_age_from_arbitrary(self, n):
        """not supported yet"""
        pass

    def sample_age(self, n):
        """Generates n-length array of samples from distribution"""
        if self.age_dist_type == 'Gauss':
            age_sample = self.sample_age_from_gauss(n)

        elif self.age_dist_type == 'Uniform':
            age_sample = self.sample_age_from_uniform(n)

        elif self.age_dist_type == 'Arbitrary':
            pass
```

353

```python
        else:
            print 'What is the age distribution type?'

        return age_sample

    def sample(self, n):
        age_sample = self.sample_age(n)
        offset_sample = self.sample_offset(n)

        asl = len(age_sample)
        osl = len(offset_sample)

        if asl > osl:
            age_sample = age_sample[0:osl]
        elif osl > asl:
            offset_sample = offset_sample[0:asl]

        sample_array = nmp.vstack([age_sample, offset_sample])

        return sample_array


def truncate_samples(sample_list):
    """truncate samples to length of shortest sample"""
    'measure length of each sample, then cut samples to shortest length'
    #d = {}
    #for i in range( len(sample_list) ):
    #    d["l"+str(i)] = len(sample_list[i])
    length_array = []
    short_list = []

    for i in range( len(sample_list) ):
        samp = sample_list[i]
        length_array.append(samp.shape[1])

    l_min = min(length_array)

    for i in range( len(sample_list) ):
        samp = sample_list[i]
        samp = samp[:, 0:l_min]
        short_list.append(samp)

    return short_list

def check_increasing(in_array):
    """Checks to see if array is monotonically increasing, returns bool value
    """
    ans_array = [1]
    for i in range(1, len(in_array)):
        if in_array[i] > in_array[i-1]:
            ans_array.append(1)
        else:
            ans_array.append(0)

    ans = bool(0 in ans_array)
    return ans

def get_log_pts(p_min, p_max, n_pts=50, base=nmp.e):
    """Generates n_pts length array of logarithmically spaced points"""
    if p_min == 0:
        pts_array = nmp.hstack([0, nmp.logspace(nmp.log(1e-5), nmp.log(p_max),
                                                num=n_pts-1, base=base)])
    else:
        pts_array = nmp.logspace(p_min, p_max, num=n_pts, base=base)
    return pts_array
```

```python
def tspline_interpolate():
    pass

def calc_stats():
    pass
```

Splines.py

```python
# -*- coding: utf-8 -*-
"""
Created on Mon Jun  4 10:26:52 2012

@author: itchy
"""

import numpy as nmp



def spline1d(x_out, x_data, y_data, x_slope, y_slope, *args):
    """
    SPLINE1D      1-D interpolation using Green's function for a spline in
tension
    SPLINE1D will find a spline-based curve using continuous curvature splines
    in tension (if set).  The algorithm uses the Green's function for the
spline.
    You can supply data constrains, slope constrains, or a mix of both.
    Solution can be evaluated at arbitrary locations

    Use one of the following 3 call formats:
        y = spline1d (x_out, x_data, y_data, x_slope, y_slope)
        y = spline1d (x_out, x_data, y_data, x_slope, y_slope, t)
        y = spline1d (x_out, x_data, y_data, x_slope, y_slope, t, cutoff)

    The input parameters are:

     x_out -  Desired output x positions
     x_data  -   coordinates of points with data constraints
     y_data  -   data constraints at the above points
     x_slope  -   coordinates of points with slope constraints
     y_slope  -   slope constraints at the above points
     t  - tension to use, 0 <= t <= 1
        if t is a vector of length 2 the second value is taken as the length-
scale
     cutoff - if set, eigenvalues whose ratio to the maximum eigenvalue are
smaller
        than cutoff are zeroed out before the curve is evaluated.

     One of (x_data, y_data) and (x_slope, y_slope) can be ([], [])
     t, if not set, defaults to 0 (cubic spline).  t = 1 gives linear interpo-
lation

       The loutput values are:
          y  - the interpolation
          l  - optionally, the eigenvalues of the linear system

      See Wessel, P, D. Bercovici, 1998, Gridding with Splines in Tension : A
      Green function Approach, Math. Geol., 30, 77-93.

    Ported to Python by Richard Styron, June 2012
    """


    # Pick a reasonable(?) lengthscale
    length_scale = (nmp.amax(x_out) - nmp.amin(x_out)) / 50.

    if len(args) == 0:  # no tension selected, set default
        t = 0.
    elif len(args) == 1:     # cutoff not set
        t = args
```

```python
        cutoff = 0.
    elif len(args) == 2:
        t = args[0]
        cutoff = args[1]


    t = nmp.array([t])
    cutoff = 0.



    nt = len(t)
    if nt == 2:      # user gave both tension and lengthscale
        length_scale = t[1]
        t = t[0]

    # TODO:  Add error/exception for values of t outside of [0,1]


    # Misc initializations
    if t < 1:
        p = nmp.sqrt(t / (1 - t))
        p = p / length_scale

    n0 = 0
    n1 = 1


        # First we must enforce the use of column vectors for the data con-
straints
        # FIX THIS: some_vector.shape unpacks to (m,) instead of (m,1)

    x_out = nmp.matrix(x_out)
    [m,n] = x_out.shape
    if m < n:
        #x_out = x_out.reshape(x_out.shape[0], -1)
        x_out = x_out.T

    x_data = nmp.matrix(x_data)
    [m,n] = x_data.shape
    if m < n:
        #x_data = x_data.reshape(x_data.shape[0], -1)
        x_data = x_data.T

        y_data = nmp.matrix(y_data)
    [m,n] = y_data.shape
    if m < n:
        #y_data = y_data.reshape(y_data.shape[0], -1)
        y_data = y_data.T

    [n0, m0] = y_data.shape

    x_slope = nmp.mat(x_slope)
    [m,n] = x_slope.shape
    if m < n:
        #x_slope = x_slope.reshape(x_slope.shape[0], -1)
        x_slope = x_slope.T

    y_slope = nmp.mat(y_slope)
    [m,n] = y_slope.shape
    if m < n:
    #y_slope = y_slope.reshape(y_slope.shape[0], -1)
        y_slope = y_slope.T

    #n1 = len(x_slope)
    n1 = 0
```

357

```python
    # Assembly final xp, yp vectors (possibly combination of data and slopes)

    #xp = nmp.array([[x_data] , [x_slope]])
    #yp = nmp.array([[y_data] , [y_slope]])

    # TODO: fix slope constrain problems by putting an 'if' statement here:
    #    if slopes exist, add to the vectors

    xp = nmp.matrix(x_data)
    yp = nmp.matrix(y_data)

    # Now build the square n x n linear system that must be solved for the al-
pha's

    n = n0 + n1

    A = nmp.zeros((n, n))

    for i in nmp.arange(0,n0):  # First add equations for data constraints

        r = xp[i] - xp
        ar = nmp.abs(r)

        if t == 0:
            B = (ar ** 3)
            A[i,:] = B.T

        elif t == 1:
            B = (ar)
            A[i,:] = B.T

        else:
            B = nmp.exp(nmp.multiply(-p, ar)) + nmp.multiply(p, ar)
            A[i,:] = B.T

    if n1 > 0:
        for i in nmp.arange(0,n1):  # Then add equations for slope constraints

            j = i + n0
            r = xp[j] - xp
            ar = nmp.abs(r)

            if t == 0:
                B = 3.0 * (r * ar)
                A[j,:] = B.T

            elif t == 1:
                B = nmp.sign(r)
                A[j,:] = B.T

    # Done building square linear system, now solve it

    # TODO: fix for cutoff > 0.0 -- deal with nargout for SVD

        if cutoff > 0.0:      # solve using SVD
        #     U, S, V = svd(A)
        #     s = nmp.diag(S)
        #     if
            pass

    else:
        alpha = nmp.linalg.solve(A, yp)
```

```
        # Now evaluate final solution at output locations

y = nmp.zeros((len(x_out),m0))

for i in nmp.arange(0,n):
    r = xp[i] - x_out
    ar = nmp.abs(r)

    if t == 0:
        y = y + (ar ** 3) * alpha[i,:]

    elif t == 1:
        y = y + ar * alpha[i,:]

    else:
        B = nmp.exp(nmp.multiply(-p, ar)) + nmp.multiply(p, ar)
        y = y + nmp.multiply(B, alpha[i,:])

y = nmp.array(y.T)

y = y[0,:]

return y
```

kf_pdfs.py

```
# -*- coding: utf-8 -*-
"""
script that makes pdfs from offset and timing information and then does a
monte carlo simulation to generate slip histories with error propagation
"""
import sys
sys.path.append('C:\\python_modules')
import numpy as nmp
import matplotlib.pyplot as plt
import Splines
from scipy import interpolate as Int
from scipy import stats
import time

then = time.time()

n = 2e5 # number of MC iterations

pdf_range = nmp.arange(0, 500) # range over which to calculate offset PDF (m)
time_max = 150 # ka
time_range = nmp.arange(0, time_max)
time_range_diff = nmp.arange(0, time_max -1)

tension = 0.95
tension2 = 1

nbins = 50

# KKRF offsets

# keys are offsets in inches measured in Illustrator (1 inch = 200 m) and val-
ues
# are

#T1_in_offset_prob = dict({'0.': 0., '0.0491': 3., '0.0961': 7., '0.1107':
10.,
#                          '0.2081': 7.5, '0.3747':2.5, '0.4202':0.})

#Qa_in_offset_prob = dict({'0.0963': 0., '0.2133': 3, '0.2777':8.5,
'0.3139':10.,
#                          '0.5285':0})

#Qao_in_offset_prob = dict({'0.1892':0., '0.2966':1., '0.4137':8.,
'0.521':10.,
#                           '0.5979':8., '0.7442':4, '0.8507':0.})


T1_in_offset_prob = dict({'0.': 0., '0.0491': 3., '0.0961': 7., '0.1107': 10.,
                          '0.2081': 7.5, '0.3747':1.5, '0.4202':0.})

Qa_in_offset_prob = dict({'0.0963': 0., '0.2133': 3, '0.2777':8.5,
'0.3139':10.,
                          '0.4357':4., '0.5285':3.25, '1.5':1.5, '1.75':0.})

Qao_in_offset_prob = dict({'0.1892':0., '0.2966':1., '0.4137':8., '0.521':10.,
                           '0.5979':8., '0.7442':4, '0.8507':2.5, '1.9':1.25,
'2.2':1.0, '2.35':0.})



# All the T1 bidnezz
```

```python
T1_offsets_in = nmp.array (map (float, T1_in_offset_prob.keys() ) )

T1_offsets_in = T1_offsets_in.copy()

T1_offset = T1_offsets_in * 200.

T1_prob = nmp.array (map (float, T1_in_offset_prob.values() ) )

# fit pmf
T1_offset_pmf = Splines.spline1d(pdf_range, T1_offset, T1_prob, [], [], ten-
sion)

# set negative values to 0
neg_vals =  T1_offset_pmf < 0  # find indices of negative values
T1_offset_pmf[neg_vals] = 0.   # change them

T1_offset_pdf = T1_offset_pmf / sum(T1_offset_pmf)    # normalize pdf from pmf

T1_offset_cdf = nmp.cumsum(T1_offset_pdf)   # make cdf

T1_icdf = Int.interp1d(T1_offset_cdf, pdf_range)    # invert cdf

T1_offset_sample = T1_icdf(nmp.random.random( (n,) ) )  # sample from pdf




# now for Qa
Qa_offsets_in = nmp.array (map (float, Qa_in_offset_prob.keys() ) )

Qa_prob = nmp.array (map (float, Qa_in_offset_prob.values() ) )

Qa_offset = Qa_offsets_in * 200.

# fit pmf
Qa_offset_pmf = Splines.spline1d(pdf_range, Qa_offset, Qa_prob, [], [], ten-
sion)

# set negative values to 0
neg_vals =  Qa_offset_pmf < 0  # find indices of negative values
Qa_offset_pmf[neg_vals] = 0.   # change them

Qa_offset_pdf = Qa_offset_pmf / sum(Qa_offset_pmf)    # normalize pdf from pmf

Qa_offset_cdf = nmp.cumsum(Qa_offset_pdf)   # make cdf

Qa_icdf = Int.interp1d(Qa_offset_cdf, pdf_range)     # invert cdf

Qa_offset_sample = Qa_icdf(nmp.random.random( (n,) ) )  # sample from pdf




# finally for Qao
Qao_offsets_in = nmp.array (map (float, Qao_in_offset_prob.keys() ) )

Qao_prob = nmp.array (map (float, Qao_in_offset_prob.values() ) )

Qao_offsets_in = nmp.array (map (float, Qao_in_offset_prob.keys() ) )

Qao_offset = Qao_offsets_in * 200.

Qao_prob = nmp.array (map (float, Qao_in_offset_prob.values() ) )
```

```python
# fit pmf
Qao_offset_pmf = Splines.spline1d(pdf_range, Qao_offset, Qao_prob, [], [],
tension)

# set negative values to 0
neg_vals =  Qao_offset_pmf < 0  # find indices of negative values
Qao_offset_pmf[neg_vals] = 0.   # change them

Qao_offset_pdf = Qao_offset_pmf / sum(Qao_offset_pmf)    # normalize pdf from
pmf

Qao_offset_cdf = nmp.cumsum(Qao_offset_pdf)   # make cdf

Qao_icdf = Int.interp1d(Qao_offset_cdf, pdf_range)    # invert cdf

Qao_offset_sample = Qao_icdf(nmp.random.random( (n,) ) )    # sample from pdf


# filter out regressive offsets
T1_offset_keep = T1_offset_sample[(T1_offset_sample < Qa_offset_sample) & (Qa_
offset_sample < Qao_offset_sample)]

Qa_offset_keep = Qa_offset_sample[(T1_offset_sample < Qa_offset_sample) & (Qa_
offset_sample < Qao_offset_sample)]

Qao_offset_keep = Qao_offset_sample[(T1_offset_sample < Qa_offset_sample) &
(Qa_offset_sample < Qao_offset_sample)]

offset_zeros = nmp.zeros(len(T1_offset_keep))
sample_offsets = nmp.vstack((offset_zeros, T1_offset_keep, Qa_offset_keep,
Qao_offset_keep))
sample_offsets = sample_offsets.T


# timing stuff


# generate age distributions, based somewhat on Chevalier et al., 2012
T1_age = 24. # central age value (median in C12, mean here)

T1_err = 8. # 1-sigma distribution

T1_age_sample = T1_err * nmp.random.randn(n) + T1_age # length n age vector

T1_age_sample = nmp.abs(T1_age_sample)

Qa_age = 50.

Qa_err = 20. #ka

Qa_age_sample = Qa_err * nmp.random.randn(n) + Qa_age # length n age vector

Qa_age_sample = nmp.abs(Qa_age_sample)

Qao_age = 100.

Qao_err = 32. #ka

Qao_age_sample = Qao_err * nmp.random.randn(n) + Qao_age # length n age vector
Qao_age_sample = nmp.abs(Qao_age_sample)
```

```
# filter out regressive ages
T1_age_keep = T1_age_sample[(T1_age_sample < Qa_age_sample) & (Qa_age_sample <
Qao_age_sample)]

Qa_age_keep = Qa_age_sample[(T1_age_sample < Qa_age_sample) & (Qa_age_sample <
Qao_age_sample)]

Qao_age_keep = Qao_age_sample[(T1_age_sample < Qa_age_sample) & (Qa_age_sample
< Qao_age_sample)]

age_zeros = nmp.zeros(len(T1_age_keep))
sample_ages = nmp.vstack((age_zeros, T1_age_keep, Qa_age_keep, Qao_age_keep))
sample_ages = sample_ages.T




# time to get slip rates


if len(Qa_age_keep) > len(Qa_offset_keep):
    k = len(Qa_offset_keep)
else:
    k = len(Qa_age_keep)

kfloat = float(k)

slip_history = nmp.zeros( (len(time_range), k) )
slip_history_percentiles = nmp.zeros((len(time_range), 6))
slip_history_hist = nmp.zeros((len(time_range), nbins))
hist_edges = nmp.zeros((nbins+1))
hist_centers = nmp.zeros(nbins)

slip_rate_history = nmp.zeros( (len(time_range_diff), k) )
slip_rate_history_percentiles = nmp.zeros((len(time_range_diff), 6))
slip_rate_history_hist = nmp.zeros((len(time_range_diff), nbins))
rate_edges = nmp.zeros((nbins+1))
rate_centers = nmp.zeros(nbins)


for run in nmp.arange(0,k):
    slip_history[:,run] = Splines.spline1d(time_range, sample_ages[run,:],
sample_offsets[run,:],
        [], [], tension2)

    slip_rate_history[:,run] = nmp.diff(slip_history[:,run])


for time_int in time_range:
    slip_history_percentiles[time_int, 0] = nmp.min(slip_history[time_int,:])
    slip_history_percentiles[time_int, 1] = stats.scoreatpercentile(slip_
history[time_int,:], per=5)
    slip_history_percentiles[time_int, 2] = stats.scoreatpercentile(slip_
history[time_int,:], per=25)
    slip_history_percentiles[time_int, 3] = stats.scoreatpercentile(slip_
history[time_int,:], per=50)
    slip_history_percentiles[time_int, 4] = stats.scoreatpercentile(slip_
history[time_int,:], per=75)
    slip_history_percentiles[time_int, 5] = stats.scoreatpercentile(slip_
history[time_int,:], per=95)
    slip_history_hist[time_int,:], hist_edges = nmp.histogram(slip_
history[time_int,:], bins=nbins, range=(0.,800.), density=False)
    slip_history_hist[time_int,:] = slip_history_hist[time_int,:] * slip_his-
tory_percentiles[time_int,2]/ (30 * kfloat)
```

```
for time_int in time_range_diff:
    slip_rate_history_percentiles[time_int, 0] = nmp.min(slip_rate_
history[time_int,:])
    slip_rate_history_percentiles[time_int, 1] = stats.scoreatpercentile(slip_
rate_history[time_int,:], per=5)
    slip_rate_history_percentiles[time_int, 2] = stats.scoreatpercentile(slip_
rate_history[time_int,:], per=25)
    slip_rate_history_percentiles[time_int, 3] = stats.scoreatpercentile(slip_
rate_history[time_int,:], per=50)
    slip_rate_history_percentiles[time_int, 4] = stats.scoreatpercentile(slip_
rate_history[time_int,:], per=75)
    slip_rate_history_percentiles[time_int, 5] = stats.scoreatpercentile(slip_
rate_history[time_int,:], per=95)
    slip_rate_history_hist[time_int,:], rate_edges = nmp.histogram(slip_rate_
history[time_int,:], bins=nbins, range=(0.,10.), density=True)

for ind in nmp.arange(nbins):
    rate_centers[ind] = (rate_edges[ind] + rate_edges[ind +1]) / 2


# TODO:  find a way to estimate the 50% (?) 'most likely' values, or the value
which is the 'top half' of the PDF




now = time.time()

duration = now-then
print duration




#plt.figure(1)
#plt.plot(, 'k--')


plt.figure(1)
#plt.plot(pdf_range, T1_offset_pdf, 'b', pdf_range, Qa_offset_pdf, 'g',
#         pdf_range, Qao_offset_pdf, 'r')

ax1 = plt.subplot(311)
plt.plot(pdf_range, T1_offset_pdf)
plt.xlabel('T1 offset (m)')
plt.ylabel('probability')

ax2 = plt.twinx()
plt.plot(pdf_range, T1_offset_cdf, 'r')
plt.ylim([0,1])
plt.ylabel('cum. probability')


ax3 = plt.subplot(312)
plt.plot(pdf_range, Qa_offset_pdf)
plt.xlabel('Qa offset (m)')
plt.ylabel('probability')
```

```
ax4 = plt.twinx()
plt.plot(pdf_range, Qa_offset_cdf, 'r')
plt.ylim([0,1])
plt.ylabel('cum. probability')


ax5 = plt.subplot(313)
plt.plot(pdf_range, Qao_offset_pdf)
plt.xlabel('Qao offset (m)')
plt.ylabel('probability')

ax6 = plt.twinx()
plt.plot(pdf_range, Qao_offset_cdf, 'r')
plt.ylim([0,1])
plt.ylabel('cum. probability')




plt.figure(2)

plt.subplot(211)
hist_extent = [time_range[0], time_range[-1], hist_edges[0], hist_edges[-1] ]
plt.imshow(slip_history_hist.T, aspect='auto', extent=hist_extent,
origin='lower')
plt.colorbar()
plt.plot(time_range, slip_history_percentiles[:,0], 'grey', linewidth = 0.75)
plt.plot(time_range, slip_history_percentiles[:,1], 'grey', linewidth = 1)
plt.plot(time_range, slip_history_percentiles[:,2], 'grey', linewidth = 1.5)
plt.plot(time_range, slip_history_percentiles[:,3], 'k-', linewidth = 1.5)
plt.plot(time_range, slip_history_percentiles[:,4], 'grey', linewidth = 1.5)
plt.plot(time_range, slip_history_percentiles[:,5], 'grey', linewidth = 1)
plt.axis([0, 148, 0, 800])
plt.gca().invert_xaxis()
plt.xlabel('age of geologic feature (ka)')
plt.ylabel('modern offset (m)')




plt.subplot(212)
rate_extent = [time_range_diff[0], time_range_diff[-1], rate_edges[0], rate_
edges[-1] ]
plt.imshow(slip_rate_history_hist.T, aspect='auto', extent=rate_extent,
origin='lower')
plt.colorbar()
plt.plot(time_range_diff, slip_rate_history_percentiles[:,0], 'grey', lin-
ewidth = 0.75)
plt.plot(time_range_diff, slip_rate_history_percentiles[:,1], 'grey', lin-
ewidth = 1)
plt.plot(time_range_diff, slip_rate_history_percentiles[:,2], 'grey', lin-
ewidth = 1.5)
plt.plot(time_range_diff, slip_rate_history_percentiles[:,3], 'k-', linewidth
= 1.5)
plt.plot(time_range_diff, slip_rate_history_percentiles[:,4], 'grey', lin-
ewidth = 1.5)
plt.plot(time_range_diff, slip_rate_history_percentiles[:,5], 'grey', lin-
ewidth = 1)
plt.axis([0,148,0,10])
plt.gca().invert_xaxis()
plt.xlabel('time before present (ka)')
plt.ylabel('slip rate (mm/a)')


plt.show()
```

365

The author on a fine mapping day in the southern Surla Range.